Membrane-associated higher-ordered protein mega-complexes for denitrification and motility in *Pseudomonas aeruginosa*

Von der Fakultät für Lebenswissenschaften

der Technischen Universität Carolo-Wilhelmina

zu Braunschweig

zur Erlangung des Grades eines

Doktors der Naturwissenschaften

(Dr. rer. nat.)

genehmigte

D i s s e r t a t i o n

von José Manuel Borrero de Acuña

aus Madrid/Spanien

1. Referent: Professor Dr. Dieter Jahn

2. Referent: Professor a. D. Dr. Kenneth Nigel Timmis

3. Referent: Professor Dr. Ralf-Rainer Mendel

eingereicht am: 01.04.2015

mündliche Prüfung (Disputation) am: 05.05.2015

Druckjahr 2015

Vorveröffentlichungen der Dissertation

Teilergebnisse aus dieser Arbeit wurden mit Genehmigung der Fakultät für Lebenswissenschaften, vertreten durch den Mentor der Arbeit, in folgenden Beiträgen vorab veröffentlicht:

Publikationen

Steen, A., Utkür, F.Ö., **Borrero-de Acuña, J.M.**, Bunk, B., Roselius, L., Bühler, B., Jahn, D. & Schobert, M. Construction and characterization of nitrate and nitrite respiring *Pseudomonas putida* KT2440 strains for anoxic biotechnical applications. Journal of Biotechnology 163(2):155-65 (2013).

Borrero-de Acuña, J.M., Bielecka, A., Häussler, S., Schobert, M., Jahn, M., Wittmann, C., Jahn, D. & Poblete-Castro, I. Production of medium chain length polyhydroxyalkanoate in metabolic flux optimized *Pseudomonas putida*. Microbial Cell Factories 19;13:88 (2014).

Tagungsbeiträge

Borrero de Acuña J. M., Arias-Rivas S., Dammeyer T., de Lorenzo V., Timmis K. & Molinari G.: Interactomic network of *Pseudomonas putida* KT2440 periplasm. (Poster). 2nd Public Retreat, Goslar-Hahnenklee (2011).

Borrero de Acuña J. M., Arias-Rivas S., Dammeyer T., de Lorenzo V., Timmis K. & Molinari G.: Interactomic network of *Pseudomonas putida* KT2440 periplasm. (Poster). 5th International PhD Symposium (HZI), Braunschweig (2011).

Borrero de Acuña J. M., Arias-Rivas S., Molinari G., Timmis K. & Schobert M.: Interactomic network of the *Pseudomonas* periplasm. (Poster). TU Braunschweig Annual Retreat, Hildesheim (2012).

Borrero de Acuña J. M.: Interactomic studies of the *Pseudomonas* periplasm. (Talk). 3rd Annual Retraet, Bad Bevensen (2012).

Borrero de Acuña J. M., Arias-Rivas S., Molinari G., Timmis K. & Schobert M.: Interactomic network of the *Pseudomonas* periplasm. (Poster). 6th International PhD Symposium, Braunschweig (2013).

Borrero de Acuña J. M. and Jahn D. Interactomic studies in the *Pseudomonas aeruginosa* denitrification pathway. (Poster). Bacterial Electron Transfer Processes and their Regulation, Conference, Vimeiro. (2015).

Table of Contents

Abbreviations and Symbols

ACN	acetonitril
AP	affinity purification
AP-MS	affinity purification coupled with mass spectrometry
AP-MS/MS	affinity purification coupled with tandem mass spectrometry
AP-QMS	affinity purification coupled with quantitative mass spectrometry
a.a.	amino acids
Ap	ampicillin
Anr	anaerobic regulation of arginine deiminase and nitrate reduction
Å	angstrom
bp	base pair(s)
CRP	cAMP receptor protein
Cb	carbenicillin
CDW	cell dry weight
ºC	Celsius degree(s)
Cm	chloramphenicol
cDNA	complementary deoxyribonucleic acid
CF	cystic fibrosis
DNA	deoxyribonucleic acid
DMSO	dimethyl sulfoxide
N_2	dinitrogen
dH_2O	distilled water
Dnr	dissimilatory nitrate respiration regulator
et al.	*et alteri* (and others)
EDTA	ethylenediamine tetraacetic acid

e.g.	*exempli gratia* (for example)
Fw	forward
GC	gas chromatography
g	gram(mes)
ppGpp	guanosine-3′,5′-bispyrophosphate
His_{6x}	hexahistidine tag
h	hour(s)
i.e.	*id est* (that is)
∞	infinity
kb	kilobase
kDa	kilodalton(s)
kg	kilogram(mes)
kV	kilovolt(s)
LC-MS/MS	liquid chromatography coupled with tandem mass spectrometry
L	litre(s)
LB	Luria-Bertani medium
MS	mass spectrometry
Mb	megabase
mRNA	messenger ribonucleic acid
µ	micro
µF	microfaradio(s)
µg	microgram(mes)
µL	microlitre(s)
µm	micrometer(s)
µM	micromolar
mg	milligram(mes)
mL	millilitre(s)
mm	millimeter(s)

mM	millimolar
min	min(s)
M	molar
MW	molecular weight
n	nano
ng	nanogram(mes)
nm	nanometer(s)
nM	nanomolar
NAD(H)	nicotinamide adenine dinucleotide (oxidized/reduced)
NADP(H)	nicotinamide adenine dinucleotide phosphate (oxidized/reduced)
NO_3	nitrate
NO	nitric-oxide
NO_2	nitrite
N_2O	nitrous oxide
nt	nucleotide(s)
Ω	ohm
ORF	open reading frame
OD	optical density
PFA	paraformaldehyde
%	percentage
PBS	phosphate buffered saline
PHA	polyhydroxyalkanoates
PCR	polymerase chain reaction
p-value	probability value
PVDF membrane	polyvinylidene difluoride membrane
Rv	reverse
rpm	revolutions per min
RNA	ribonucleic acid

rRNA	ribosomal ribonucleic acid
RBS	ribosomal binding site
SEM	scanning electron microscopy
sec	sec(s)
SDS-PAGE	sodium dodecyl sulfate polyacrylamide gel electrophoresis
Sm	streptomycin
TAP	tandem affinity purification
TEM	transmission electron microscopy
Tn	transposon
TCA-cycle	tricarboxylic acid cycle
TCA-precipitation	trichloroacetic acid precipitation
TFA	trifluoroacetic acid
TAE	tris acetate EDTA
UV	ultraviolet light
λ	lambda
v/v	volume/volume
wt	wild-type
w/v	weight/volume
x *g*	gravitational force

1 Introduction

1.1 The genus *Pseudomonas*

Pseudomonas species belong to the Gram-negative Gammaproteobacteria. Most of them are straight or slightly curved rods that bear one or more polar flagella which endow the bacterium with motility (Palleroni *et al.*, 1972). Members of the genus *Pseudomonas* are ubiquitous bacteria that inhabit a wide variety of environments from terrestrial to aquatic niches (Silby *et al.*, 2011). They are known due to their metabolic versatility being able to assimilate a wide range of compounds (Rojo, 2010), e.g. sugars, fatty acids, alcohols, glycols, aromatic compounds, amines or amino acids (Palleroni, 1993). Certain *Pseudomonas* species are opportunistic pathogens such as *P. syringae* and *P. aeruginosa*. Others as *P. putida* are of high biotechnological importance, for instance due to their ability to degrade xenobiotic compounds and produce biofuels or bioplastics (Palleroni, 2003).

1.1.1 *Pseudomonas putida*

P. putida is a Gram-negative rod-shaped Gammaproteobacterium which is able to effectively thrive in diverse niches, such as temperate soils and waters, and the rhizosphere of a number of plants (Aranda-Olmedo *et al.*, 2002). The full genome of *P. putida* KT2440 (6.18 Mb) was the first one sequenced among *P. putida* strains (Nelson *et al.*, 2002). This bacterium is known for its versatility to degrade a wide variety of aromatic compounds. Five major degradation pathways have been elucidated in *P. putida* strains: β-ketoadipate, gentisate, homogentisate, phenylacetyl-CoA, and the homo-proto-catechuate (Jimenez *et al.*, 2002). Furthermore, *P. putida* is capable of recycling organic waste in aerobic compartments of the environment, thereby playing a key role in the maintenance of environmental quality (Timmis, 2002). In addition, *P. putida* strain has been shown to be an optimal host strain for expression of heterologous genes.

1.1.1.2 Systems metabolic engineering in *P. putida*

The term systems metabolic engineering refers to the manipulations of complex biological systems in order to alter the nature and production of compounds of biotechnological importance towards the benefits released by these alterations (better structure, higher production of a determined compound, higher specificity, etc). The

prediction and construction of gene-regulatory networks is intrincate and requires extensive mathematical designing in order to reconstitute enzymes systems (Gardner *et al.*, 2000). Here, carry out a modeling in *P. putida* that enhances its PHA production to an extent never reported before.

1.1.1.3 Metabolic engineering

Metabolic engineering of microorganisms has significantly contributed to the biotechnological production of chemicals in a sustainable manner (Khosla & Keasling, 2003, Stephanopoulos & Vallino, 1991). Insertion of heterologous pathways and modification of the host metabolism, via deletion or amplification of genes, has been a common procedure to enhance the synthesis of a desired compound. Nevertheless, these modifications often evoke detrimental effects on the cell metabolism which lead to decreased growth and low performance of the constructed cell factory (Lee *et al.*, 2011). *In silico* reconstruction of the metabolism of bacterial production hosts in combination with metabolic flux modeling can help to design the optimal pathways towards a product of interest (Kohlstedt *et al.*, 2010, Otero & Nielsen, 2010). Multiple efforts have been made to engineer microorganisms to obtain sustainable polymers which have the potential to replace petroleum-based plastics. In this regard, *mcl*-PHAs are among the most promising biodegradable polymers synthesized by microorganisms which can be used in a wide range of applications (Borrero-de Acuna *et al.*, 2014).

1.1.1.4 *P. putida* as a producer of *mcl*-PHAs

P. putida can naturally synthesize *mcl*-PHAs. These polymers are accumulated as inclusion bodies in the cytoplasm of a wide range of bacterial strains (Figure 1). These inclusion bodies are utilized as reservoir of carbon and energy to cope with the changing environmental conditions of their natural habitats (Chung *et al.*, 2009). The accumulation of these polymers is generally promoted by a high carbon supply and the limitation of an inorganic nutrient such as nitrogen, oxygen, or phosphorous (Madison & Huisman, 1999).

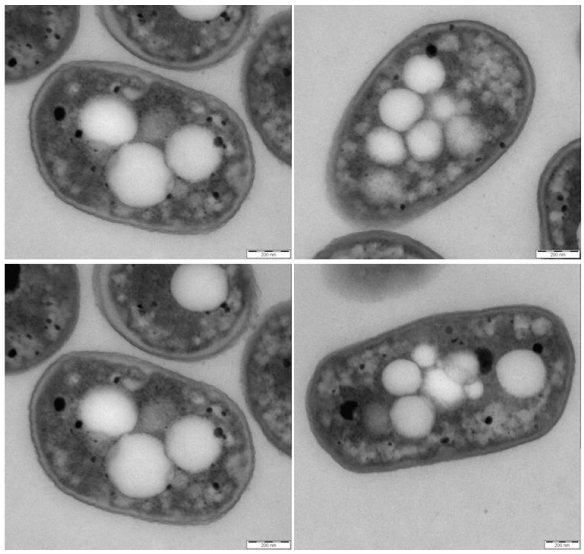

Figure 1. Electron micrographs of thin sections of *P. putida* KT2440 (provided by Dr. Ignacio Poblete Castro, HZI).

For decades, studies for biotechnological *mcl*-PHA production focused on the use of fatty acid as carbon source. This approach led to PHA accumulation in the cell, yielding more than 80% of its dry weight as PHA (Poblete-Castro *et al.*, 2012). Additionally, engineering of the β-oxidation pathway in *P. putida* allowed for production of novel *mcl*-PHAs, which implies a broad range of applications in biomedicine and for biomaterials (Tripathi *et al.*, 2013). Much less attention has been given to the engineering of metabolic pathways involved in sugar or polyalcohol utilization in *P. putida* (Escapa *et al.*, 2013).

1.1.2 *Pseudomonas aeruginosa*

P. aeruginosa causes approximately 9 - 10% of hospital infections (Hancock & Speert, 2000). It is the most prevalent cause of nonsomical infections being found in burn wounds, chronic wounds and chronic obstructive pulmonary disorders. Surface growth on implanted biomaterials, on hospital surfaces and in water supplies was observed. In general terms, *P. aeruginosa* is considered an opportunistic human pathogen, assigned to the death of immunocompromised patients, associated with skin and soft tissue infections, nosocomial pneumonia, and sepsis (Damron & Goldberg, 2012). *P. aeruginosa* is the most predominant cause of both acute and chronic infections of the lung of cystic fibrosis (CF) patients (Stover *et al.*, 2000, Van Alst *et al.*, 2009b). It is capable of colonizing the dehydrated mucus of the CF lung. The ability of *P. aeruginosa* to grow in a biofilm manner enhances its ability to cause infections by

conferring protection to the bacteria from host defenses and chemotherapy (Mulcahy *et al.*, 2014). It has been recently found that sharp O_2 gradients exist across the mucus of the CF lung indicating that *P. aeruginosa* must adapt its energy metabolism to the changing oxygen concentrations from high to low O_2 and on to anaerobic environments within the CF lung (Williams *et al.*, 2007). *P. aeruginosa* cell is shown in Figure 2.

Figure 2. *P. aeruginosa* (red) on a HELA cell (green). The image was taken by SEM (Prof. Dr. Manfred Rohde, HZI). Colored with Photoshop (Dr. Gabriella Molinari, HZI).

Significant research efforts have been invested into studying its capability of forming biofilms (O'Toole *et al.*, 2000), as well as cell-to-cell signaling employing quorum sensing (Withers *et al.*, 2001, Juhas *et al.*, 2005). As a pathogen, *P. aeruginosa* is especially difficult to treat due to this high antibiotic resistance (Hancock & Speert, 2000).

1.1.2.1 Cystic fibrosis and anaerobic growth of *P. aeruginosa*

One out of approximately 30,000 individuals in United States and a comparable number in Europe is affected by the autosomal disease CF. Due to the thickness of this cystic fibrosis airway mucus there is a decreasing oxygen gradient across it which represents a stress situation to be overcome by bacteria (Su & Hassett, 2012). *P. aeruginosa* is able to grow in low oxygen tensions conditions, like those created in the lung environment of CF afflicted patients, through dissimilatory denitrification. In this pathway nitrate and nitrite, also found in the mucus generated by this affection (Zetterquist *et al.*, 2009), are utilized as terminal electron acceptors to gain energy by proton motive force generation instead of oxygen. Alternatively, *P. aeruginosa* is also

able to persist under anaerobic stress by the arginine and the pyruvate fermentation. In general, the most effective mode of biological energy generation is oxygen respiration. During this process electrons are transported from donor molecule, like NADH, via membrane localized large multi-protein complexes along a redox cascade to the electron acceptor oxygen. The generated free energy is recovered via the formation of a H^+/Na^+ gradient at the membrane, ultimately driving ATP synthesis by ATP synthases (Singleton & Wigley, 2003). Under conditions of oxygen-depletion many microorganisms are capable of replacing oxygen by an alternative electron acceptor including nitrate, sulphate, fumarate or dimethyl sulfoxide DMSO (Oren, 2009). Furthermore, the electron acceptors are combined with a whole variety of electron donors by these organisms (Unden & Bongaerts, 1997). In this context, every electron donor and acceptor requires an own complex enzymatic system, either soluble or membrane-associated and often accompanied by additional intermediate transfer complexes, like the bc_1 complex. The structure and biochemistry of these different enzyme complexes and enzymatic systems are well understood (Zumft, 1997, Williams *et al.*, 2007). In contrast, much less is known about the dynamic interactions of these protein complexes in the respiratory chains. For prokaryotes, only a few investigations report on the supra-molecular organization of these respiratory chains (Magalon *et al.*, 2012).

1.1.2.2 Denitrification pathway of *P. aeruginosa*

Denitrification occurs mainly in the periplasmic space of the cell with the exception of the first reduction step which takes place at the cytoplasmic site of the inner membrane. In this process nitrate is utilized as terminal electron acceptor and comprises stepwise reductions as follows: nitrate (NO_3^-) → nitrite (NO_2^-) → nitric-oxide (NO) → nitrous oxide (N_2O) → molecular nitrogen (N_2) (Williams *et al.*, 2007, Toyofuku *et al.*, 2012b). The positive redox potentials E_0 of nitrate (NO_3^-/NO_2^- = + 0.43 V), nitrite (NO_2^-/NO = + 0.35 V), nitric-oxide (NO/N_2O = + 1.175 V) and nitrous oxide (N_2O/N_2 = +1.355 V) are employed for energy conservation (Zumft, 1997, Berks *et al.*, 1995). These reactions represent an important part of the world´s N-cycle (Bannert *et al.*, 2011). These sequential steps lead to a gain of energy by proton motive force and are catalyzed consecutively by the enzymes nitrate reductase (Nar), nitrite reductase (Nir), nitric-oxide reductase (Nor) and nitrous oxide reductase (Nos) (Hassett *et al.*, 2002, Arai, 2011). Nitrate and nitric-oxide, in addition of being respiratory substrates,

have been both identified as signaling molecules for the induction of the distinct N oxide-metabolizing enzymes (Zumft, 1997). The genes encoding these reductases *narGHI*, *nirS*, *norCB* and *nosZ* are found throughout the genome in tightly regulated operons (Hassett *et al.*, 2002). *P. aeruginosa* possesses a second, periplasmic nitrate reductase, NapAB which can compensate in the absence of Nar (Van Alst *et al.*, 2009a). An overview of the denitrification pathway is depicted in Figure 3.

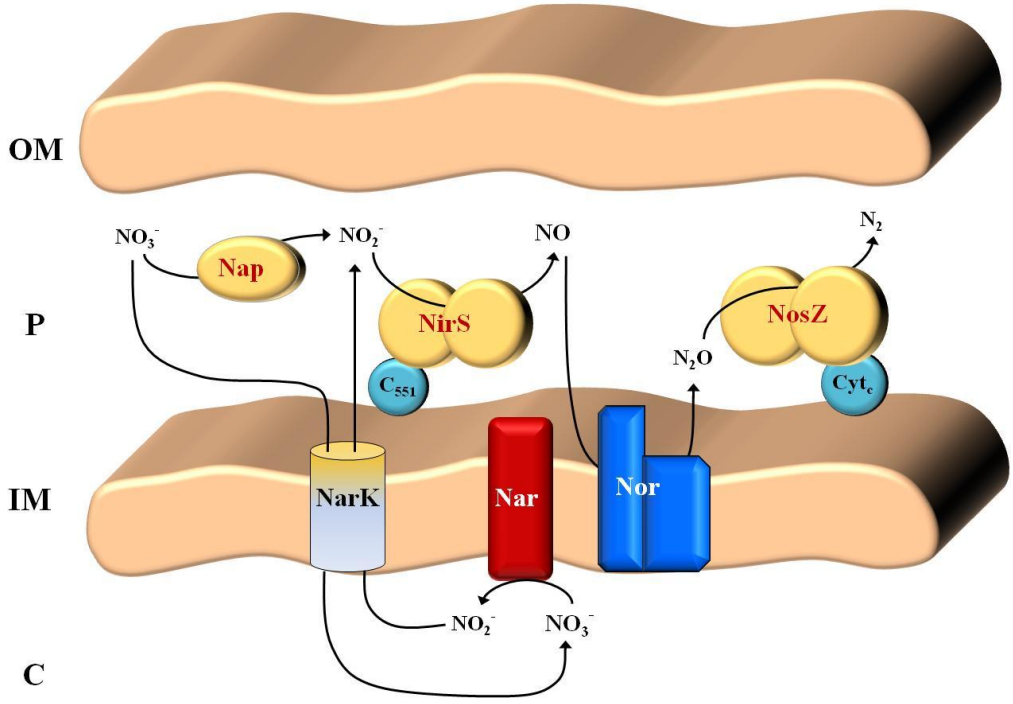

Figure 3. Schematic view of the denitrification pathway of *P. aeruginosa* illustrating its reduction steps. P = periplasm. IM = inner membrane. C = cytoplasm. OM = outer membrane.

Nitrate reductase

During the first step of denitrification in *P. aeruginosa* respiratory nitrate reductase (NarGHI) catalyzes the reaction: $NO_3^- + 2e^- + 2H^+ \leftrightarrow NO_2^- + H_2O$. Multiple biochemical and structural data revealed that these quinol-nitrate oxidoreductases receive electrons from ubiquinol via the two heme groups of the membrane spanning small subunit NarI. Electrons get transferred through a linear arrangement of Fe-S clusters of the NarI attached subunit NarH to the active site of the molybdenum cofactor (MoCo) containing subunit NarG. NarH and NarG are directed into the cytoplasm of *P. aeruginosa* (Einsle & Kroneck, 2004, Bertero *et al.*, 2003, Dias *et al.*, 1999). The protein NarJ and cardiolipins are involved in the complex assembly of

the various protein subunits with their corresponding cofactors (Lanciano *et al.*, 2007, Arias-Cartin *et al.*, 2012). *P. aeruginosa* additionally contains the periplasmic nitrate reductase NapAB. Electrons are supplied by the membrane anchored tetraheme cytochrome *c* NapC. Interestingly, NapABC can compensate for NarGHI deficiency (Van Alst *et al.*, 2009a).

Nitrite reductase

The periplasmic nitrite reductase NirS catalyzes the reaction: $NO_2^- + 2H^+ + e^- \leftrightarrow NO + H_2O$. The *P. aeruginosa* enzyme is a cytochrome cd_1 carrying an electron receiving heme *c* and a catalytic site with heme d_1 (3,8-dioxo-17-acrylate-porphyrindione); (Nurizzo *et al.*, 1997, Rinaldo *et al.*, 2011, Farver *et al.*, 2009). The two *c*-type cytochromes NirM and NirC act as electron donors (Hasegawa *et al.*, 2001a). NirN and NirF form protein-protein interactions with the nitrite reductase NirS during enzyme maturation (Nicke *et al.*, 2013). NirF is involved in heme d_1 insertion (Bali *et al.*, 2010). The final step of heme d_1 biosynthesis, mainly localized in the periplasm, involves the uroporphyrin-III *c*-methyltransferase NirE (Storbeck *et al.*, 2011), siroheme decarboxylase NirDL/NirGH (Haufschildt *et al.*, 2014) and a novel electron-bifurcating dehydrogenase NirN (Adamczack *et al.*, 2014). Nitrate from the environment gets transported into the cytoplasm by the nitrate/nitrite antiporter NarK2, converted by the activity of NarGHI into nitrite, which then returns via NarK2 into the periplasm to serve as substrate for NirS (Sharma *et al.*, 2006).

Nitric-oxide reductase

The integral membrane protein nitric-oxide reductase NorCB catalyzes the reaction: $2NO + 2H^+ + 2e^- \leftrightarrow N_2O + H_2O$. The heterodimeric *P. aeruginosa* enzyme utilizes heme *c* and heme *b* for electron delivery to a heme *b* and non-heme iron in the active site which coordinates the two NO substrates (Hino *et al.*, 2010, Shiro, 2012). Interestingly, the small subunit C covers most of the surface of the enzyme towards the periplasm (Hino *et al.*, 2010, Shiro, 2012). The ATP-binding protein NirQ seems to be involved in NorCB maturation (Hayashi *et al.*, 1998).

Nitrous oxide reductase

The periplasmic enzyme nitrous oxide reductase NosZ catalyzes the reaction: $N_2O + 2e^- + 2H^+ \leftrightarrow N_2 + H_2O$. Catalysis of the head-to-tail homodimeric enzyme

requires two copper centers (Wust *et al.*, 2012, Pomowski *et al.*, 2011). The periplasmic domain of the transmembrane iron-sulfur flavoprotein NosR was found essential for NosZ function (Wunsch & Zumft, 2005). The periplasmic lipoprotein NosL anchored to the outer membrane is a copper binding protein involved in NosZ maturation (Taubner *et al.*, 2004, McGuirl *et al.*, 2001). However, the denitrification further relies on electron donating primary dehydrogenases (Dell'acqua *et al.*, 2011, Williams *et al.*, 2007) and multiple other components of the electron transport chain (Ugidos *et al.*, 2008, Kawakami *et al.*, 2010).

1.1.2.3 Regulation of denitrification supra-complex formation

Formation of the denitrification pathway is controlled by complex regulatory networks (Benkert *et al.*, 2008, Vollack & Zumft, 2001). During the shift from aerobic to anaerobic denitrifying conditions oxygen-depletion is detected by the Fe-S-cluster containing Fnr-type regulator Anr (Kuroki *et al.*, 2014). Nitrate is measured by the two-component regulatory system NarXL. Finally, NO is targeted by the hemoprotein Dnr, again an Fnr/Crp-type regulator. All these regulators are inducing nitrate reductase NarGHI formation (Schreiber *et al.*, 2007). The formation of NirS, NorCB and NosZ is mainly depending on Dnr (Trunk *et al.*, 2010, Arai *et al.*, 2003).

Anr and Dnr regulators

The anaerobic regulator of arginine deiminase and nitrate reduction (Anr), an analogue of *Escherichia coli* regulator of fumarate and nitrate reduction (Fnr), has been reported to be essential for denitrification in *P. aeruginosa* (Schobert & Tielen, 2010). Oxygen limitation is sensed by the Anr transcriptional regulator via a Fe-S cluster what leads to activation of the nitrate reductase operon and a large additional regulon (Trunk *et al.*, 2010). The dissimilatory nitrate respiration regulator (Dnr), a cAMP receptor protein CRP/Fnr related regulator protein has also been shown to be crucial for this pathway. *dnr* gene transcription is regulated by Anr (Arai *et al.*, 1997). Transcriptional activation of *nirS*, *norCB* and *nosZ* genes relies on the Dnr regulator (Trunk *et al.*, 2010) which is presumed to sense NO (Arai *et al.*, 2003) by a bound heme cofactor (Giardina *et al.*, 2008). The NO molecule is an intermediate of the denitrification pathway.

The NarXL two-component system

Upon oxygen limitation a two-component system is activated: NarXL. The NarX protein is a sensor kinase which perceives nitrate or nitrite. NarL is the response regulator to NarX. Both proteins form a two-component system which activates expression of *hemA*, *narK1*, *nirQ* and *dnr*, whereas it represses expression of arginine fermentation genes. NirQ in turn seems to modulate *nirS* expression (Schobert & Tielen, 2010).

1.1.2.3 Arginine fermentation

Although *P. aeruginosa* preferentially obtains its energy by aerobic or anaerobic respiration, it is able to carry out arginine and pyruvate fermentation when required (Williams *et al.*, 2007, Eschbach *et al.*, 2004). Arginine fermentation is accomplished by the arginine deiminase pathway which catalyzes the conversion of L-arginine into L-ornithine resulting in ATP generation (Vander Wauven *et al.*, 1984). In this pathway three enzymes are involved: the arginine deiminase, a catabolic ornithine carbamoyltransferase and the carbamate kinase (Mercenier *et al.*, 1980). In Figure 4 the fermentative steps are illustrated.

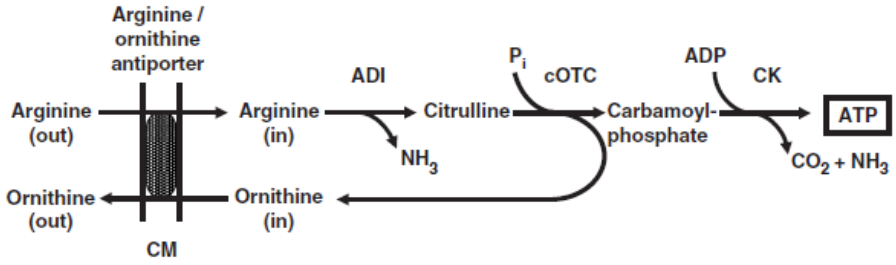

Figure 4. Reduction steps during arginine fermentation (Williams *et al.*, 2007).

The structural genes encoding these enzymes are *arcABC* which are flanked upstream by the *arcD*, being all of them arranged in the *arcDABC* operon. The *arcD* gene encodes for an arginine-ornithine antiporter. This operon is induced by the presence of arginine. Moreover, the expression of the operon is activated in an Anr-dependent manner at low-oxygen tension. It has been reported that no anaerobic growth in the presence of arginine is possible in *anr* mutants. The ArgR regulatory protein mediates arginine induction by binding to a conserved sequence motif upstream of the Anr site in the *arcD* promoter (Williams *et al.*, 2007). Apart from that, another binding region

(-60 nucleotides upstream) is recognized for NarL which represses the *arcDABC* operon in the presence of nitrate (Benkert *et al.*, 2008). In Figure 5 the transcriptional regulation of the *arcDABC* operon is shown.

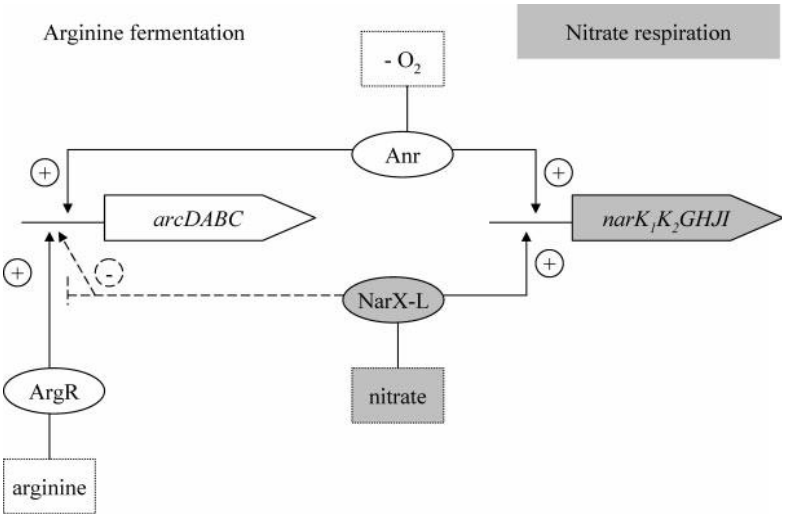

Figure 5. Schematic view of the modulation system that interlinks the Anr protein, the NarXL two-component system and the arginine fermentation operon activation (Benkert *et al.*, 2008).

1.1.2.4 Pyruvate fermentation

P. aeruginosa was originally described as a strict respiratory, not fermentative bacterium. However, the *P. aeruginosa* genome presented an *ldhA* gene which encodes for a fermentative D-lactate dehydrogenase (LDH) (Eschbach *et al.*, 2004). Regarding pyruvate fermentation, several loci have been identified to be involved in this metabolism. The *ackA-pta* loci encodes for an acetate kinase and a phosphotransacetylase, respectively. Furthermore, the *adhA* locus was found to encode for an alcohol dehydrogenase (Williams *et al.*, 2007). The pyruvate fermentation provides with low energy levels to *P. aeruginosa* and therefore it is used rather when nitrate or nitrite is available. Pyruvate fermentation has been identified to rather sustain long-term anaerobic survival than significant aerobic growth. The pyruvate fermentation pathway is shown in Figure 6.

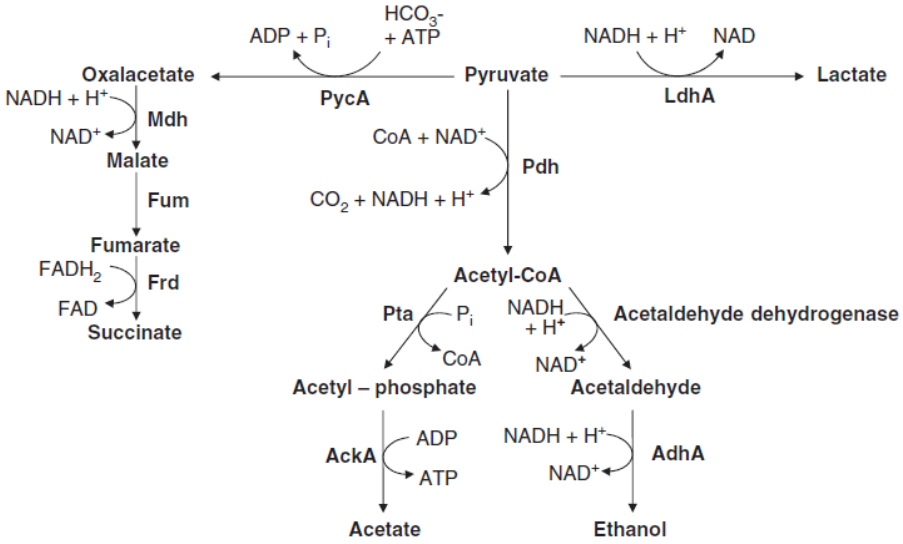

Figure 6. Overview of the pyruvate fermentation in *P. aeruginosa* (Williams *et al.*, 2007).

1.1.2.5 Regulatory network for the anaerobic energy metabolism of *P. aeruginosa*

In Figure 7 the transcriptional modulation of denitrification and fermentations pathways is displayed. As observed in the figure, the arginine and pyruvate fermentations seem to be interlinked with anaerobic stress and denitrification. Fermentation and denitrification are thereby tightly regulated and switched on and off in agreement one with another.

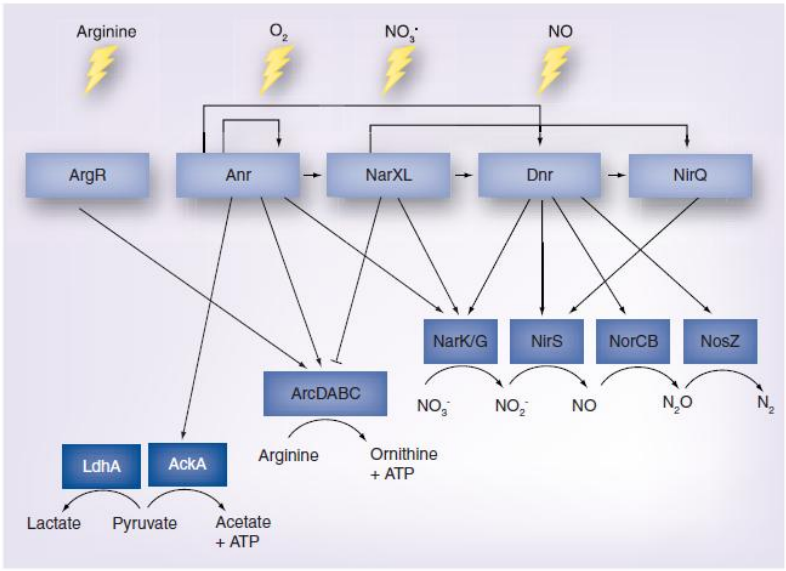

Figure 7. Transcriptional regulation of the denitrification and fermentation pathways of *P. aeruginosa* (Schobert & Tielen, 2010).

In contrast to the in depth understanding of the gene regulatory circuits, the assembly of the denitrification machinery at the protein level is only poorly investigated.

1.2 Interactomic studies

Most proteins function within intricate cellular pathways interacting with other proteins either in pairs or as components of larger complexes. Therefore, a proper understanding of these protein interactions could bring insights into the mechanisms by which cellular pathways operate and interlink (Kumar & Snyder, 2002). Elucidating protein-protein interactions sheds light on how human diseases can be treated (Sutherland *et al.*, 2008). Furthermore, the identification of protein networks is a requisite to better understand cellular processes since proteins interactions give insights into protein functions (Stelzl & Wanker, 2006). The underlying concept is termed guilt-by-association, what means that if two proteins interact they usually participate in the same, or related, cellular functions (Oliver, 2000). A known function for the bait (protein of interest under study) can be attributed to the resulting preys (potential interaction partner) which function was beforehand unclear. Over the last decades, several approaches have been used to identify protein complexes: yeast-two hybrid system (Figure 8), double immunogold labeling (see Results section), immunoprecipitation, phage display (Figure 9), affinity purification (AP) coupled with mass spectrometry (MS), shortened as AP-MS (Figure 10), etc (Gingras *et al.*, 2007).

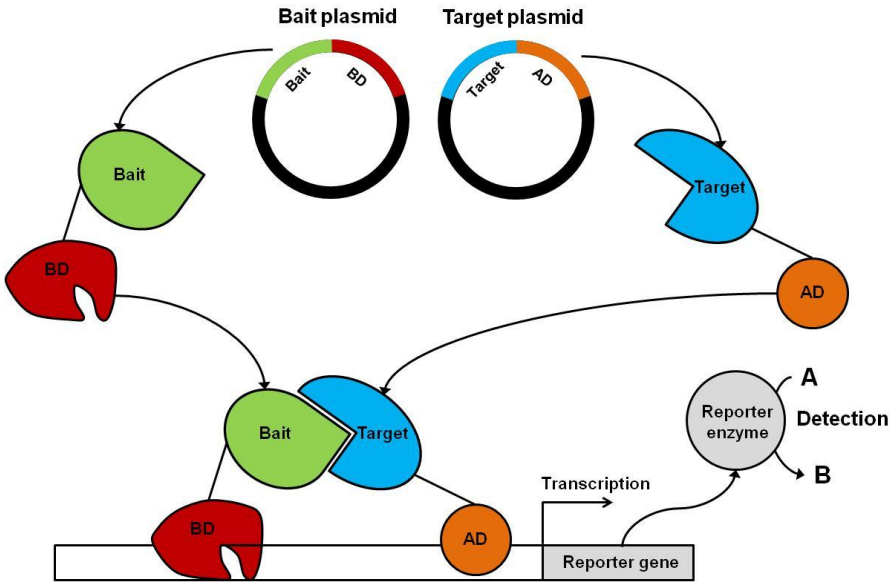

Figure 8. Two-hybrid system for detection of interaction partners. The bait is fused to a binding domain (BD) which recognizes a specific region of a reporter gene promoter region and the prey (target) is fused to an activation domain (AD) which coordinates the assembly

of the elements required for transcription. Only if both proteins (bait-prey) interact, the expression of the reporter gene is feasible. The gene product is used for detection, after coupled to color or fluorescent generator. A = substrate; B = fluorophore.

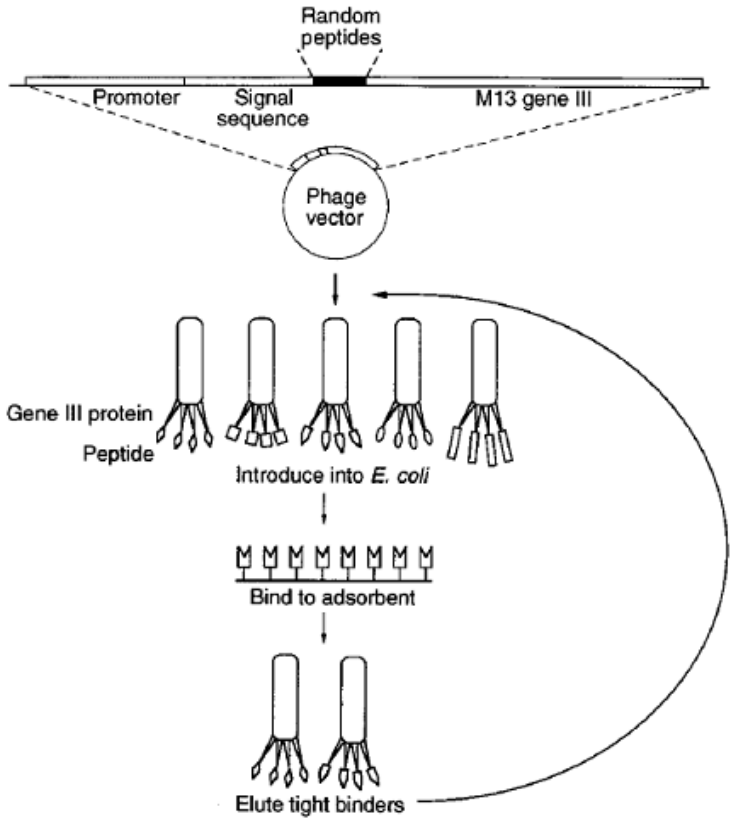

Figure 9. Schema of the Phage Display system for identification of protein-protein interactions (Berggard *et al.*, 2007). Random sequences along the whole genome of *E. coli* encoding for peptides (possible preys regions) are cloned into a phage plasmid and subsequently expressed. These peptides encoding sequences are recombinantly fused to a signal sequence that determines their export to the outside of the phage and being exposed as epitopes attached to the phage surface. Afterwards, the phages are introduced into *E. coli*. Once the phages are released they are incubated along with the immobilized bait (in a matrix for instance) or undergo affinity purification and only phages exposing specific peptides will bind to it and subsequently elute.

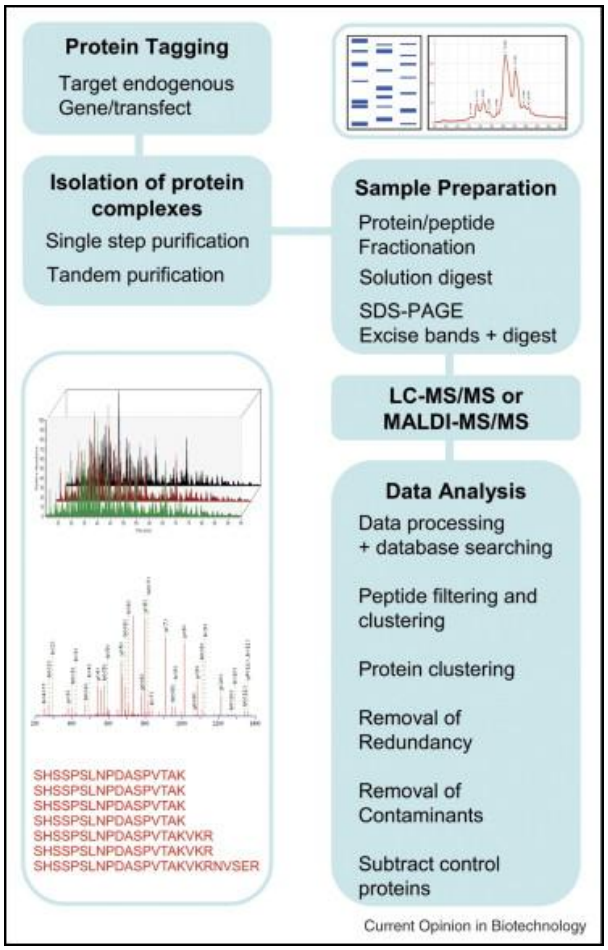

Figure 10. Generic workflow by which AP of tagged proteins coupled MS is performed. Eluted protein complexes can be resolved by SDS-PAGE or protein chromatography. Alternatively, a solution digest of the eluted complexes can be carried out and peptides can be straightforward analysed by MS methods. The most common MS are liquid chromatography coupled with tandem MS (LC-MS/MS) or by two-dimension LC-MS/MS (2D-LC-MS/MS). The election of one technique or another depends on the sample complexity (Collins & Choudhary, 2008).

The choice of a certain technique depends on factors, such as number of preys, *in vivo* or *in vitro* conditions or if the experiment carried out is confirmatory. We chose an AP-MS approach for this study.

1.2.1 Affinity purification coupled with mass spectrometry methods

A widely used technique for scrutiny of protein complexes implicates AP for bait-preys isolation, followed by MS identification of the constituent proteins (Ranish *et al.*, 2003). AP-MS methods can rely on SDS-PAGE i.e. gel-mediated or on gel-free approaches. 1D- or 2D-dimension SDS-PAGE gel can be employed depending on the

complexity of the sample in the case of the gel-mediated approach. Moreover, MS or tandem MS (MS/MS) can be used depending on the accuracy needed. MS/MS is recommended for complex samples and quantitative methods, whereas MS can be used for lower complex samples and qualitative methods (simple determination of the protein). Nevertheless, in this work AP-MS/MS is employed for identification of interaction partners in both, the gel-mediated and gel-free approaches. In particular we used LC-MS/MS to identify interaction partners after AP. In the recent years AP coupled with MS/MS (AP-MS/MS) has become a technique of high relevance for detection of protein complexes. As intuited in the previous paragraph, AP-MS/MS is a variety within the AP/MS methododology. In this approach, target proteins (baits) are purified along with their preys (potential interaction partners) by means of an epitope tag-based affinity chromatography procedure. The protein mixture then is digested resulting in peptides that are identified using MS/MS. By performing additional AP-MS/MS experiments for interlaced baits, additional information can be gained related to the assembly of proteins into interaction networks and delineation of protein complexes involving shared components (Choi *et al.*, 2010). Over the last years, researchers have witnessed a huge development in AP-MS methods in general which relied on powerful MS (which permits identification and quantification of interaction partners) and the advance in protein purification protocols (Gingras *et al.*, 2007, Sutherland *et al.*, 2008). An overview of this method is shown in Figure 11.

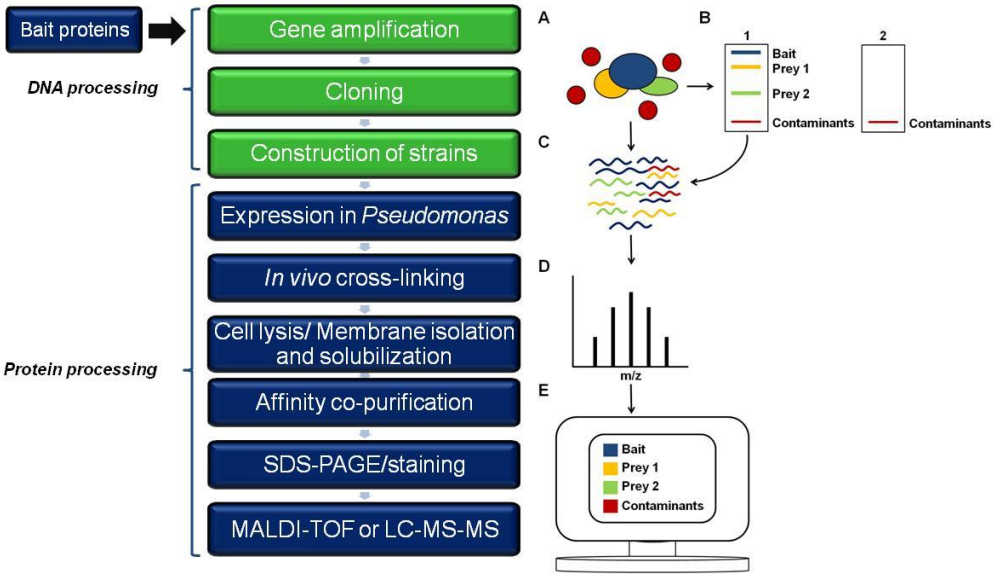

Figure 11. Overview of an AP-MS experiment. The workflow (left) step by step to elucidate protein-protein interactions is shown.

On the right, A) the tagged protein of interest (bait) is purified from the cell extract along with its potential interaction partners (preys). B) As an optional step proteins can be separated by SDS-PAGE (gel dependent approach). Contaminants are identified by contrasting the elution (1) and the control (2). C) Proteins are subjected to proteolysis. D) MS analysis of peptides. Normally, this involves peptide separation by reversed-phase liquid chromatography followed by two MS events: in the first scan, the mass/charge ratio (m/z) of the intact peptide is measured. The most abundant peptides are then specifically selected and subjected to fragmentation, yielding a MS/MS spectrum. E) Softwares are employed to identify the MS data and thereby identify the bait, potential interaction partners and contaminants. Based on the model by Gingras *et al*. (Gingras *et al*., 2007).

For detection of interaction partners of periplasmic proteins, we employed the so-called SPINE (‘‘Strep-protein interaction experiment’’) method (Muller *et al.*, 2011, Herzberg *et al.*, 2007a) which implicates a Strep-tagged bait. Generally, a C-terminal tag is used since periplasmic proteins normally harbour a N-terminal leader peptide which is cleaved off once they are exported into the periplasmic compartment (Dalbey & Kuhn, 2012). For membrane residing proteins, baits were His-tagged at the C-terminus and solubilized to elude the problems derived from their hydrophobic and amphiphilic nature. To circumspect the drawbacks derived from protein overproduction such as generation of false positives due to protein abundance, gene expression under their natural promoters has been presented as a good alternative (Choi *et al.*, 2010). Furthermore, we used the strengthening of protein-protein interactions by *in vivo* cross-linking (CL), what assures to hook transient interaction partners (Ogierman & Braun, 2003, Manting *et al.*, 1999).

1.2.1.2 Affinity purification coupled with mass mass spectrometry methods employed in the current work

Two different AP-MS/MS methods were used to identify protein-protein interactions in this work, gel-mediated and gel-free quantitative. The selection of one or another depended on the complexity of the eluates being the first one employed when a lower number of proteins were spotted on previous control gel and the second one when samples seemed to be more complex.

SDS-PAGE gel-mediated method

A widely used AP-MS/MS relies on SDS-PAGE gel proteins visualization. After protein complexes affinity tag purification, eluted proteins are resolved by a SDS-

PAGE and protuberant bands are excised for further protein identification by LC-MS/MS. This approach was used in lower complex samples and it has been proven to be successful for the elucidation of protein-protein interactions in yeast, prokaryotes and human cells (Rigaut *et al.*, 1999, Butland *et al.*, 2005). An overview of this method is shown in Figure 12.

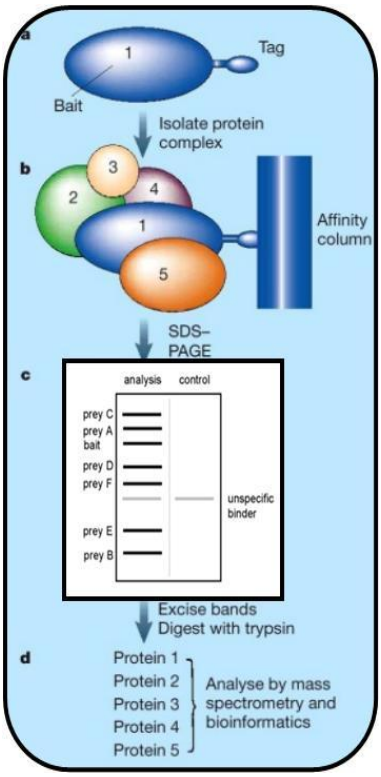

Figure 12. SDS-PAGE gel-mediated method for protein-protein interactions identification. Slightly modified illustration (Kumar & Snyder, 2002). Method based on gel electrophoresis and subsequent band excision.

In this technique most prominent bands correspond to the most abundant proteins in the protein-complex and therefore they are considered to be binding more specifically to the bait.

SDS-PAGE gel-free method

This approach relies on AP skipping the gel step and quantitative proteomics. There are two categories of quantitative proteomic methods: labeled-based and label-free. The first one is accurate when determining the protein relative or absolute amount in very complex proteomics samples (Trinkle-Mulcahy, 2012) and includes, among others, the stable isotope labeling with amino acids in cell culture (SILAC), isotope-

coded affinity tag (ICAT) and the isobaric tags for relative and absolute quantification (iTRAQ) (Liang *et al.*, 2012). Label-free (semi)-quantification has been extensively reported as highly reliable to establish the interactions specificity (Tate *et al.*, 2013) by determining the relative protein amount determination (Armean *et al.*, 2013, Bildl *et al.*, 2012). A concept termed "Protein Abundance Index" (PAI) is used to quantify protein abundance (Ong & Mann, 2005, Bachi & Bonaldi, 2008). The intensity of the signal while the peptide elutes is extracted over time and the area beneath this curve corresponds to the ion current (XIC). The average of the three peptides with the largest peak area, related to a certain protein defines the so-called "xPAI" of the protein (Ong & Mann, 2005, Lambert *et al.*, 2013). The larger this value confined to a protein is, the more concentrated it is in the eluate and therefore considered to be binding more specifically to the protein complex. An overview of this technique is shown in Figure 13.

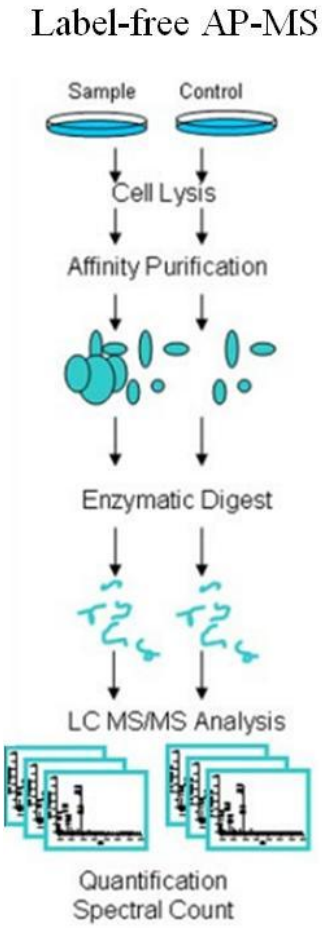

Figure 13. Overview of the unlabelled AP-MS approach designed to elucidate protein-protein interactions, omitting gel step (Kaake *et al.*, 2010).

In vivo cross-linking

Loss of specific components of a protein complex during the purification process can be prevented by *in vivo* cross-linking (Sutherland *et al.*, 2008) which stabilizes transient interactions and thereby complexes maintain structural integrity (Vasilescu *et al.*, 2004). Cell lysis converts the highly ordered protein assemblies inside a cell into disordered protein solutions, disturbing the spatial and temporal constraints that govern protein interactions in cells. Hence, the importance of performing *in vivo* cross-linking (Toews *et al.*, 2008). There are infinite cross-linkers such as glutaraldehyde or osmonium tetroxide. Nevertheless, one of the most commonly used is the formaldehyde which holds several profitable features such as being compatible with AP-MS/MS; rapid penetration through membranes is guaranteed due to its molecule size (2.3-2.7 A°) what entails as well that only proteins in close proximity are cross-linked (Klockenbusch & Kast, 2010). Moreover, formaldehyde cross-links are reversible by prolonged heating times (Orlando *et al.*, 1997). The course of action of this cross-linking agent is shown in Figure 14.

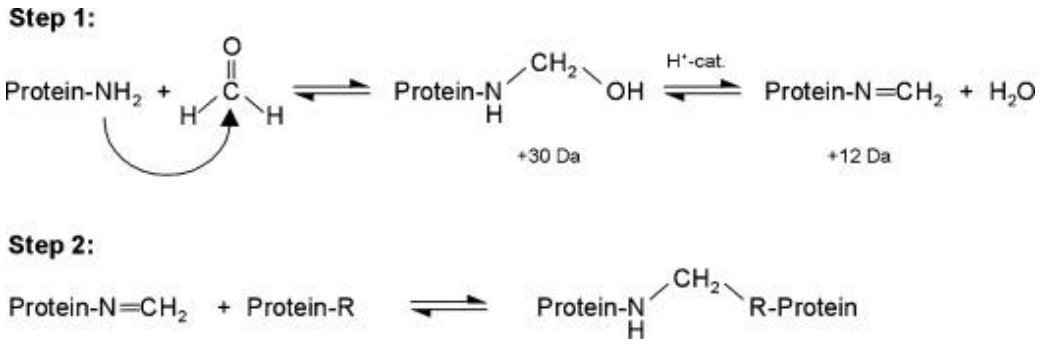

Figure 14. Mechanism by which the formaldehyde cross-linker reaction is driven. The aldehyde group can react with nitrogen and some other atoms of proteins. First, the functional groups of the cross-linker react with an amino acid residue, thereby attaching the cross-linker to the protein by covalent bond. In the second step, the remaining functional group on the cross-linker then generates a second covalent bond with another amino acid residue, effectively bridging two amino acid residues.

A cross-linking treatment was effectuated in this study intended to strengthen protein interactions within complexes (Sutherland *et al.*, 2008).

1.3 Aim of this work

In this thesis two pronounced *Pseudomonas* species, *P. aeruginosa* and *P. putida*, should be used as model systems to investigate general and biotechnologically applicable principles of bacterial physiology. *P. aeruginosa* was employed to answer the question for the constitution and assembly of the denitrification respiratory supra-complex. Using for this purpose a previously established interactomics method based on various bait proteins for the assumed complex, interaction partners should be cross-linked *in vivo*, isolated and identified by proteomics. Obtained results should serve for a first model for the overall structure of the respirasome in the periplasm of this bacterium. *P. putida* should be used as target for the directed optimization of a biotechnological process, in this case the production of the biopolymer PHA. Based on a previous bioinformatic prediction of the corresponding metabolism, genetic engineering approach should be performed. Overall, general conclusions from the results of both approaches should be drawn.

2 Materials and Methods

2.1 Instruments and software

Table 1. List of devices used in this work.

Application	Device model	Company
Agarose gel electrophoresis	Agagel	Biometra, Göttingen, Germany
Agarose gel visualization	UV transilluminator	Wealtec, Sparks, USA
	DeVision DBox	DCscienceTec, Ontario. Canada
Anaerobic incubation of Petri dishes	BBL GasPak GasPack Jars	Difco, VGD, Lawrence, USA
Bioreactor fermentation	Top-bench	Sartorius BP Systems GmbH,
	BIOSTAT B1 bioreactor	Göttingen, Germany
	Flow controller PR4000	MKS Instruments, Waltham, USA
Camera	Optio E20	Pentax, Denver , USA
Cell lysis	French Pressure Cell Press	Thermo Scientific, Waltham, USA
Centrifugation	Avanti J-26 XP centrifuge	Beckman Coulter, Krefeld, Germany
	Centrifuge 5424	Eppendorf, Hamburg, Germany
	Eppendorf 5810 R	Eppendorf, Hamburg, Germany
	Megafuge 1.0 R Heraus	Thermo Scientific, Waltham, USA
Clean bench work	HeraSafe	Thermo Scientific, Waltham, USA
DNA concentration determination	Nanodrop ND-1000-UV/VIS	Peqlab, Erlangen, Germany
Fluorescence microscopy	Axio Imager A1, AxioCam MRm cámara	Carl Zeiss, Oberkochen, Germany
Gel electrophoresis power supply (agarose, PAGE)	Power Basic gel electrophoresis	BioRad, Munich, Germany
Incubation of cell cultures	Water bath incubator Aquatron	Infors-HT, Bottmingen, Switzerland

Application	Device model	Company
Incubation of Petri dishes	Incubator Fine Line Heraeus	Thermo Scientific, Waltham, USA
MS analysis	Dionex Ultimate 3000 n-RSLC connected to Orbitrap Velos	Thermo Scientific, Waltham, USA
Optical density determination of cells	Spectrophotometer Biomate3	Thermo Scientific, Waltham, USA
Polymerase chain reaction (PCR)	CFX96 Real Time System Thermocycler	BioRad, Munich, Germany
pH measurement	Microprocessor pH Meter 211	Hanna Instruments, Kehl am Rhein, Germany
Pipetting	Eppendorf Research	Eppendorf, Hamburg, Germany
Protein visualization (SDS-PAGE)	GS-800 calibrated densitometer	BioRad, Munich, Germany
Protein transference	Trans-Blot Turbo transfer system	BioRad, Munich, Germany
RNA fragmentation	Covaris Adaptive Focused Acoustics device	Covaris, LGC Genomics, Ausburg, Germany
SDS-PAGE electrophoresis	Mini Protean II	BioRad, Munich, Germany
Sequencing	Genetic Analyzer ABI Prism	GATC, Constance, Germany
	Illumina HiSeq 2500	Illumina, San Diego, USA
Sterilization	Autoclaves EL3850	Systec, Wettenberg, Germany
Thermomixer	Thermomixer comfort	Eppendorf, Hamburg, Germany
Transmission electron microscopy (TEM)	TEM910 transmission electron microscope	Carl Zeiss, Oberkochen, Germany
	Slow-Scan CCD-Camera	ProScan, Lagerlechfeld, Germany
Ultracentrifugation	Ultracentrifuge Optima L-90K	Beckman Coulter, Krefeld, Germany
Vortex	Vortex Genie 2	Scientific Industries, New York, USA
Water purification	MilliQ Synthesis	Millipore, Billerica, USA

Table 2. List of softwares and databases employed in this work.

Application	Software/Database
DNA sequence alignment	BioEdit
Immunofluorescence imaging	AxioVision Rel. 4.6 Software using AxioVision 4 Module Multichannel Fluorescence and Filters 49, 44 and 50
Genome comparison	www.pseudomonas.com
MS data analysis (LC-MS/MS)	Proteome Discoverer
MS data analysis	Mascot
RNA raw data analysis	Stampy/DESeq (R software)
Transmission microscopy imaging	ITEM-Software, Olympus Soft Imaging Solutions

2.2 Kits and special materials

Table 3. Kits employed throughout this study.

Application	Kit	Company
DNA extraction (Gel), purification (PCR) and plasmid isolation	QIAquick Gel extraction kit, QIAquick PCR purification kit and QIAquick Spin Miniprep kit	Qiagen, Hilden, Germany
NADP/NADPH quantification	NADP/NADPH Colorimetric Quantitation Kit	Biovision, Milpitas, USA
Ribosomal RNA removal	MICROExpress Bacterial RNA enrichment kit	Ambion, Life Technologies, Darmstadt, Germany
RNA extraction	RNeasy kit	Qiagen, Hilden, Germany

2.3 Media and additives

Standard complex medium for *P. aeruginosa*, *P. putida* and *E. coli* was LB medium (Sambrook & Russell, 2001).

Table 4. Luria-Bertani medium (LB).

Component	g/L
NaCl	5
Tryptone	10
Yeast extract	5

When *P. aeruginosa* was required to be grown under anaerobic denitrifying conditions, the LB medium was supplemented with 50 mM KNO_3 or 10 mM $NaNO_2$ and cells were grown in rubber stoppered serum flasks. For certain immunofluorescence experiments, swimming medium supplemented with arginine was used (Table 5). Cells were grown anaerobically in rubber stoppered serum flasks for 5 days (Williams *et al.*, 2007).

Table 5. Swimming medium supplemented with 20 mM L-arginine.

Component	g/L
NaCl	5
Tryptone	10
$C_6H_{14}N_4O_2$	3.484

Swimming motility of the *P. aeruginosa* strains was analyzed on L-arginine agar (3 g/L) plates swimming medium as described before (Rashid & Kornberg, 2000). *P. putida* KT2440 was grown in M9 minimal medium for PHA production experiments as shown in Table 6 (Borrero-de Acuna *et al.*, 2014).

Table 6. M9 Mineral medium.

Component	g/L
$Na_2HPO_4{\cdot}7H_2O$	12.8
KH_2O_4	3
NH_4Cl	1
NaCl	0.5

Basic solution.

Afterwards, 0.12 g of $MgSO_4{\cdot}H_2O$ and a trace element solution were added (Table 7).

Table 7. Trace elements solution.

Component	mg/L
$FeSO_4{\cdot}7H_2O$	6
$CaCO_3$	2.7
$ZnSO_4{\cdot}H_2O$	2
$MnSO_4{\cdot}H_2O$	1.16
$CoSO_4{\cdot}7H_2O$	0.37
$CuSO_4{\cdot}5H_2O$	0.33
H_3BO_3	0.08

Finally, 20 mg/L of glucose were added to the whole mixture. The antibiotics used in this study for the different strains are listed in Table 8.

Table 8. Antibiotics concentrations employed throughout this study.

Antibiotic	*E. coli*	*P. aeruginosa*	*P. putida*
Carbenicillin (Cb)	100	250	-
Ampicillin (Ap)	100	-	-
Streptomycin (Sm)	62.5	-	100

The antibiotics concentration is expressed in µg/mL (Sambrook & Russell, 2001).

2.4 Bacteria, plasmids and primers

The constructed plasmids, bacterial strains and primers used for the study of protein-protein interactions in *P. aeruginosa* and the enhancement of PHA production in *P. putida* are shown in sections 2.4.1 and 2.4.2, respectively.

2.4.1 Bacteria, plasmids and primers used for the construction of *P. aeruginosa* recombinant strains

All bacteria, plasmids and primers used for the construction of *P. aeruginosa* recombinant strains and their subsequent application in the investigation of protein-protein interactions are listed in Table 9.

Table 9. Bacteria, plasmids and primers used for the investigation protein-protein interactions in *P. aeruginosa*.

	Relevant characteristics	Source/ reference
Strains		
E. coli		
DH10b	F$^-$ *end*A1 *rec*A1 *gal*E15 *gal*K16 *nup*G rps*L* Δ*lac*X74 Φ80*lacZ*Δ M15 *ara*D139 Δ(*ara*,*leu*)7697 *mcrA* Δ(*mrr-hsd*RMS-*mcr*BC) λ$^-$	Invitrogen, Darmstadt, Germany
BL21	B F- *dcm omp*T *hsd*S(r_B- m_B-) *gal* [*malB*$^+$]$_{K-12}$(λ^S)	Stratagene, Santa Clara, USA
DH10b pJET 1.2-*nirS*	DH10b carrying intermediate promoter-*nirS* untagged plasmid	This study
DH10b pJET 1.2-*fliC*	DH10b carrying intermediate promoter-*fliC* untagged plasmid	This study

	Relevant characteristics	Source/ reference
DH10b pJET 1.2-*nosZ*	DH10b carrying intermediate *nosZ* untagged plasmid	This study
DH10b pJET 1.2-*nosPR*	DH10b carrying intermediate *nos*-promoter plasmid	This study
DH10b pJET 1.2-*nosR*	DH10b carrying intermediate promoter-*nosR* untagged plasmid	This study
DH10b pJET 1.2-*norC*	DH10b carrying intermediate promoter-*norC* untagged plasmid	This study
DH10b pJET 1.2-*norCB*	DH10b carrying intermediate promoter-*norCB* untagged plasmid	This study
DH10b pAS40-*nirS*	DH10b harboring the expression vector pAS40-promoter-*nirS* Strep-tag II fusion gene	This study
DH10b pAS40-*fliC*	DH10b harboring the expression vector pAS40-promoter-*fliC* Strep-tag II fusion gene	This study
DH10b pAS40-*nosZ*	DH10b harboring the expression vector pAS40-promoter-*nosZ* Strep-tag II fusion gene	This study
DH10b pAS40-*nosR*	DH10b harboring the expression vector pAS40-promoter-*nosR* His_{6x} fusion gene	This study
DH10b pAS40-*norC*	DH10b harboring the expression vector pAS40-promoter-*norC* His_{6x} fusion gene	This study
DH10b pAS40-*norCB*	DH10b harboring the expression vector pAS40-promoter-*norCB* (*norB* His_{6x} fusion gene)	This study
BL21-pET14b-*dnaK*	BL21 harboring the overexpression vector pET14b-*dnaK* His_{6x} fusion gene	This study
P. aeruginosa		
PA14 wild-type	Parental strain	(Rahme *et al.*, 1995)
PAO1 wild-type	Parental strain	DSMZ, Braunschweig, Germany
PA14 *nirS*	PA14*MAR2xT7 nirS* Tn mutant	(Liberati *et al.*, 2006)
PA14 *fliC*	PA14*MAR2xT7 fliC* Tn mutant	(Liberati *et al.*, 2006)
PA14 *nosZ*	PA14*MAR2xT7 nosZ* Tn mutant	(Liberati *et al.*, 2006)
PA14 *norB*	PA14*MAR2xT7 norB* Tn mutant	(Liberati *et al.*, 2006)
PA14 *narH*	PA14*MAR2xT7 narH* Tn mutant	(Liberati *et al.*, 2006)
PA14 pAS40	PA14 wild-type harboring empty plasmid	This study
PAO1 pAS40	PAO1 wild-type harboring empty plasmid	This study
PA14 $nirS^{-}/nirS^{+}$	PA14 *nirS* Tn mutant complemented with *nirS*-	This study

	Relevant characteristics	Source/ reference
	pAS40 expression plasmid	
PA14 *nirS*$^{-}$/*fliC*$^{+}$	PA14 *nirS* Tn mutant carrying the *fliC*-pAS40 expression plasmid	This study
PA14 *fliC*$^{-}$/*fliC*$^{+}$	PA14 *fliC* Tn mutant complemented with *fliC*-pAS40 expression plasmid	This study
PA14 *fliC*$^{-}$/*nirS*$^{+}$	PA14 *fliC* Tn mutant carrying *nirS*-pAS40 expression plasmid	This study
PA14 *nosZ*$^{-}$/*nosZ*$^{+}$	PA14 *nosZ* Tn mutant complemented with *nosZ*-pAS40 expression plasmid	This study
PAO1 *nosR*	PAO1mini-Tn*5 lux nosR* mutant	(Lewenza *et al.*, 2005)
PAO1 *norC*	PAO1mini-Tn*5 lux norC* mutant	(Lewenza *et al.*, 2005)
PAO1 *norB*	PAO1mini-Tn*5 lux norB* mutant	(Lewenza *et al.*, 2005)
PAO1 *nosR*$^{-}$/*nosR*$^{+}$	PAO1 *nosR* Tn mutant complemented with *nosR*-pAS40 expression plasmid	This study
PAO1 *norC*$^{-}$/*norC*$^{+}$	PAO1 *norC* Tn mutant complemented with *norC*-pAS40 expression plasmid	This study
PAO1 *norB*$^{-}$/*norB*$^{+}$	PAO1 *norB* Tn mutant complemented with *norCB*-pAS40 expression plasmid	This study
Plasmids		
pJET 1.2	Ap^{r}, carrier vector, toxin expressed upon self-ligation	Fermentas, Darmstadt, Germany
pAS40	Cb^{r}, expression vector in *P. aeruginosa* derived from the pUCPT20t lacking the *Bsa*I restriction site (mutation: GGTCTC → GCTCTC). Blue/white colonies selection possible	TU Braunschweig, Germany (Annika Steen)
pET14b	Ap^{r}, T7 promoter, IPTG inducible plasmid	Novagen, Darmstadt, Germany
pJET 1.2-*nirS*	Ap^{r}, pJET 1.2, carrying promoter-*nirS* untagged gene	This study
pJET 1.2-*fliC*	Ap^{r}, pJET 1.2, carrying promoter-*fliC* untagged gene	This study
pJET 1.2-*nosPR*	Ap^{r}, pJET 1.2, carrying *nos* operon promoter	This study
pJET 1.2-*nosZ*	Ap^{r}, pJET 1.2, carrying *nosZ* gene untagged gene	This study
pJET 1.2-*nosR*	Ap^{r}, pJET 1.2, carrying promoter-*nosR* untagged gene	This study
pJET 1.2-*norC*	Ap^{r}, pJET 1.2, carrying promoter-*norC* untagged gene	This study

	Relevant characteristics	Source/ reference
pJET 1.2-*norCB*	Ap^r, pJET 1.2, carrying promoter-*norCB* untagged genes	This study
pJET 1.2-*nosPR*	Ap^r, pJET 1.2, carrying *nos*-promoter (≈500 bp)	This study
pJET 1.2-*nosZ*	Ap^r, pJET 1.2, carrying *nosZ* untagged gene	This study
pAS40-Strep-tag II (S)	Cb^r, pAS40 carrying the Strep-tag II module with *Bsa*I restriction sites designed for promoter-*nirS* cloning	This study
pAS40-Strep-tag II (F)	Cb^r, pAS40 carrying the Strep-tag II module with *Bsa*I restriction sites designed for promoter-*fliC* cloning	This study
pAS40-Strep-tag II (Z)	Cb^r, pAS40 carrying the Strep-tag II module with *Bsa*I restriction sites designed for promoter-*nosZ* cloning	This study
pAS40-His_{6x} (R)	Cb^r, pAS40 carrying the His_{6x} tag module with *Bsa*I restriction sites designed for promoter-*nosR* cloning	This study
pAS40-His_{6x} (C)	Cb^r, pAS40 carrying the His_{6x} tag module with *Bsa*I restriction sites designed for promoter-*norC* cloning	This study
pAS40-His_{6x} (CB)	Cb^r, pAS40 carrying the His_{6x} tag module with *Bsa*I restriction sites designed for promoter-*norCB* cloning	This study
pAS40-*nirS*	Cb^r, pAS40 carrying promoter-*nirS* Strep-tag II tagged	This study
pAS40-*fliC*	Cb^r, pAS40 carrying promoter-*fliC* Strep-tag II tagged	This study
pAS40-*nosZ*	Cb^r, pAS40 carrying promoter-*nosZ* Strep-tag II tagged	This study
pAS40-*nosR*	Cb^r, pAS40 carrying promoter-*nosR* His_{6x} tagged	This study
pAS40-*norC*	Cb^r, pAS40 carrying promoter-*norC* His_{6x} tagged	This study
pAS40-*norCB*	Cb^r, pAS40 carrying promoter-*norCB* with *norB* His_{6x} tagged	This study
pET14b-*dnaK*	Ap^r, Overexpressing plasmid for *dnaK* His_{6x} fusion gene	This study
Primers (5´-3´)		
nirSFw	TGCTGGTCTCCAGCAGATACCGCCTTC GCGCA	Invitrogen, Darmstadt, Germany

	Relevant characteristics	Source/ reference
nirSRv	GTACGGTCTCCGTACACGTCGTGCTGG GTGTT	Invitrogen, Darmstadt, Germany
*nirS*StreptagIIFw	AATTAGCACGAGACCAGATCTGATATCGG TCTCCGTACTGGAGCCACCCGCAGTTCGA AAAATGA	Invitrogen, Darmstadt, Germany
*nirS*StreptagIIRv	AGCTTCATTTTTCGAACTGCGGGTGGCTCC AGTACGGAGACCGATATCAGATCTGGTCT CGTGCT	Invitrogen, Darmstadt, Germany
*fliC*Fw	GGTCTCGCGACTGGATGCTCGAAGGCGC	Invitrogen, Darmstadt, Germany
*fliC*Rv	GGTCTCTGCGCAGCAGGCTCAGGACCGC	Invitrogen, Darmstadt, Germany
*fliC*StreptagIIFw	AATTCGACTGAGACCAGATCTGATATCGG TCTCAGCGCTGGAGCCACCCGCAGTTCGA AAAATGA	Invitrogen, Darmstadt, Germany
*fliC*StreptagIIRv	AGCTTCATTTTTCGAACTGCGGGTGGCTCC AGCGCTGAGACCGATATCAGATCTGGTCT CAGTCG	Invitrogen, Darmstadt, Germany
*nosZ*Fw	TACCGGTCTCTGGTAACCTCTGACCTGGCT CC	Invitrogen, Darmstadt, Germany
*nosZ*Rv	GGCTGGTCTCTAGCCTTTTCCACCAGCATC CG	This study
*nosPR*Fw	GATAGGTCTCGTATCTCACCTGCGGCAAC GAC	Invitrogen, Darmstadt, Germany
*nosPR*Rv	GGTAGGTCTCGTACCGGCGAAAAAAGGG ACGC	Invitrogen, Darmstadt, Germany
*nosZ*StreptagIIFw	AATTTATCCGAGACCAGATCTGATATCGG TCTCCGGCTTGGAGCCACCCGCAGTTCGA AAAATGA	Invitrogen, Darmstadt, Germany
*nosZ*StreptagIIRv	AGCTTCATTTTTCGAACTGCGGGTGGCTCC AAGCCGGAGACCGATATCAGATCTGGTCT CGGATA	Invitrogen, Darmstadt, Germany
*nosR*Fw	CACCGGTCTCGGGTGTATCTCACCTGCGG CAA	Invitrogen, Darmstadt, Germany
*nosR*Rv	CCTCGGTCTCTGAGGTTCTCCGCGGGTATC CG	Invitrogen, Darmstadt, Germany

	Relevant characteristics	Source/ reference
*nosR*His6xFw	AATTGGTGTGAGACCAGATCTGATATCGG TCTCACCTCCATCATCATCATCATCATTGA	Invitrogen, Darmstadt, Germany
*nosR*His6xRv	AGCTTCAATGATGATGATGATGATGGAGG TGAGACCGATATCAGATCTGGTCTCACAC C	Invitrogen, Darmstadt, Germany
*norC*Fw	GCCAGGTCTCGCTGATGCTCTACTGGCAC ATGGTC	Invitrogen, Darmstadt, Germany
*norC*Rv	CAAGGGTCTCTACCCTCCTTGTTCGGCGGC CA	Invitrogen, Darmstadt, Germany
*norC*His6xFw	AATTCTGATGAGACCAGATCTGATATCGG TCTCAGGGTCATCATCATCATCATCATTGA	Invitrogen, Darmstadt, Germany
*norC*His6xRv	AGCTTCAATGATGATGATGATGATGACCC TGAGACCGATATCAGATCTGGTCTCATCA G	Invitrogen, Darmstadt, Germany
*norCB*Fw	GCCAGGTCTCGCTGATGCTCTACTGGCAC ATGGTC	Invitrogen, Darmstadt, Germany
*norCB*Rv	CAAGGGTCTCTGGCGGCCGCCTTGCCGCG CCG	Invitrogen, Darmstadt, Germany
*norCB*His6xFw	AATTCTGATGAGACCAGATCTGATATCGG TCTCACGCCCATCATCATCATCATCATTGA	Invitrogen, Darmstadt, Germany
*norCB*His6xRv	AGCTTCAATGATGATGATGATGATGGGCG TGAGACCGATATCAGATCTGGTCTCATCA G	Invitrogen, Darmstadt, Germany
*dnaK*Fw	CAGCCATATGGGCAAAATCATTGGCATCG	Invitrogen, Darmstadt, Germany
*dnaK*Rv	CATGGATCCTTACTTGTTGTCCTTGACC	Invitrogen, Darmstadt, Germany

Antibiotic resistance: Ap^r = Ampicillin resistance; Cb^r = Carbenicillin resistance. *Bsa*I, *Nde*I and *BamH*I restriction sites are underlined, the 4 first nucleotides of the gene amplicon sequence and the 4 last are colored in red. The *Bgl*II-*Eco*RV restriction sites are colored in green. (R), (C) and (CB) refer to the distinct pAS40-His_{6x} plasmids with *Bsa*I restriction sites designed for promoter and each gene *nosR*, *norC* and *norCB* cloning, respectively. (S) refers to the pAS40-Strep-tag II plasmid with *Bsa*I restriction sites designed for *nirS* gene and promoter cloning. (F) refers to the pAS40-Strep-tag II plasmid with *Bsa*I restriction sites designed for *fliC* gene and promoter cloning. (Z) refers to the pAS40-Strep-tag II plasmid with *Bsa*I restriction sites designed for *nosZ* gene and promoter cloning.

2.4.2 Bacteria, plasmids and primers used for the construction of *P. putida* recombinant strains

All bacteria, plasmids and primers used for the study of PHA production improvement in *P. putida* are listed in Table 10.

Table 10. Bacteria, plasmids and primers used for improvement of PHA production in *P. putida*.

	Relevant features/genotype	**Source/reference**
Strains		
E. coli		
DH10b	F⁻ *end*A1 *rec*A1 *gal*E15 *gal*K16 *nup*G rps*L* Δ*lac*X74 Φ80*lac*Z*Δ*M15 *ara*D139 Δ(*ara,leu*)7697 *mcrA* Δ(*mrr-hsd*RMS-*mcr*BC) λ⁻	Invitrogen, Darmstadt, Germany
XL10-Gold	*end*A1 *gln*V44 *rec*A1 *thi*-1 *gyr*A96 *rel*A1 *lac* Hte Δ(*mcr*A)183 Δ(*mcr*CB-*hsd*SMR-*mrr*)173 *tet*^{R} F'[*pro*AB *lac*I^{q}ZΔM15 Tn10(Tet^R Amy Cm^R)]	Stratagene, Santa Clara, USA
DH10b-*acoA*	DH10b carrying the *P. putida acoA* gene cloned in pJET 1.2	This study
DH10b-*pgl*	DH10b carrying *P. putida pgl* gene cloned in pJET 1.2	This study
XL10-Gold-*acoA*	XL10-Gold harboring *acoA* overexpression vector pSEVA-*acoA*	This study
XL10-Gold-*pgl*	XL10-Gold harboring *pgl* overexpression vector pSEVA-*pgl*	This study
P. putida		
KT2440	Parental strain	DSMZ
KT2440-*acoA*	KT2440 harboring *acoA* expression vector pSEVA424	This study
KT2440-*pgl*	KT2440 harboring *pgl* expression vector pSEVA424	This study
KT2440Δ*gcd*	KT2440 carrying *gcd* mutation	(Poblete-Castro *et al.*, 2013)
KT2440Δ*gcd-acoA*	KT2440 carrying the *gcd* knockout mutation harboring *acoA* overexpression vector pSEVA-*acoA*	This study

	Relevant features/genotype	Source/reference
KT2440Δ*gcd-pgl*	KT2440 carrying the *gcd* knockout mutation harboring *pgl* overexpression vector pSEVA-*pgl*	This study
Plasmids		
pJET 1.2	Carrier vector, toxin expressed upon self-ligation, Ap^r	Fermentas
pSEVA424	Sm^r, expression vector for *P. putida*, IPTG-inducible *tac* promoter	De Lorenzo´s lab
pJET 1.2-*acoA*	Ap^r, plasmid pJET 1.2 carrying *acoA* gene for propagation	This study
pJET 1.2-*pgl*	Ap^r, plasmid pJET 1.2 carrying *pgl* gene for propagation	This study
pSEVA-*acoA*	Sm^r, *acoA* overexpression vector, based on pSEVA424	This study
pSEVA-*pgl*	Sm^r, *pgl* overexpression vector, based on pSEVA424	This study
Primers (5´-3´)		
*acoA*Fw	CCG*GAATTC*AGGAGGAAAAACATATGTC CAATCAACTCAGT	Invitrogen, Darmstadt, Germany
*acoA*Rv	TGC*TCTAGA*GCATCAGGGGTAGGCGACG TA	Invitrogen, Darmstadt, Germany
*pgl*Fw	CCG*GAATTC*AGGAGGAAAAACATATGGG AGGGCGTGGTATG	Invitrogen, Darmstadt, Germany
*pgl*Rv	TGC*TCTAGA*GCATCATGGGCACCAGTAG AT	Invitrogen, Darmstadt, Germany

Antibiotic resistance: Ap^r = ampicillin resistance; Sm^r = streptomycin resistance. *Eco*RI and *Xba*I restriction sites are shown in italics. Shine Dalgarno or ribosomal binding site (RBS) sequences are displayed in bold whereas the eight conserved nucleotides upstream the RBS are depicted in bold and italics.

2.5 Microbiological techniques

Bacterial growth conditions, determination of cell density and storage of the strains are explained in detail in the following sections.

2.5.1 General growth conditions for *E. coli* and *P. aeruginosa*

For aerobic growth, all strains were incubated in LB medium as described previously (Schreiber *et al.*, 2006). For anaerobic growth, except for

immunofluorescence experiments, *P. aeruginosa* bacterial strains were grown in LB supplemented with 50 mM nitrate in rubber stoppered serum flasks until late exponential phase. For the immunofluorescence assays, *P. aeruginosa* strains were mainly cultivated in swimming medium (Rashid & Kornberg, 2000) supplemented with 20 mM L-arginine aerobically until they reached an optical density (OD) at 578 of 1.0 and immediately shifted into anaerobic flasks and further grown for 5 days. All strains described above were grown at 37°C. Immunofluorescence was also tested aerobically in LB medium.

2.5.2 General growth conditions for *P. putida*

P. putida was grown in M9 minimal medium (Borrero-de Acuna *et al.*, 2014). Single colonies were then picked from the plate and inoculated in 50 mL shake flasks containing 10 mL LB and incubated overnight under aerobic conditions at 30°C and shaking at 180 rpm. To start the PHA-producing process 1 L baffled shake flasks containing 200 mL of defined culture medium were inoculated to an initial OD_{595} of 0.05 and placed in a rotary shaker (180 rpm) under aerobic conditions at 30°C (Borrero-de Acuna *et al.*, 2014).

2.5.3 Bioreactor fermentations

P. putida strains were grown in M9 medium supplemented with 18.5 g/L glucose and antibiotic as required. Bioreactor batch fermentations were carried out in a 2 L top-bench BIOSTAT B1 bioreactor (Sartorius B Systems GmbH, Melsungen, Germany) with a working volume of 1.5 L at 30°C. The aeration rate was set to 500 mL/L*min using a mass flow controller (PR4000, MKS Instruments, Wilmington, MA, USA). The dissolved oxygen level was kept above 20% air saturation by control of the agitation speed up to a maximum of 900 rpm. The pH was maintained at 7.0 by automatic pH controlled addition of 500 mM H_2SO_4 or 1 M of KOH. Cell growth was monitored via OD measurements at 600 nm (Ultraspec 2000, Hitachi, Japan). The cell dry weight (CDW) was determined gravimetrically after harvesting bacteria from 10 mL culture broth for 10 min at 4°C and 10,000 rpm (Eppendorf 5810 R, Hamburg, Germany), washing with distilled water (dH_2O), and drying of the obtained pellet at 100°C. The ammonium concentration in cell-free extracts was measured by a

photometric test (LCK 303 kit, Hach Lange, Danaher, USA). The glucose concentration in the cultivation supernatant was analyzed after appropriate dilution by HPLC chromatography (HPLC Agilent 1260, Agilent, Krefeld, Germany) through an 8 mm Rezex ROA-organic acid H column (Phenomenex, USA) at a flow rate of 0.5 mL/min at 65°C using 0.013 N H_2SO_4 as the mobile phase, followed by detection using a RID detector (Agilent series1260). Gluconate and 2-keto-gluconate were quantified by HPLC chromatography using an Aminex HPX 87 H column (Biorad, Hercules, CA, USA) on a Hitachi HPLC system (Hitachi Elite LaChrom, Krefeld, Germany) and 12.5 mM H_2SO_4 as the mobile phase at a flow rate of 0.5 mL/min at 45°C. Compounds were quantified by UV detection at 220 nm.

2.5.4 Determination of cell density

In order to determine the cell density of liquid cultures, the OD was measured at a wavelength of 578 and 595 nm for *E. coli*/*P. aeruginosa* and *P. putida*, respectively. An OD of 1.0 corresponded to 1 x 10^9 cells/mL, approximately.

2.5.5 Long-term storage of bacterial strains

In order to store the bacterial strains employed in this study, aerobic LB-overnight cultures, at 200 rpm were grown. *P. aeruginosa* and *E. coli* strains were grown at 37ºC, whereas *P. putida* was grown at 30ºC. Afterwards, 10 mL cells were harvested at 4,000 x *g* for 20 min and resuspended in 1 mL fresh LB. This suspension was further diluted 1:3 into 100% glycerol and further stored at -80ºC.

2.6 Molecular biology techniques

General DNA manipulations carried out in this study in order to achieve the subsequent construction of the recombinant strains are specified in the upcoming sections.

2.6.1 Genomic DNA isolation

All centrifugation steps were carried out at 13,000 rpm (Eppendorf centrifuge, Eppendorf, Hamburg, Germany). Cells (4 mL) were grown overnight in an aerobic manner. Afterwards, cells were harvested by centrifugation for 20 min and the pellet

further resuspended in 700 µL P1 buffer (QIAquick Spin Miniprep kit, Qiagen, Hilden, Germany) and incubated for 5-10 min. Later, 700 µL of phenol:chloroform:isoamyl alcohol (25:24:1) solution (Life Technologies, Darmstadt, Germany) was added and thoroughly mixed by vortexing. Phase separation was achieved by centrifugation of the reaction mixture for 2 min. The supernatant was transferred into a new reaction tube and the previous step was repeated twice. Chloroform was added to the supernatant (1:1) and centrifuged for 2 min. The remaining supernatant was mixed with 60 µL of 3 M sodium acetate (pH 5.0) and 700 µL of isopropanol and incubated for 20 min at room temperature. The mixture was subjected to 15 min centrifugation. Afterwards, the resulting DNA pellet was washed with 70% v/v ethanol and centrifuged for 5 min. Finally, pellet was allowed to dry and dissolved in 100 µL dH_2O (if the pellet did not dissolve properly, it was incubated overnight at 4°C). DNA concentration was determined with a Nanodrop ND-1000-UV/VIS (Peqlab, Erlangen, Germany).

2.6.2 Polymerase chain reaction (PCR)

In order to amplify targeted DNA regions, genomic DNA was isolated as described before and subjected to PCR. The subsequent mixture volume was of 50 µL. The Polymerase employed in all amplifications was the Phusion®High-Fidelity DNA Polymerase (NEB, Ipswich, USA). The general PCR mixture composition was prepared as described in Table 11.

Table 11. PCR strategy employed for amplification of the DNA regions in this study.

Component	Volume (µL)
5x Phusion HF or GC Buffer	10
10 mM dNTPs	1
Forward Primer (10 µM)	2.5
Reverse Primer (10 µM)	2.5
Genomic DNA (50 ng/µL)	1-2
DMSO (optional)	3 or 6
$MgCl_2$ (optional)	1-5
Phusion DNA Polymerase	0.5
Nuclease-free H_2O	Up to 50

Resulting DNA amplicons were in all the cases inserted first in the blunt end commercial pJET 1.2 plasmid for propagation in *E. coli* prior to subcloning in pAS40 or pSEVA424.

2.6.3 DNA sequencing

Constructed plasmids harboring the genes of interest were sent for Sanger sequencing to GATC Biotech (Constance, Germany). Primers employed for sequencing apart of those used for amplification are listed in Table 12 and were purchased from Invitrogen (Darmstadt, Germany).

Table 12. List of primers used for the sequencing of genes inserted into the plasmids utilized in this work (pJET 1.2, pAS40, pSEVA424).

Primer name	Sequence (5´-3´)
pJET 1.2Fw	CGACTCACTATAGGGAGAGCGGC
pJET 1.2Rv	AAGAACATCGATTTTCCATGGCAG
pAS40Fw	GGCCTCTTCGCTATTACGC
pAS40Rv	ATTAGGCACCCCAGGCTTTA
pSEVA424Fw	GCACTCCCGTTCTGGATAAT
pSEVA424Rv	GATCTATCAACAGGAGTCCAA

2.6.4 Gel electrophoresis of DNA

Intending to visualize the proper arrangements of the DNA modules or correct PCR-amplification, gel electrophoresis was performed using Agagel device (Biometra, Göttingen, Germany). After electrophoresis, the 1% w/v gels were incubated in 0.1% v/v ethidium bromide solution for 20 min. Subsequently, DNA could be visualized under UV light at 312 nm. QIAquick Gel Extraction Kit was employed if required in order to excise desired bands.

2.6.5 General recombinant DNA techniques

Plasmid preparations were obtained following the manufacturer´s instructions (QIAGEN Miniprep Kit). Molecular DNA techniques were performed as formerly described (Sambrook & Russell, 2001). *Bsa*I cloning was conducted following a slightly modified cloning procedure (Engler *et al.*, 2009, Engler & Marillonnet, 2014).

2.6.6 Double digestion (*EcoR*I and *Xba*I) of pJET 1.2-*acoA* and pJET 1.2-*pgl*

Exclusively for insertion of *acoA* and *pgl* amplicons into the expression plasemid pSEVA424, the pJET 1.2-*acoA* and pJET 1.2-*pgl* plasmids were digested by *EcoR*I and *Xba*I as specified in Table 13. The restriction reaction was performed for 1 h at 37ºC.

Table 13. Digestion of pJET 1.2-*acoA* and pJET 1.2-*pgl* plasmids for insertion in pSEVA424.

Component	Volume (µL)
Plasmid (300 ng/µL)	3-4
10X NEBuffer	5
*EcoR*I Restriction Enzyme (20,000 units/mL)	0.5
XbaI Restriction Enzyme (20,000 units/mL)	0.5
MilliQ H_2O	Up to 50

The empty pSEVA424 plasmid was digested in the same fashion. If required, the reaction was terminated by incubating the sample at 65ºC for 20 min. All enzymes used in these digestions were purchased in NEB. This digestion protocol is valid for other digestions employing the same amount of each component (varying the sort of restriction enzyme, plasmid, etc). It was applied for *EcoR*I-*Hind*III pAS40 digestion too.

2.6.7 Insertion of *acoA* and *pgl* fragments into pSEVA424

To insert the desired *EcoR*I-*Xba*I digested amplicons into pSEVA424, resulting in pSEVA424-*acoA* and pSEVA-*pgl* expression plasmids, the following reaction was performed overnight at 16ºC. The ligation mixture is shown in Table 14. 10x T4 DNA Ligase Buffer

Table 14. Mixture composition generally used to insert the targeted genes into pSEVA424.

Component	Volume (µL)
Digested pSEVA424 plasmid (75 ng/µL)	1
10x T4 DNA Ligase Buffer	1
Purified insert of DNA	3
T4 DNA ligase (400,000 units/mL)	1
MilliQ H_2O	Up to 10

A helpful formula employed for the calculation of DNA concentration needed for such ligations reads as follows (Sambrook & Russell, 2001):
((Ng of the vector x Kb of the insert)/Kb of the vector)) x Molar ratio (insert/vector)
All enzymes used in these ligations were purchased in NEB. Construction of genetically manipulated *P. aeruginosa* strains was carried out differently, as referred to in section 2.7.

2.6.8 Transformation of *E. coli* with constructed plasmids

E. coli cells were grown aerobically in 100 mL LB at 37°C and 200 rpm to an OD_{578} of 0.5. The culture was chilled on ice for 10 min before cells were harvested by 10 min centrifugation at 4,000 x *g* and 4°C (Heraeus Megafuge 1.0 R, Thermo Scientific, Waltham, USA). The cell pellet was then resuspended in 10 mL of ice cold $CaCl_2$ buffer (100 mM $CaCl_2$, 10% glycerol in dH_2O) and centrifuged as described above. The supernatant was discarded and cells were resuspended in 1 mL of $CaCl_2$ buffer. 50 µL aliquots were prepared and either immediately used for transformation or stored at -80°C. For transformation of $CaCl_2$ competent *E. coli*, cells were first thawed on ice for 15 min and then mixed with 10 to 50 ng of plasmid DNA. After incubation on ice for 20 min, the cells were subjected to a heat shock by incubation at 42°C for 45 sec. Immediately, cells were chilled on ice for two additional min. Afterwards, 450 µL of fresh LB were added for recovery of the cells. After incubation at 37°C for 60 min, 250 µL were streaked on LB agar plates containing the selective antibiotic and plates were incubated overnight at 37°C.

2.6.9 Transformation of *P. aeruginosa* with constructed plasmids

In order to transform *P. aeruginosa* strains with the plasmids of interest, cells were streaked on LB agar plates and incubated overnight at 37ºC. A portion of the biomass was scraped off the plate and resuspended in 500 µL dH_2O and centrifuged at 13,000 rpm for 10 min. The resulting pellet was resuspended and washed again in 500 µL dH_2O by centrifuging at the same speed for 1 min. Next, cells were resuspended in 50 µL dH_2O and kept on ice. Approximately 50-100 ng DNA were added and the mixture incubated for 10 min on ice. Afterwards, cells were transferred into a 1 mm electroporation cuvette (Peqlab, Erlangen, Germany). Electroporation was performed

settling the electroporator at the following parameters set: 200Ω, 25μF, 1.9kV. Cells were rapidly resuspended in 450 μL fresh LB and further incubated at 37ºC for 1 h. Finally, grown cells were plated on LB agar plates containing the corresponding antibiotics concentrations and incubated overnight at 37ºC.

2.6.10 Transformation of *P. putida* with constructed plasmids

A 100 mL *P. putida* culture was grown overnight in LB medium at 30°C under vigorous aeration. Cells were subsequently centrifuged at 4,000 x *g* at room temperature for 10 min. Afterwards, the supernatant was removed and the pellet gently resuspended in 50 mL of 300 mM sucrose in dH_2O (sucrose buffer) and centrifuged likewise. The supernatant was discarded again and 1 mL of 300 mM sucrose buffer was added. Cells were resuspended and transferred into a fresh tube. Cells were then centrifuged at 8,000 rpm at room temperature for 2 min. The supernatant was disposed and 500 μL of 300 mM sucrose added to resuspend the cells. At last, 100 μL aliquots were distributed in tubes and used immediately or stored at -80ºC. For electroporation, 100 μL of electrocompetent cells were gently mixed with 200 ng of the vector DNA. Afterwards, cells were transferred into a 2 mm gap electroporation cuvette (Peqlab, Erlangen, Germany) and incubated on ice for 10 min. Electroporation was performed according to the following parameters: voltage = 1.25 v/1mm gap cuvette or 2.5 v/2 mm gap cuvette, resistance: 200 Ω (set up between 200 min and 600 maximum) and capacitance: 25 μFD. Electroporated cells were resuspended in 400 μL fresh LB and incubated at 30ºC for 1 h. At last, cells were streaked on LB plates supplemented with the corresponding antibiotics.

2.7 Construction of the recombinant strains

For the contruction of the *P. aeruginosa* recombinant strains a recent protocol was employed based on the work by Carola Engler and colleages (Engler *et al.*, 2009), whereas the *P. putida* recombinant strains were constructed following traditional cloning procedures (Sambrook & Russell, 2001).

2.7.1 *P. aeruginosa* strains construction

All plasmids employed in this work are listed in Table 9. Plasmids throughout this study were constructed according to a slightly modified cloning protocol (Engler *et al.*, 2009) so-called Golden Gate Shuffling cloning. By this method different DNA modules can be arranged.

By single-step PCR, *nirS, fliC, nosR, norC* and *norCB* genes including a region between 400-500 nucleotides upstream their start codon were amplified by using the primers *nirS*Fw/*nirS*Rv, *fliC*Fw/*fliC*Rv, *nosR*Fw/*nosR*Rv, *norC*Fw/*norC*Rv and *norCB*Fw/*norCB*Rv, respectively. The upstream region flanking each gene comprised the natural promoters for each operon, *nir*, *fli*, *nos* and *nor*, respectively (Arai *et al.*, 2003, Arai *et al.*, 1995, Frisk *et al.*, 2002). *nosZ* was amplified separately from the *nosRZDFYL* (*nos*) promoter (termed here *nosPR*) by PCR using the *nosZFw*/*nosZRv* and *nosPRFw*/*nosPRRv*, respectively. Blunt ends were generated since the High Fidelity Phusion polymerase was used and therefore all amplicons could be ligated into the commercial intermediate vector pJET 1.2 following the manufacturer´s guidelines (Thermo Scientific, Darmstadt, Germany). All amplicons included a *Bsa*I (GGTCTC) restriction site at the 5´ and at the 3´ extremes. The resulting plasmids were pJET 1.2-*nirS*, pJET 1.2-*fliC*, pJET 1.2-*nosR*, pJET 1.2-*norC*, pJET 1.2-*norCB*, pJET-*nosZ* and pJET 1.2-*nosPR* (see Table 9). The partial chromosomal arrangements of the *nir*, *fli*, *nos* and *nor* operons are shown in Figure 15 for the sake of clarity.

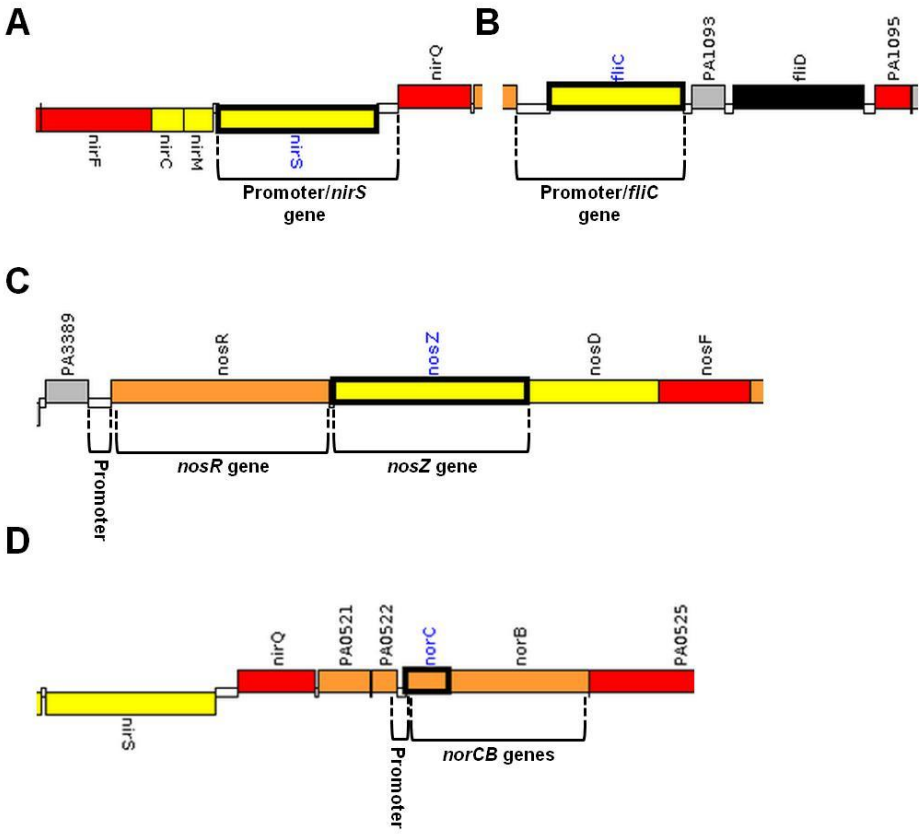

Figure 15. Chromosomal arrangements of the *nir, fli, nos* and *nor* operons. A) *nir* operon chromosomal arrangement. *nirS* gene and its promoter region are highlighted. B) *fli* operon chromosomal arrangement. *fliC* gene and its promoter region are highlighted. C) *nos* operon chromosomal arrangement. *nosR*, *nosZ* genes and their promoter region are highlighted. D) *nor* operon chromosomal arrangement. *norC*, *norB* genes and their promoter region are highlighted.

In parallel a DNA modules specific for the further cloning of each desired gene were constructed by annealing two single-DNA strands (primers). The annealed pairs of primers were *nirS*StreptagIIFw/*nirS*StreptagIIRv, *fliC*StreptagIIFw/*fliC*StreptagIIRv, *nosZ*StreptagIIFw/*nosZ*StreptagIIRv, *nosR*His6xFw/*nosR*His6xRv, *norC*His6xFw/*norC*His6xRv and *norCB*His6xFw/*norCB*His6xRv, respectively (see Table 9). These primers consisted in general terms of (5´ to 3´): *Eco*RI, 4 first nucleotides of the amplicon (~400-500 bp upstream flanking our gene of interest), one random nucleotide, *Bsa*I (inversed orientation: GAGACC), *Bgl*II, *Eco*RV, *Bsa*I (GGTCTC), one random nucleotide, the last 4 nucleotide the gene (stop codon skipped), Histag (for *nosR*, *norC* and *norCB*)/Strep-tag II (for *nirS*, *fliC* and *nosZ*) and the TCA-

stop codon (Table 9). The complementary strand lacked *EcoR*I at the 5´ and included a *Hind*III restriction site at the 3´ end. The pairs of primers were annealed and inserted into pAS40 as shown in Tables 15, 16 and 17. All enzymes utilized in this protocol were provided by NEB. First, each pair of primers was phosphorilated (Table 15).

Table 15. Phosphorilation of the oligos required for subsequent insertion. PCR program employed in this phosphorilation is shown.

Component	**Volume (µL)**
T4-Polynucleotidekinase (10U)	1
T4-DNA-Ligase Buffer with ATP (10x)	5
Oligo (100 pmol/µL)	3
MilliQ H_2O	Up to 50
PCR program	
Temperature (ºC)	**Time (min)**
37	30
65	20
4	Pause

Then, the phosphorilated oligos were combined and aliquoted in 20 µL per PCR tube and subsequently aligned generating a DNA module (Table 16).

Table 16. PCR program for the alignment of the oligos pair.

PCR program	
Temperature (ºC)	**Time (min)**
95	3
Tm	1
55	1
4	Pause

Tm corresponds to the melting temperature of the pairs of oligos.

Last, the ligation of the aligned DNA module into an *EcoRI-Hind*III digested pAS40 (see section 2.6.6 for general digestions) was carried out as described in Table 17.

Table 17. Ligation of the aligned DNA module into *EcoR*I-*Hind*III digested pAS40 plasmid.

Component	Volume (µL)
pAS40 *EcoR*I-*Hind*III digested vector (100 ng/µL)	1
Aligned oligos (different dilutions)	1
T4-DNA-Ligase Buffer	1
T4-DNA-Ligase (400,000 U/mL)	1
MilliQ H_2O	Up to 10

Different dilutions of the aligned module were assessed for ligation (1:1, 1:10, 1:100, 1:100). This annealed module was *EcoR*I-*Hind*III inserted into the digested expression vector pAS40 as referred above. The resulting plasmids were pAS40-Strep-tag II (S), (F) and (Z) and pAS40-His_{6x} (R), (C) and (B) harboring the Strep-tag II and His_{6x} tag, respectively. In addition, these plasmids were suitable for further insertion of *nirS*, *fliC*, *nosZ* and promoter, *nosR*, *norC* and *norCB* once they were cleaved from the pJET 1.2 intermediate plasmids. Ligation was performed overnight at 16ºC. Ligation mixtures were used for *E.coli* DH10b transformation and streaked on LB agar plates with the respective antibiotic concentration, 0.1 mM IPTG and 40 µg/mL of X-GAL and white colonies were selected.

The plasmids pJET 1.2-*nirS*, pJET 1.2-*fliC*, pJET 1.2-*nosR*, pJET 1.2-*norC* and pJET 1.2-*norCB* were pooled together with their respective suitable pAS40 vectors harboring the modules abovementioned. pJET-*nosZ*, pJET 1.2-*nosPR* and its suitable pAS40 plasmid were combined. Afterwards, 50 cycles of 5 min *Bsa*I-digestion followed by 5 min ligation were implemented resulting in the expression vectors, pAS40-*nirS*, pAS40-*fliC*, pAS40-*nosR*, pAS40-*norC*, pAS40-*norCB* and pAS40-*nosZ* harboring fusion genes (Table 9). The mixture composition and PCR program employed in order to accomplish the shuffling events is shown in Table 18.

Table 18. Golden Gate Shuffling cloning procedure mixture composition and PCR program.

Component	**Volume (µL)**
pAS40 harboring DNA aligned module (75 ng/µL)	1
pJET 1.2 harboring the genes of interest (75 ng/µL)	1
*Bsa*I restriction enzyme (10 U/µL)	0.5
T4-DNA-Ligase (4 U/µL)	3.75
T4-DNA-Ligase Buffer 10x	1.5
MilliQ H_2O	Up to 15
PCR program	
Temperature (ºC)	**Time (min)**
50	5
16	5
4	Pause

U = units of enzyme. PCR program was repeated 50 cycles.

The corresponding background mutant strains PA14 *nirS*, PA14 *fliC* and PAO1 *nosR*, *norC*, *norB* and *nosZ* were transformed with their complementing constructs. Additionaly, the pAS40-*nirS* and pAS40-*fliC* plasmids were introduced into the PA14 *fliC* and PA14 *nirS* Tn mutants, respectively, in order to carry out the interacting peptides determination experiments. The pAS40 empty plasmid was introduced in *P. aeruginosa* PAO1/PA14 wild-type strains and the generated strains were further employed as negative controls for interactomic studies. A schematic view of this cloning procedure is represented in Figures 16A and B.

A

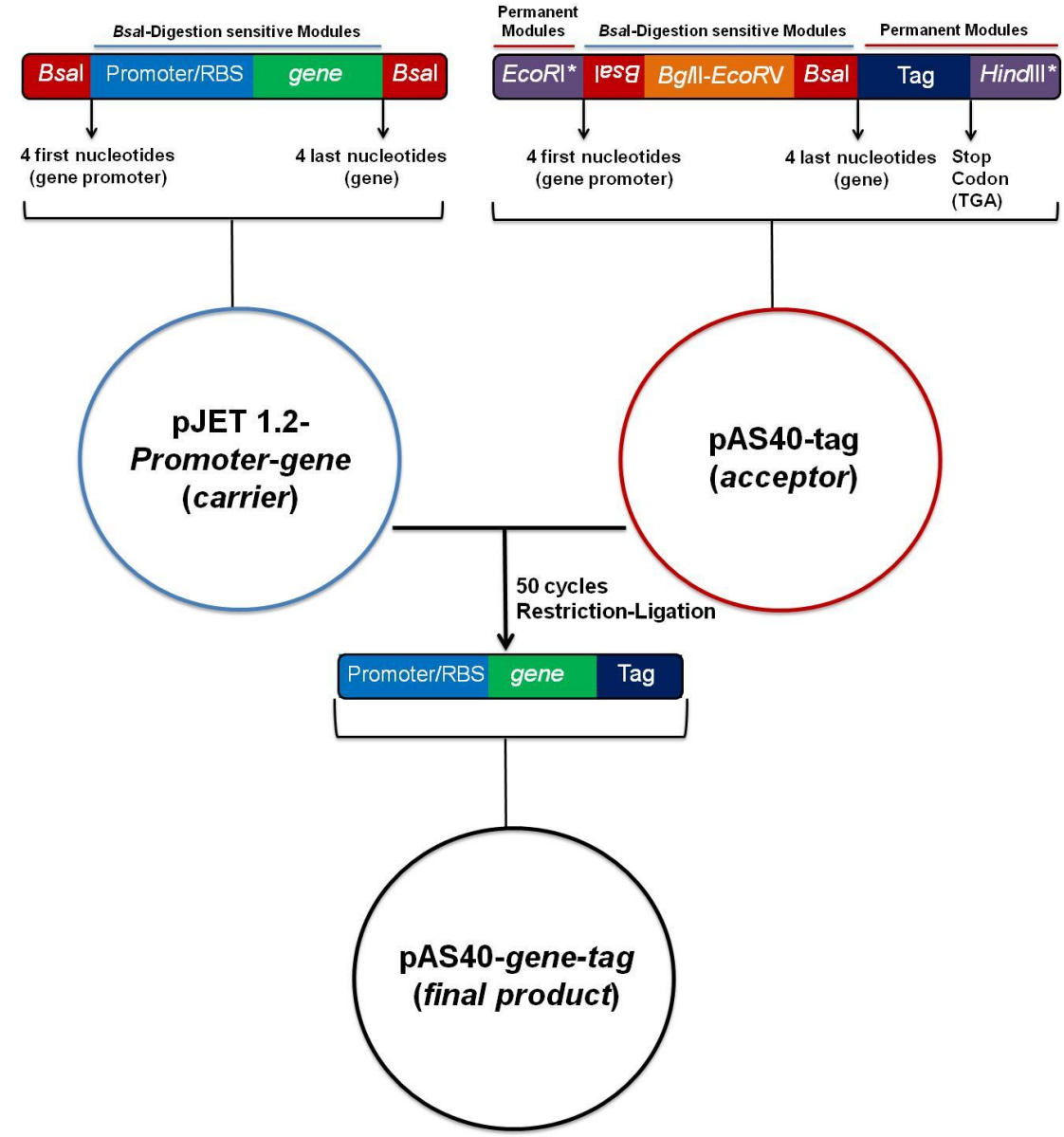
BsaI-Digestion sensitive Modules
BsaI
Promoter/RBS
gene
BsaI
4 first nucleotides (gene promoter)
4 last nucleotides (gene)
Permanent Modules
BsaI-Digestion sensitive Modules
Permanent Modules
EcoRI*
BsaI
BglII-EcoRV
BsaI
Tag
HindIII*
4 first nucleotides (gene promoter)
4 last nucleotides (gene)
Stop Codon (TGA)
pJET 1.2- Promoter-gene (carrier)
pAS40-tag (acceptor)
50 cycles Restriction-Ligation
Promoter/RBS
gene
Tag
pAS40-gene-tag (final product)

B

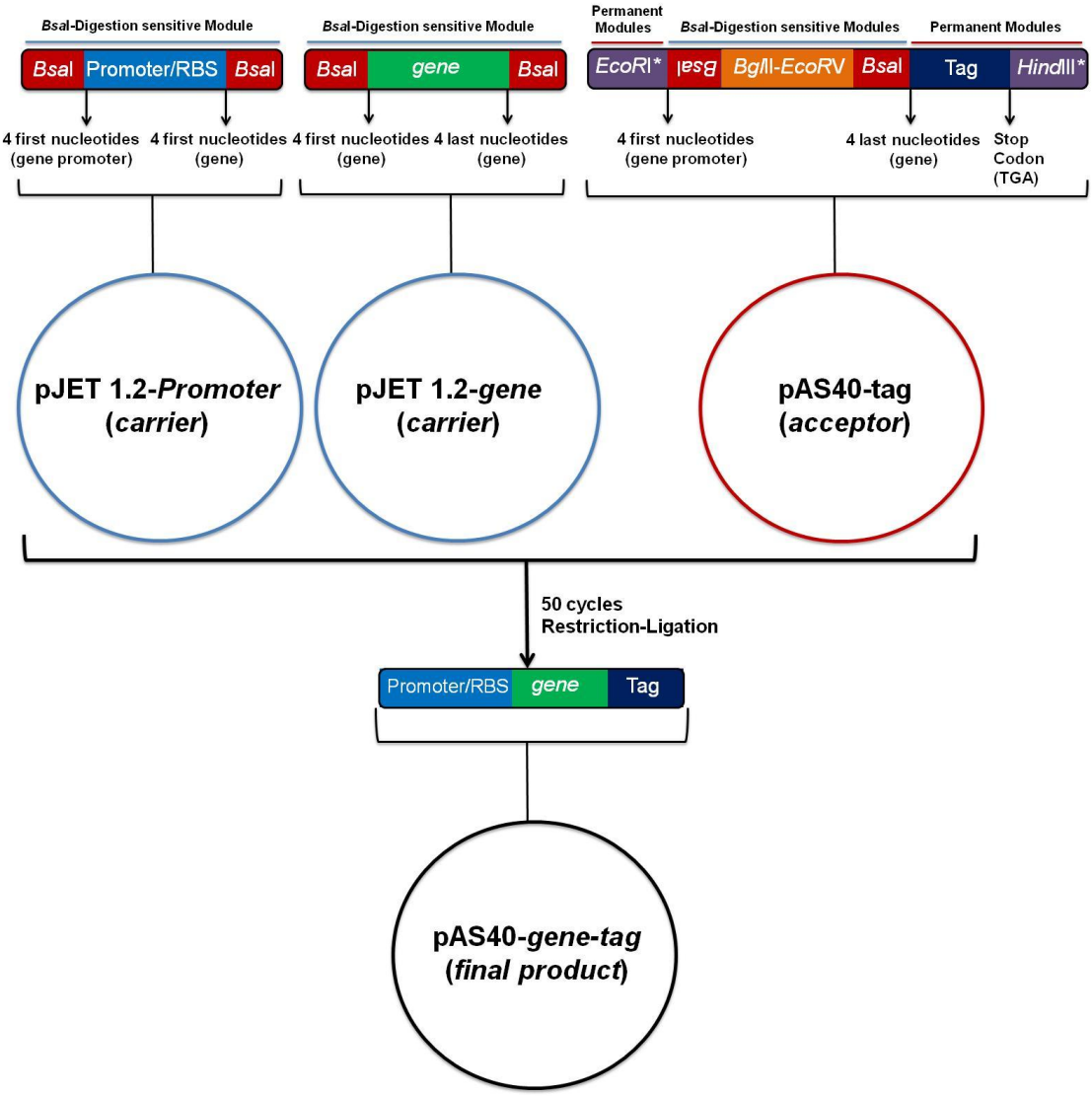

Figure 16. Schematic representation of the Golden Gate Shuffling cloning strategy for complex DNA modules arrangements. A) Overview of *nirS*, *fliC*, *nosR*, *norC* and *norCB* cloning procedures. The acceptor plasmid corresponds to pAS40-His6x (R), (C) and (B) or pAS40-Strep-tag II (S) and (F) suitable for *nosR*, *norC*, *norCB*, *nirS* and *fliC* ligations, respectively, whereas the carrier was pJET 1.2 harboring *nosR*, *norC*, *norCB*, *nirS* and *fliC* untagged genes (see Table 9). The promoter region (including the RBS) is shown upstream the gene. B) Overview of *nosZ* cloning procedure. In this case the acceptor is pAS40-Strep-tag II (Z) suitable for *nosZ* ligation, while one of the carrier plasmids harbors the *nosZ* untagged gene and the other one the *nos* promoter (*nosPR*). Promoter and *nosZ* gene were first cloned independently into the pJET 1.2 vector and subsequently subjected to restriction-ligation protocol leading to the final pAS40-*nosZ* product. *Eco*RI* and *Hind*III* refer to the truncated versions enclosing only the 4 intermediate nucleotides of both

restriction sites which are sufficient to be ligated into an *Eco*RI-*Hind*III digested plasmid. Upside down *Bsa*I indicates that this restriction site sequence is inverse orientated in comparison to the other ones. RBS refers to the ribosomal binding site of the within a promoter region. All genes are fused to their natural promoters in the final construct product. This method relies on the specific digestion fashion of *Bsa*I restriction enzyme. Therefore, a proper design of the *Bsa*I restriction sites is needed in order to assemble the different DNA modules in the expected manner.

The proper complementation of all recombinant strains was tested by nitrate/nitrite consumption (50 and 10 mM, respectively) and anaerobic denitrifying growth (PAO1 *nirS*$^-$/*nirS*$^+$; PAO1 *nosR*$^-$/*nosR*$^+$; PAO1 *norC*$^-$/*norC*$^+$ and PAO1 *norCB*$^-$/*norCB*$^+$;) or by swimming motility recovery (PA14 *fliC*$^-$/*fliC*$^+$).

2.7.2 *P. putida* strains construction

The 978 bp *acoA* and 729 bp *pgl* genes were PCR amplified using the primer pairs *acoA*Fw/*acoA*Rv and *pgl*Fw/*pgl*Rv, respectively. Used primers sequences are listed in Table 10. The forward primers (*acoA*/Fw, *pgl*/Fw) of both genes encoded an *Eco*RI restriction site, a consensus Ribosomal Binding Site (RBS) sequence (AGGAGG), eight conserved nucleotides downstream (AAAAACAT) and 18 nucleotides from the gene of interest. Both reverse primers (*acoA*/Rv, *pgl*/Rv) encoded an *Xba*I restriction site and the last 18 nucleotides of target gene sequences (Table 10). Amplified genes were cloned into pJET 1.2 resulting in pJET 1.2-*acoA* and pJET 1.2-*pgl*, respectively. The cloned genes were excised from their host vectors via *Eco*RI and *Xba*I restriction and subsequently cloned into the *Eco*RI-*Xba*I sites of pSEVA424 resulting in pSEVA-*pgl* and pSEVA-*acoA*, respectively.

2.8 *In vivo* cross-linking of protein interaction partners

In vivo cross-linking of protein complexes was carried out as described previously (Nicke *et al.*, 2013). The formaldehyde cross-linker agent was injected through a syringe into the culture at the late exponential phase to a final concentration of 0.125% v/v. Cultures were incubated shaking at 150 rpm to facilitate cross-linker penetration at 37ºC for 20 additional min. Thereby, transient protein interactions are ensured to be hooked. Free aldehyde groups were quenched by addition of 135 mM glycine and incubating the cultures at 37ºC for 5 min shaking at 150 rpm. Afterwards,

cells were harvested at 3,000 x *g*, for 20 min at 4ºC. The pellet was washed twice with phosphate-buffered saline (PBS; 137 mM NaCl, 2.7 mM KCl, 4.3 mM $Na_2HPO_4 \cdot 7H_2O$ and 1.4 mM KH_2PO_4, pH 7.3) via centrifugation at 4,000 x *g*, for 20 min at 4ºC.

2.9 Purification of fusion proteins

Two different approaches conducted purification accordingly to the location of the fusion proteins (periplasm or membrane). The purification of periplasmic soluble proteins was performed by osmotic cold shock whereas for membrane proteins cells were subjected to lysis and insoluble proteins were subsequently treated with a detergent.

2.9.1 Purification of periplasmic soluble proteins

After the cross-linking treatment, cells were harvested by centrifugation at 4,000 x *g*, 4ºC and 20 min. Pellets were washed twice in PBS buffer by resuspending and centrifuging as before specified. Periplasmic isolations were accomplished by osmotic cold shock as previously described (Dammeyer *et al.*, 2013) by resuspending washed cells in a slightly modified PE buffer (20% w/v sucrose, 50 mM Tris, 1 mg/mL polymyxin B, pH 8.0) supplemented with 1 tablet of protease cocktail inhibitor (Roche, Penzberg, Germany) per each 10 mL of sample. Cells suspensions were incubated overnight at 4ºC thoroughly rotating. To separate insoluble fractions, periplasmic extraction samples were transferred to the 70.1 Ti rotor (Beckman Coulter, Krefeld, Germany) and centrifuged at 100,000 x *g* for 1 h at 4ºC, employing the Optima L-90K ultracentrifuge (Beckman Coulter, Krefeld, Germany). The resulting supernatant constituted the periplasmic fraction. Periplasmic fractions underwent affinity co-purification attempting to resolve interaction partners along with the bait. Samples were applied to a previously equilibrated gravity Strep-Tactin superflow high capacity column (IBA GmbH, Göttingen, Germany). Washing steps were implemented using the washing buffer recommended by the manufacturer (100 mM Tris.Cl, 150 mM NaCl, 1 mM EDTA, pH 8.0) and protein elution was succeeded with elution buffer (100 mM Tris.Cl, 150 mM NaCl, 1 mM EDTA, 2.5 mM desthiobiotin, pH 8.0). Protein elutions were concentrated by centrifugation at 1,000 x *g* for ≈60 min through Vivaspin 15, 10 kDa cutoff centrifugal concentrators (Sartorius AG, Göttingen, Germany). *P.*

aeruginosa wild-type harboring the empty plasmid was subjected to the same procedure as control in order to identify possible unspecific binding proteins to the column material or protein complexes. Protein concentrations were determined by Bradford assay (Noble & Bailey, 2009). NosZ-Strep-tag II fusion protein purification from the periplasmic fraction was taken as a negative control since it is highly present in this compartment and considered a marker for denitrification.

2.9.2 Purification of membrane residing proteins

Throughout fusion proteins purifications, samples were kept at 4ºC. Since an overall interactome was aspired, outer and inner membranes were isolated. Washed cells were resuspended in 2-3 pellet volumes lysis buffer (50 mM NaH_2PO_4, 300 mM NaCl, pH 8.0). Lysis buffer was supplemented with 1 tablet of Protease Inhibitor Cocktail (Roche, Penzberg, Germany) for every 10 mL buffer. Intact cells were lysed by subjecting them to French Press cycles at 1100 psi (1 psi = 6.9 kPa) for two consecutive runs. Cell debris was removed by centrifugation at 20,000 x *g* for 30 min. In order to isolate the recombinant membrane-bound proteins, lysates were ultra-centrifuged at 100,000 x *g* for 1 h at 4ºC. Supernatants containing the cell soluble fractions were discarded and membrane insoluble fractions stored at -20ºC until further use. Aiming to solubilize membrane residing proteins, roughly 200 µg of membrane fraction biomass were withdrawn and dissolved in 500 µL 20 mM Potassium buffer (pH 8.0) supplemented with 2% Triton X-100. Afterwards, samples were incubated at 4ºC, gently rotating for 1 h in order to expedite solubilization. Cell debris and insolubilized membranes were removed by centrifuging at 16,000 x *g* for 30 min. Ni-NTA agarose for His_{6x} tagged protein purification, was equilibrated with NPI-10 (50 mM NaH_2PO_4, 300 mM NaCl, 10 mM imidazole, pH 8.0). Solubilized membrane protein suspension present in the supernatant was blended with 1/5 its volume of equilibrated Ni-NTA agarose. The binding of fusion proteins to Ni^{2+} ions was addressed by incubating the mixture at 4ºC for 1 h kindly rotating. Affinity co-purification of bait-prey complexes was accomplished by means of low-centrifugation steps (500 x *g* for 5 min) using Spin columns F (MoBiTech, Göttingen, Germany). Stringent washing steps were performed by washing the immobilized protein complexes within the column with increasing imidazole concentrations, 20 (NPI-20), 30 (NPI-30), 40 (NPI-40) and 50 mM (NPI-50),

consecutively. Flow-through, whole membrane fraction and the last washing step were stored at -20ºC for interactomic purposes. Either last washing steps or negative control elutions (wild-type harboring plasmid without insert) were confirmed to have negligible protein content by SDS-PAGE and Bradford assay (Noble & Bailey, 2009). Eluates containing recombinant proteins along with their potential interaction partners were accomplished by addition of 300 mM imidazole (NPI-300).

2.10 SDS-PAGE gel electrophoresis and Western blot detection

After bait-preys co-purification, the presence of the fusion protein under study and its potential interaction partners was tested by SDS-PAGE and Western blot.

2.10.1 SDS-PAGE gel electrophoresis

Periplasmic and membrane fractions, flow-through, washing steps and protein samples in each case were prepared and gel electrophoresis performed as previously described (Righetti, 1990). When required trichloroacetic acid (TCA)-precipitation was carried out (see section 2.11). Protein samples were mixed with 1x SDS-loading buffer (1.5% v/v glycerol, 0.5% v/v beta-mercaptoethanol, 0.24% w/v SDS, 0.1% w/v bromophenolblue, 0.08% w/v Tris, pH 6.8). cross-linking of proteins complexes was reversed by heating the samples at 95ºC for extensive periods of 20-30 min prior to gel loading (Orlando, 2000). Gels employed in this study consisted of 12.5% polyacrilamide. The protein ladders used to visualize relative molecular weight of the proteins were the PageRuler Prestained Protein Ladder and PageRuler Unstained Protein Ladder (Thermo scientific, Darmstadt, Germany) for His-tagged and Strep-tag II fusion proteins, respectively. The buffers needed for SDS-PAGE are shown in Tables 19 and 20.

Table 19. Separation gel.

Reagents	Volume (mL)
Rotiphorese G.30	3.75
2x Separation Buffer (1.5 M Tris pH 8.8, 0.2% w/v SDS)	4.5
MilliQ dH_2O	0.75
10% w/v amonium persulfate	0.03
Temed	0.007

Once this mixture was poured between the SDS plates it was let to be dried for approximately 20 min, overlaid with isopropanol. Consecutively the isopropanol was removed and the stacking gel was prepared and poured onto the former face (Table 20).

Table 20. Stacking gel

Reagents	Volume (mL)
Rotiphorese G.30	0.4
2x Stacking Buffer (1 M Tris pH 6.8, 0.2% w/v SDS)	2
MilliQ dH_2O	1.6
10% w/v amonium persulfate	0.030
Temed	0.007

The SDS-PAGE was filled up to the edge and the comb inserted. When the complete gel was dried, SDS-PAGE electrophoresis was carried out at 100 V for 2h in 1x Laemmelli buffer (250 mM Tris, 2.5M glycine, 1% w/v SDS). Resolved proteins were stained with Coomassie Staining Solution (25 % v/v isopropanol, 10% v/v acetic acid and 0.05% w/v and 0.05 w/v Brilliant Blue G-250) and destained with Destaining Solution (10% v/v acetic acid, 30% v/v ethanol) for further visualization under a GS-800 calibrated densitometer. Required chemicals were purchased in BioRad (Munich, Germany).

2.10.2 His-tagged protein detection by Western blot

His-tagged recombinant proteins were detected by Western blot according to the manufacturer´s recommendations (Sigma-Aldrich, Munich, Germany). Primary antibodies against His_{6x} were incubated with GST-alkaline phosphatase conjugate secondary antibodies. Coomassie stained SDS-PAGE gels and PVDF blotted membranes were visualized on a GS-800 calibrated densitometer (Biorad, Munich, Germany). Six whatman papers and 1 PVDF membrane were excised to the same size of the separation gel. The stacking gel was separated and disposed. The PVDF membrane was briefly soaked in methanol, the whatman papers and the separation gel in 1x Towbin buffer (14.86 g/L glycine, 3.03 g/L, 15% v/v methanol, pH 8.5). Afterwards, the PVDF membrane was briefly soaked in Towbin buffer. Three Whatman papers were piled up followed by the PVDF membrane, the SDS-PAGE gel and the

other three Whatman papers, on the Semy-dry and rapid Blotting. The protein transfer was carried out at 25 V, 300 mA for 6-8 min. All following steps were carried out at room temperature and gently shaking. The PVDF membrane was briefly washed in TBS buffer (6.06 g/L Tris pH 7.6 and 8.77 g/L NaCl) and immediately transferred to 20 mL of Blocking buffer (TBS buffer, 5% w/v Milk powder) and incubated for 1 h. Afterwards, the membrane was incubated in 20 mL Primary Antibody Solution (Blocking buffer, 1:1000 primary antibodies dilution) for an additional h. The PVDF membrane was washed three times in 20 mL TBS-Tween buffer (TBS buffer, 0.1% v/v Tween 20) for 10 min each step. The membrane was then incubated for 1 h in 20 mL Secondary Antibody Solution (Blocking buffer, 1:10,000 secondary antibodies dilution). Then the membrane was washed three times in 20 mL TBS-Tween buffer for 10 min each step. Finally the chromogenic detection was carried out by adding 20 mL of APB Staining Solution (12.11 g/L Tris, 5.84 g/L NaCl, 0.48 g/L $MgCl_2$, 0.083 µg/mL 5-bromo-4-chloro-3-indolylphosphate (BCIP) and 0.66 µg/mL Nitrotetrazolium Blue Chloride (NBT)) and incubating for 5 min maximum. The reaction was terminated by washing with dH_2O. The fusion proteins (baits) were visualized under a GS-800 scanner (BioRad, Munich, Germany).

2.10.3 Strep-tag II tagged protein dectection by Western blot analysis

Strep-tag II fusion protein presence was corroborated by Western blot analysis. Proteins were transferred to a PVDF membrane and further detected according to the supplier (IBA GmbH, Göttingen, Germany). Primary Alkaline-Phosphatase conjugated antibodies were immunochemically detected by chromogenic reaction (IBA GmbH, Göttingen, Germany). SDS-PAGE was performed and the protein was electrotransferred to a PVDF membrane. Then, the membrane was briefly washed in PBS-buffer (4 mM KH_2PO_4, 16 mM Na_2HPO_4, 115 mM NaCl, pH 7.4). The membrane was blocked with 20 mL PBS-blocking buffer (PBS buffer with 3% BSA and 0.5% v/v Tween 20). Afterwards, the membrane was incubated for 1 h at room temperature or overnight at 4°C gently shaking. Then, the membrane was washed three times with 20 mL PBS-Tween buffer (PBS-buffer with 0.1% v/v Tween 20) for 5 min each time at room temperature. After the last washing step 10 mL PBS-Tween buffer were added to the membrane. Subsequently, 2.5 µl of Strep-Tactin alkaline phosphatase conjugate

(1:4000) were added. The membrane was incubated for 1 h at room temperature. Next, the membrane was washed twice with PBS-Tween buffer for 1 min each time at room temperature. After that the membrane was washed twice with PBS-buffer for 1 min each time at room temperature. Afterwards, the membrane was transferred in 20 mL Reaction buffer (100 mM NaCl, 5 mM $MgCl_2$, 100 mM Tris·Cl, pH 8.8), 10 µL of NBT solution (7.5% w/v nitrotetrazolium blue in 70% v/v dimethylformamid) and 60 µL BCIP solution (5% w/v 5-bromo-4-chloro-3-indolyl-phosphate in dimethyl-formamid) were added. The chromogenic reaction was allowed gently shaking for a maximal time frame of 5 minutes to avoid much background. The reaction was terminated by washing the membrane with dH_2O. The fusion proteins (baits) were visualized under a GS-800 scanner(BioRad, Munich, Germany).

2.11 Protein precipitation

When required, TCA-precipitation was carried out in order to precipitate the protein content and thereby achieve a higher protein concentration. Total protein elutions were diluted with 2.5 volumes of 50% w/v trichloroacetic acid and 9 volumes of 0.1% w/v sodium deoxycholate, mixed and incubated for 30 min on ice. Afterwards, samples were centrifuged at 13,000 rpm for 20 min. Protein pellets were washed twice with cold acetone by centrifuging for 10 additional min. Precipitated proteins were diluted with 20 µL of 1x SDS-loading buffer and loaded onto an SDS-gel.

2.12 Antibodies

All polyclonal antibodies were raised in rabbits by Metabion (Metabion, Planegg/Steinkirchen, Munich, Germany).

2.12.1 NosZ antibodies

P. aeruginosa PA14 bearing the *nosZ* fusion plasmid was grown under anaerobic conditions and nitrate supplementation in rubber stoppered serum flasks at 100 rpm and 37ºC. NosZ fusion protein was purified as follows: Intact cells were subjected to French Press lysis leading consequently to soluble proteins release. Ultracentrifugation was carried out as specified before. Upcoming soluble fractions were withdrawn and affinity co-purification undertaken as recommended by the

manufacturer´s instructions (IBA, Göttingen, Germany). Protein solutions immobilized at the column beads were subjected to intensive washing steps and a final protein elution was accomplished by addition of 2.5 mM desthiobiotin buffer. Samples were collected and concentrated through Vivaspin 15, 10 kDa cutoff centrifugal concentrators (Sartorius AG, Göttingen, Germany). Approximately 1 mg of NosZ-Strep-tag II recombinant protein was produced and polyclonal antibodies were raised against the resulting fusion protein (Metabion, Planegg/Steinkirchen, Munich, Germany).

2.12.2 NosR, NarH, NorC antibodies

For the generation of anti-NosR, anti-NarH and anti-NorC antibodies several peptides were synthesized. The amino acid residues 50-61, 102-116 and 118-132 for NorC and 106-130, 190-203 and 404-418 for NosR were selected for this purpose, respectively. These amino acid residues corresponded to medium-length periplasmic loops of these proteins resulting in soluble peptides. For the generation of anti-NarH polyclonal antibodies a mixture of three peptides corresponding to the amino acids 1-276, 277-392 and 418-513 were selected.

2.12.3 NirS, FliC and DnaK antibodies

In order to generate specific antibodies against NirS, FliC the following strategy was chosen. NirS peptides covering the regions of the amino acids 379-392, 526-540 and 541-555 where synthesized by Metabion and its mixture was employed for raising polyclonal antibodies in rabbit by Metabion. The peptide spanning the first 174 amino acids of FliC was used for rabbit immunization.

2.12.4 DnaK antibodies

DnaK-His_{6x} was overproduced in *E. coli* BL21 via 1 mM IPTG induction sustained by the pET14b plasmid. Purification of 2 mg/mL recombinant protein was achieved following the manufacturer´s guidelines (Protino, Macherey Nagel). Polyclonal antibodies were generated against the recombinant protein by Metabion (Planegg/Steinkirchen, Germany) for further polyclonal antibodies generation in rabbit.

2.13 Double-immunogold labeling and TEM

Immunogold labeling with the generated antibodies was performed and visualized by TEM to confirm protein-protein interactions *in vivo* in the *P. aeruginosa* cells. The co-localizations of NosR-NarH-NirS-NorC-NosZ and NirS-DnaK-FliC corresponded to two separate studies and were performed in PAO1 and PA14, respectively. Antibody concentrations were differently employed depending on the proteins being labeled. Therefore, the procedures are separated into two sections.

2.13.1 Co-localization of NosR, NarH, NirS, NorC and NosZ in *P. aeruginosa* PAO1 by double-immunogold labeling and TEM

P. aeruginosa PAO1 wild-type strain was grown anaerobically in LB supplemented with 50 mM nitrate for 8 h. Bacteria were fixed with 1% formaldehyde in the growth medium overnight at 5°C. After centrifugation, cells were resuspended in 10 mM glycine to quench the formaldehyde cross-linker. Afterwards, bacteria were dehydrated according to the progressive lowering of temperature procedure (PLT embedding) with ethanol and subsequently embedded in Lowicryl K4M resin. After polymerization with UV-light ultrathin, sections were cut with a diamond knife, collected onto butvar coated nickel grids and incubated with the specific antibodies. First, sections were incubated with the first round of purified IgG antibodies overnight at 5°C. After washing with PBS bound antibodies were rendered visible by adding protein A/G gold-nanoparticles (PA/GG 15 nm in size, 1:75 dilution of the stock solution) for 30 min at room temperature. After washing with PBS containing 0.1% Tween 100 sections were further incubated with a protein A solution (0.1 mg/mL) for 15 min at room temperature. After washing in PBS, sections were incubated for 3 h at room temperature with the second round of different purified IgG. Antibodies dilutions were established at 1:25 for the first IgG and 1:15 for the second. After PBS washing, sections were incubated with PA/GG (10 nm in size, 1:200 dilution of the stock solution) for 30 min at room temperature. Subsequently, sections were washed with PBS containing 0.1% Tween 100, TE-buffer and dH_2O. Sections were counterstained with 45 aqueous uranyl acetate for 1 min. Samples were then examined in a TEM910 transmission electron microscope (Carl Zeiss, Oberkochen) at an acceleration voltage of 80 kV. Images were recorded digitally at calibrated magnifications with a Slow-Scan

CCD-Camera (ProScan, 1024x1024, Scheuring, Germany) with ITEM-Software (Olympus Soft Imaging Solutions, Münster, Germany). Contrast and brightness were adjusted with Adobe Photoshop CS4.

2.13.2 Co-localization of NirS, DnaK and FliC in *P. aeruginosa* PA14 by double-immunogold labeling and TEM

P. aeruginosa PA14 wild-type strain was grown anaerobically in LB supplemented with 50 mM nitrate until late exponential phase was reached (8 h) Bacteria were fixed with 1% formaldehyde in the growth medium for overnight at 5°C. After centrifugation bacteria were resuspended in TE buffer containing 10 mM glycine to quench free aldehyde groups. Bacteria were then dehydrated according to the progressive lowering of temperature protocol (PLT embedding) with ethanol and embedded in Lowicryl K4M resin. After polymerization with UV-light ultrathin sections were cut with a diamond knife, collected onto butvar coated nickel grids and incubated with the specific antibodies. First sections were incubated with a 1:25 dilution of the purified DnaK IgG antibodies for overnight at 5°C. After washing with PBS bound antibodies were made visible with protein A/G gold-nanoparticles (PA/GG 15 nm in size, 1:75 dilution of the stock solution) for 30 min at room temperature. After washing with PBS containing 0.1% Tween 100 sections were incubated with a protein A solution (0.1 mg/mL) for 15 min at room temperature. After washing in PBS sections were incubated either with anti NirS antibodies (1:20 dilution of the purified IgG antibodies) or with anti-FliC antibodies (1:20 dilution of the purified IgG antibodies) for 3 h at room temperature. After a PBS washing step sections were incubated with PA/GG (10 nm in size, 1:200 dilution of the stock solution) for 30 min at room temperature. Subsequently, sections were washed with PBS containing 0.1% Tween 100, TE-buffer and dH_2O. Sections were counterstained with 45 aqueous uranyl acetate for 1 min. Samples were then examined in a TEM910 transmission electron microscope (Carl Zeiss, Oberkochen) at an acceleration voltage of 80 kV. Images were recorded digitally at calibrated magnifications with a Slow-Scan CCD-Camera (ProScan, 1024x1024, Scheuring, Germany) with ITEM-Software (Olympus Soft Imaging Solutions, Münster, Germany). Contrast and brightness were adjusted with Adobe

Photoshp CS4. The co-localization experiments were carried out in collaboration with Prof. Dr. Manfred Rohde (HZI, Braunschweig, Germany).

2.14 AP-MS/MS by gel-mediated and gel-free identification of interaction partners

Protein elutions were routinously spotted on a SDS-gel and a gel-mediated or a gel-free procedure was chosen depending on the complexity of the sample.

2.14.1 AP-MS/MS by gel-mediated identification of the interaction partners

When the protein-complexes resulted to be of low complexity since only a few bands were observed by gel electrophoresis, the approach employed was the AP-MS/MS by gel-mediated identification of the interaction partners.

2.14.1.1 Protein extraction and LC-MS/MS analysis

Prominent bands found in the gels co-purification insets were excised and further processed in order to analyze peptide content by LC-MS/MS analysis.

2.14.1.2 Protein Extraction

Bands were excised from the gels and prepared for HPLC-MS analysis according to (Toyofuku *et al.*, 2012a). Protein samples of approximately 300 µL were precipitated by adding 1 µL GlycoBlue (Ambion, Darmstadt, Germany), 80 µL 2.5 M sodium acetate pH 5.0 and 1500 µL ethanol overnight. The precipitated proteins were pelleted (16,000 rpm, 30 min, 4°C) and air dried.

2.14.1.3 Tryptic digestion

Air dried proteins were resolubilized in 50 mM Triethylammonium bicarbonate buffer (TEAB), reduced by the addition of 20 mM Tris-(2-carboxyethyl)-phosphine-hydrochloride (TCEP), alkylated with Methyl methanemethylthiosulfonate (MMTS), digested by the addition of trypsin at a final ratio of 50:1 (protein: protease) and incubated at 37°C overnight.

2.14.1.4 Protein purification using reverse phased HPLC chromatography of the protein preparations employing vacuum-driven centrifugation

After evaporation of all fluid in the SpeedVac, the peptides were desalted onto Stage Tips with an additional layer of 5 µL of 10 µm RP18 material (Lichrosorb; Merck, Darmstadt, Germany). Peptides were resolubilized in 3% acetonitril (ACN) containing 0.2% TFA and adsorbed to the RP18 material. After washing with binding solution, the peptides were eluted with 60% ACN containing 0.2% TFA. To remove the organic phase the peptides were dried by vacuum centrifugation, resolubilized in 12 µL 3% ACN containing 0.2% TFA and centrifuged in an ultracentrifuge. Peptides were used for HPLC-MSMS analyses.

2.14.1.5 LC-MS/MS and data analyses

LC-MS/MS analyses were performed on a Dionex UltiMate 3000 n-RSLC system connected to an LTQ Orbitrap Velos mass spectrometer (Thermo Scientific, Darmstadt, Germany). Peptides were loaded onto a C18 pre-column (3 µm, Acclaim, 75 µm x 20 mm, Dionex), washed for 3 min at a flow rate of 6 µL/min. Subsequently, peptides were separated on a C_{18} analytical column (3-µm, Acclaim PepMap RSLC, 75 µm x 25 cm, Dionex) at 350 µL/min via a linear 120-min gradient with UPLC buffer A (0.1% formaldehyde in water) and UPLC buffer B (0.1% formic acid in 80% ACN). The LC system was operated with Chromeleon Software (version 6.8, Dionex), which was embedded in the Xcalibur software (version 2.1, Thermo Scientific, Darmstadt, Germany). The effluent from the column was electro-sprayed (Pico Tip Emitter Needles, New Objectives) into the mass spectrometer. The mass spectrometer was controlled by Xcalibur software and operated in the data-dependent mode allowing the automatic selection of a maximum of 10 doubly and triply charged peptides and their subsequent fragmentation. Peptide fragmentation was carried out using the CID mode in the ion trap. MS/MS raw data files were processed via Proteome Discoverer 1.3.0.339 mediated searches against a PA14 database, extracted from SwissProt on a Mascot server (V. 2.4, Matrix Science). The following search parameters were used: enzyme, trypsin; maximum missed cleavages, 1; fixed modification, carbamidomethylation (C); variable modification, oxidation (M), peptide tolerance, 5 ppm; MS/MS tolerance, 0.5 Da.

2.14.2 AP-MS/MS by gel-free identification of interaction partners

When protein-complexes turned out to be more complex, interaction partners were identified by AP-MS/MS gel-free procedure.

2.14.2.1 LC-MS/MS and data analyses

Eluates in triplicates (NosR-His_{6x}, NorC-His_{6x} and NorB-His_{6x}) resulted in sufficient proteins amounts and were subsequently evaluated by LC-MS-MS as described and proteins identified by an unlabelled quantitative proteomics approach. This approach is the so-called label-free quantitative MS (AP-QMS) (Kaake *et al.*, 2010). This quantification method can be very useful to determine a cut-off for interaction specificity. The area value approach based on labelled-free protein quantitation has been already introduced in other studies (Bachi & Bonaldi, 2008) (Lambert *et al.*, 2013) and it is referred to as xPAI (Protein Abundance Index). This method is highly useful when handling low complex samples which is the case of the protein-protein interactions (Hubner & Mann, 2011). It is a relative quantitation of the protein contents in protein-protein interactions studies (Ong & Mann, 2005). Each eluate was loaded onto LC-MS/MS at the same concentration. To each protein identified by MS an area value was attributed on the basis of peptide abundance. This area value derives from the label-free quantitative proteomics resulting data. The area value displays the average area of the three unique peptides with the largest peak area. If only one peptide is found the value corresponds to the peak area of this peptide. That means, the higher an area value attributed to a certain protein is, the more abundant this protein is present in the co-purification. It indicates higher interaction specificity in comparison to less abundant proteins. More intense bands were reflected afterwards by elevated area values assigned by LC-MS-MS analysis what underlines the robustness of the approach.

LC-MS/MS analyses were performed on a Dionex UltiMate 3000 n-RSLC system connected to an LTQ Orbitrap Velos mass spectrometer (Thermo Scientific, Darmstadt, Germany). Tryptic digested peptides were loaded onto a C18 pre-column (3 µm, Acclaim, 75 µm x 20 mm, Dionex), washed for 3 min at a flow rate of 6 µL/min. Subsequently, peptides were separated on a C_{18} analytical column (3-µm, Acclaim

PepMap RSLC, 75 μm x 25 cm, Dionex) at 350 μL/min via a linear 120-min gradient from 100% buffer A to 25% B followed by a 50 min gradient from 25% buffer to 80% UPLC buffer B (buffer A = 0.1% formic acid in water; B = 99.9% acetonitrile with 0.1% formic acid). The LC system was operated with Chromeleon Software (version 6.8, Dionex), which was embedded in the Xcalibur software (version 2.1, Thermo Scientific, Darmstadt, Germany). The effluent from the column was electro-sprayed (Pico Tip Emitter Needles, New Objectives) into the mass spectrometer (Orbitrap Velos Pro). The mass spectrometer was controlled by Xcalibur software and operated in the data-dependent mode allowing the automatic selection of a maximum of 10 doubly and triply charged peptides and their subsequent fragmentation. A dynamic exclusion allowed a new spectrum of a peptide after each 18 sec. Peptide fragmentation was carried out using LTQ settings (Min signal 2000, Isolation width 4, Normalized collision energy 35, Default Charge State 4 and Activation time 10 ms). MS/MS raw data files were processed via the Proteome Discoverer program Version 1.4 (Thermo Scientific, Darmstadt, Germany) on a Mascot server (V. 2.3.02, Matrix Science) using a *Pseudomonas aeruginosa* PAO1 database extracted from SwissProt. The following search parameters were used: enzyme, trypsin; maximum missed cleavages, 1; fixed modification: MMTS (C); variable modifications: oxidation (M), peptide tolerance, 10 ppm; MS/MS tolerance, 0.4 Da. The results were evaluated and quantified using Proteome Discoverer 1.4. The LC-MS/MS analysis was performed in cooperation with Dr. Josef Wissing (HZI, Braunschweig, Germany).

2.15 Insoluble protein composition determination

In order to assess whether potential interaction partners (found for the membrane baits) constituted specific interactions or rather an artifact derived from protein abundance in the cross-linked membrane fractions, *P. aeruginosa* PAO1 membranes were isolated and residing proteins solubilized as described before. Overall solubilized proteins were extracted following a previously described method (Wessel & Flugge, 1984) and thereby excess of detergent and remaining lipids were discarded. Four volumes methanol were added to 1 volume sample, mixed and incubated on ice for 15 min. Subsequently, 1 volume of chloroform was applied and samples incubated as in the previous step. Afterwards, 3 volumes of dH_2O were added and incubated likewise.

Samples were then centrifuged for 5 min at 9,000 x *g* at 4ºC. Upper and lower phases were withdrawn and 3 volumes of methanol added to wash the sample. Finally, samples were centrifuged at the same speed at 4ºC for 10 min and pellets dried to be immediately after resuspended in PBS buffer. Same protein concentrations as those ones employed before for the co-purifications were loaded into LC-MS/MS. Experiments were carried out in three independent replicates.

2.16 Nitrate and nitrite consumption rate determination

In order to measure the nitrate and nitrite reducing activity *in vivo* of the diverse *Pseudomonas* strains, a nitrate/nitrite colorimetric test was utilized (Roche, Penzberg, Germany). Samples were withdrawn and heated up to 95ºC in order to lyse the cell and release intracellular nitrate/nitrite. The test was performed following the manufacturer´s guidelines. Strains were grown in LB medium supplemented with 4.5 mM $NaNO_2$ or 50 mM KNO_3 initial concentration. Nitrate/Nitrite concentrations were quantified over 24 h and the intrinsic consumption rate determined. Consumption rates were expressed in mg/L*h. For the *in vitro* nitrate and nitrite reductase activities PAO1 *narG*, *nirS* and *norB* mutant strains as well as the wild type were grown aerobically in LB supplemented with 50 mM nitrate as described before, until an optical density of 0.8 was reached. Afterwards, cultures were shifted to anaerobic growth as previously specified. Cells were grown for 2 h in order to induce denitrification (Hartig & Zumft, 1999) and the pellet was collected by centrifuging at 4ºC for 20 min, at 4000 x *g*. Further work was carried out in anaerobic conditions in a glove box. Cells were washed twice in PBS buffer in order to get rid of the remaining nitrate and subsequently subjected to French Press for cell lysis as described before. One tablet of Protease Cocktail Inhibitor (Roche) was added per 10 ml of sample volume. Cell debris was removed by centrifugation at 4000 x *g* for 20 min, at 4ºC. Whole cell extracts were kept on ice while the nitrate activity measurements were being carried out. The nitrate assay is based on a described procedure, slightly modified (Bedzyk *et al.*, 1999). The reaction mixture was composed of 100 µl of the whole cell extract diluted into 500 µl dH_2O, 50 mM Potassium Phosphate buffer (pH 7.3), 500 µM of KNO_3 and 200 µM of methyl viologen. The reaction was initiated by adding 100 µl of fresh sodium dithionite solution (16 mg/ml) in 0.8% $NaHCO_3$.

For the *in vitro* nitrite consumption determination, the reaction mixture was composed of 100 µl cell extract diluted in 690 µl dH_2O, 50 mM Potassium Phosphate buffer (pH 7.3), 720 µM $NaNO_2$ and 100 µM NADH. The reaction was started by adding 10 µM of phenazine methosulfate. The reaction mixture was incubated at 37ºC for 1 hour and 100 µl samples were taken every after 1, 2, 5, 10, 15, 30 and 60 min. The reaction was terminated by diluting the withdrawn 100 µl-aliquot into 900 µl of NaOH solution (0.6 g/l). The reaction without cells was taken as a control and no variations in the nitrate concentration were observed. Nitrate and nitrite concentrations were determined by following the manufacturer´s instructions with the nitrate/nitrite colorimetric test (Roche).

2.17 Immunofluorescence

For immunofluorescence staining of flagella, bacteria were grown aerobically in swimming medium supplemented with 20 mM arginine to an OD_{578} of 1.0 and then switched to anaerobic growth (as described before) for 5 days. LB aerobic cultures were as well included as control. Samples were processed without washing and centrifugation steps to avoid possible damage of the flagellar structures. A drop (25 µL) of bacterial culture was placed on a glass coverslip and was fixed with 3% paraformaldehyde (PFA) in PBS for 30 min at room temperature. The coverslips were washed twice and fixed cells were permeabilized using PBS containing 0.01% Triton X-100 for 3 min. Fixed coverslips were rinsed twice after each immunostaining step with PBS. Samples were blocked in blocking buffer (10% FCS in PBS) for 1h at room temperature; this same buffer was used for the preparation of all the antibody solutions used. Coverslips were incubated with the primary rabbit polyclonal antibody (anti-FliC, anti-DnaK or both) for 1 h at room temperature. After washing, samples were incubated with the fluorescently labeled secondary antibody (goat anti-rabbit Alexa 488 or goat anti-rabbit Alexa 568, Life Technologies, Darmstadt, Germany). For the double staining with anti-FliC and anti-DnaK separate antibody incubations were performed. Anti-FliC was the first primary antibody used followed by goat anti-rabbit Alexa 488. After another blocking step, anti-DnaK was the second primary antibody used followed by goat anti-rabbit Alexa 568. Coverslips were mounted using ProLong Gold DAPI (Life Technologies, Darmstadt, Germany). Fluorescence images were obtained with an Axio Imager A1,

AxioCam MRm camara (Zeiss, Göttingen, Germany) and AxioVision Rel. 4.6 Software using AxioVision 4 Module Multichannel Fluorescence and Filters 49, 44 and 50. This work was performed in collaboration with Dr. Gabriella Molinari (HZI, Braunschweig, Germany).

2.18 Swimming motility assays

Swimming motility determination of the distinct strains was tested on swimming medium as described before (Rashid & Kornberg, 2000). Overnight cultures were settled from the following strains: PA14 wild-type, PA14 *nirS*, *nirS*$^{-}$/*nirS*$^{+}$, *nosZ*, *narH*, *norB*, *fliC* and *fliC*$^{-}$/*fliC*$^{+}$ in 1% w/v tryptone, 0.5% w/v NaCl, 0.3% w/v agarose (BD Biosciences, Heidelberg, Germany) and 20 mM L-arginine (Sigma-Aldrich, Munich, Germany) as energy source instead of nitrate to rule out negative interferences of this source on denitrifying enzyme mutants and therefore focus exclusively on swimming deficiencies associated to protein absence. Agar plates were point inoculated in the middle by stabbing with an overnight culture tip-soaked toothpick. Plates were placed in a chamber (Difco, VGD, Lawrence, USA) containing one piece of Anaerocult (Merck Millipore, Darmstadt, Germany) to generate anaerobic environment and oxygen-depletion was confirmed colorimetrically by an Anaerotest stripe (Merck Millipore, Darmstadt, Germany). The plates were faced up and incubated at 37ºC over 5 days. Swimming motility of the corresponding strains was determined by measuring the swimming halo diameter. Swimming plates were photographed in a dark box (DCscienceTec, Ontario. Canada).

2.19 NirS-FliC interacting domains determination

To investigate the peptides involved in the interaction between NirS and FliC, eluates obtained from PA14 *nirS*$^{-}$/*nirS*$^{+}$, PA14 *fliC*$^{-}$/*nirS*$^{+}$ and PA14 *nirS*$^{-}$/*fliC*$^{+}$ construct-containing cells, were digested by trypsin and analyzed by LC-MS/MS for complete peptide composition analysis. All bacteria used in this assay were grown in LB supplemented with nitrate anaerobically. First, NirS was purified in the *nirS* Tn mutant (PA14 *nirS*$^{-}$/*nirS*$^{+}$), afterwards NirS in the *fliC* mutant strain (PA14 *fliC*$^{-}$/*nirS*$^{+}$) and finally FliC in the *nirS* mutant (PA14 *nirS*$^{-}$/*fliC*$^{+}$). The purifications were carried out as described previously for periplasmic soluble proteins. All elutions were subsequently

subjected to tryptic digestion and MS analysis as formerly described. In the first scenario, NirS is expected to bind with FliC, but not in the second or the third one. In the first case, the lysines and arginines of NirS and FliC involved in their interaction remain inaccessible for tryptic digestion what is reflected in this set of peptides. In the second NirS purification, the NirS lysines and arginines responsible for NirS-FliC interaction are liberated due to the lack of FliC. In the last case, this effect takes place with the FliC lysines and arginines since NirS is devoid. Hence, once the three sets of peptides were analyzed, the interacting moieties for NirS-FliC interaction were determined comparing the peptides of NirS and FliC missing in the first sample which appeared in the second and third ones. These experiments were carried out in three separate replicates.

2.20 Optimization of *P. putida* KT2440 PHA production by metabolic engeneering

Metabolic engineered *P. putida* strains were employed for an enhancement of PHA production. The determination of genes which had to be deleted or overexpressed to lead to a higher PHA accumulation was conducted by *in silico* predictions.

2.20.1 PHA characterization and quantification

Composition analyses of the polymer produced and cellular PHA content concentration determination were performed by gas chromatography (GC) and MS of the methanolyzed polyester. For PHA production corresponding *P. putida* strains were streaked on LB agar plates and incubated for one day at 30°C. Single colonies were then picked from the plate, inoculated in a 50 mL shake flask containing 10 mL of the above described medium and incubated overnight under aerobic conditions at 30°C and 180 rpm (Innova, Enfield, USA). To begin the PHA accumulating process, 1 L baffled shake flasks containing 200 mL of culture medium were inoculated at an initial OD_{595} of 0.05 and incubated under aerobic conditions at 30°C for 50 h. Subsequently, 10 mL of the culture were centrifuged for 10 min at 4°C and 9,000 x *g*, followed by a washing step with dH_2O and lyophilization. Methanolysis was carried out by suspending 5 to 10 mg of lyophilized cell pellet in 2 mL of chloroform and 2 mL of methanol containing 15% sulfuric acid and 0.5 mg/mL 3-methylbenzoic acid as internal standard. Incubation

followed at 100°C for 4 h. After cooling, 1 mL of demineralized water was added. The organic phase containing the resulting methyl esters of the monomers of the polymers of interest were analyzed by GC-MS on a Varian GC-MS system 450GC/240MS ion trap mass spectrometer operated by the software MS Workstation 6.9.3 (Varian Inc., Agilent Technologies, Böblingen, Germany). For this purpose, 1 mL of the organic phase was injected into the gas chromatograph at a split ratio of 1:10. Separation of the analytes of interest (i.e. the methyl esters of 3-hydroxyexanoate, 3-hydroxyoctanoate, 3-hydroxydecanoate, 3-hydroxydodecanoate, 3-hydroxy-5-cis-dodecanoate, 3-hydroxytetradecanoate) was achieved by chromatography through a FactorFour VF-5 ms capillary column (30 m X 0.25 mm i.d. X 0.25 mm film thickness). Helium was used as carrier gas at a flow rate of 0.9 mL/min. The injector and transfer line temperature were 275°C and 300°C, respectively. The temperature program was: initial temperature 40°C for 2 min, then to 150°C at a rate of 5°C/min and finally 280°C at a rate of 10°C/min. Positive ions were obtained using electron ionization at 70 eV. The mass spectrum was generated by scanning ions of m/z 50 to m/z 650. The PHA content (%wt) was defined as the percentage of PHA in the CDW (Borrero-de Acuna *et al.*, 2014). This procedure was carried out in collaboration with Dr. Ignacio Poblete Castro (HZI, Braunschweig, Germany).

2.20.2 NADH and NADPH quantification

The intracellular NAD^+, NADH, $NADP^+$ and NADPH concentrations were measured employing an NADP/NADPH Colorimetric Quantitation Kit (Biovision, Abcam, UK). Crude cell lysates were obtained by undertaking various freeze-thaw lysis cycles. Cofactors concentrations were photometrically quantified by measuring colorimetric changes at 450 nm (Borrero-de Acuna *et al.*, 2014).

2.20.3 Transcriptome analysis via RNAseq

Isolation of total RNA from corresponding 10 mL *P. putida* culture was performed using the RNeasy kit (Qiagen, Venlo, Netherland), according to the instructions provided by the manufacturer. Briefly, ribosomal RNA removal was performed with the MICROExpress Bacterial RNA enrichment kit using the *Pseudomonas* module (Ambion, Life Technologies, Darmstadt, Germany) according to

the manufacturer's instructions. The RNA was fragmented to a median fragment size of 200 nt by sonication using Covaris Adaptive Focused Acoustics device (Covaris, LGC Genomics, Herts, UK Strand-specific cDNA libraries were generated by previous RNA-Adapter ligation and subsequent reverse transcription. Hereby the ligated 5′-RNA-Adapter contained one of 24 different 6 nt barcode sequences, which allowed multiplexing of several libraries in a single Illumina lane for sequencing. Up to 20 libraries were pooled and treated with duplex-specific nuclease (DSN) for additional rRNA removal. Sequencing was performed on an Illumina HiSeq generating single-end reads with a length of 50 base pairs. Computational analysis of the raw sequence data obtained in Illumina FASTQ-format was performed as described previously (Dotsch *et al.*, 2012). Mapping was performed using stampy, a short-read aligner that allows for gapped alignments (Lunter & Goodson, 2011) for quantification of gene expression. The reads per gene (rpg) values of all genes were calculated from the SAM output files. Testing for differential expression against KT2440 (four biological replicates) was performed with DESeq (Anders & Huber, 2010), an R software package that uses a statistical model based on the negative binomial distribution (Borrero-de Acuna *et al.*, 2014). This work was performed in cooperation with Agata Bielecka (HZI, Braunschweig, Germany).

3 Results and Discussion

3.1 Proteins mega-complexes of *P. aeruginosa* for energy generation and motility

The investigation of the biochemistry, physiology and genetics of bacterial metabolism focused during the last decades mainly on the structure and function of involved enzymes. Moreover, a detailed picture of the corresponding underlying gene regulatory circuits was obtained. However, the observed speed and accuracy of the investigated cellular processes suggest a fine-tuned interplay of involved components via transient, specific and regulated protein-protein interactions. Several examples exist for the interaction of various enzymes of a certain pathway for metabolic channeling, ensuring the necessary precision and speed of the coupled synthetic processes (Smith *et al.*, 2013, Baker *et al.*, 2012). For example solvent sensitive or toxic intermediates are further metabolized prior to their detrimental side activities. In contrast to the obvious cellular importance of outlined protein complex formations the current knowledge of the involved protein-protein interactions is only poor. Therefore, a combined genetic-biochemical-proteomic approach was undertaken in the framework of this thesis to determine the structure of mega-complexes involved in anaerobic energy generation and motility of *P. aeruginosa*. For this purpose assembly platform proteins were selected and employed as bait for the residual complex. The corresponding chromosome copy of the bait protein gene was replaced with a copy encoding a His-tagged counterpart. Appropriate conditions for this gene expression were chosen and protein interaction partners of the bait protein were fixed to the bait via *in vivo* cross-linking. Corresponding protein megacomplexes were isolated from cell-free extracts via affinity chromatography. Attached proteins were identified through proteomics. Enrichment of proteins via this procedure was determined against a background of the proteome of not treated cell-free extracts.

Focus was laid on the denitrification machinery of *P. aeruginosa*. The system was intensively studied at the biochemical and structural biology level. For example for all four involved enzyme systems (Nar, Nir, Nor and Nos) crystal structures were available (Hino *et al.*, 2012, Nurizzo *et al.*, 1997, Pomowski *et al.*, 2011).

In a second approach the cooperation of energy generation and flagella synthesis was studied.

3.2 Structure of the denitrification mega-complex of *P. aeruginosa*

Williams and coworkers proposed a model of the overall aerobic and anaerobic respiratory energy metabolism of *P. aeruginosa* (Williams *et al.*, 2007). Figure 17 illustrates a scenario for the participating electron donating at the top and the electron accepting counterparts at the bottom. Thus, the repertoire of expected protein partners in a supra-complex was set.

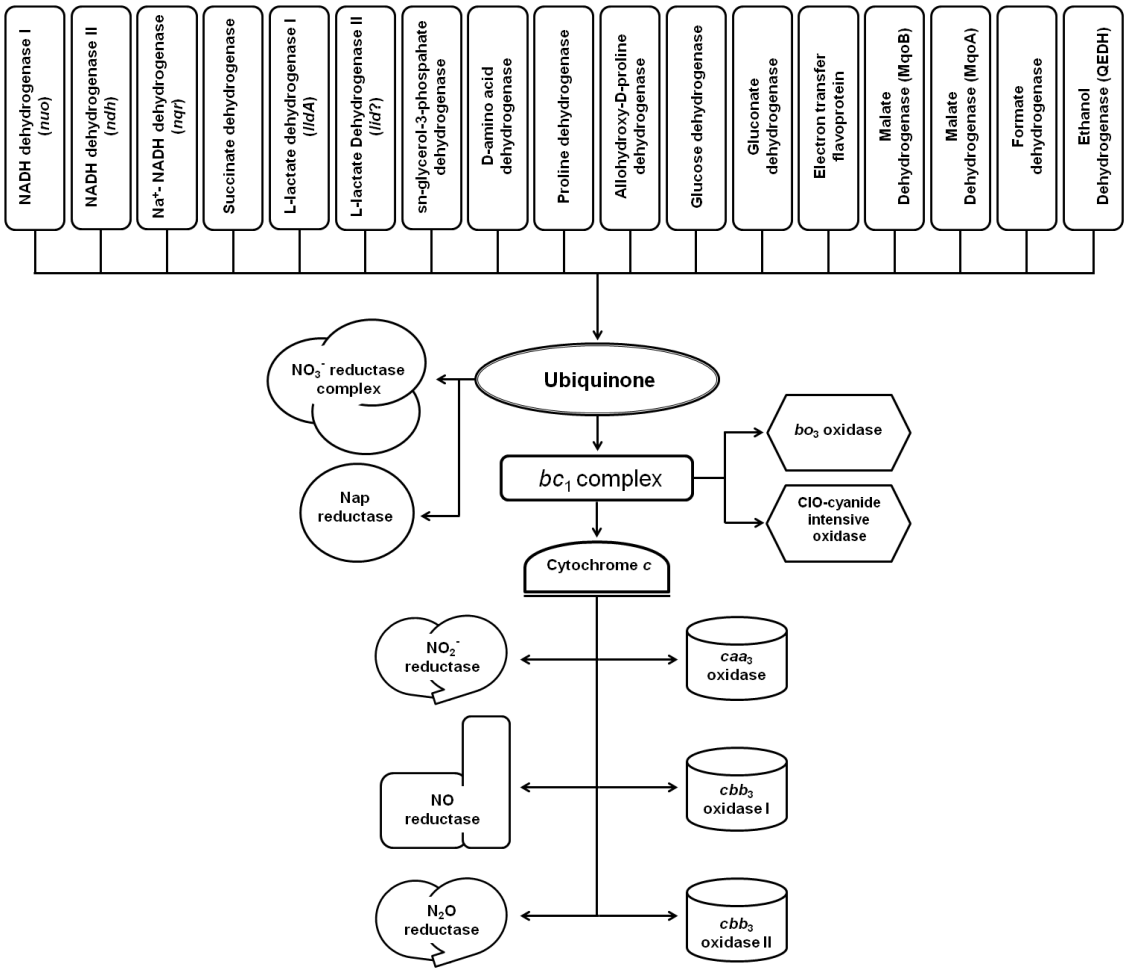

Figure 17. Proposed aerobic and anaerobic respiratory chains of *P. aeruginosa* based on the model by Williams, H.D. et al. (Williams *et al.*, 2007).

In order to investigate the process of the coordinated assembly of a complete respiratory machinery at the inner membrane of a bacterium, we chose the thoroughly investigated multi-enzyme system of anaerobic denitrification. The system consists of four multi-subunit, cofactor containing enzyme complexes (Nar, Nir, Nor and Nos) localized in the inner membrane and in the periplasm of the bacterium. Due to the toxic and the signaling characteristics of NO_2^- and NO, a tight channeling complex was expected. Additionally, proteins delivering the electrons to these enzymes, transporting the reaction intermediates, detoxifying detrimental radicals and regulating the overall process were expected to be part of the supra-molecular protein complex.

In order to visualize the protein network involved in these processes, an interactome approach previously described was employed (Ong & Mann, 2005, Lambert *et al.*, 2013). As outlined above, this approach utilizes chromatographically immobilized tagged proteins of a system of interest as baits to physically fish interaction partners and subsequently to identify their preys via proteomics techniques. Prior chromatographic co-purification potential protein complexes were stabilized via CL. Appropriate background controls were essential to the approach. For some of the found central protein-protein interactions control experiments via electron microscopy were realized, using antibodies and corresponding gold-labeling of potential interaction partners.

3.2.1 Mutants of *P. aeruginosa* nitric-oxide oxidoreductase genes *norCB* and of *nosR* revealed reduced nitrate and nitrite formation

For the selection of the initial bait proteins for our interactomic approach, our primary assumption was that the complex should somehow be stably localized, most likely anchored to the membrane, while proton gradient formation occurs, the ultimate goal of the process. Only NarI, NorB, NorC and NosR were confirmed as integral membrane proteins. In order to investigate the roles of the membrane proteins NorCB and NosR in the overall denitrifying process, the nitrate and nitrite consumption rates of the corresponding *P. aeruginosa* mutants were determined and compared to nitrate reductase (*narG*) and nitrite reductase (*nirS*) mutants. *P. aeruginosa* background mutant strains and the wild-type were grown anaerobically in LB supplemented with 50 mM KNO_3 for 24 h in rubber stoppered serum flasks. Every 2 h, culture samples were withdrawn and heated up to 95ºC to lyse the cells and release intracellular nitrate and

nitrite. Overall nitrate and nitrite concentrations were measured at each time point as specified by the manufacturer (Roche, Penzberg, Germany) and thereby a consumption rate of both molecules was determined for each strain (Figure 18).

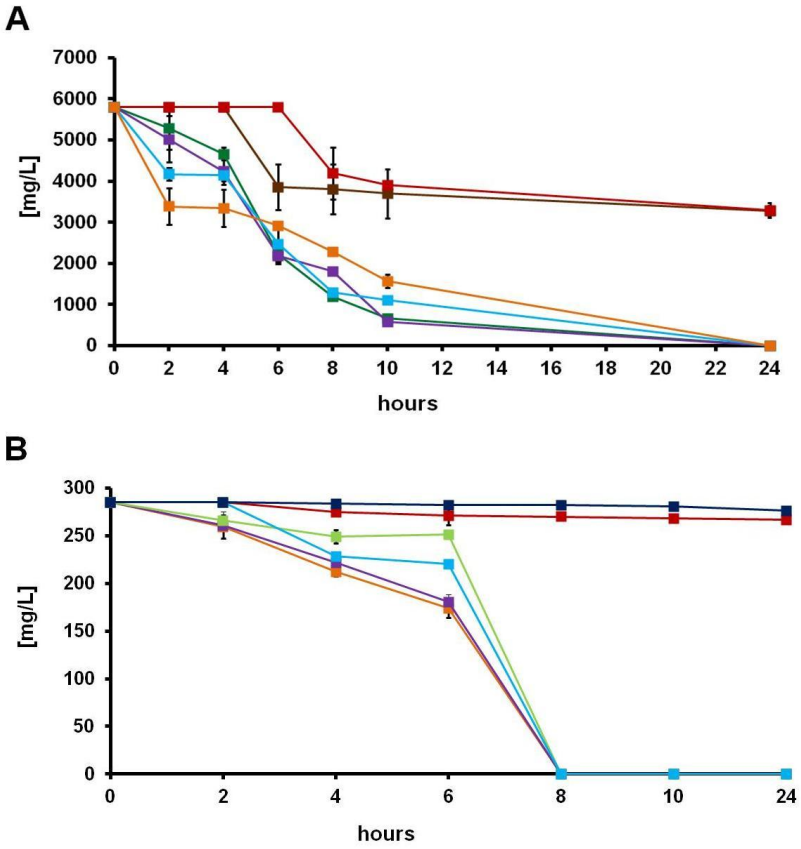

Figure 18. Nitrate and nitrite consumption *in vivo* of wild-type and PAO1 mutant strains with defect in denitrification enzymes. The nitrate (A) and nitrite (B) decay over 24 h was measured as described in Materials and Methods and the mg/L concentration at each time point (every 2 h) is depicted. In A) the results for PAO1 *narG* (brown), *norB* (red), *norC* (green), *nosZ* (purple), *nosR* (light blue) mutants and wild-type (orange) are shown. In B) the results for PAO1 *nirS* (navy blue), *nosR* (light blue), *norB* (red), *norC* (green), *nosZ* (purple) mutants and the wild-type (orange) are shown.

Surprisingly, the nitric-oxide reductase mutant *norB* failed to convert nitrate into nitrite to similar extent as detected for the nitrate reductase *narG* mutant. Again, the *norB* mutant failed to reduce nitrite to a similar extent as the nitrite reductase mutant *nirS*. Interestingly, *norC* and *nosR* mutants showed significantly reduced nitrite reduction capacity. Since NorCB and NosR are not enzymatically involved in nitrate and nitrite reduction, an important alternative contribution to the overall denitrification

process was deduced. Therefore, we tested NorCB and NosR for their function in denitrification supra-complex formation.

Furthermore, the nitrate and nitrite consumption rates were determined in the whole cell extract for the wild-type, *narG* and *norB* mutants for the first case and for the wild-type, *nirS* and *norB* mutants for the second case (Figure 19).

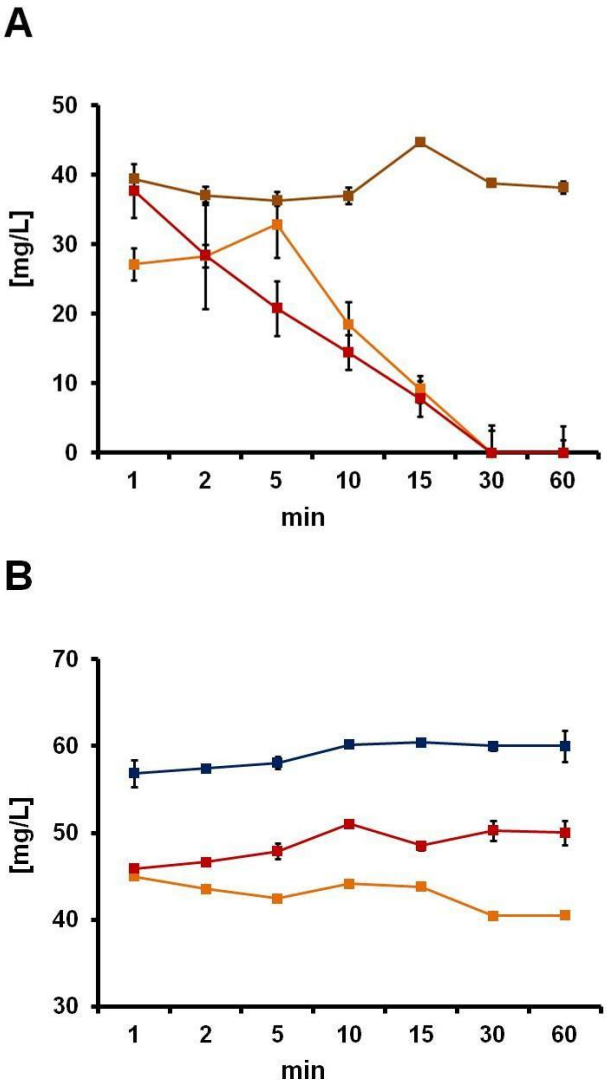

Figure 19. Nitrate and nitrite consumption *in vitro* of wild-type and PAO1 mutant strains with defect in denitrification enzymes. The nitrate (A) and nitrite (B) decay over 60 min was measured as described in Materials and Methods and the mg/L concentration at each time point is depicted. In A) the results for PAO1 *narG* (brown), *norB* (red) and wild-type (orange) are shown. In B) the results for PAO1 *nirS* (navy blue), *norB* (red) and wild-type (orange) are shown.

As shown above, the *norB* mutant free-cell extract presented a positive nitrate reducing activity (similar to the wild-type) when compared to the *narG* mutant strain which was deficient reducing nitrate. On the other hand the *norB* mutant free-cell seemed to have low nitrite reducing activity.

In conclusion, these results indicate that NorB must be present *in vivo* for the proper assembly of the denitrification machinery since the nitrate reducing activity of this mutant is almost abolished, but it contains a functional nitrate reductase that conducts its activity as observed *in vitro*. It is possible that norB mutants do not produce enough nitrite reductase. Hence, a deficient nitrite reducing activity is observed *in vivo* and *in vitro*.

3.2.2 Interactomic studies using *P. aeruginosa* NosR, NorC and NorB as bait proteins

For the determination of the denitrification mega-complex interactome, recombinant *P. aeruginosa* strains were incubated for 8 h under denitrifying conditions. The recombinant strains PAO1 $nosR^-/nosR^+$ producing His-tagged NosR in a *nosR* deficient background, PAO1 PAO1 $norC^-/norC^+$ producing His-tagged NorC in a *norC* deficient background and PAO1 $norB^-/norB^+$ producing His-tagged NorB in a *norB* deficient background were analyzed in comparison to the PAO1 wild-type harboring the control vector pAS40. Stabilization of the formed protein complexes was accomplished by formaldehyde treatment of the cells prior to AP. Cells were harvested, disrupted and His-tagged bait proteins were subjected to affinity-chromatography. First, protein eluates from the affinity material were TCA-precipitated and evaluated by SDS-PAGE (Figure 20).

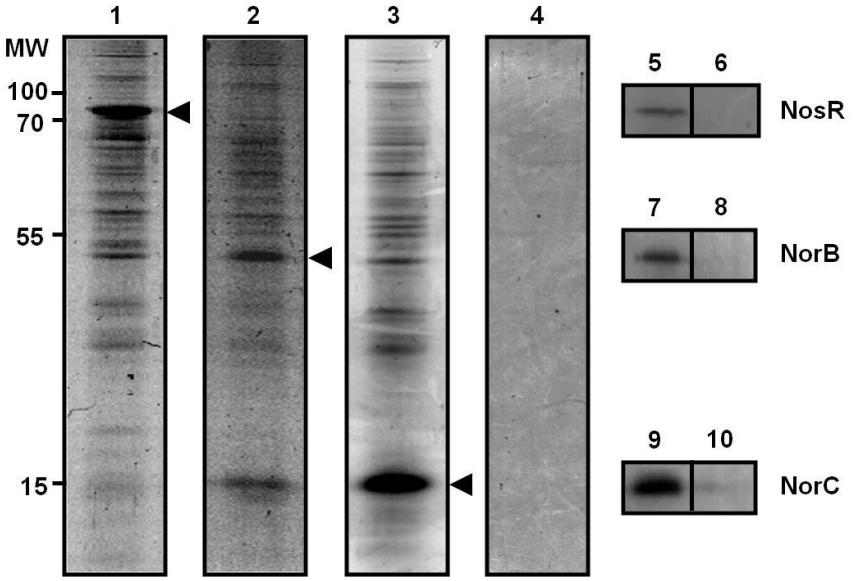

Figure 20. Interactomics using NosR, NorC and NorB as bait proteins revealing multiple interaction partners. Affinity co-purified proteins resolved on an SDS-PAGE gel and Western blot analysis of the bait-preys complexes of NosR, NorC and NorB. A) NosR-His_{6x} fusion protein and its prey proteins co-purification, B) NorB-His_{6x} fusion protein and its prey proteins co-purification, C) NorC-His_{6x} fusion protein and its prey proteins co-purification, D) PAO1 carrying pAS40 served as a control, E) Western blot analysis of NosR-His_{6x} fusion protein, F) Western blot analysis of wild-type PAO1 carrying pAS40 as control, G) Western blot analysis of NorB-His_{6x} fusion protein, H) wild-type PAO1 carrying pAS40 as control, I) Western blot analysis of NorC-His_{6x} fusion protein, J) wild-type PAO1 carrying pAS40 as control. The anti-His_{6x} immunodetection was performed using alkaline phosphatase coupled anti-mouse secondary antibodies with the corresponding chromogenic reaction. The recombinant strains PAO1 *nosR*$^-$/*nosR*$^+$ (A and E), PAO1 *norB*$^-$/*norB*$^+$ (B and G) and PAO1 *norC*$^-$/*norC*$^+$ (C and I) were subjected to the outlined interactomic studies. The relative molecular weights are indicated (left). The arrows indicate the presence of the bait fusion proteins NosR-His_{6x} (A), NorB-His_{6x} (B) and NorC-His_{6x} (C) as further confirmed by Western blot (E, G and I).

The purification of the His-tagged proteins yielded sufficient protein concentrations (0.1-0.5 mg/mL) for the determination of bound protein partners. The NosR-His_{6x} eluates revealed a protein with a relative molecular mass of approximately 80,000 +/- 5,000 as a major component that was identified as NosR-His_{6x} by immunoblot detection (see Figure 20). The SDS-PAGE showed a number of additional protein bands visible above and below the NosR-His_{6x} representing potential interaction partners. Likewise, NorC-His_{6x} and NorB-His_{6x} eluates contained prominent proteins which were identified as NorC-His_{6x} and NorB-His_{6x}, respectively. Again several potential interaction partners

were observed (see Figure 20). As expected control reactions with PAO1 carrying the control vector failed to co-purify additional proteins as documented by SDS-PAGE (Figure 20).

Next, the various eluates were subjected to a proteomics approach and analyzed by LC-MS/MS. The protein abundance index (xPAI) was attributed to each protein of the sample mixture as explained in Materials and Methods section and an "area value" was deduced. A proteomic analysis of all cell-free extracts from identically grown *P. aeruginosa* cell, however, without further enrichment procedure served as background (protein natural abundance determined). A list of potential interaction partners harboring an area value was generated for each bait. The percentage of interactors belonging to each area value range (i.e. 10^9, 10^8, etc) was plotted against the protein abundance (Figure 21). Standard deviations were calculated from the biological triplicates. In Figure 21A all potential protein interaction partners were graphed. Interaction partners exclusively involved in denitrification were extracted and are shown in Figure 21B.

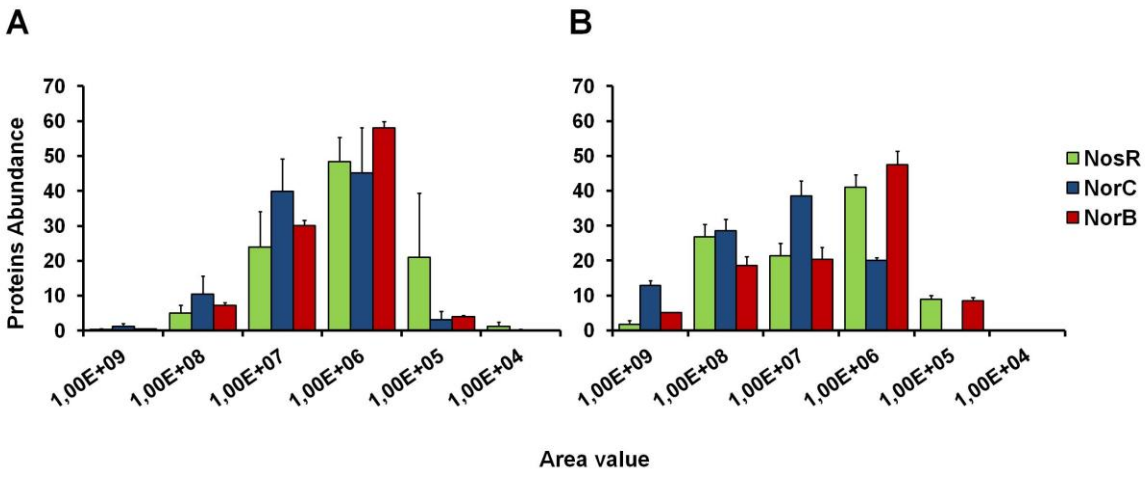

Figure 21. Identified interaction partners of NosR, NorC and NorB without (A) and with (B) relation to the process of denitrification. A) Graph representing the area value distribution of detected interaction partners (overall) encountered after the outlined co-purification procedure. B) Potential interaction partners involved in denitrification. Percentage of proteins (Y axis) is plotted against the area value (X axis). The area value is a quantitative indication. The distributions of the preys of NosR, NorC and NorB are illustrated in this plot in triplicates with the corresponding area value averages and standard deviations.

As shown in Figure 21, most of the protein interaction partners were detected at the area range of 10^6 - 10^7. We concluded that high affinity interaction partners belong to the area value ranges of 10^8 - 10^9. Abundant proteins of an average bacterial cell, such as chaperones and translation elongation factors, were encountered within the area value range of 10^6. Therefore, proteins within higher area values were considered specific and interaction partners below 10^6 area value were not further considered throughout this study. Obtained candidate proteins were separated into the categories of "denitrification related proteins" and "other proteins", as shown in two tables and described in two different chapters.

As our focus was on protein-protein interactions involved in the denitrification pathway, a condensed list of corresponding proteins were analyzed separately and integrated in a box-plot (Figure 22).

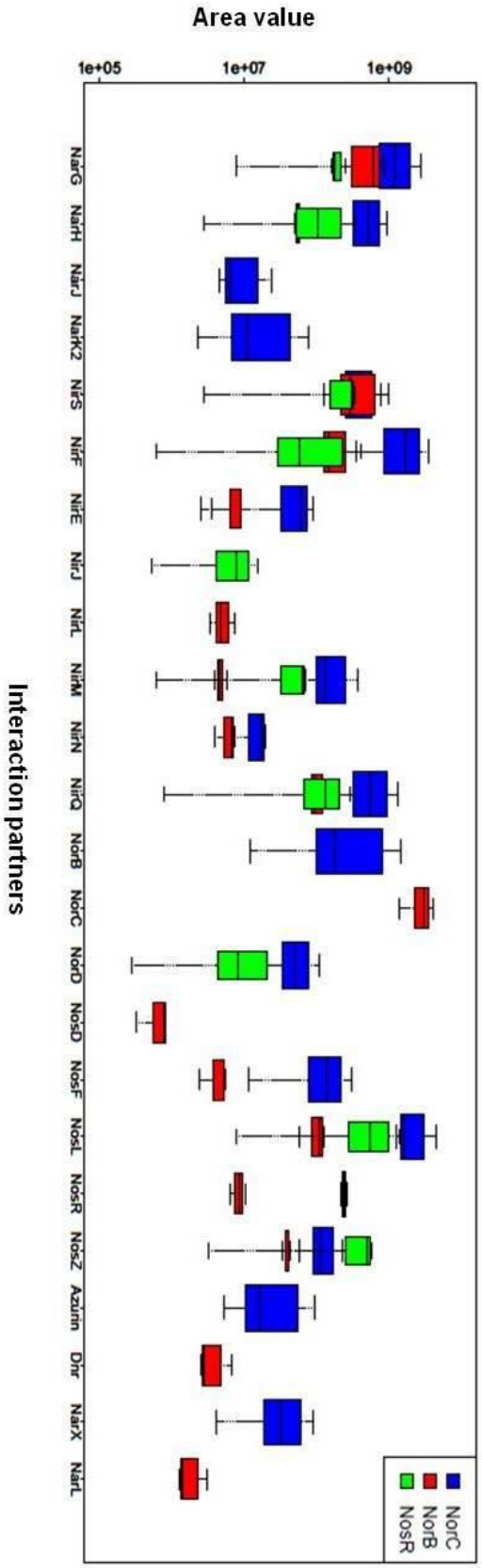

Figure 22. Detailed quantitative analysis of protein interaction partners for NorB, NorC and NosR involved in denitrification. Box-plot representing interaction partners

found for NorC (blue), NorB (red) and NosR (green) plotted against corresponding area value. Only protein-protein interactions partners found reproducibly are depicted. Boxes height represents the difference between the first and the third quartiles of the values enclosing the 50% of the data. Lines extending vertically (whiskers) denote maximal and minimal values encountered. The median (second quartile) is presented as a black band within the boxes. The area value (Y axis) is given in logarithmic scale. The protein-protein interactions interaction partners are shown in the X axis. This plot was generated with the R program.

As shown in Figure 22, most of the interaction partners involved in denitrification found for NorB, were also encountered in NorC eluates, what is in concordance with the dimeric structure of the enzyme. NorC revealed the largest number of protein partners what is in agreement with its dominant periplasmic surface, in contrast to the small periplasmic surface of NorB and NosR (Hino *et al.*, 2012). The majority of the proteins related to denitrification that interacted with one of these baits did it with an area value of 10^7, what is an indication of high specific protein-protein interactions. NorC, NorB and NosR shared several partners what is the first evidence on a tight supra-complex anchored to these membrane proteins.

3.2.3 The nitric-oxide reductase NorCB represents the major assembly platform protein for the denitrification assembly supra-complex

The area values of the potential interaction partners were divided by their own area value registered for the cell-free extract proteome control giving rise to the fold-change enrichment factor for these proteins. This enrichment factor is a direct sign of the specficicity of the interaction over general protein abundance. The higher this enrichment factor was, the more specific the interaction was considered. The fold-change is therefore a factor which is shown in the following tables as a reference of protein-protein interactions specificity.

Crystal structures of the heterodimeric nitric-oxide reductase revealed that subunit B forms a tight complex with its second subunit C. In agreement, our interatomics approach showed the strongest interaction of NorB with NorC and *vice versa*, providing a proof of principle to our approach (Table 21). Overall, found interactions to the majority of the detected proteins for NorC were significantly stronger compared to NorB with only a few exceptions. Most likely, this is due the NorCB

structural arrangement where most of the subunit NorC surfaces towards the periplasm. Alternatively, simple differences in the solubility properties between NorB and NorC during the experimental approach might explain the obtained results. The differences in the affinity of NorB (bait) for NorC (prey) of 10 and NorC (bait) for NorB (prey) of 435 might argue for this assumption. The majority of strongly bound prey proteins were associated to NorC and to a similar but weaker degree to NorB. This identified the nitric-oxide reductase NorCB as the major membrane-anchored platform for the denitrification supra-complex. In the following, the interactions of other enzyme systems related to denitrification with NorCB are outlined.

Table 21. Interaction partners from the denitrification pathway for NosR, NorC and NorB identified by proteomics and immunogold co-localization by electron microscopy.

PA Nº	Interaction Partners	NorB	NorC	NosR	NarH	NosZ
PA4292	Azurin	ND	0.6	ND		
PA0527	Transcriptional regulator Dnr	∞	ND	ND		
PA3875	Respiratory nitrate reductase alpha chain NarG	0.98	**7.08**	2.46		
PA3874	Respiratory nitrate reductase beta chain NarH	1.26	**12.06** ++	3.41 ++	-	++
PA3873	Respiratory nitrate reductase delta chain NarJ	ND	∞	ND		
PA3876	Nitrite extrusion protein NarK2	ND	**3.11**	ND		
PA3879	Two-component response regulator NarL	∞	ND	ND		
PA3878	Two-component sensor NarX	ND	∞	ND		
PA0510	Uroporphyrin-III *c*-methyltransferase NirE	∞	∞	ND		
PA0516	Heme d_1 biosynthesis protein NirF	**18.89**	**163.94**	**14.42**		
PA0511	Heme d_1 biosynthesis protein NirJ	ND	ND	∞		
PA0514	Heme d_1 biosynthesis protein NirL	∞	ND	ND		
PA0518	Cytochrome c_{551} NirM	0.11	**4.17**	1.00		
PA0509	Putative *c*-type cytochrome NirN	0.96	2.27	ND		
PA0520	Regulatory protein NirQ	1.75	**10.54**	2.26		
PA0519	Nitrite reductase NirS	2.17	1.97 +++	0.98 ++	++	+++
PA0524	Nitric-oxide reductase subunit B NorB		**435.73**	ND		

PA Nº	Interaction Partners	NorB	NorC	NosR	NarH	NosZ
PA0523	Nitric-oxide reductase subunit C NorC	**10.61**		ND ++	++	+++
PA0525	Probable denitrification protein NorD	ND	**15.73**	3.81		
PA3393	NosD protein	∞	ND	ND		
PA3394	NosF protein	∞	∞	ND		
PA3396	NosL protein	2.82	**68.91**	**18.65**		
PA3391	Regulatory protein NosR	1.91	**52.88** ++		++	+++
PA3392	Nitrous oxide reductase NosZ	0.77	2.61 +++	**7.11** +++	++	-

The proteomic data reveals the enrichment of proteins in the co-purification using NorB, NorC and NosR as bait expressed as protein abundance (area value) in comparison to the appropriate experiment control. Each number represents the average area of the protein in the bait-preys co-purifications versus the average area of the protein in the control experiment. ND = proteins not reproducibly detected as prey. ∞ = proteins detected as a prey but not found in the control. ++ = found interacting specifically with the bait in the double immunogold labeling experiments. +++ = found interacting **very** tightly with the bait in the double immunogold labeling experiments. Values shown in bolt correspond to the proteins with often detected interactions in the co-purification experiments. PA accession numbers are shown.

The following chapters discuss the involvement of the interaction partners identified as key players in the supra-complex via an interactomics approach.

3.2.4 Nitrate reductase NarGHI is attached to the denitrification supra-complex via interaction to NorCB

Cytoplasmic oriented nitrate reductase subunits NarG and NarH strongly interact with NorB and NorC, obviously causing the fixation of the initial enzyme to the denitrification supra-complex (Table 21). Interestingly, no detectable interaction with the periplasmic nitrate reductase NapAB was observed. In agreement, only the *narGHI* operon and not the *nap* operon is co-regulated with the expression of the other denitrification genes (Schreiber *et al.*, 2007).

3.2.5 The nitrate/nitrite antiporter NarK2 is integrated into the denitrification complex via interaction with NorC

Respiratory nitrate reductase NarGHI reduces nitrate to nitrite with its cytoplasmic subunit NarG. The succeeding nitrite to NO reduction catalyzed by NirS occurs in the periplasm. Consequently, toxic nitrate has to be transported into the

cytoplasm and cytotoxic nitrite has to be returned into the periplasm without further exposure to cytoplasmic components. Therefore, the integration of the observed nitrate/nitrite antiporter $NarK_2$ via interaction with NorC (Table 21) into the supra-complex seems to be logical (Sharma *et al.*, 2006).

3.2.6 Attachment of the nitrite reductase NirS and its maturation apparatus to NorCB

Interestingly, the interaction of NorBC to nitrite reductase NirS was visible, but not of strong nature. The strongest interaction of NorCB (bait) for an isolated prey protein was detected for NirF, the last enzyme in heme d_1 synthesis and insertion, a unique cofactor of sulfite and nitrite reductases (Nicke *et al.*, 2013). NirF is a periplasmic, membrane attached lipoprotein. For the final insertion of heme d_1 into NirS, the system uses NirN, a structural homologue of NirS without nitrite reductase activity. NirS, NirF and NirN form a stable complex during nitrate reductase maturation (Nicke *et al*., 2013). In agreement, protein interactions of NorB and NorC with NirN were also detected (Table 21). Furthermore, strong interactions of the *c*-type cytochrome NirM, serving as electron donor system for the nitrite reductase (Hasegawa *et al*., 2001), mainly to NorC was detected (Table 21). Additionally, strong interaction of NorC to the ATP-binding protein NirQ was found (Table 21). Accordingly, deletion of the *nirQ* gene resulted in the simultaneous loss of nitrite and NO reduction in *P. aeruginosa*, *P. stutzeri* and *Paracoccus denitrificans* (Jüngst and Zumft, 1992, Hayashi *et al*., 1998). Posttranslational enhancement of nitrite and nitric-oxide reducase activitiy was observed for *P. aeruginosa* NirQ and analogously for the NirQ homologue CbbQ for the posttranslational activation of 1, 5 bisphosphate carboxylase/oxygenase (Hayashi *et al.*, 2000). Our observation nicely contributes to the overall posttranslational maturation function of both enzymes including the observed *nirQ* deletion phenotype. NirQ might fulfill its function as nitrite and nitric-oxide reductase specific assembly factor.

The nitrite reductase NirS itself showed stronger interaction to NorB than to NorC. Our electron microscopy approach confirmed the NirS-NorC interaction. In conclusion, the nitrite reductase NirS is obviously bound via NirF to the denitrification supra-complex, while the electron donor system NirM and the enzyme maturation machinery NirN - NirF - NirQ interacting with NirS are attached directly to NorC.

3.2.7 Electron transferring blue copper protein azurin is bound to the supra-complex via NorC

The cytochrome c_{551} NirM, the electron donor of nitrite reductase NirS, forms a tight complex with azurin (Santini *et al.*, 2014). The NirM and NirC cytochromes strongly bind to the nitrite reductase NirS. Their location in the periplasm has been shown previously. NirM and NirC are reduced by azurin. The NirS heme *c* receives the electron from these two cytochromes *c* and passes it to the heme d_1 (Hasegawa *et al.*, 2001b). Consistently, NorC strongly interacts either with NirM or with azurin. Consequently, we demonstrate that NorC is crucial for the proper electron transfer to NirS. This might explain the inability of NorB and NorC deficient strains to convert nitrite into NO (see 3.1.2).

3.2.8 NosR is the third denitrification supra-complex assembly platform protein

Deletion of the *nosR* gene for the third integral membrane protein of the denitrification machinery besides NorCB caused a significant failure of the denitrification (Figure 18). To understand this pleiotropic phenotype the contribution of NosR to denitrification supra-complex formation was tested.

Originally, NosR was discovered as a component necessary for the expression of the nitrous reductase (Cuypers *et al.*, 1992). *P. sturtzeri* NosR is a polytopic membrane protein found required for the formation of the N_2O reductase NosZ. However, NosZ purified from a *nosR* deficient background revealed N_2O activity *in vitro* (Wunsch & Zumft, 2005). NosR is an iron-sulfur flavoprotein with its flavin cofactor directed towards the periplasm and the redox centers towards the cytoplasm. The exact biochemical function of the protein is currently unknown. Zumft and coworkers suggested NosR function to be involved in the maturation of the NosZ copper-site (Wunsch and Zumft, 2005). Here, we demonstrated the physical interaction of multiple periplasmic and others proteins of the apparatus with the transmembrane protein NosR as the major logistic support player of the assembly platform for the denitrification supra-complex.

3.2.9 Nitrous oxide reductase NosZ and the assembly protein NosL are integrated via interaction with NosR into the supra-complex

As outlined above, NosR was found strongly attached via NorC to the NorCB platform which in turn showed strong interactions with nitrate and nitrite reductase systems. In agreement NosR significantly co-localized with NorC in the double immunogold experiments. Moreover, strong interactions to NarG and NarH of nitrate reductase as well as to NirF, NirQ, NirS and NirM of nitrite reductase were observed, indicating a tightly bound complex at the NorCB-NosR platform. Most importantly, further major contacts were observed to the N_2O reductase NosZ (Table 21). In contrast to the previous findings for the other enzymes of denitrification, the NorCB platform only revealed weak interactions to NosZ. Clearly, NosZ is attached via NosR to the denitrification supra-complex. The nitrous oxide reductase NosZ is a homodimeric metalloprotein containing two unusual Cu-centers, CuA as binuclear, valence-delocalized cluster and CuZ as a tetranuclear active site center. Catalysis is performed by bottle centers (Schneider *et al.*, 2014). Obviously, these centers require additional proteins for maturation. Multiple proteins encoded by the *nosDFYLtat*E operon were proposed to be involved in this process (Honisch & Zumft, 2003). We detected strong protein interactions of NosL with NorC and NosR.

Achromobacter cycloclastes NosL was identified as a copper-binding protein (McGuirl *et al.*, 2001). The protein contains a putative lipobox, a signal peptide that targets the protein for translocation through the inner membrane, followed by cleavage of the signal leader sequence and amino-acylation of the N-terminal cysteine to diacylglycerol (Narita *et al.*, 2004). NosL is most likely shuttled through the periplasm where the resulting anchor tethers the protein to the outer membrane. NMR analysis of NosL identified the structural homology to MerB, an organomercury lyase involved in bacterial mercury resistance (Schaefer *et al.*, 2004), sustaining a potential role as a copper chaperone (Taubner *et al.*, 2006). However, in *P. stutzeri* only NosD, NosF, NosR and NosY were found to be essential for active nitrous oxide formation *in vivo* (Wunsch *et al.*, 2003).

3.2.10 Immunogold labeling for co-localization of NosR and the 4 reductases of the denitrification pathway in *P. aeruginosa*

To reconfirm some of the major observed protein-protein interactions with a second, independent method co-localization studies using antibody-labelled proteins and electron microscopy were performed. Antibodies specific for NarH, NirS, NorC, NosZ and NosR were raised as described in Materials and Methods section. Due to the large domains of these proteins embeeded in the inner membrane, the selection of peptides for the antibodies generation was rather difficult. Only the soluble parts of the proteins could be chosen (in order to prevent complete failure of labeling since transmembrane domains cannot be accessed by the antibodies). To determine whether these proteins co-localize in *P. aeruginosa*, indicating their interaction, cells were fixated and double immunogold labeling was performed matching all possible combinations. As can be deduced from quantitative data from the double labeling studies (Table 22) it is obvious that all the enzymes localized as an integral protein in the cytoplasmic membrane and in the periplasm show a higher percentage of co-localization events, well above 1, when compared with proteins separated by the cytoplasmic membrane, average of co-localization well under 1.

Table 22. Quantification of double labeling studies.

Figure 23	**Interaction**	**Average in 20 cells**	**Average in 20 cells**	**Total N° co-localization in 20 cells**	**Average co-localization in 20 cells**
		PAG 15	**PAG 10**		
A	NarH-NirS	NarH	NirS		
		3	1.95	3	0.15
B	NarH-NorC	NarH	NorC		
		7.5	4.8	14	0.7
C	NorC - NirS	NorC	NirS		
		8.35	3.65	25	1.25
D	NosZ-NirS	NosZ	NirS		
		8.6	4.6	25	1.25
E	NosR - NorC	NosR	NorC		
		9.95	2.7	17	0.85
F	NosZ-NosR	NosZ	NosR		
		7.45	4.4	20	1.7
G	NosZ-NarH	NosZ	NarH		
		8.25	3	12	0.6
H	NarH - NosR	NarH	NosR		
		6.05	3.15	12	0.6
I	NosZ - NorC	NosZ	NorC		
		10.5	7.2	36	1.8
J	NosR-NirS	NosR	NirS		
		8.05	3.55	22	1.1

For 20 longitudinal sections with approximately the same area large and small gold-particles as well as co-localization events in those cells were counted. The average co-localization value was then calculated for the 20 cells.

Thus, NosZ-NirS, NorC-NirS, NosZ-NorC and NosZ-NosR double immunogold labeling occurred to present a higher number of events of co-localization, whereas NarH-NirS, NarH-NosZ, NarH-NorC, NosR-NirS, NarH-NosR and NorC-NosR presented a reduced number of co-localizations (Figure 23). These results are in concordance with the AP-QMS data. Regarding these results, it is observed that denitrification elements seem to be close in proximity forming a complex scaffold. Taking into account that the generated antibodies were directed against only short-length hydrophilic loop peptides of the respective NosR, NorBC proteins, the incidents of co-localization within the *P. aeruginosa* cells are to be evaluated as significant. An important aspect to be considered is that proteins more distant in denitrification in regard to the reduction step that they carry out (for instance the nitrate reductase and the nitrous-oxide reductase) might be as well located more separately. If a chain of reactions is presumed, the proteins involved in intermediate steps (NirS and NorCB) might be in the middle and the distance between the gold particles of NarH and NosZ could correspond to the sum of the two other protein sizes in nm.

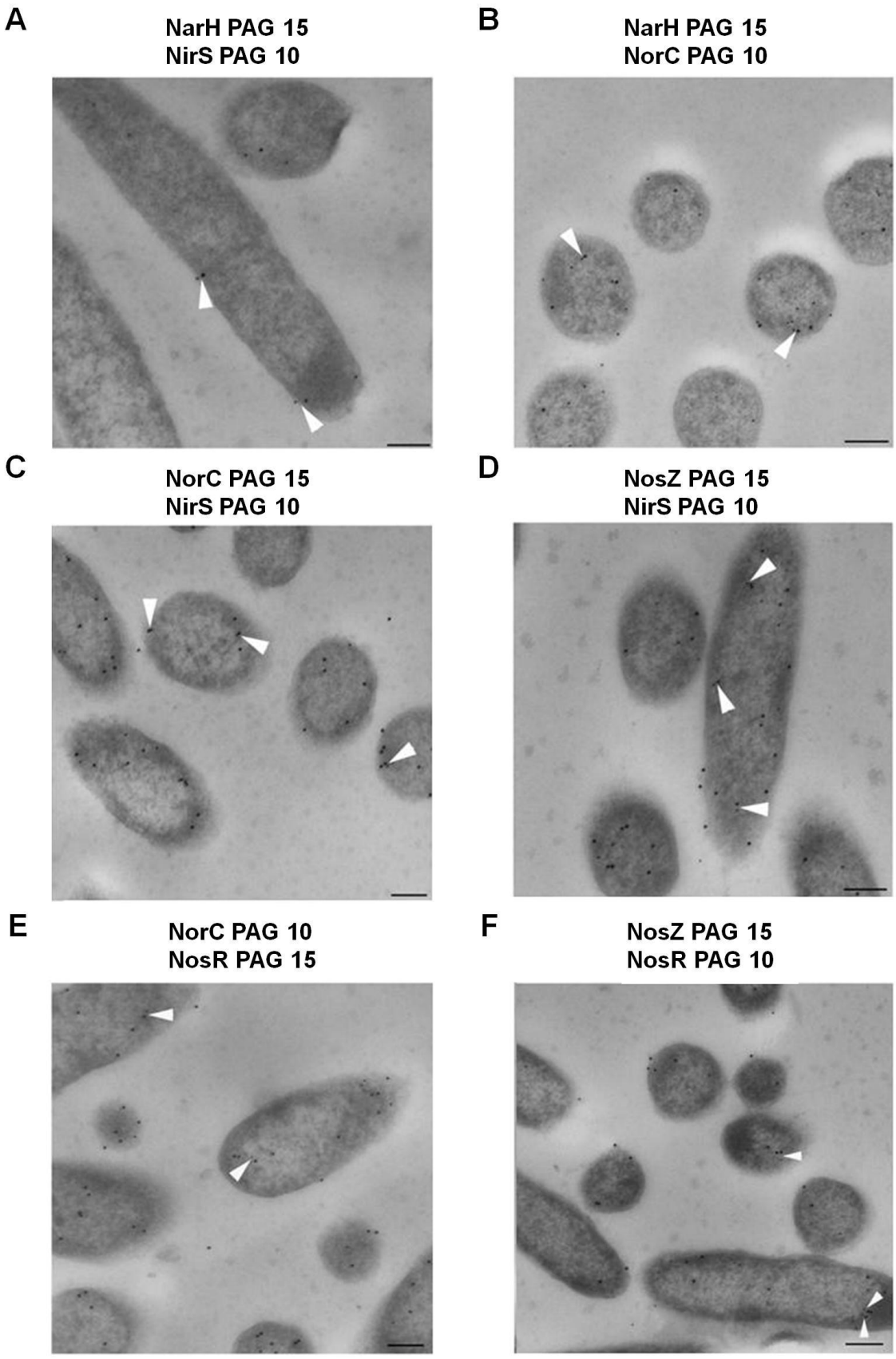
A
NarH PAG 15
NirS PAG 10
B
NarH PAG 15
NorC PAG 10
C
NorC PAG 15
NirS PAG 10
D
NosZ PAG 15
NirS PAG 10
E
NorC PAG 10
NosR PAG 15
F
NosZ PAG 15
NosR PAG 10

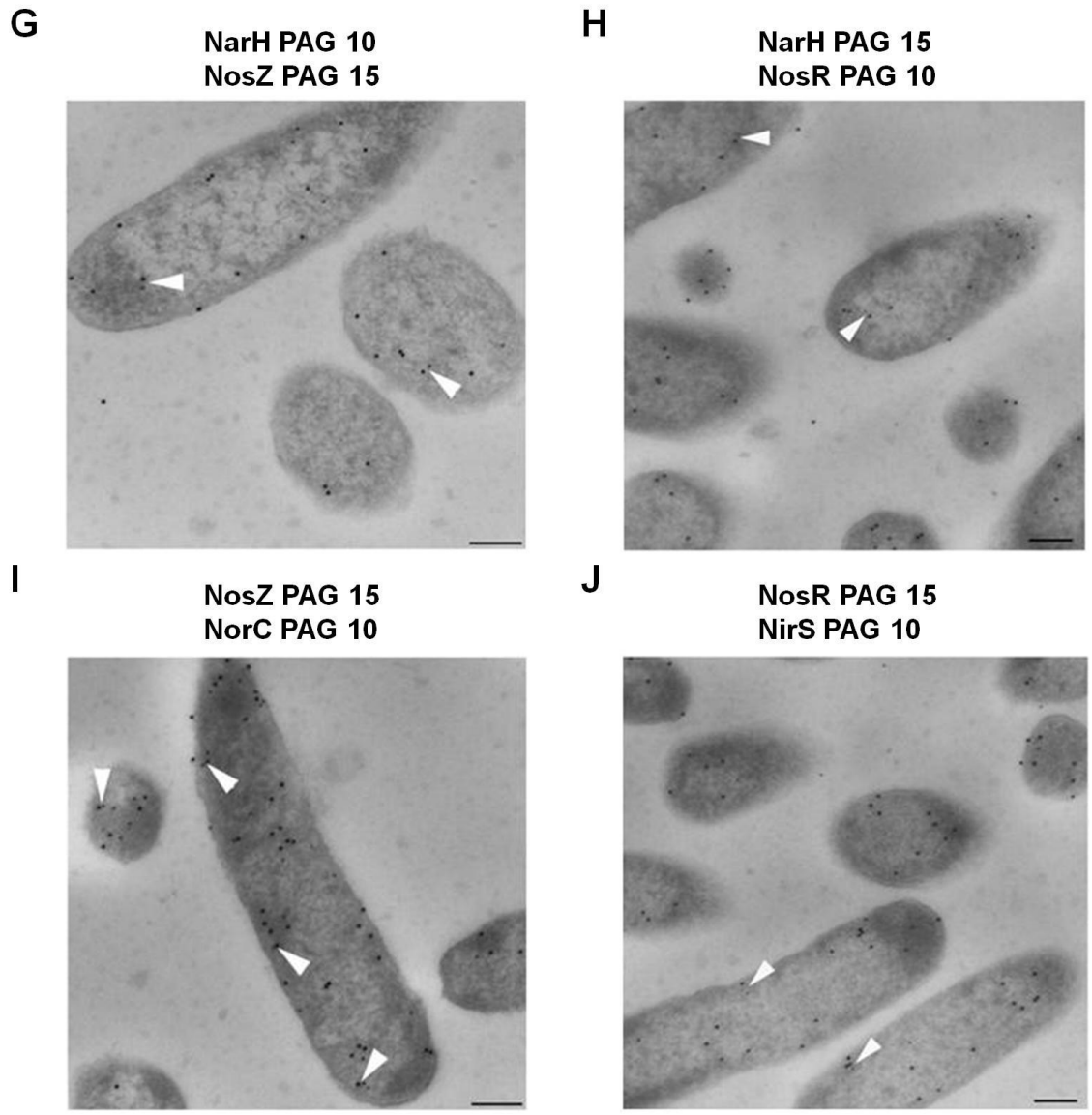

Figure 23. Double Immunogold labeling of NosR, NarH, NirS, NorC and NosZ to determine their co-localization in *P. aeruginosa* cells. Names shown above illustrate the proteins that were immunogold labeled and tested. Numbers aside each protein represent the gold particle size employed for each labeling. Bars size corresponds to 200 nm. Arrows indicate co-localized proteins only if the distance between both were less than 25 nm. Double immunogold co-localization of NarH-NirS (A), NarH-NorC (B), NorC-NirS (C), NosZ-NirS (D), NorC-NosR (E), NosZ-NosR (F), NarH-NosZ (G), NarH-NosR (H), NosZ-NorC (I) and NosR-NirS (J) were carried out.

These outcomes are in concordance with the proteomics data. It was observed that the components of the denitrification machinery seemed to be close in proximity forming a complex scaffold. Taking into account that the generated antibodies were directed against only short-length hydrophilic loop peptides of the respective NosR, NorCB

proteins, the incidents of co-localization within the *P. aeruginosa* cells were evaluated as significant. An important aspect to be considered is that proteins more distant in denitrification in regard to the reduction step that they carry out (for instance the nitrate reductase and the nitrous oxide reductase) might be as well located more separately. If a chain of reactions is presumed, the proteins involved in intermediate steps (NirS and NorCB) might be in the middle and the distance between the gold particles of NarH and NosZ could correspond to the sum of the two other proteins size in nm. A schematic view of the denitrification supra-complex elucidated by two different methods is represented in Figure 24.

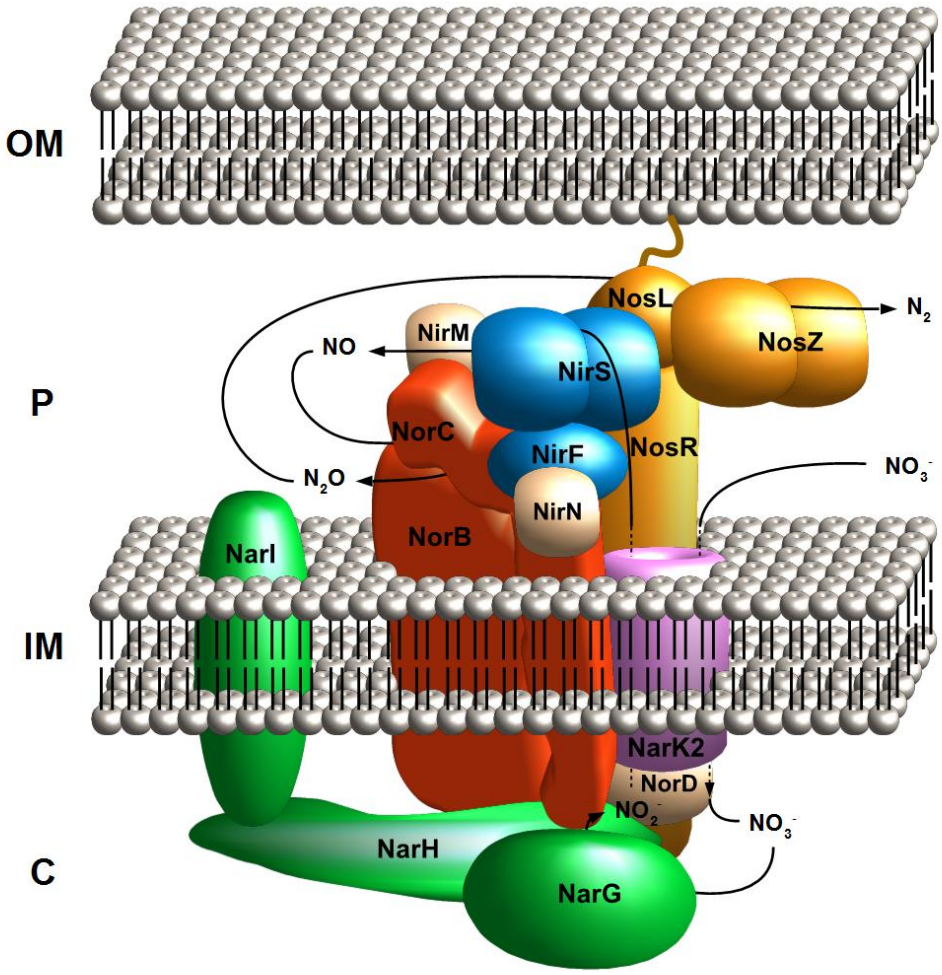

Figure 24. Denitrification supra-complex assembly model proposed in this study. The figure has been elucidated relying on the interactomics and immunogold labeling data. C = cytoplasm; IM = inner membrane; P = periplasm and OM = outer membrane.

This supra-complex (Figure 24) formed by several proteins involved in denitrification has therefore been validated by AP-QMS and double immunogold labeling couple with TEM what gives consistency to the model. NorC-NorB coupled with NosR seem to play a crucial role in keeping the denitrification machinery hooked what benefits the electron channeling and facilitates the enzyme maturation and insertion of cofactors since all components (including accessory proteins and chaperones) are in close vicinity.

3.2.11 The denitrification supra-complex as part of the anaerobic respirasome of *P. aeruginosa*

Other than proteins involved in the denitrification pathway additional proteins of the electron transport chain were found to be important for sustaining the NorBC-NosR platform (Figure 25, Table 23 and Appendix). These included electron donating succinate dehydrogenase (PA1582, PA1583 and PA1584), D-amino acid dehydratase and malate:quinone oxidoreductase (PA3452 and PA4640). Two of these enzymes are participating in the TCA cycle. Accordingly, aconitate hydratase (PA1562 and PA0794), succinyl-CoA synthase (PA1588 and PA1589), isocitrate dehydrogenase (PA2623 and PA2624), citrate synthase (PA1580 and PA5006) and enzymes of the pyruvate knot, including various subunits of pyruvate dehydrogenases (PA5015 and PA5016), pyruvate kinase (PA4329), phosphopyruvate hydratase (PA3635), acetyl-CoA carboxylase (PA3112) and phosphoenolpyruvate synthase (PA1770) were also found attached. Additionally, multiple subunits of the F0F1 ATP synthase (PA5553, PA5554, PA5555 and PA5556) are part of the supra-complex. Furthermore, various subunits of the chemotactic complex (PA0413, PA1457, PA3349, PA1459, PA2788, PA5072, PA4307, PA4309, PA4310 , PA2654, PA0415, PA1646, PA4290, PA0180, PA2867, PA2652, PA4633 and PA1608) and the aerotaxis receptor AER were found attached to NorBC-NosR. The Hcp1 protein of type IV secretion system preferentially bound to NorC. Interestingly, some components of the SecYEG/SecAB secretion system (PA4403, PA5128, and PA4747) and the YidC (PA5568) insertase were coupled to the supra-complex. Surprisingly, multiple subunits of nucleotide metabolizing ribonucleotide reductases NrdA and NrdB (PA1156, PA1155) and of the iron storage protein bacterioferritin (PA3531 and PA4235) were also found strongly attached to the denitrification platform. All these proteins including the PA accession number, factor of

enrichment and cellular process in which they are implicated are shown in the Appendix.

Table 23. Interaction partners categories found for NorB, NorC and NosR involved in the respiratory chains of *P. aeruginosa*.

Group	Interaction Partners
1	Electron transport chain
1.1	NADH dehydrogenases
1.2	Other primary dehydrogenases
1.3	Succinate dehydrogenase
2	ATP synthase
3	Cytochrome oxidases
4	Fermentation
5	Cofactor formation
6	Cell division
7	TCA cycle and pyruvate knot
8	Cell wall/membrane/envelope
9	Chemotaxis/motility
10	Protein transport
11	Amino acid metabolism
12	Iron-sulfur proteins
13	Alginate
14	Proteases/chaperones
15	Stress/detoxification
16	DNA/RNA metabolism
17	Inorganic ion transport and metabolism

NorCB and NosR interacted with proteins from all categories listed above. The detailed table is shown in Appendix.

3.2.12 Model of the nitrate respirasome of *P. aeruginosa*

Today, respirasome research, the investigation of mega-complexes involved in respiration, almost exclusively focuses on the mitochondrial electron transport chain of eukaryotes (Bansal *et al.*, 2012, Lombardi *et al.*, 2009). Herein, we present a mega-complex of spanning proteins of the different electron transport chains of *P. aeruginosa* involved in the generation of energy. Summarizing the data obtained in this study we propose a model of the key players of the supra-complex during the denitrification in *P. aeruginosa* attached to a mega-complex which we define as "respirasome". Proteins of different chain systems involved in the electron transfer were found to strongly interact with the NorB-NorC and NosR supra-complex (Figure 25). The succinate

dehydrogenase, the NADH dehydrogenase complex, the cytochrome c_1 and several enzymes from the TCA cycle were interacting with this supra-complex (Figure 25). Furthermore, several components of the ATP synthase were found as well to link to the complex as the last piece of the puzzle, essential responsible to convert the proton motive force into ATP. Moreover, certain elements of the SecYEG/SecAB system were found to interact with the system (Figure 25). A model was derived integrating all these interactions (Figure 25).

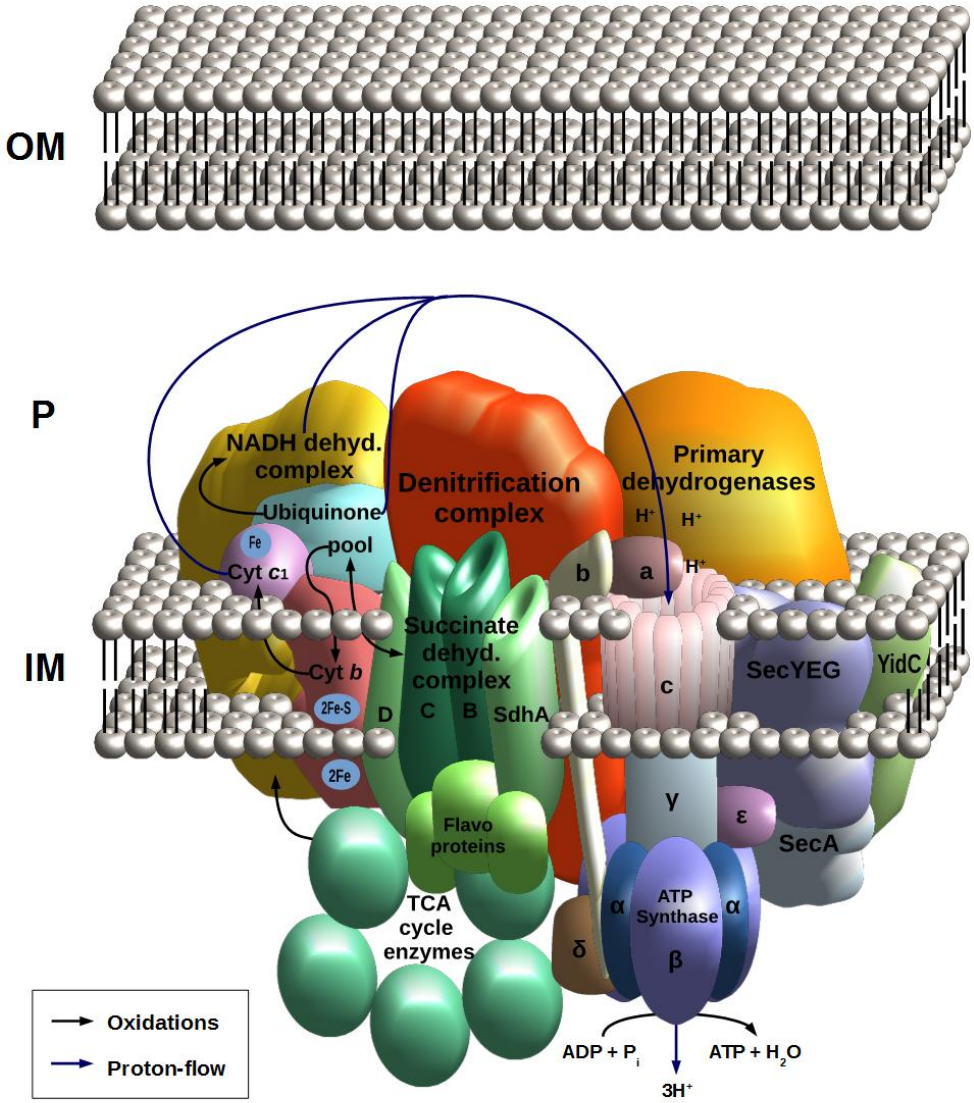

Figure 25. Schematic model of the respirasome relying on the NorCB-NosR supra-complex. C = cytoplasm; IM = inner membrane; P = periplasm and OM = outer membrane.

In conclusion: we denominate the "respirasome" of *P. aeruginosa* to all these electron transfer systems which are interconnected in the cell (denitrification supra-complex, the succinate dehydrogenase and other primrary dehydrogenases, the NADH dehydrogenase complex, ubiquinone biosynthesis proteins, the cytochrome c_1 and several enzymes from the TCA cycle) coupled with the ATP synthase forming a system itself intended to repire. This global system was elucidated by proteomics and double immunogold labeling followed by transmission electron microscopy. This is the first experimental evidence for an energy generation mega-complex which combines all necessary electron transport chains proteins for their formation in the periplasm and the ATP synthase for the ATP generation. This system comprises large number of interactions interlacing different cellular processes and cell components.

3.3 NirS interactome. Investigation of the NirS functions by means of interactomic studies

Within the denitrification pathway of *P. aeruginosa*, the Nir enzyme, the cytochrome cd_1 nitrite reductase (NirS) provides the cell with a crucial function since it converts the toxic nitrite into the NO, a gas with toxic but also signal function. The complex studies described above already revealed a tight protein network involved in Nir function. The enzyme is a homodimer composed of two distinct domains, the N-terminal domain which encloses small *c*-type cytochromes and accommodates a covalently bound heme *c*, and a C-terminal domain which harbors the catalytically essential heme d_1 molecule (Nurizzo *et al.*, 1998, Arese *et al.*, 2003). Due to the outlined crucial function of NirS we have sought the interaction partners of the enzyme, through application of interactomic methods in combination with phenotypic characterizations and imaging.

3.3.1 The NirS, FliC and DnaK form a periplasmic complex in *P. aeruginosa* grown under denitrifying conditions

The interaction partners of the periplasmic cytochrome cd_1 nitrite reductase NirS were investigated in a strep-protein interaction experiment (SPINE) (Herzberg *et al.*, 2007b), with NirS as a "bait" protein. The *nirS* gene and its upstream sequence (approximately 500 bp) were cloned in plasmid pAS40, as described in detail in Materials and Methods. In this construct, *nirS* expression under denitrification

conditions is controlled by the native transcriptional regulation machinery (Trunk *et al.*, 2010). The hybrid plasmid was introduced into the PA14 *nirS* mutant strain to yield the PA14 *nirS*$^{-}$/*nirS*$^{+}$ complemented strain. Two parallel samples were taken from cultures grown under anaerobic denitrification conditions, treated or not (control) with cross linker. Periplasmic extracts were prepared and subjected to AP of NirS. SDS-PAGE analyses of the column eluates demonstrated that two distinct bands, in addition to the affinity-bait protein NirS, were always present as tested in triplicate experiments (Figure 26A). These additional bands were confirmed by Western blot detection. The co-purifying proteins were identified by LC-MS/MS analyses as FliC (flagellin type B) and the DnaK molecular chaperone. This information led us to carry out a reciprocal experiment using FliC as the bait protein in the PA14 *fliC* mutant complemented strain (PA14 *fliC*$^{-}$/*fliC*$^{+}$). In this case, NirS and DnaK co-purified with FliC (Figure 26B). The NirS-FliC-DnaK triad was observed in samples from both *in vivo* cross-linked cultures and untreated cultures, indicating that the interactions are rather strong, although the yields of co-purifying proteins were substantively lower from non-cross-linked cultures (Figure 26A). No column-binding proteins were observed with periplasmic samples from control cells of the wild-type PA14 strain bearing the cloning vector alone (PA14 pAS40; Figure 26C). In a further control experiment involving another periplasmic denitrification pathway enzyme, the nitrous oxide reductase NosZ as a bait protein, the FliC and DnaK bands did not appear, which supports the specificity of the NirS-FliC-DnaK interactions.

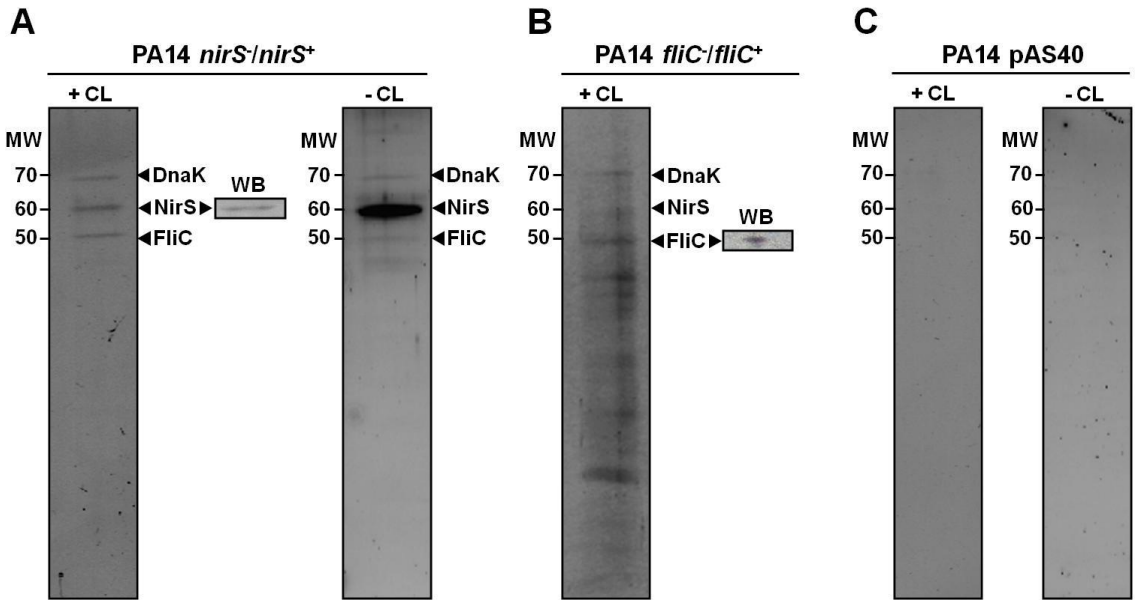

Figure 26. Interaction partners of NirS and FliC. SDS-PAGE analyses of periplasmic proteins co-purifying with affinity purified bait proteins NirS (A) and FliC (B). The negative control showed no purified proteins (C). +CL and -CL indicate whether or not the cell samples were treated with cross linker prior to protein isolation. WB (inset) indicates Western blot confirmation of the identity of the bait protein using anti Strep-Tactin antibodies conjugated to alkaline phosphatase. Proteins obtained from cross-linked samples were heated to 95°C in SDS-sample buffer to reverse cross-linking before loading the gel. The bands indicated by arrows were excised from the gels, the proteins were eluted and tryptic digests were analyzed by LC-MS/MS, as described in Materials and Methods.

In conclusion, this interactomic study of *P. aeruginosa* cells growing anaerobically revealed a strong protein-protein interactions triad in the bacterial periplasm consisting of the NirS protein, a cytochrome cd_1 nitrite reductase which plays a central role in energy generation by denitrification, FliC, the subunit protein of the flagellar filament, the organ of bacterial motility, and DnaK, a molecular chaperone. Evidence for the triad and for its localization in the periplasm, consisted of bait:prey experiments, involving NirS and FliC as baits to capture and affinity purify interaction partners from periplasmic extracts of cells treated with a cross linker. An overview of the denitrification pathway from *P. aeruginosa* and the flagellar assembly model based on the knowledge gathered in *Salmonella enterica* and *E. coli* is shown below (Figure 27).

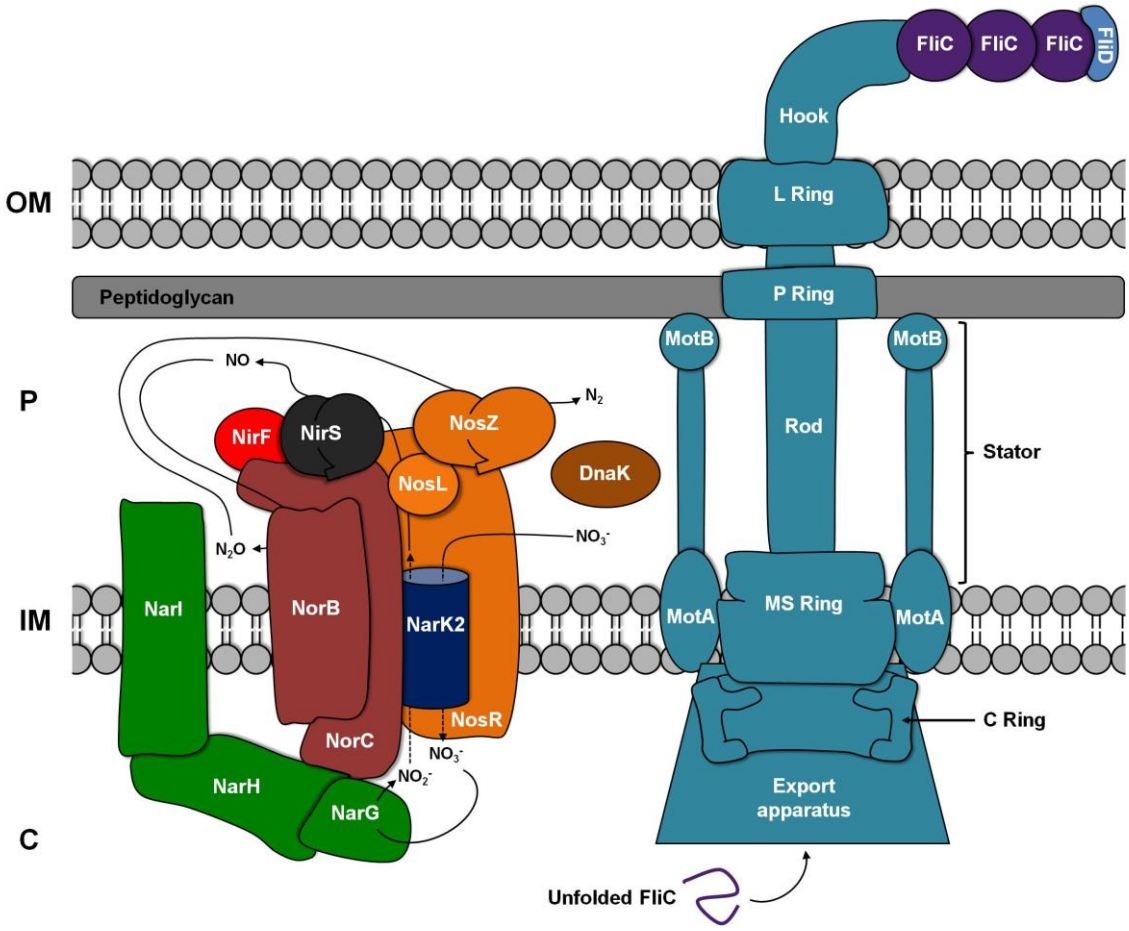

Figure 27. Schematic model of the denitrification pathway and the flagellar apparatus. The denitrification model (left) shows the proteins that are involved in the *P. aeruginosa* anaerobic respiration. The flagellar apparatus (right) was constructed based on the models described for *S. enterica* and *E. coli* (Zhao *et al.*, 2014). DnaK periplasmic location is postulated in this work.

Interestingly, a *nirS* knockout mutant of *P. aeruginosa* PA14 showed deficiency in swarming motility (de la Fuente-Nunez *et al.*, 2013) which *in P. aeruginosa* involves both flagella and pili, unlike swimming motility which is accomplished exclusively by flagella (Kohler *et al.*, 2000). The flagellum, in combination with the chemotaxis system, mediates directional movement of the bacterium in response to attractants and repellents (Kohler *et al.*, 2000), and plays a crucial role in initial cell-cell and cell-surface interactions and biofilm formation (O'Toole & Kolter, 1998). A *nirS* mutant produces poorly-dispersing biofilms, which partially regain dispersal ability upon addition of exogenous nitric-oxide (Barraud *et al.*, 2006, Barraud *et al.*, 2009). These observations suggest a coupling between denitrification and motility, though direct evidence for this is currently lacking. The presence of usually extracellular flagellum

protein FliC in the periplasm is of unknown nature. Nevertheless, monomers have been found in this fraction previously (Imperi *et al.*, 2009b) and the role of secreted monomers as cytotoxic agents which promote immunological response has been shown (Miao *et al.*, 2008). We presume that these monomers might be exported in a convergent manner other than flagellum-like secretion system known in other bacteria.

The role of DnaK in this triad is more mysterious and its presence in the periplasm even more since it is considered an ATP-dependent chaperone located mostly in the cytoplasm (Allen *et al.*, 2009, Ben-Zvi & Goloubinoff, 2001). However, DnaK was also found in the periplasmic fraction (Imperi *et al.*, 2009a) and its complementary role in secretion in SecB lacking mutants has been confirmed (Sala *et al.*, 2014). Thus, another function besides its cytoplasmic ATP-dependent chaperone one, maybe at the periplasmic, membrane or outside fraction of the cell is likely.

3.3.2 A PA14 *nirS* mutant is deficient in swimming motility

To investigate the relevance of denitrification functions in *P. aeruginosa* motility, bacterial swimming motility was scored in mutant strains defective in different denitrification reductases. The PA14 wild-type and *fliC* mutant strains served as positive and negative controls, respectively. Because denitrification mutants are unable to grow anaerobically, the fermentable substrate arginine was provided to enable anaerobic growth of the mutants. Under these conditions, any swimming defect should be related to a malfunction in the swimming machinery rather than to impaired denitrification. As shown in Figure 28, the PA14 *nirS* mutant was impaired in its swimming ability, and the degree of impairment was comparable to that of the *fliC* mutant strain. The *nirS* complemented strain PA14 $nirS^-/nirS^+$, and *fliC* complemented strain PA14 $fliC^-/fliC^+$ both exhibited normal motility, i.e. the characteristic large swimming halo of the wild-type parental strain (Figure 28). The PA14 *narH* and *nosZ* mutant strains were also able to swim, unlike the *nirS* mutant, showing that these other denitrification reductases are not important for efficient motility. Thus, an involvement of the denitrification machinery in motility appears to be NirS-specific. In the PA14 *norB* mutant, both swimming motility and bacterial growth were strongly inhibited, so any specific effect on motility could not be assessed. Perhaps NorB is also required as platform for these processes.

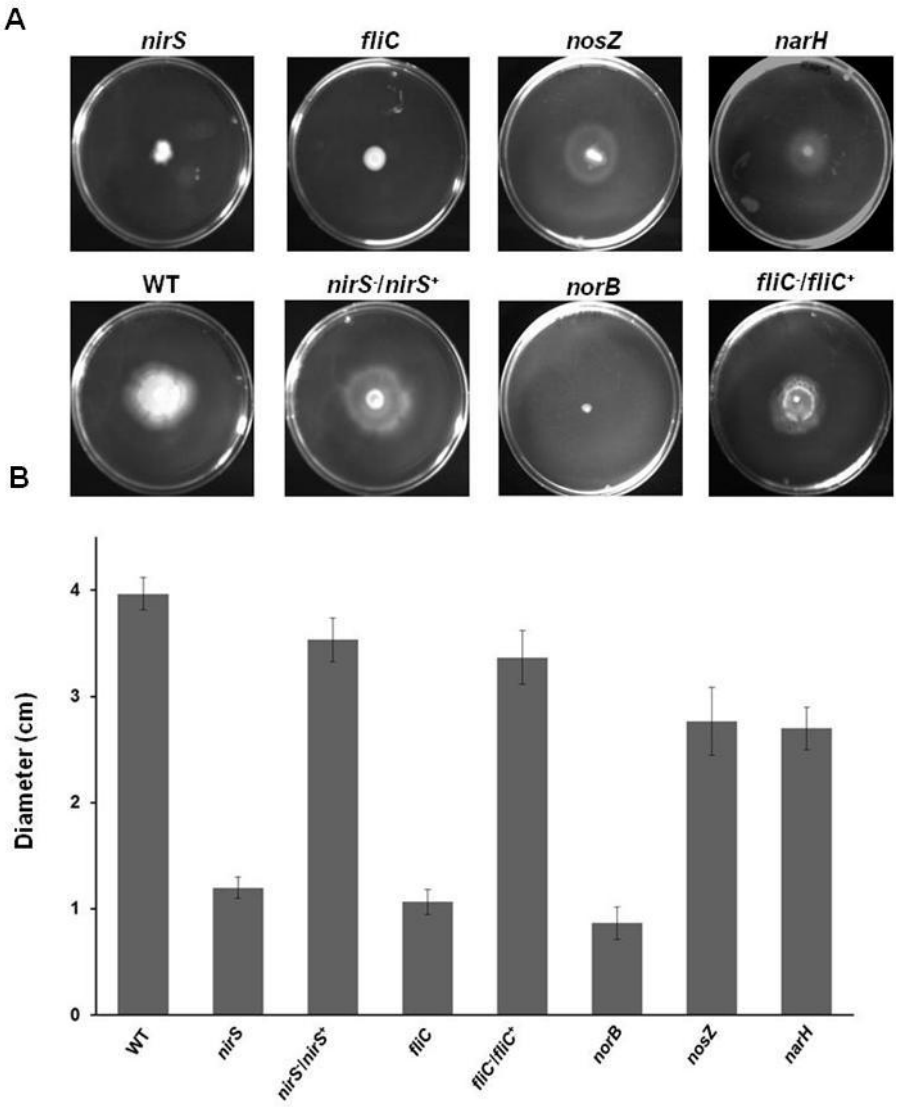

Figure 28. Swimming motility assays of the PA14 wild-type (WT) and denitrification mutant strains. A) Soft agar plates containing arginine as energy source were point inoculated with overnight cultures of the strains to be tested, incubated anaerobically at 37°C for 5 days, as described in Materials and Methods, and then photographed. B) The diameters of the halos of bacterial growth, representing the distance migrated by swimming, were measured. The plots in B show the mean halo-diameters of triplicate measurements, and their standard deviations.

Swimming motility, unlike swarming motility, is mediated solely by flagella (Kohler *et al.*, 2000). The finding of a protein interaction between NirS and FliC prompted us to examine the swimming phenotype of a *nirS* mutant. The *nirS* mutant, but not control *narH* (nitrate reductase) and *nosZ* (nitrous oxide reductase) mutants, macroscopically exhibited impaired swimming motility and microscopically were

observed to have no or only aberrant (shortened, non-spiral) flagella. Thus: NirS appears to play a key role in the formation and/or stability and/or function of flagella. The NirS:FliC protein-protein interactions would seem to be the most likely underlying mechanism, although an indirect mechanism, such as NirS-mediated production of nitric-oxide (NO), a known signaling molecule in *P. aeruginosa* that influences motility and biofilm formation, is also possible.

3.3.3 Impaired flagellation of the PA14 *nirS* mutant

The findings of impairment of swimming motility in the PA14 *nirS* mutant and a protein interaction between NirS and FliC suggested the possibility of impairment of flagellar structure or function in this mutant. The flagella abundance and morphology were therefore investigated by immunofluorescence staining of FliC, the structural protein component of the flagellar filament. The wild-type parental strain expressed flagella under all growth conditions tested, aerobic and anaerobic, when grown in LB, as shown in Figure 29A, although flagellar abundance varied from cell-to-cell. To facilitate the visualization of individual cells, they were permeabilized with Triton X-100 and immunolabeled using an anti-DnaK rabbit antibody. With this staining procedure, cells were very well labeled and DnaK was observed to be evenly distributed around the cell envelope (Figure 29B). Double immunofluorescence staining was used to compare the production of flagella by *P. aeruginosa* PA14 wild-type and the *nirS* mutant. The number of flagellated PA14 *nirS* mutant bacteria was much lower than observed in the parental strain and many short, incomplete and abnormal non-spiral (non-rotating) flagella were seen (Figure 29C).

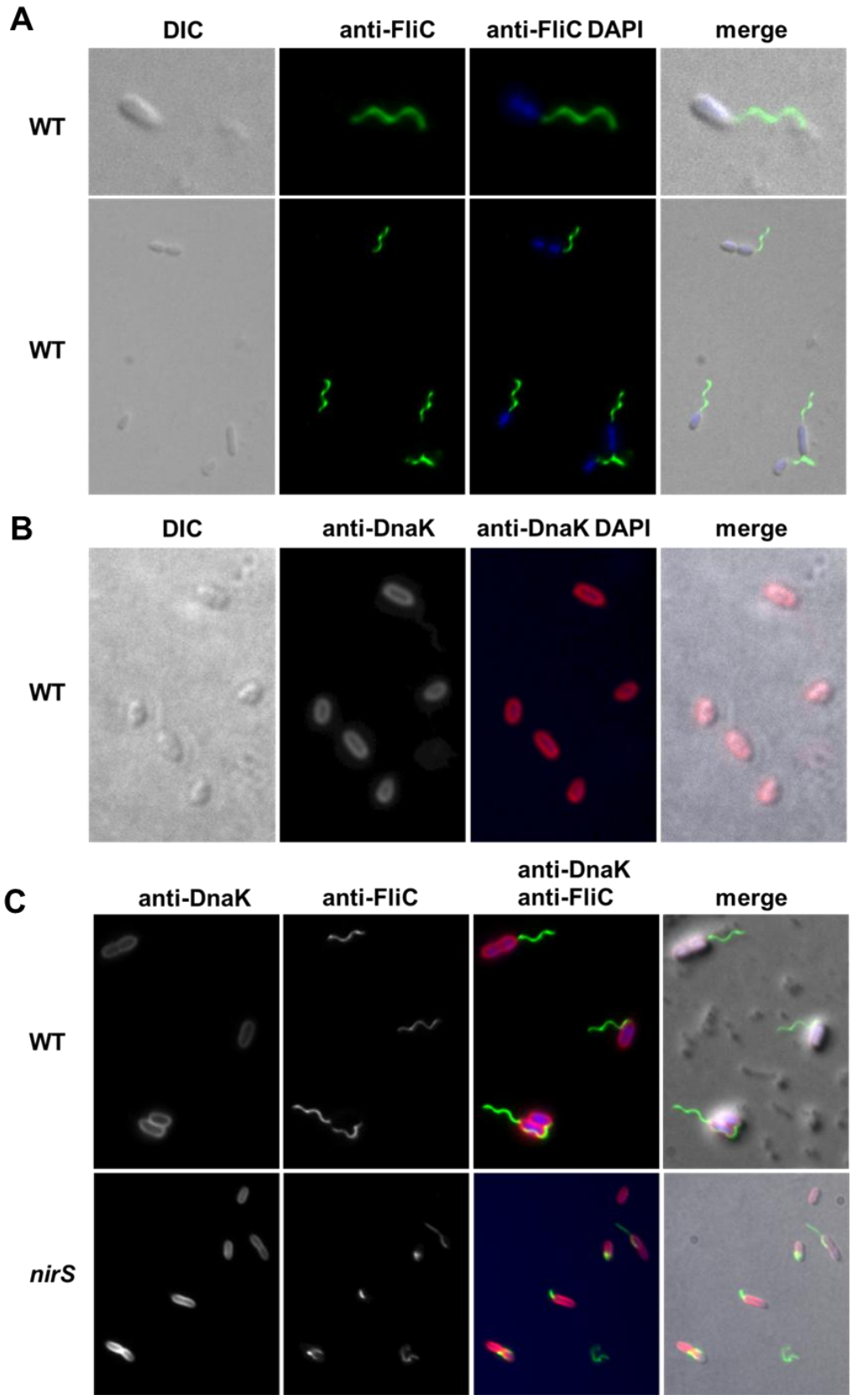

Figure 29. Flagella morphology and DnaK distribution in *P. aeruginosa* PA14 wild-type and the corresponding *nirS* mutant analyzed by immunofluorescence staining.

For visualization of extracellular FliC protein (A), samples of bacteria cultured anaerobically in LB containing arginine were incubated with the primary anti-FliC rabbit antibody, washed, incubated with the secondary goat anti-rabbit antibody Alexa 488, and prepared for fluorescence microscopy, as described in Materials and Methods. For visualization of intracellular/non-external DnaK and FliC proteins (B, C), bacteria were first permeabilized with Triton X-100 0.1% in PBS.

In A, the primary antibody used was rabbit anti-FliC. In B, the primary antibody was rabbit anti:DnaK. In C, two series of stainings were carried out: initially, the primary antibody was anti-FliC was followed by goat anti-rabbit Alexa 488. After, a second staining with anti-DnaK antibody was followed again by goat anti-rabbit Alexa 568. All cover slips were mounted with ProLong Gold DAPI. Similar results were obtained with bacteria cultured in swimming medium and thus correlated ultrastructure analysis with the lack of swimming motility in the PA14 *nirS* mutant strain (Figure 30).

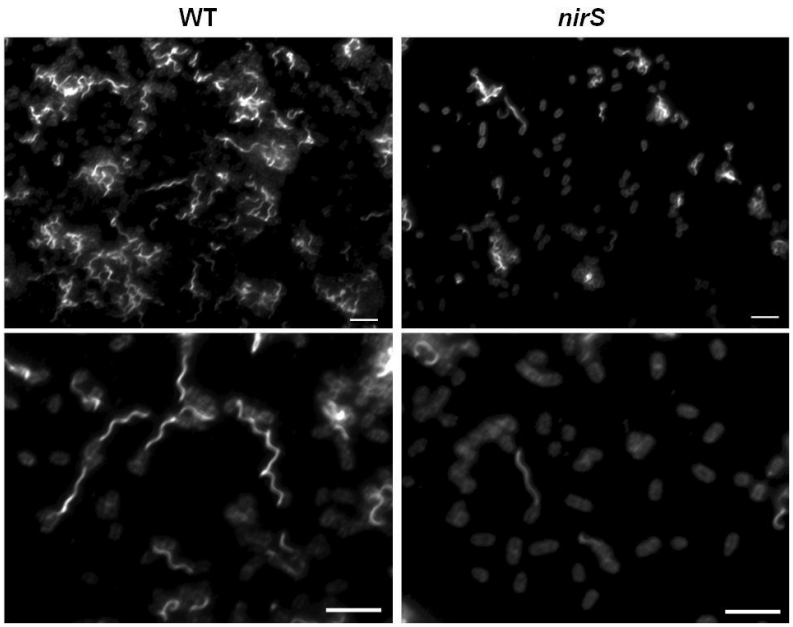

Figure 30. Flagellation of *P. aeruginosa* strains PA14 wild-type (WT) and the corresponding *nirS* mutant in swimming liquid medium. Flagella and bacteria cells were visualized at low (upper panels) and higher (bottom panels) magnification using immunofluorescence staining with anti-FliC and anti-DnaK antibodies and goat anti-rabbit Alexa 488. Scale bars: 10 µm.

As observed in Figure 30, the PA14 *nirS* mutant strain population was drastically lower flagellated than the wild-type. Therefore a deficiency in flagellar assembly or stability was present when NirS was devoid. These results establish a functional relationship

between the NirS protein and flagellation that reflects the detected NirS:FliC protein interaction.

3.3.4 Immunolocalization of NirS-FliC-DnaK

In order to directly visualize the spatial distribution of NirS, FliC and DnaK in living cells, purified IgG antibodies were used for labeling of ultrathin sections of *P. aeruginosa* PA14 with gold nanoparticle (PAG)-conjugated antibodies. First, anti-DnaK and anti-FliC antibodies conjugated with different sizes of gold-particles (15 and 10 nm in size, respectively) were incubated onto ultrathin sections of *P. aeruginosa* and thereby the DnaK and FliC proteins were immunogold labeled and subsequently their location in the cell was observed by TEM. Second, the anti-DanK (15 nm) and the anti-NirS (10 nm) nanoparticle (PAG)-conjugated antibodies were used, revealing the location of DnaK and NirS in the cell. Co-localizations studies for these proteins are shown in Figure 31.

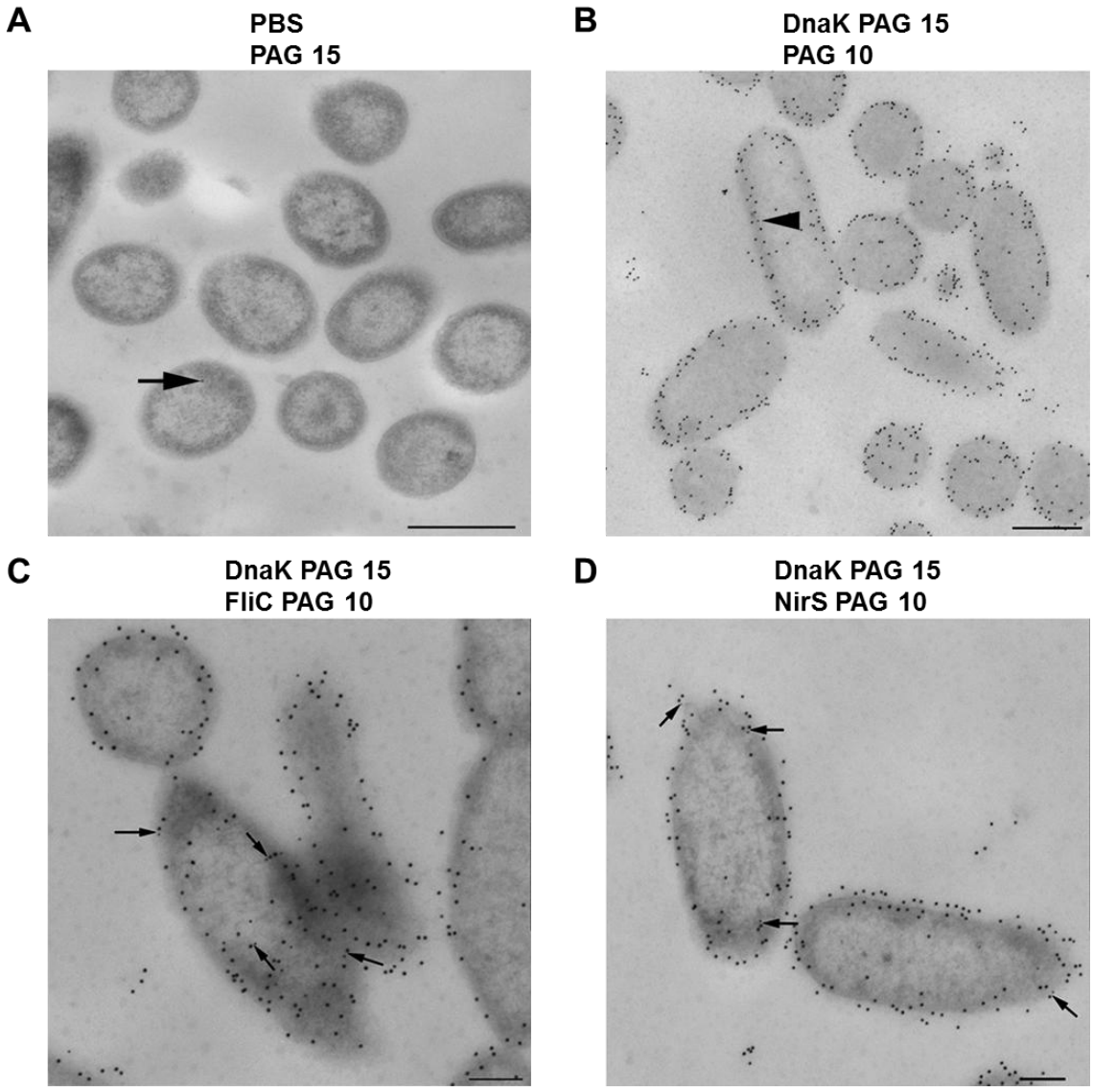

Figure 31. Cellular localization and co-localization of DnaK, FliC and NirS in anaerobically-grown, denitrifying cells of *P. aeruginosa* PA14. Cells were prepared for TEM, treated with specific antibody and Protein A/G conjugated with 10 or 15nm diameter gold nanoparticles (PAG 10, PAG 15, respectively), counterstained, and examined in a TEM910 transmission electron microscope, as described in Materials and Methods. A) antibody-negative control with the PAG 15 particles alone; B) anti-DnaK antibodies with PAG 15, followed by protein A blocking, then PAG 10; C) anti-DnaK antibodies with PAG 15, followed by protein A blocking, then anti-FliC antibodies with PAG 10; D) anti-DnaK antibodies with PAG 15, followed by protein A blocking, then anti-NirS antibodies with PAG 10. DnaK is seen to be distributed mostly in the extracytoplasmic region; several co-complexes between DnaK and FliC, and DnaK and NirS are observed and indicated by arrows. Scale bars are 500 nm for A, B and 200 nm for C, D.

In the presence of anti-DnaK antibodies, PAG conjugated with 15 nm diameter gold nanoparticles revealed that DnaK is abundant and predominantly localized at the cell periphery and/or in the extracytoplasmic region (Figures 31B-D). This was in accordance with the immunofluorescence microscopy observations. In double-immunogold labeling, protein-protein complexes are indicated by differently sized gold particles co-localizing less than 25 nm from each other, since each of the two applied antibodies can maximally span a distance of approximately 12 nm due to the hinge in the Fab region. Double labeling with anti-DnaK and anti-FliC or anti-NirS antibodies revealed that both FliC and NirS proteins are much less abundant than DnaK (Figures 31C and D). However, when they are detected, they are mostly co-localized with DnaK, provides ultrastructural support for direct DnaK:NirS and DnaK:FliC interactions, most probably in the bacterial periplasm. Almost no labeling of *P. aeruginosa* PA14 was observed using PAG nanoparticles alone in the absence of specific antibody (Figure 31A).

3.3.5 The NirS cytochrome *c* domain is involved in the NirS-FliC interaction

A simple notion of the configuration of the triad is either a triangular arrangement, with each protein contacting both of the others, or a linear chain arrangement of the type (1) DnaK-NirS-FliC, (2) DnaK-FliC-NirS and (3) FliC-DnaK-NirS. In order to obtain further information on the interactions in the triad, we repeated the bait:prey interaction experiment shown in Figure 26, but using *fliC* and *nirS* mutant backgrounds, to eliminate the involvement of FliC or NirS in the triad. First, NirS-Strep-tag II was purified from the PA14 *fliC* background mutant while FliC-Strep-tag II was purified from the PA14 *nirS* mutant strain (Figure 32). Cells were grown anaerobically in LB medium supplemented with 50 mM KNO_3 for 8 h. *In vivo* cross-linking was performed prior to periplasmic extractions. As can be seen in Figure 32A and B, FliC is not required for interaction of NirS with DnaK, which eliminates possibility 2, nor is NirS required for FliC interaction with DnaK, which eliminates option 1, leaving only the option of NirS and FliC being linked via DnaK (3).

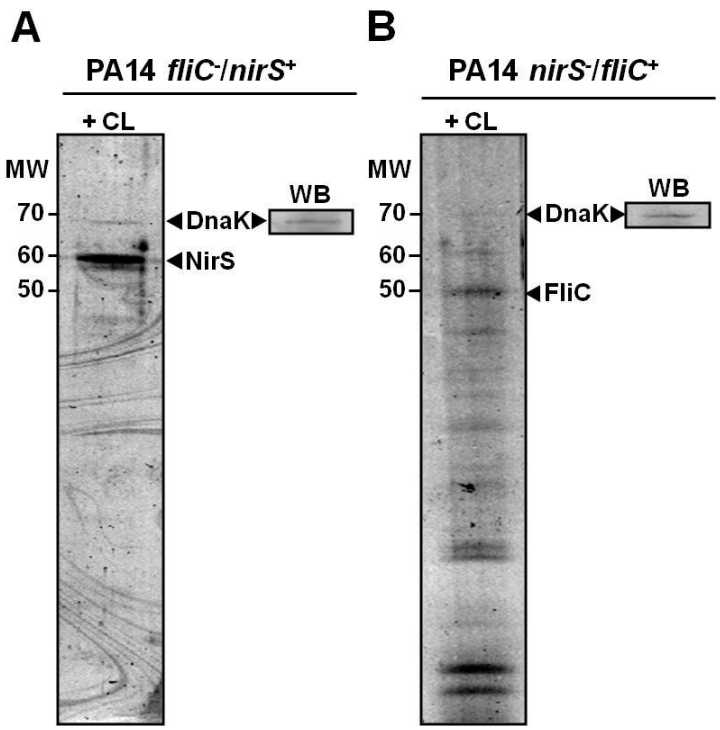

Figure 32. NirS-FliC-DnaK interactions. A) NirS co-purification in the PA14 *fliC*$^{-}$/*nirS*$^{+}$ strain and B) FliC co-purification in the PA14 *nirS*$^{-}$/*fliC*$^{+}$ strain.

In order to distinguish between a linear arrangement with DnaK functioning as a link between NirS and FliC, and the triangular format, we analyzed and compared the complete peptide composition from the samples obtained from the *fliC* and *nirS* background mutants, respectively, after subjecting them to trypsinisation and peptide analysis by LC-MS/MS. In this experiment NirS:FliC cross-linked peptides were identified, showing a direct interaction between these two members of the triad, excluding linear arrangements 3, and supporting a triangular configured triad. Figure 33 illustrates the approach for a better understanding.

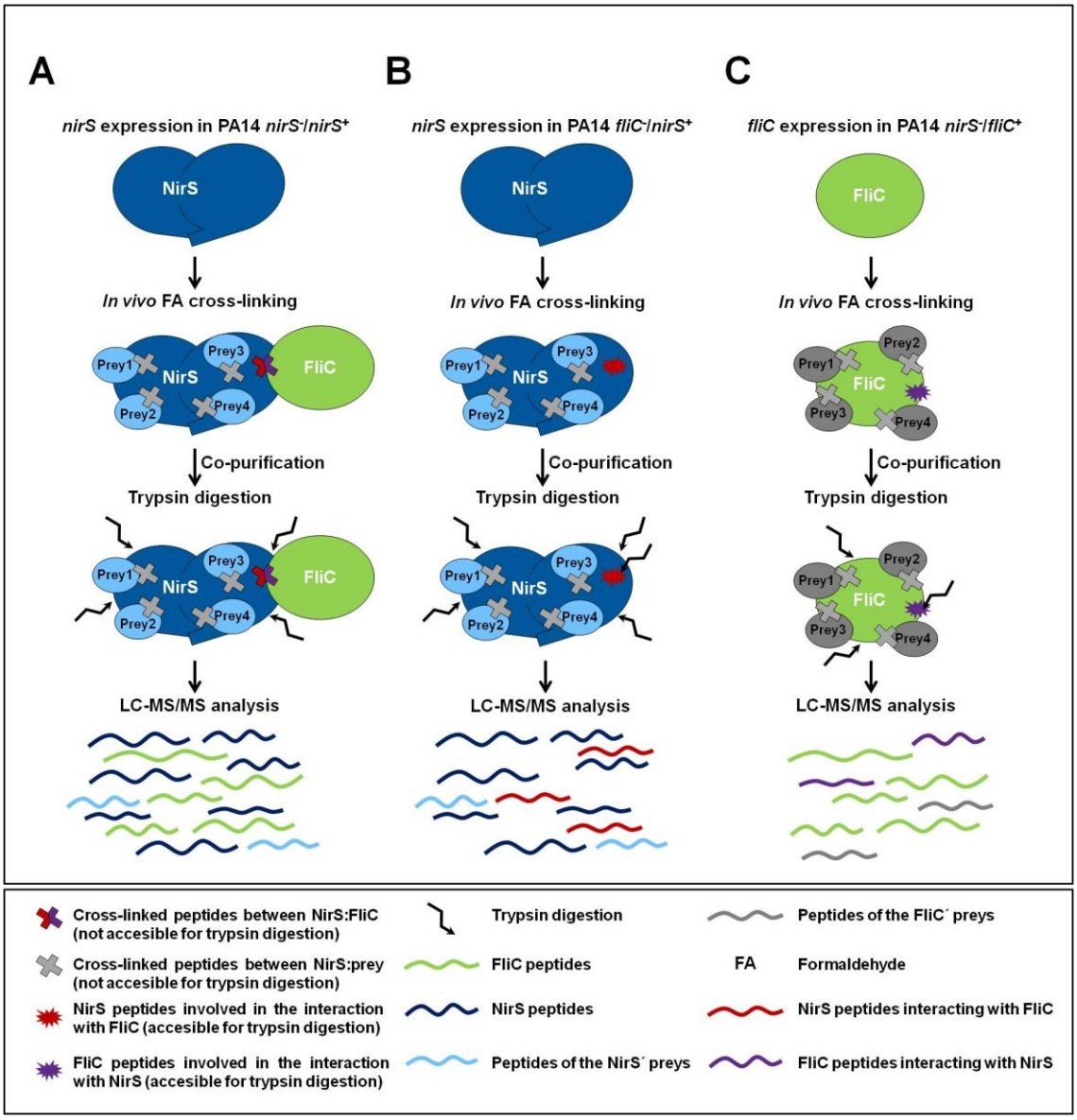

Figure 33. Strategy designed with the purpose of identifying the peptides directly involved in the NirS-FliC interaction. The recombinant strains PA14 *nirS*⁻/*nirS*⁺ (A) PA14 *fliC*⁻/*nirS*⁺ (B) and PA14 *nirS*⁻/*fliC*⁺ (C) were grown anaerobically supplemented with nitrate. Cross-linking was applied *in vivo* and the resulting periplasmic extracts were subjected to AP. Eluates were digested with trypsin and analysed by LC-MS/MS. The different peptides were compared over the samples. Missing peptides of NirS in A and found in B were considered the NirS peptides involved in this interaction. The FliC peptides not found in A but encountered in C were presumed as the FliC peptides involved in this interaction.

The NirS:FliC peptides from the cross-linked complex were AAEQYQGAASAVDPTHVVR, CAGCHGVLRK and GQQYLEALITYGTPLGMPNWGSSGELSK, from NirS, and NQVLQQAGTAILAQANQLPQAVLSLLR and LGITASINDK, from FliC. Since

interaction surfaces of the complex are potentially contained within these peptides, we wanted to map them onto available structure models. Figure 34, highlights the NirS peptides that cross-link to FliC in the NirS structure model (obtained from the PDB database (pdb accession code 1NIR (Nurizzo *et al.*, 1997)). These peptides were located in the cytochrome *c* domain of NirS (Zumft, 1997, Nurizzo *et al.*, 1997). Further work is required to test this model and deduce its predictions by site-directed mutagenesis.

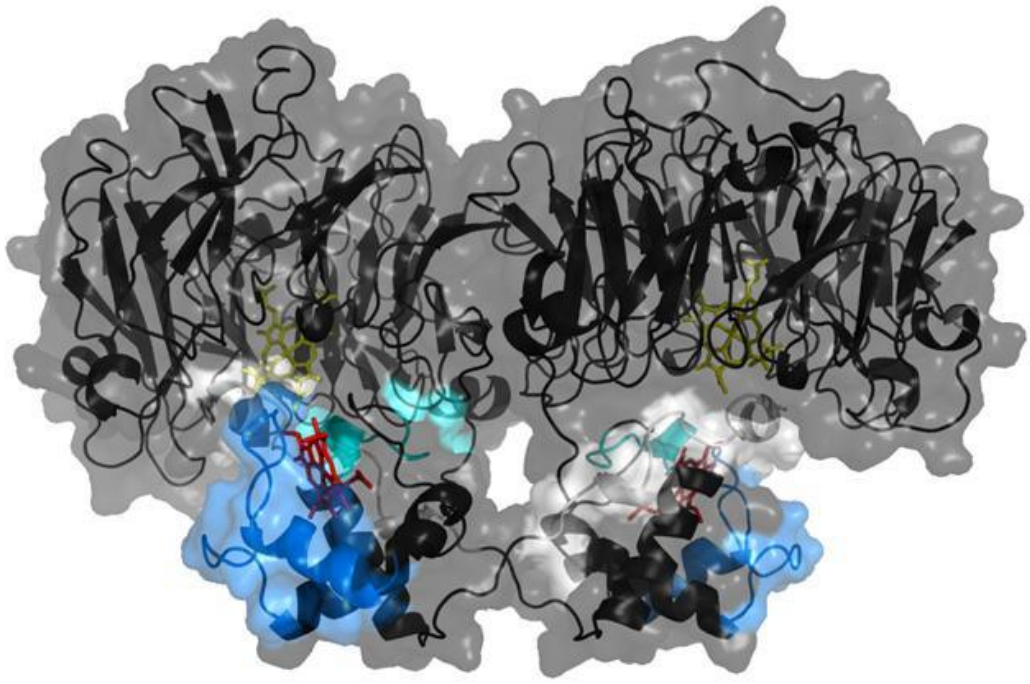

Figure 34. NirS peptides involved in the interaction with FliC. Structural model of dimeric PA14 NirS showing the peptides hypothesized to participate in the interaction with FliC. NirS structure displayed as cartoon model with transparent surface as inferred from pdb 1NIR (Nurizzo *et al.*, 1997). Stick models indicate the heme *c* (red) and heme d_1 molecules (yellow). Potential interacting peptides are shown in light gray (AAEQYQGAASAVDPTHVVR), cyan (CAGCHGVLRK) and light blue (GQQYLEALITYGTPLGMPNWGSSGELSK).

FliC was demonstrated previously to be present in the periplasm (Imperi *et al.*, 2009a) and in outer membrane vesicles (Choi *et al.*, 2011) of *P. aeruginosa*. It was predicted to participate in a thus far poorly understood manner in the assembly and transport of the flagellum. The flagellum transport system itself has some interaction with/functional redundancy with/reciprocity between the Type III secretion system, so it

will be interesting to explore further a possible role of the NirS-FliC-DnaK triad in this cross-talk of vital transport systems.

Tryptic digests of cross-linked NirS-FliC complexes approximately localized the interacting peptides of the two proteins and an available structural model of NirS allowed identification of the approximate region of the docking surface. Unfortunately, the absence of a model of the FliC protein prevented identification of its corresponding reciprocal surface. Nevertheless, it is interesting to note that the region of NirS involved in the interaction is its cytochrome *c* heme domain, which is the domain receiving electrons from cytochrome c_{551} (Hasegawa *et al.*, 2001b, Nurizzo *et al.*, 1998, Nurizzo *et al.*, 1997). This in turn might suggest a possible bioenergetic basis of the interaction, and it will be interesting in future to assess this possibility, along with others, by means of site-directed mutagenesis.

The role of DnaK in the triad is even more enigmatic. DnaK is generally considered to be a ubiquitous ATP-dependent chaperone functioning in the cytoplasm, where ATP is generally to be found in concentrations physiologically relevant to DnaK function (Allen *et al.*, 2009, Ben-Zvi & Goloubinoff, 2001). It was therefore surprising to find it by fluorescence and TEM to be an abundant protein concentrated in the cell envelope, and co-localized with NirS (but not the abundant periplasmic denitrification protein NosZ) and FliC in the periplasm, in anaerobically-grown, denitrifying cells. There are, however, a few reports suggesting that DnaK may not only have a cytoplasmic location: it has been shown to be involved in the export of proteins in *E. coli* (Qi *et al.*, 2002, el Yaagoubi *et al.*, 1996, Perez-Rodriguez *et al.*, 2007, Imperi *et al.*, 2009a), to be released by osmotic shock from *E. coli* (Berrier *et al.*, 2000), to be associated with Bayer adhesion sites in *E. coli* and *Vibrio cholerae*, and to be detected in the periplasmic proteome of *P. aeruginosa* (Berrier *et al.*, 2000, el Yaagoubi *et al.*, 1994, Jyot *et al.*, 1999, Imperi *et al.*, 2009a). Importantly, the present identification of one complex of DnaK periplasmic interaction partners now points to an experimental route of *in vitro* studies with purified proteins to determine periplasmic DnaK requirements.

In summary: we have demonstrated the existence of a protein interaction triad in the periplasm of anaerobically-grown, denitrifying *P. aeruginosa* cells that links denitrification with motility and the molecular chaperone DnaK. This constitutes a new

insight into the interconnection of two cellular functions essential for *P. aeruginosa* pathogenicity, namely energy generation under low oxygen conditions, and motility, key activities underlying the biofilm lifestyle. We suggest that the NirS-FliC-DnaK protein interaction triad may constitute a molecular hub of biofilm biology in general and pathogenicity in particular. DnaK is a ubiquitous molecular chaperone involved in protein folding and stabilization, and has also been implicated in membrane protein export and in modulation of gene expression. Given its accepted dependency on ATP for activity, its role and functional mechanism in the periplasm in general and as partner in the protein triad we demonstrated, remain to be elucidated. It is clear from our study that further analyses of interaction partners of periplasmic proteins will reveal new surprises that channel investigations to previously unsuspected metabolic partnerships which, in turn, will deliver new insights and new levels of understanding of the functioning of this unique interface between the cytoplasm and the external environment.

3.4 Improvement of PHA production by *P. putida* KT2440 through genetic manipulations derived from metabolic engineering

In a third part of this thesis the metabolic capacities of *Pseudomonas* strains were employed for biotechnological applications. Our research focused on the development of *P. putida* strains which can accumulate high amounts of *mcl*-PHA when grown on glucose as the sole carbon source. Recently, novel bioengineering approaches for the directed optimization of *mcl*-PHA production from glucose were undertaken (Poblete-Castro *et al.*, 2013). Initially, a genome-based *in silico* model of the *P. putida* metabolism was established and used for the prediction of optimal metabolic fluxes towards PHA and its precursor molecules. Among a list of different genetic targets, elementary flux mode analysis suggested an inactivation of glucose dehydrogenase encoded by *gcd* to prevent undesired by-product formation and excretion. In agreement with the prediction from the *in silico* model the constructed *P. putida* Δ*gcd* mutant strain showed an increased PHA production in batch (Poblete-Castro *et al.*, 2012) and Fed-Batch cultivations (Poblete-Castro *et al.*, 2014). The central metabolism of *P. putida* KT2440 is shown in Figure 35 as well as the enzymes involved in PHA production for a better understanding.

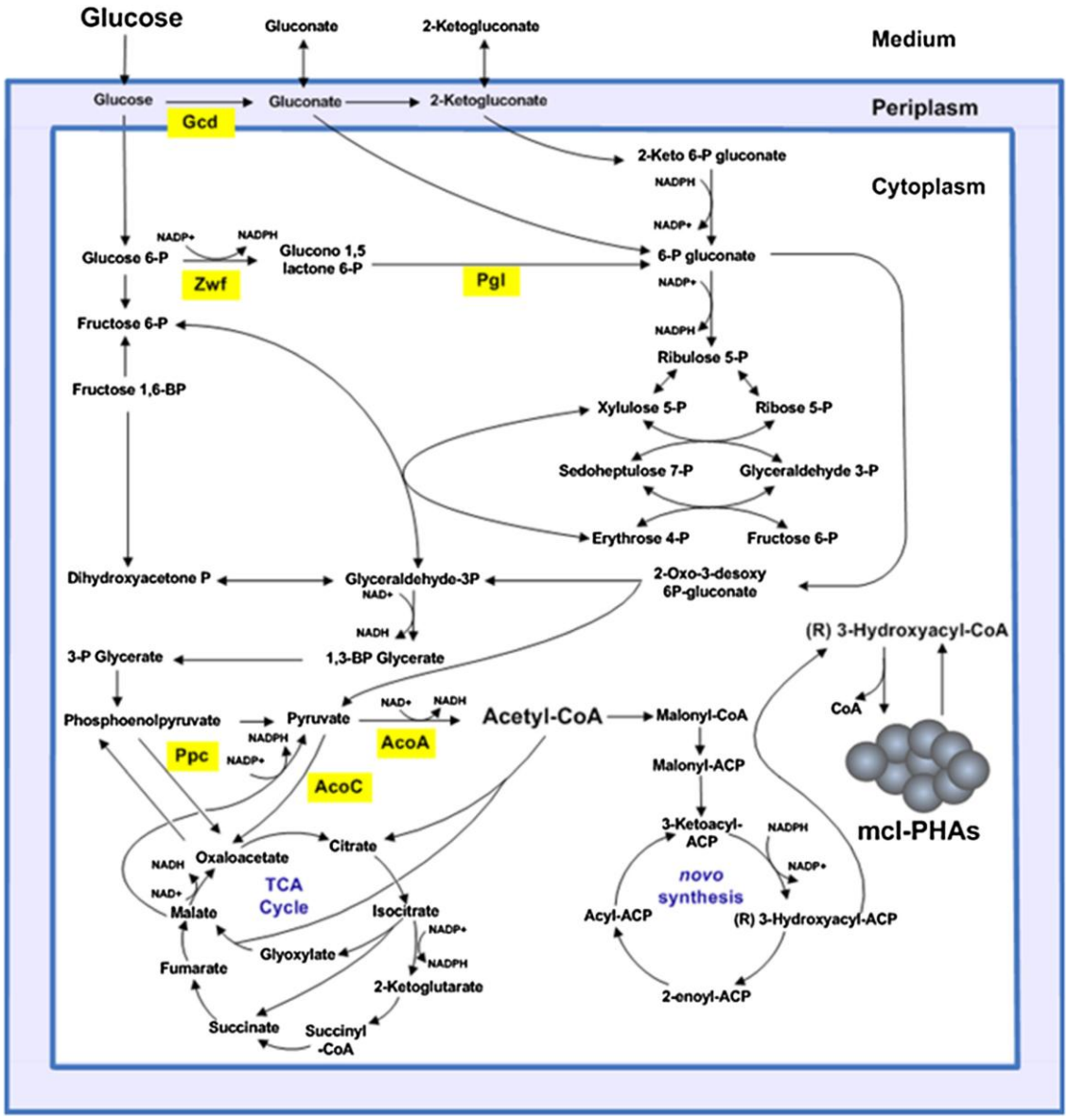

Figure 35. Central metabolism of *P. putida* KT2440 (Borrero-de Acuna *et al*., 2014).

The proteins marked in yellow are considered of high importance in the metabolite efflux for PHA production in our *in silico* model. Here, we continued to experimentally verify the predictions of our *in silico* model for the optimization of *mcl*-PHA production in *P. putida*. We tested for the proposed positive impact of the overexpression of the genes for pyruvate dehydrogenase (*acoA*) and 6-phosphogluclactonase (*pgl*) on *mcl*-PHA production. As observed in the figure, AcoA is involved in the conversion of pyruvate into acetyl-CoA, whereas Pgl catalyzes the conversion of glucono-1,5-lactone 6-P into 6-P-gluconate.

3.4.1 Overexpression of the genes for the pyruvate dehydrogenase AcoA and 6-phosphoglucolactonase Pgl for improved PHA production

The *acoA* and *pgl* genes were separately cloned into the broad host range vector pSEVA424 and then transformed into the *P. putida* KT2440 and the Δ*gcd* mutant strains. A list of all used strains, vectors and primers is provided in Table 10. Wild-type *P. putida* KT2440 and the corresponding Δ*gcd* mutant strain carrying the vector without insert served as controls. Cells were grown in defined M9 mineral minimal medium supplemented with 20 (g/L) glucose and 62.5 μg/mL streptomycin as described in the Methods section. Protein production was induced at an initial OD_{600nm} of 0.05. Cells were harvested after 60 h by centrifugation prior to protein composition analyses and PHA-extraction and quantification. SDS-PAGE analyses were used to assess the overproduction of the AcoA and the Pgl proteins. Successful overproduction of AcoA (M_r = 35,000) and Pgl (M_r = 23,000) was observed, which is in good agreement to the deduced relative molecular mass of approximately 34,700 Da for AcoA and 25,500 Da for Pgl (Figure 36).

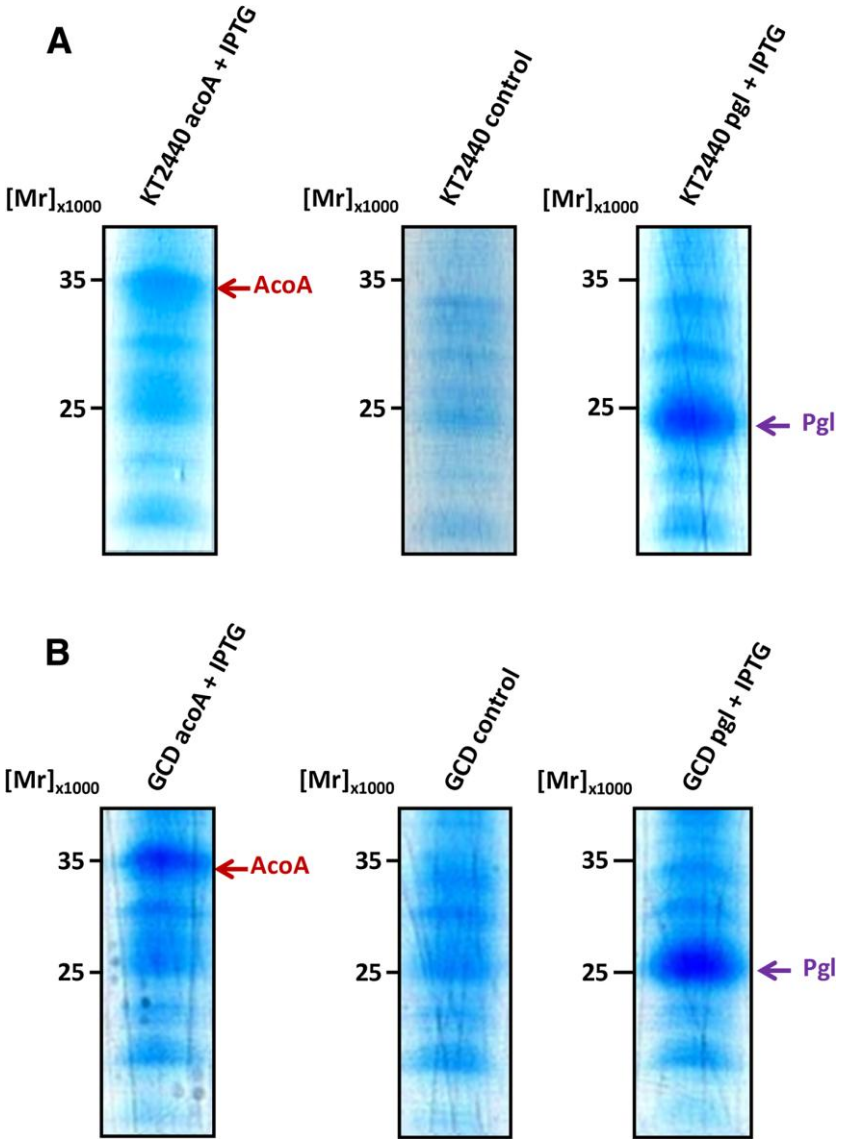

Figure 36. SDS-PAGE gels demonstrating the recombinant production of pyruvate dehydrogenase and 6-phosphogluconolactonase by the recombinant *P. putida* strains. A) Shown the separations of whole cell protein extracts from KT2440 (lane 1), KT2440-*acoA* (lane 2), KT2440-*pgl* (lane 3), and B) KT2440Δ*gcd* (lane 4), KT2440Δ*gcd-acoA* (lane 5) and KT2440Δ*gcd-pgl* (lane 6). Proteins were visualized by Coomassie Brilliant Blue staining.

In conclusion, the targeted proteins seemed to be highly over-produced as documented by the gels. The cloning strategy of the encoding genes by the insertion of a consensus RBS and the T7 promoter turned out to be optimal for our purpose. Thereby further analysis of the PHA yield in these strains was done.

3.4.2 Increased *mcl*-PHA production in *P. putida* by overexpression of the pyruvate dehydrogenase gene *acoA*

In order to evaluate the effect of *acoA* and *pgl* overexpression on PHA versus biomass production GC-MS analyses of the extracted PHA and biomass determination were performed (Figure 37). Triplicate aerobic cultures of *P. putida* strains KT2440 (wt), KT2440-*acoA*, KT2440-*pgl*, KT2440Δ*gcd*, KT2440Δ*gcd-acoA*, and KT2440Δ*gcd-pgl* were tested. For this purpose, cells were grown in defined minimal medium for 60 h until glucose as the sole carbon source was completely consumed (in all tested strains no glucose was detected via HPLC at 60 h). As predicted by the *in silico* design the pyruvate dehydrogenase-producing KT2440-*acoA* and KT2440Δ*gcd-acoA* mutant strains both showed an increased PHA content amassing 33.3 wt % and 42.1 wt % as *mcl*-PHA, respectively (Figure 37A).

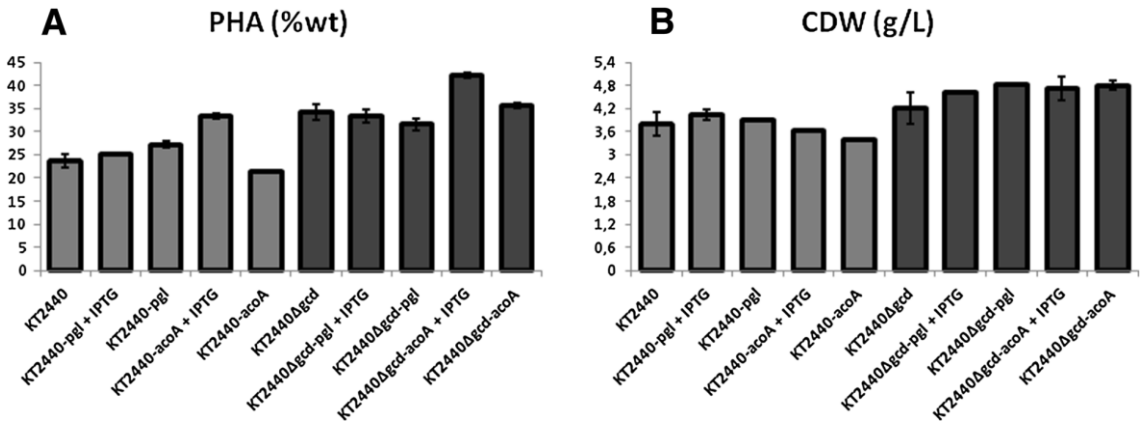

Figure 37. *mcl*-PHA A) content and CDW. B) of different metabolically engineered indicated *P. putida* strains.

This was not the case for the phosphoglucolactonase-overproducing KT2440-*pgl* (25.7 wt %) and KT2440Δ*gcd-pgl* (33.2 wt %) strains in which the PHA concentration remained at the basic level. In addition, no obvious major changes of the *mcl*-PHA momomer composition between the various producing *P. putida* strains were observed (Table 24). Next, the yield of biomass of engineered strains grown on glucose was determined. As initially desired, the biomass production of the various recombinant strains was found very similar to the one determined for the wild-type *P. putida* KT2440 strain (Figure 37B).

Table 24. Monomer composition of *mcl*-PHA produced by metabolically *engineered P. putida* strains in flask experiments.

Strain	C6[∞]	C8[∞]	C10[∞]	C12[∞]	C12:1[∞]	C14[∞]
KT2440	n.d.	11.8 ± 0.2	73.0 ± 0.1	4.7 ± 0.2	9.4 ± 0.7	0.8 ± 0.3
KT2440Δ*gcd*	n.d.	14.0 ± 0.4	71.1 ± 0.8	4.6 ± 0.9	8.5 ± 0.4	1.1 ± 0.2
KT2440-*acoA*	n.d.	13.0 ± 0.6	69.1 ± 1.2	3.4 ± 0.7	10.5 ± 0.2	3.9 ± 0.2
KT2440Δ*gcd-acoA*	n.d.	14.8 ± 0.7	70.2 ± 1.4	5.1 ± 0.3	8.8 ± 0.1	0.7 ± 0.3
KT2440-pgl	n.d.	12.2 ± 0.9	74.1 ± 1.5	3.8 ± 0.5	9.9 ± 0.8	n.d.
KT2440Δ*gcd-pgl*	n.d.	14.6 ± 0.3	73.1 ± 0.8	3.7 ± 0.2	8.1 ± 0.5	0.5 ± 0.1

n.d.: not detected, less than 0.2%.

[∞]: The data were determined by GC/MS and are given as relative molar fraction (%) of C6: 3-hydroxyexanoate, C8: 3-hydroxyoctanoate, C10:3-hydroxydecanoate, C12: 3-hydroxydodecanoate, C12:1: 3-hydroxy-5-cis-dodecanoate, and C14: 3-hydroxytetradecanoate.

In summary, the most efficient PHA producer was KT2440*Δgcd-acoA* strain, where the PHA concentration was doubled compared to *P. putida* wild-type strain (Figure 37A) and enhanced by 21% compared to the KT2440Δ*gcd* mutant strain (Figure 37A). Thus, the predicted engineering strategy was successful in increasing the *mcl*-PHA synthesis of *P. putida*.

3.4.3 Batch fermentation in the bioreactors for controlled *mcl-PHA* production

To ensure well-controlled *mcl*-PHA production using our metabolically engineered *P. putida* strains, aerobic batch fermentations of the KT2440-*acoA* and KT2440Δ*gcd-acoA* strains on glucose were performed in a bioreactor. Figure 38 shows the time-resolved measurements for *mcl*-PHA formation, biomass production and the corresponding concentrations of ammonium, gluconate, 2-ketogluconate, and glucose formation. As expected, the KT2440-*acoA* strain, gluconate and 2-ketogluconate were excreted into the medium during consumption of the available glucose (Figure 38A, Table 25). In contrast, during the fermentation of the flux optimized KT2440Δ*gcd-acoA* strain (Figure 38B) excreted organic acids were below the detection limit (Table 25).

Table 25. Physiological parameters of the wild-type *P. putida* KT2440 and metabolically engineered strains in batch culture grown with glucose.

Strain	μ_{max} (/h)	$Y_{X/S}$ § (g/g)	$Y_{2\text{-ketoglut/S}}$ (g/g)	$Y_{gluconate/S}$ (g/g)	$Y_{PHA/S}$ (g/g)
KT2440	0.56	0.22	<0.001	0.64	0.05
KT2440Δ*gcd*	0.42	0.23	<0.001	<0.001	0.08
KT2440-*acoA*	0.40	0.21	0.04	0.38	0.07
KT2440Δ*gcd-acoA*	0.25	0.25	<0.001	<0.001	0.11
KT2440-*pgl*	0.33	0.21	0.07	0.55	0.05
KT2440Δ*gcd-pgl*	0.21	0.24	<0.001	<0.001	0.08

§ $Y_{x/s}$ is calculated based on the total biomass concentration (true biomass + PHA content). Standard deviations of less than 10% were obtained in 3 independent experiments.

A recent study compared *mcl*-PHA synthesis in *P. putida* KT2440 and KT2442 when grown on gluconate (Follonier *et al.*, 2011). *P. putida* KT2440 accumulated 17% of its CDW as PHA, whereas KT2442 only synthesized 1.7 wt % as PHA, demonstrating the large differences between the two *P. putida* strains. *P. putida* KT2440 can re-consume gluconate and 2-ketogluconate once secreted to the medium. We recently demonstrated that this process is not efficient to improve *mcl*-PHA synthesis (Poblete-Castro *et al.*, 2014), resulting in a lower volumetric PHA productivity compared to the one shown by the Δ*gcd P. putida* mutant strain under the same growth conditions. Several investigations have shown that the volumetric productivity is the key parameter for the industrial production of PHAs and thus, any factor influencing this parameter affects the economics and cost competitiveness of PHAs synthesis via microbial fermentation (Follonier *et al.*, 2011, Lee & Na, 2013, Oehmen *et al.*, 2014, Choi & Lee, 1999). Ammonium was completely consumed at 12 h by the KT2440-*acoA* strain, while KT2440Δ*gcd-acoA* took more than 15 h to deplete the entire amount of nitrogen. In addition, a large proportion of carbon was directed towards gluconate in the KT2440-*acoA* strain. More than 5 g/L of gluconate was produced after 24 h, (Figure 38A).

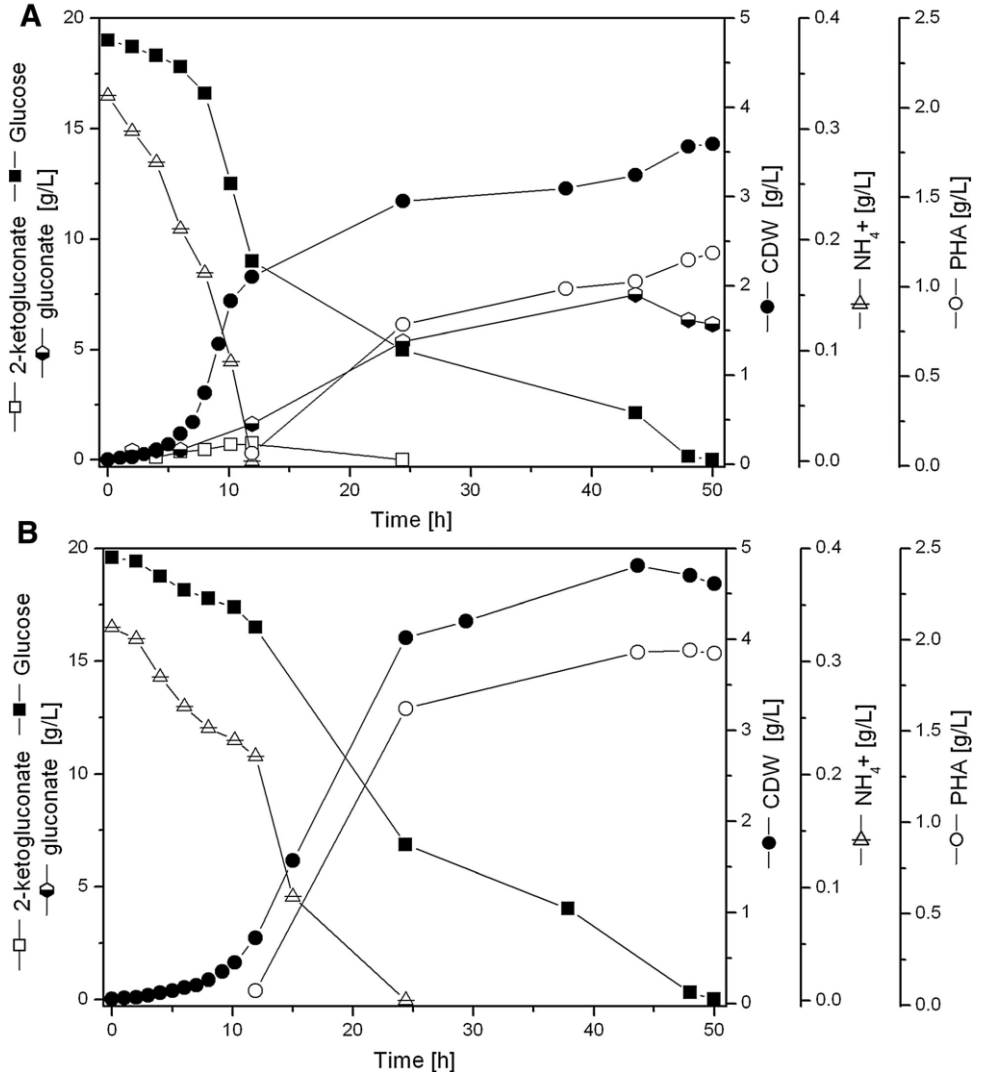

Figure 38. Growth and *mcl*-PHA production of the metabolically engineered strains KT2440-*acoA* (A) and KT2440Δ*gcd-acoA* (B) in batch cultures. Cells were grown in lab scale bioreactor in the presence of glucose 18.5 (g/L). Data are presented as mean values obtained from two independent experiments.

Furthermore, the lower biomass of 2 g/L obtained for this strain prior ammonium limitation was most likely due to the increased production of cellular compounds including nucleic acids and proteins due to less PHA formation. These findings might explain the reduced PHA and biomass yield on glucose in comparison to the KT2440Δ*gcd-acoA* mutant strain. The genetic modification of the KT2440Δ*gcd-acoA* led to the lowest μ_{max} of all strains (0.25/h versus 0.56/h for KT2440). Nevertheless, the KT2440Δ*gcd-acoA* strain biomass (CDW = 4.71 g/L after 50 hrs) and *mcl*-PHA 42.1 wt % contents were higher in comparison to the KT2440-*acoA* strain (CDW = 3.63 g/L after 50 hrs and *mcl*-PHA = 33.3 wt %). To our knowledge this is the highest *mcl*-PHA

accumulation ever reported using a *P. putida* strain in the presence of glucose in batch cultures.

3.4.4 Transcriptome analysis of the engineered *P. putida* PHA production strains

Glucose is metabolized in *P. putida* that utilizes three pathways converging at the level of 6-phosphogluconate prior to the formation of 2-keto-3-deoxy-6-phosphogluconate KDPG; (del Castillo *et al.*, 2007). The repressor HexR regulates the expression of major genes of the pathway including the *zwf-1*, *pgl*, *eda* operon and the *gap1* gene encoding glyceraldehyde-3-phosphate dehydrogenase. Accumulation and binding of KDPG to HexR lead to derepression (Daddaoua *et al.*, 2009, del Castillo *et al.*, 2008, Kim *et al.*, 2008). Furthermore, the genes of PHA synthesis are subjected to a complex control by catabolite regulation and various stress responses mediated by the complex RNA-dependent GacS and Crc regulating systems, besides others (Garcia-Maurino *et al.*, 2013, La Rosa *et al.*, 2014, Ryan *et al.*, 2013). In order to understand the gene regulatory adaptation of the newly engineered strains to enhanced PHA production the gene expression compared to the parental strains was analyzed using next generation sequencing of transcripts (RNA_{Seq}). We are fully aware that major adaptation processes might take place at the level of enzyme regulation which cannot be made visible with the employed approach. Samples were taken after 60 h of cultivation, when the PHA concentration in the cell reached its highest level. Strict cut-off parameters (log change > 2 and a *p*-value < 0.05) were applied. First, the gene expression of *acoA* overexpressing strains was compared to the wild-type KT2440 strain and the KT2440Δ*gcd* mutant strain (Table 26). Overall, 53 open reading frames (ORFs) were found differentially transcribed (12 up-regulated and 41 down-regulated) between the KT2440 wild-type strain with or without overexpressed *acoA*. Moreover, 108 ORFs (59 up-regulated and 49 down-regulated) were found changed in their transcription between the KT2440Δ*gcd* strain with or without overexpressed *acoA*. As expected, the strongest up-regulated gene in both variant strains overexpressing *acoA* was PP_0555 (*acoA*). Interestingly, also PP_0554 (*acoB*) was found upregulated, however to a lesser extent (Table 26). Most of the genes encoding for enzymes related to the central and PHA synthesis metabolic pathways showed only slight variations in their expression levels (Table 26). Interestingly, the increased flux toward acetyl-CoA and as a consequence citrate induced the expression of the isocitrate lyase gene, which encodes the first

enzyme of the glyoxylate shunt. One metabolic consequence is a reduced NADH production in the TCA cycle. A second consequence might be the channeling of acetyl-CoA into the glyoxylate cycle. In agreement, it was previously shown that inactivation of the isocitrate lyase gene leads to increased PHA production (Klinke *et al.*, 2000). Overall, the gene expression data do not provide conclusive explanations for the observed increase in PHA production. Most likely regulatory effects at the enzyme level might be responsible.

Table 26. Expression profile of the genes belonging to PHA biosynthesis and central metabolic pathways in the metabolically engineered *P. putida* strains compared to their parental strains.

Gene name	Locus tag	Description	Fold change	
			Δ*gcd-acoA*	**KT2440-a*coA***
PHA synthesis				
phaI	PP5008	PHA granule-associated	0.7	0.9
phaF	PP5007	PHA granule-associated	−0.3	0.2
phaC1	PP5003	PHA polymerase	−0.2	0.7
phaC2	PP5005	PHA polymerase	−0.6	−0.2
phaZ	PP5004	PHA depolymerase	0.3	0.5
phaD	PP5006	Transcriptional regulator	−0.4	0.3
phaG	PP1408	Acyl-transferase	**1.5**	−0.1
Transporters				
oprB-1	PP1019	Porin	−0.7	**−1.0**
oprB-2	PP1445	Porin	−0.5	−0.6
Glycolysis/ gluconeogenesis				
glk	PP1011	Glucokinase	0.2	−0.2
pgi	PP1808	Glucose-6-phosphate isomerase	−0.5	0.0
fbp	PP5040	Fructose-1,6-bisphosphatase	0.6	0.4
fda	PP4960	Fructose-1,6-bisphosphate aldolase	0.9	0.1

tpiA	PP4715	Triosephosphate isomerase	0.8	0.6
gap1	PP1009	Glyceraldehyde dehydrogenase, type I	**−1.2**	−0.4
gap2	PP2149	Glyceraldehyde dehydrogenase, type II	0.2	0.3
pgk	PP4963	Phosphoglycerate kinase	0.2	0.1
pgm	PP5056	Phosphoglyceromutase	0.4	0.1
eno	PP1612	Phosphopyruvate hydratase	0.3	0.0
pyk	PP1362	Pyruvate kinase	−0.3	0.4
Pentose phosphate pathways				
zwf1	PP1022	Glucose-6-phosphate dehydrogenase	0.9	0.2
zwf2	PP4042		0.1	−0.3
zwf3	PP5351		0.2	0.4
pgl	PP1023	6-phosphogluconate dehydrogenase	0.5	−0.9
gnd	PP4043	6-phosphoglucolacto dehydrogenase	−0.6	−0.1
gnuK	PP3416	Carbohydrate kinase	**−1.1**	−0.6
kguK	PP3378	Dehydroglucokinase	0.45	−0.4
kguD	PP3376	2-Ketogluconate 6-phosphate reductase	−0.7	−0.5
rpiA	PP5150	Ribose-5-phosphate isomerase A	0.3	0.0
rpe	PP0415	Ribulose-phosphate 3-epimerase	−0.5	−0.1
tktA	PP4965	Transketolase	0.3	0.7
tal	PP2168	Transaldolase B	0.4	0.3
Entner-Doudoroff pathway				
edd	PP1010	6-Phosphogluconate dehydratase	−0.3	−0.3

eda	PP1024	2-keto-3-deoxy-6-phosphogluconate aldolase	0.0	−0.5
Pyruvate metabolism				
acoA	PP0555	Pyruvate dehydrogenase	**12.4**	**5.3**
acoB	PP0554	Pyruvate dehydrogenase	**1.5**	**1.0**
acoC	PP0553	Pyruvate dehydrogenase	0.7	0.7
	PP0545	Aldehyde dehydrogenase	0.1	**−1.0**
acsA	PP4487	Acetyl-CoA synthetase	0.8	**1.4**
accC-2	PP5347	Pyruvate carboxylase	0.5	0.2
ppsA	PP2082	Phosphoenolpyruvate synthase	0.5	0.4
ppc	PP1505	Phosphoenolpyruvate carboxylase	0.5	0.4
TCA cycle				
gltA	PP4194	Citrate synthase	0.7	0.7
acnA	PP2112	Aconitate hydratase	0.4	−0.4
acnB	PP2339	Aconitate hydratase	0.7	0.3
icd	PP4011	Isocitrate dehydrogenase	0.3	−0.5
sucA	PP4189	2-Oxoglutarate dehydrogenase	−0.7	−0.2
sucD	PP4185	Succinyl-CoA synthetase sub alpha	−0.1	−0.3
sucC	PP4186	Succinyl-CoA synthetase sub beta	0.2	0.3
sdhA	PP4191	Succinate dehydrogenase	0.3	0.4
fumC	PP0944	Fumarate hydratase	0.5	**−1.1**
mdh	PP0654	Malate dehydrogenase	−0.4	**−1.3**
Glyoxylate shunt				
aceA	PP4116	Isocitrate lyase	**2.9**	**1.3**
glcB	PP0356	Malate synthase	0.8	0.8

p-value < 0.05. Grey color represents a differentiated expression pattern.

Next, the *pgl* overexpressing strains without increased PHA production were analyzed for potential compensatory gene regulatory activities. Of the 86 ORFs differentially expressed in KT2440-*pgl* mutant strain compared to the wild-type strain, 77 corresponded to genes that were transcriptionally up-regulated, whereas 9 genes were found with decreased expression levels (Table 27).

Table 27. Expression profile of the genes belonging to PHA biosynthesis and central metabolic pathways in the metabolically engineered strains compared to their parental strains.

Gene name	Locus tag	Description	Fold change	
			Δ*gcd-pgl*	**KT2440-*pgl***
PHA synthesis				
phaI	PP5008	PHA granule-associated	0.6	−0.3
phaF	PP5007	PHA granule-associated	0.3	−0.4
phaC1	PP5003	PHA polymerase	−0.8	−0.1
phaC2	PP5005	PHA polymerase	−0.7	−0.4
phaZ	PP5004	PHA depolymerase	−0.4	0.0
phaD	PP5006	Transcriptional regulator	0.2	0.1
phaG	PP1408	Acyl-transferase	**2.1**	0.2
Transporters				
oprB-1	PP1019	Porin	0.4	−0.1
oprB-2	PP1445	Porin	−0.4	−0.4
Glycolysis/gluconeogenesis				
glk	PP1011	Glucokinase	0.3	0.2
pgi	PP1808	Glucose-6-phosphate isomerase	−0.4	0.0
fbp	PP5040	Fructose-1,6-bisphosphatase	0.3	−0.1
fda	PP4960	Fructose-1,6-bisphosphate aldolase	0.6	−0.1
tpiA	PP4715	Triosephosphate isomerase	0.4	0.5
gap1	PP1009	Glyceraldehyde dehydrogenase, type I	−0.4	−0.2

gap2	PP2149	Glyceraldehyde dehydrogenase, type II	−0.3	−0.2
pgk	PP4963	Phosphoglycerate kinase	0.1	0.0
pgm	PP5056	Phosphoglyceromutase	0.5	−0.3
eno	PP1612	Phosphopyruvate hydratase	0.5	0.1
pyk	PP1362	Pyruvate kinase	−0.5	0.6
Pentose phosphate pathways				
zwf1	PP1022	Glucose-6-phosphate dehydrogenase	**5.2**	**3.6**
zwf2	PP4042		0.2	−0.6
zwf3	PP5351		−0.1	−0.3
Pgl	PP1023	6-phosphogluconate dehydrogenase	**9.3**	**7.8**
gnd	PP4043	6-phosphoglucolacto dehydrogenase	0.2	−0.3
gnuK	PP3416	Carbohydrate kinase	−0.1	0.3
kguK	PP3378	Dehydroglucokinase	0.6	0.5
kguD	PP3376	2-Ketogluconate 6-phosphate reductase	0.1	−0.1
rpiA	PP5150	Ribose-5-phosphate isomerase A	0.3	−0.4
rpe	PP0415	Ribulose-phosphate 3-epimerase	0.2	−0.1
tktA	PP4965	Transketolase	0.7	0.3
tal	PP2168	Transaldolase B	0.2	0.1
Entner-Doudoroff pathway				
edd	PP1010	6-Phosphogluconate dehydratase	0.2	0.1
eda	PP1024	2-keto-3-deoxy-6-phosphogluconate aldolase	0.4	−0.2
Pyruvate metabolism				
acoA	PP0555	Pyruvate dehydrogenase	**1.3**	**−2.7**

acoB	PP0554	Pyruvate dehydrogenase	0.7	−0.8
acoC	PP0553	Pyruvate dehydrogenase	0.5	**−1.2**
	PP0545	Aldehyde dehydrogenase	0.5	−0.9
acsA	PP4487	Acetyl-CoA synthetase	−0.3	−0.6
accC-2	PP5347	Pyruvate carboxylase	0.8	**2.3**
ppsA	PP2082	Phosphoenolpyruvate synthase	0.2	−0.1
ppc	PP1505	Phosphoenolpyruvate carboxylase	0.0	**1.4**
TCA cycle				
gltA	PP4194	Citrate synthase	−0.2	0.7
acnA	PP2112	Aconitate hydratase	0.8	−0.5
acnB	PP2339	Aconitate hydratase	−0.2	0.3
icd	PP4011	Isocitrate dehydrogenase	−0.3	−0.3
sucA	PP4189	2-Oxoglutarate dehydrogenase	−0.6	0.2
sucD	PP4185	Succinyl-CoA synthetase sub alpha	−0.2	0.5
sucC	PP4186	Succinyl-CoA synthetase sub beta	−0.1	0.1
sdhA	PP4191	Succinate dehydrogenase	−0.7	0.3
fumC	PP0944	Fumarate hydratase	**1.1**	−0.4
mdh	PP0654	Malate dehydrogenase	0.8	−0.8
Glyoxylate shunt				
aceA	PP4116	Isocitrate lyase	**1.2**	**−1.1**
glcB	PP0356	Malate synthase	−0.4	−0.1

p-value < 0.05. #Grey color represents a differentiated expression pattern.

For KT2440Δ*gcd-pgl* mutant strain compared to the KT2440Δ*gcd* mutant, 15 genes were found down-regulated while 117 ORFs were found induced. As expected, the *pgl* overexpressing strains revealed an increase of *pgl* mRNA. Glucose-6-phosphate dehydrogenase (encoded by PP_1022, *zwf*) was found to be highly up-regulated (>12 fold) in both strains harboring the overexpression system (Table 27). Obviously, the

initial goal to enhance the flux from glucose toward 2-keto-3-deoxy-6-phosphogluconate was achieved. The increased amounts of the metabolite might have enhanced *zwf-1* expression via HexR derepression. Furthermore, expression differences were detected for the pyruvate metabolism, where the genes encoding pyruvate dehydrogenase (PP_0554), pyruvate carboxylase (PP_5347) and phosphoenoylpyruvate (PP_1505) showed differential expression levels (Table 27). At least for the wild-type strain harboring the overexpressed *pgl* a problematic rearrangement of pyruvate metabolization occurred which might be responsible for the observed production phenotype. While the pyruvate dehydrogenase gene *acoA* was found reduced, the pyruvate carboxylase gene *acoC-2* was found induced (Table 27). In addition, induction of the phosphoenolpyruvate carboxylase gene *ppc* was detected. The KT2440Δ*gcd* mutant carrying overexpressed *pgl* did not reveal this response. For the *pgl* overexpression the observed gene regulatory response provides reasonable explanations for the observed PHA production phenotype.

3.4.5 The role of NADPH and NADH in *P. putida* PHA production

The production of *mcl*-PHAs in *P. putida* KT2440 requires NADPH + H^+. *P. putida* catabolizes glucose via the Entner-Doudoroff pathway and hence the NADPH + H^+ producing glucose-6-phosphate dehydrogenase (Zwf) is highly active. However, the attempts to further increase the metabolic flux through this step by overproducing the rate-limiting, succeeding enzyme (Pgl) failed to increase PHA production (Figure 37). However, the flux of carbon towards PHA was most likely hampered at the pyruvate metabolization step in the *pgl* overexpression strain. Interestingly, the transcriptome analyses revealed an increased *zwf* gene expression. In order to determine the contribution of the NADPH + H^+ level in *P. putida* to PHA production, NADPH + H^+ versus $NADP^+$ levels were determined for the various bioengineered strains (Table 28) The ratios of NADPH to $NADP^+$ were measured using UV/Vis spectrometry and quantified according to their colorimetric changes at λ = 450 nm. At the maximum *mcl*-PHA accumulation in the cell (60 h culture), we found the NADPH/$NADP^+$ ratios of all the PHA-overproducing strains were lower compared to the corresponding wild-type *P. putida* KT2440 (Table 28). Clearly, the employed metabolic engineering strategy increased the polyester production in both strains (Table 24, Figure 37). As a consequence of this increased flux of carbon into PHA synthesis, more NADPH is

needed to turn 3-ketoacyl-ACP into (R)-3-hydroxyacyl-ACP. Therefore, the levels of NADPH/$NADP^+$ were lower for the engineered *P. putida* strains (Table 28), in which pyruvate dehydrogenase was overproduced. A totally different picture was observed for the strains in which the *pgl* gene was overexpressed. Here, an increase of the NADPH/$NADP^+$ levels was detected (Table 28). As already deduced from the transcriptome data, the initial flux through the Entner-Doudoroff pathway might have been induced, leading to a KDPG accumulation and an increased *zwf-1* expression. Consequently, sufficient NADPH was produced. However, the increased flux of carbon towards PHA was lost at least in one case at the *pgl* overexpression strains. Overall, gene and most likely enzyme activity regulatory phenomena prohibited further flux towards PHA production and resulted in increased NADPH + H^+ levels.

Table 28. Levels of the NAD+, NADH, NADP+, and NADPH cofactors and their ratios of various *P. putida* strains under PHA producing conditions.

Strain	Cofactor level (mmol/g rCDW)*				Cofactor ratio	
	NAD^+	NADH	$NADP^+$	NADPH	$NADH/NAD^+$	$NADPH/NADP^+$
KT2440	7.62 ± 0.86	0.67 ± 0.08	3.22 ± 0.38	2.67 ± 0.07	0.09	0.83
KT2440Δ*gcd*	6.01 ± 0.67	1.75 ± 0.36	4.49 ± 0.12	1.31 ± 0.32	0.30	0.29
KT2440-*acoA*	6.25 ± 0.42	2.02 ± 0.15	6.48 ± 0.48	0.87 ± 0.27	**0.32**	0.13
KT2440Δ*gcd-acoA*	6.88 ± 0.33	2.94 ± 0.15	3.98 ± 0.46	0.96 ± 0.36	**0.43**	0.24
KT2440-*pgl*	5.59 ± 0.14	1.82 ± 0.10	2.58 ± 0.40	3.07 ± 0.41	0.33	1.19
KT2440Δ*gcd-pgl*	10.81 ± 0.50	2.18 ± 0.38	2.30 ± 0.15	3.71 ± 1.23	0.20	1.62

*rCDW: residual cell dry weight.

By overproducing the AcoA subunit of the pyruvate dehydrogenase complex, there was a significant change on $NADH/NAD^+$ values in comparison to those found in their parental strains (Table 28, bolt values). *P. putida* strains with high PHA production revealed high $NADH/NAD^+$ ratio values. It was shown before that intracellular NADH concentrations are crucial for cell growth (Berrios-Rivera *et al.*, 2004, Sanchez *et al.*, 2005). Similar observations of the importance of the $NADH/NAD^+$ ratio for PHA

synthesis from fatty acids in *P. putida* were published before (Ren *et al.*, 2009, Lee *et al.*, 1996, Escapa *et al.*, 2012).

In conclusion, we have successfully continued our in silico metabolic modeling based approach for the improvement of PHA formation in *P. putida*. The predicted overexpression of the pyruvate dehydrogenase subunit gene *acoA* in combination with the deletion of the glucose dehydrogenase gene *gcd* resulted in an increase of PHA production by 120%. Potential explanation for the observed PHA production phenotypes were derived from gene expression and cofactor quantification analyses. Beyond this work on microbial biopolymer production, *in silico* based metabolic engineering has proven truly valuable for succinate (Lee *et al.*, 2006), 1,4 butandiol (Yim *et al.*, 2011), bio-ethanol (Bro *et al.*, 2006), and amino acids (Becker *et al.*, 2011, Park *et al.*, 2007), suggesting this strategy as highly promising to breed superior producers industrial biotechnology.

4 Summary

The two bacterial species of the genus *Pseudomonas* were used during to investigate questions of fundamental and applied microbiology. *Pseudomonas aeruginosa* served as target for the identification and functional characterization of membrane-associated higher ordered protein complexes involved in anaerobic energy generation and motility. Using a combined affinity chromatography and proteomic approach the mega-complex for anaerobic denitrification, the conversion of nitrate via nitrite, NO, N_2O to molecular N_2, was isolated and its composition elucidated. All four enzymes of denitrification (Nar, Nir, Nor and Nos) and multiple accessory proteins were assembled at a membrane anchored platform consisting of NorBC and NosR. In agreement, mutants of *norBC* and *nosR* revealed abolished or hampered overall denitrification. Furthermore, various electron donating enzymes systems of cofactor biosynthesis, proteins export, the complete ATP synthase and multiple other compounds were part of the mega-complex. Protein-protein interactions were confirmed by electron microscopy. Interestingly, a trimeric complex of the nitrite reductase NirS, the flagella protein FliC and the chaperone DnaK were detected by a similar experimental approach in the periplasm of *P. aeruginosa*. Mutants of *nirS* revealed a defect in swimming motility. The cellular location of the three proteins was visualized by electron microscopy and protein domains of NirS responsible for protein-protein interaction with FliC were identified. The exact biological function of the complex, possibly in flagellum assembly, remains to be determined. Finally, *P. putida* were employed for the *in silico* metabolic modeling based directed optimization of PHA production. For this purpose the *acoA* gene encoding pyruvate dehydrogenase was successfully overexpressed. Combination with a glucose dehydrogenase gene (*gcd*) deficient genetic background enhanced PHA production by 120%. The functional background for the observed improvement was fully investigated by transcriptome and NADH /NAD^+ ratio analysis. In summary, this thesis provides for the first time evidences for the existence of a bacterial respirasome which seems to directly be coupled to motility.

5 Outlook

5.1 *P. aeruginosa* NirS interactome

- Mutagenic analysis on NirS and FliC to determine the exact peptides of the interaction and impact on flagellar production.
- RT-PCR of *nirS* mutant variants and wild-type and analysis of flagellar components expression.
- Beta-galactosidase activity assays with *nir* promoter and correlation of transcription with flagellar production.
- Generation of *dnaK* mutant and assessment of swimming motility, flagellar presence and determination of the transcriptional levels of flagellar gene expression.
- ATP tests to relate whether DnaK functions in the periplasm with ATP hydrolysis.
- Encountering signal peptides of DnaK or FliC generating constructs with different lengths at the N- or C-terminus.
- Determination of the immunological response of eukaryotic cells to FliC monomers.
- Elucidation of FliC membrane interaction partners to identify possible alternative export pathways.

5.2 *P. aeruginosa* NorCB-NosR interactome

- Determination of the order of these interactions by systematically purifying the different prey proteins in the distinct available mutants. This experiment permits as well the determination of the interacting peptides.
- Western-blot analysis for the determination of the nitrate and nitrite reductase presence in the whole cell extract of the *nirS*, *norB*, *narH* mutants and wild-type when grown under anaerobic denitrifying conditions.

5.3 Enhancement of PHA production in *P. putida*

- Overexpression in the Δ*gcd* mutant the three pyruvate dehydrogenase subunits (*acoA*, *acoB* and *acoC*) to possibly enhance the PHA yield.
- Knockout of target genes to deviate metabolite flux might increase PHA production according to the *in silico* model.

6 References

Adamczack, J., M. Hoffmann, U. Papke, K. Haufschildt, T. Nicke, M. Broring, M. Sezer, R. Weimar, U. Kuhlmann, P. Hildebrandt & G. Layer, (2014) NirN Protein from *Pseudomonas aeruginosa* is a Novel Electron-bifurcating Dehydrogenase Catalyzing the Last Step of Heme d_1 Biosynthesis. *J Biol Chem* **289**: 30753-30762.

Allen, W.J., G. Phan & G. Waksman, (2009) Structural biology of periplasmic chaperones. *Adv Protein Chem Struct Biol* **78**: 51-97.

Anders, S. & W. Huber, (2010) Differential expression analysis for sequence count data. *Genome Biol* **11**: R106.

Arai, H., (2011) Regulation and Function of Versatile Aerobic and Anaerobic Respiratory Metabolism in *Pseudomonas aeruginosa*. *Front Microbiol* **2**: 103.

Arai, H., Y. Igarashi & T. Kodama, (1995) Expression of the *nir* and *nor* genes for denitrification of *Pseudomonas aeruginosa* requires a novel CRP/FNR-related transcriptional regulator, DNR, in addition to ANR. *FEBS Lett* **371**: 73-76.

Arai, H., T. Kodama & Y. Igarashi, (1997) Cascade regulation of the two CRP/FNR-related transcriptional regulators (ANR and DNR) and the denitrification enzymes in *Pseudomonas aeruginosa*. *Mol Microbiol* **25**: 1141-1148.

Arai, H., M. Mizutani & Y. Igarashi, (2003) Transcriptional regulation of the *nos* genes for nitrous oxide reductase in *Pseudomonas aeruginosa*. *Microbiology* **149**: 29-36.

Aranda-Olmedo, I., R. Tobes, M. Manzanera, J.L. Ramos & S. Marques, (2002) Species-specific repetitive extragenic palindromic (REP) sequences in *Pseudomonas putida*. *Nucleic Acids Res* **30**: 1826-1833.

Arese, M., W.G. Zumft & F. Cutruzzola, (2003) Expression of a fully functional cd_1 nitrite reductase from *Pseudomonas aeruginosa* in *Pseudomonas stutzeri*. *Protein Expr Purif* **27**: 42-48.

Arias-Cartin, R., S. Grimaldi, P. Arnoux, B. Guigliarelli & A. Magalon, (2012) Cardiolipin binding in bacterial respiratory complexes: structural and functional implications. *Biochim Biophys Acta* **1817**: 1937-1949.

Armean, I.M., K.S. Lilley & M.W. Trotter, (2013) Popular computational methods to assess multiprotein complexes derived from label-free affinity purification and mass spectrometry (AP-MS) experiments. *Mol Cell Proteomics* **12**: 1-13.

Bachi, A. & T. Bonaldi, (2008) Quantitative proteomics as a new piece of the systems biology puzzle. *J Proteomics* **71**: 357-367.

Baker, P., C. Hillis, J. Carere & S.Y. Seah, (2012) Protein-protein interactions and substrate channeling in orthologous and chimeric aldolase-dehydrogenase complexes. *Biochemistry* **51**: 1942-1952.

Bali, S., M.J. Warren & S.J. Ferguson, (2010) NirF is a periplasmic protein that binds $d(_1)$ heme as part of its essential role in $d(_1)$ heme biogenesis. *FEBS J* **277**: 4944-4955.

Bannert, A., K. Kleineidam, L. Wissing, C. Mueller-Niggemann, V. Vogelsang, G. Welzl, Z. Cao & M. Schloter, (2011) Changes in diversity and functional gene abundances of microbial communities involved in nitrogen fixation, nitrification, and denitrification in a tidal wetland versus paddy soils cultivated for different time periods. *Appl Environ Microbiol* **77**: 6109-6116.

Bansal, S., S. Srinivasan, S. Anandasadagopan, A.R. Chowdhury, V. Selvaraj, B. Kalyanaraman, J. Joseph & N.G. Avadhani, (2012) Additive effects of mitochondrion-targeted cytochrome CYP2E1 and alcohol toxicity on cytochrome *c* oxidase function and stability of respirasome complexes. *J Biol Chem* **287**: 15284-15297.

Barraud, N., D.J. Hassett, S.H. Hwang, S.A. Rice, S. Kjelleberg & J.S. Webb, (2006) Involvement of nitric oxide in biofilm dispersal of *Pseudomonas aeruginosa*. *J Bacteriol* **188**: 7344-7353.

Barraud, N., D. Schleheck, J. Klebensberger, J.S. Webb, D.J. Hassett, S.A. Rice & S. Kjelleberg, (2009) Nitric oxide signaling in *Pseudomonas aeruginosa* biofilms mediates phosphodiesterase activity, decreased cyclic di-GMP levels, and enhanced dispersal. *J Bacteriol* **191**: 7333-7342.

Becker, J., O. Zelder, S. Hafner, H. Schroder & C. Wittmann, (2011) From zero to hero--design-based systems metabolic engineering of *Corynebacterium glutamicum* for L-lysine production. *Metab Eng* **13**: 159-168.

Bedzyk, L., T. Wang & R.W. Ye, (1999) The periplasmic nitrate reductase in *Pseudomonas* sp. strain G-179 catalyzes the first step of denitrification. *J Bacteriol* **181**: 2802-2806.

Ben-Zvi, A.P. & P. Goloubinoff, (2001) Review: mechanisms of disaggregation and refolding of stable protein aggregates by molecular chaperones. *J Struct Biol* **135**: 84-93.

Benkert, B., N. Quack, K. Schreiber, L. Jaensch, D. Jahn & M. Schobert, (2008) Nitrate-responsive NarX-NarL represses arginine-mediated induction of the *Pseudomonas aeruginosa* arginine fermentation *arcDABC* operon. *Microbiology* **154**: 3053-3060.

Berks, B.C., S.J. Ferguson, J.W. Moir & D.J. Richardson, (1995) Enzymes and associated electron transport systems that catalyse the respiratory reduction of nitrogen oxides and oxyanions. *Biochim Biophys Acta* **1232**: 97-173.

Berrier, C., A. Garrigues, G. Richarme & A. Ghazi, (2000) Elongation factor Tu and DnaK are transferred from the cytoplasm to the periplasm of *Escherichia coli* during osmotic downshock presumably via the mechanosensitive channel mscL. *J Bacteriol* **182**: 248-251.

Berrios-Rivera, S.J., A.M. Sanchez, G.N. Bennett & K.Y. San, (2004) Effect of different levels of NADH availability on metabolite distribution in Escherichia coli fermentation in minimal and complex media. *Appl Microbiol Biotechnol* **65**: 426-432.

Bertero, M.G., R.A. Rothery, M. Palak, C. Hou, D. Lim, F. Blasco, J.H. Weiner & N.C. Strynadka, (2003) Insights into the respiratory electron transfer pathway from the structure of nitrate reductase A. *Nat Struct Biol* **10**: 681-687.

Bildl, W., A. Haupt, C.S. Muller, M.L. Biniossek, J.O. Thumfart, B. Huber, B. Fakler & U. Schulte, (2012) Extending the dynamic range of label-free mass spectrometric quantification of affinity purifications. *Mol Cell Proteomics* **11**: M111 007955.

Borrero-de Acuna, J.M., A. Bielecka, S. Haussler, M. Schobert, M. Jahn, C. Wittmann, D. Jahn & I. Poblete-Castro, (2014) Production of medium chain length polyhydroxyalkanoate in metabolic flux optimized *Pseudomonas putida*. *Microb Cell Fact* **13**: 88.

Bro, C., B. Regenberg, J. Forster & J. Nielsen, (2006) *In silico* aided metabolic engineering of *Saccharomyces cerevisiae* for improved bioethanol production. *Metab Eng* **8**: 102-111.

Butland, G., J.M. Peregrin-Alvarez, J. Li, W. Yang, X. Yang, V. Canadien, A. Starostine, D. Richards, B. Beattie, N. Krogan, M. Davey, J. Parkinson, J. Greenblatt & A. Emili, (2005) Interaction network containing conserved and essential protein complexes in *Escherichia coli*. *Nature* **433**: 531-537.

Collins, M.O. & J.S. Choudhary, (2008) Mapping multiprotein complexes by affinity purification and mass spectrometry. *Curr Opin Biotechnol* **19**: 324-330.

Cuypers, H., A. Viebrock-Sambale & W.G. Zumft, (1992) NosR, a membrane-bound regulatory component necessary for expression of nitrous oxide reductase in denitrifying *Pseudomonas stutzeri*. *J Bacteriol* **174**: 5332-5339.

Choi, D.S., D.K. Kim, S.J. Choi, J. Lee, J.P. Choi, S. Rho, S.H. Park, Y.K. Kim, D. Hwang & Y.S. Gho, (2011) Proteomic analysis of outer membrane vesicles derived from *Pseudomonas aeruginosa*. *Proteomics* **11**: 3424-3429.

Choi, H., S. Kim, A.C. Gingras & A.I. Nesvizhskii, (2010) Analysis of protein complexes through model-based biclustering of label-free quantitative AP-MS data. *Mol Syst Biol* **6**: 385.

Choi, J. & S.Y. Lee, (1999) Factors affecting the economics of polyhydroxyalkanoate production by bacterial fermentation. *Applied Microbiology and Biotechnology* **51**: 13-21.

Chung, A., Q. Liu, S.P. Ouyang, Q. Wu & G.Q. Chen, (2009) Microbial production of 3-hydroxydodecanoic acid by pha operon and *fadBA* knockout mutant of *Pseudomonas putida* KT2442 harboring *tesB* gene. *Appl Microbiol Biotechnol* **83**: 513-519.

Daddaoua, A., T. Krell & J.L. Ramos, (2009) Regulation of glucose metabolism in *Pseudomonas*: the phosphorylative branch and entner-doudoroff enzymes are regulated by a repressor containing a sugar isomerase domain. *J Biol Chem* **284**: 21360-21368.

Dalbey, R.E. & A. Kuhn, (2012) Protein traffic in Gram-negative bacteria--how exported and secreted proteins find their way. *FEMS Microbiol Rev* **36**: 1023-1045.

Dammeyer, T., K.N. Timmis & P. Tinnefeld, (2013) Broad host range vectors for expression of proteins with (Twin-) Strep-tag, His-tag and engineered, export optimized yellow fluorescent protein. *Microb Cell Fact* **12**: 49.

Damron, F.H. & J.B. Goldberg, (2012) Proteolytic regulation of alginate overproduction in *Pseudomonas aeruginosa*. *Mol Microbiol* **84**: 595-607.

de la Fuente-Nunez, C., F. Reffuveille, K.E. Fairfull-Smith & R.E. Hancock, (2013) Effect of nitroxides on swarming motility and biofilm formation, multicellular behaviors in *Pseudomonas aeruginosa*. *Antimicrob Agents Chemother* **57**: 4877-4881.

del Castillo, T., E. Duque & J.L. Ramos, (2008) A set of activators and repressors control peripheral glucose pathways in *Pseudomonas putida* to yield a common central intermediate. *J Bacteriol* **190**: 2331-2339.

del Castillo, T., J.L. Ramos, J.J. Rodriguez-Herva, T. Fuhrer, U. Sauer & E. Duque, (2007) Convergent peripheral pathways catalyze initial glucose catabolism in *Pseudomonas putida*: genomic and flux analysis. *J Bacteriol* **189**: 5142-5152.

Dell'acqua, S., I. Moura, J.J. Moura & S.R. Pauleta, (2011) The electron transfer complex between nitrous oxide reductase and its electron donors. *J Biol Inorg Chem* **16**: 1241-1254.

Dias, J.M., M.E. Than, A. Humm, R. Huber, G.P. Bourenkov, H.D. Bartunik, S. Bursakov, J. Calvete, J. Caldeira, C. Carneiro, J.J. Moura, I. Moura & M.J. Romao, (1999) Crystal structure of the first dissimilatory nitrate reductase at 1.9 A solved by MAD methods. *Structure* **7**: 65-79.

Dotsch, A., D. Eckweiler, M. Schniederjans, A. Zimmermann, V. Jensen, M. Scharfe, R. Geffers & S. Haussler, (2012) The *Pseudomonas aeruginosa* transcriptome in planktonic cultures and static biofilms using RNA sequencing. *PLoS One* **7**: e31092.

Einsle, O. & P.M. Kroneck, (2004) Structural basis of denitrification. *Biol Chem* **385**: 875-883.

el Yaagoubi, A., M. Kohiyama & G. Richarme, (1994) Localization of DnaK (chaperone 70) from *Escherichia coli* in an osmotic-shock-sensitive compartment of the cytoplasm. *J Bacteriol* **176**: 7074-7078.

el Yaagoubi, A., M. Kohiyama & G. Richarme, (1996) Defect in export and synthesis of the periplasmic galactose receptor MglB in *dnaK* mutants of *Escherichia coli*, and decreased stability of the *mglB* mRNA. *Microbiology* **142 (Pt 9)**: 2595-2602.

Engler, C., R. Gruetzner, R. Kandzia & S. Marillonnet, (2009) Golden gate shuffling: a one-pot DNA shuffling method based on type IIs restriction enzymes. *PLoS One* **4**: e5553.

Engler, C. & S. Marillonnet, (2014) Golden Gate cloning. *Methods Mol Biol* **1116**: 119-131.

Escapa, I.F., C. del Cerro, J.L. Garcia & M.A. Prieto, (2013) The role of GlpR repressor in *Pseudomonas putida* KT2440 growth and PHA production from glycerol. *Environ Microbiol* **15**: 93-110.

Escapa, I.F., J.L. Garcia, B. Buhler, L.M. Blank & M.A. Prieto, (2012) The polyhydroxyalkanoate metabolism controls carbon and energy spillage in *Pseudomonas putida*. *Environ Microbiol* **14**: 1049-1063.

Eschbach, M., K. Schreiber, K. Trunk, J. Buer, D. Jahn & M. Schobert, (2004) Long-term anaerobic survival of the opportunistic pathogen *Pseudomonas aeruginosa* via pyruvate fermentation. *J Bacteriol* **186**: 4596-4604.

Farver, O., M. Brunori, F. Cutruzzola, S. Rinaldo, S. Wherland & I. Pecht, (2009) Intramolecular electron transfer in *Pseudomonas aeruginosa cd*$_{(1)}$ nitrite reductase: thermodynamics and kinetics. *Biophys J* **96**: 2849-2856.

Follonier, S., S. Panke & M. Zinn, (2011) A reduction in growth rate of *Pseudomonas putida* KT2442 counteracts productivity advances in medium-chain-length polyhydroxyalkanoate production from gluconate. *Microb Cell Fact* **10**: 25.

Frisk, A., J. Jyot, S.K. Arora & R. Ramphal, (2002) Identification and functional characterization of *flgM*, a gene encoding the anti-sigma 28 factor in *Pseudomonas aeruginosa*. *J Bacteriol* **184**: 1514-1521.

Garcia-Maurino, S.M., I. Perez-Martinez, C.I. Amador, I. Canosa & E. Santero, (2013) Transcriptional activation of the CrcZ and CrcY regulatory RNAs by the CbrB response regulator in *Pseudomonas putida*. *Mol Microbiol* **89**: 189-205.

Gardner, T.S., C.R. Cantor & J.J. Collins, (2000) Construction of a genetic toggle switch in *Escherichia coli*. *Nature* **403**: 339-342.

Giardina, G., S. Rinaldo, K.A. Johnson, A. Di Matteo, M. Brunori & F. Cutruzzola, (2008) NO sensing in *Pseudomonas aeruginosa*: structure of the transcriptional regulator DNR. *J Mol Biol* **378**: 1002-1015.

Gingras, A.C., M. Gstaiger, B. Raught & R. Aebersold, (2007) Analysis of protein complexes using mass spectrometry. *Nat Rev Mol Cell Biol* **8**: 645-654.

Hancock, R.E. & D.P. Speert, (2000) Antibiotic resistance in *Pseudomonas aeruginosa*: mechanisms and impact on treatment. *Drug Resist Updat* **3**: 247-255.

Hartig, E. & W.G. Zumft, (1999) Kinetics of nirS expression (cytochrome cd_1 nitrite reductase) in *Pseudomonas stutzeri* during the transition from aerobic respiration to denitrification: evidence for a denitrification-specific nitrate- and nitrite-responsive regulatory system. *J Bacteriol* **181**: 161-166.

Hasegawa, N., H. Arai & Y. Igarashi, (2001a) Two *c*-type cytochromes, NirM and NirC, encoded in the nir gene cluster of *Pseudomonas aeruginosa* act as electron donors for nitrite reductase. *Biochem Biophys Res Commun* **288**: 1223-1230.

Hassett, D.J., J. Cuppoletti, B. Trapnell, S.V. Lymar, J.J. Rowe, S.S. Yoon, G.M. Hilliard, K. Parvatiyar, M.C. Kamani, D.J. Wozniak, S.H. Hwang, T.R. McDermott & U.A. Ochsner, (2002) Anaerobic metabolism and quorum sensing by *Pseudomonas aeruginosa* biofilms in chronically infected cystic fibrosis airways: rethinking antibiotic treatment strategies and drug targets. *Adv Drug Deliv Rev* **54**: 1425-1443.

Haufschildt, K., S. Schmelz, T.M. Kriegler, A. Neumann, J. Streif, H. Arai, D.W. Heinz & G. Layer, (2014) The crystal structure of siroheme decarboxylase in complex with iron-uroporphyrin III reveals two essential histidine residues. *J Mol Biol* **426**: 3272-3286.

Hayashi, N.R., H. Arai, T. Kodama & Y. Igarashi, (1998) The *nirQ* gene, which is required for denitrification of *Pseudomonas aeruginosa*, can activate the RubisCO from *Pseudomonas hydrogenothermophila*. *Biochim Biophys Acta* **1381**: 347-350.

Hayashi, N.R., K. Terazono, T. Kodama & Y. Igarashi, (2000) Structure of ribulose 1,5-bisphosphate carboxylase/oxygenase gene cluster from a thermophilic hydrogen-oxidizing bacterium, *Hydrogenophilus thermoluteolus*, and phylogeny of the fructose 1,6-bisphosphate aldolase encoded by *cbbA* in the cluster. *Biosci Biotechnol Biochem* **64**: 61-71.

Herzberg, C., L.A. Weidinger, B. Dorrbecker, S. Hubner, J. Stulke & F.M. Commichau, (2007a) SPINE: a method for the rapid detection and analysis of protein-protein interactions *in vivo*. *Proteomics* **7**: 4032-4035.

Hino, T., Y. Matsumoto, S. Nagano, H. Sugimoto, Y. Fukumori, T. Murata, S. Iwata & Y. Shiro, (2010) Structural basis of biological N_2O generation by bacterial nitric oxide reductase. *Science* **330**: 1666-1670.

Hino, T., S. Nagano, H. Sugimoto, T. Tosha & Y. Shiro, (2012) Molecular structure and function of bacterial nitric oxide reductase. *Biochim Biophys Acta* **1817**: 680-687.

Honisch, U. & W.G. Zumft, (2003) Operon structure and regulation of the *nos* gene region of *Pseudomonas stutzeri*, encoding an ABC-Type ATPase for maturation of nitrous oxide reductase. *J Bacteriol* **185**: 1895-1902.

Hubner, N.C. & M. Mann, (2011) Extracting gene function from protein-protein interactions using Quantitative BAC InteraCtomics (QUBIC). *Methods* **53**: 453-459.

Imperi, F., F. Ciccosanti, A.B. Perdomo, F. Tiburzi, C. Mancone, T. Alonzi, P. Ascenzi, M. Piacentini, P. Visca & G.M. Fimia, (2009a) Analysis of the periplasmic proteome of *Pseudomonas aeruginosa*, a metabolically versatile opportunistic pathogen. *Proteomics* **9**: 1901-1915.

Imperi, F., F. Tiburzi & P. Visca, (2009b) Molecular basis of pyoverdine siderophore recycling in *Pseudomonas aeruginosa*. *Proc Natl Acad Sci U S A* **106**: 20440-20445.

Jimenez, J.I., B. Minambres, J.L. Garcia & E. Diaz, (2002) Genomic analysis of the aromatic catabolic pathways from *Pseudomonas putida* KT2440. *Environ Microbiol* **4**: 824-841.

Juhas, M., L. Eberl & B. Tummler, (2005) Quorum sensing: the power of cooperation in the world of *Pseudomonas*. *Environ Microbiol* **7**: 459-471.

Jyot, J., J.K. Gautam, M. Raje & A. Ghosh, (1999) Localization of DnaK and GroEL in *Vibrio cholerae*. *FEMS Microbiol Lett* **172**: 165-171.

Kaake, R.M., X. Wang & L. Huang, (2010) Profiling of protein interaction networks of protein complexes using affinity purification and quantitative mass spectrometry. *Mol Cell Proteomics* **9**: 1650-1665.

Kawakami, T., M. Kuroki, M. Ishii, Y. Igarashi & H. Arai, (2010) Differential expression of multiple terminal oxidases for aerobic respiration in *Pseudomonas aeruginosa*. *Environ Microbiol* **12**: 1399-1412.

Khosla, C. & J.D. Keasling, (2003) Metabolic engineering for drug discovery and development. *Nat Rev Drug Discov* **2**: 1019-1025.

Kim, J., C.O. Jeon & W. Park, (2008) Dual regulation of *zwf*-1 by both 2-keto-3-deoxy-6-phosphogluconate and oxidative stress in *Pseudomonas putida*. *Microbiology* **154**: 3905-3916.

Klinke, S., M. Dauner, G. Scott, B. Kessler & B. Witholt, (2000) Inactivation of isocitrate lyase leads to increased production of medium-chain-length poly(3-hydroxyalkanoates) in *Pseudomonas putida*. *Appl Environ Microbiol* **66**: 909-913.

Klockenbusch, C. & J. Kast, (2010) Optimization of formaldehyde cross-linking for protein interaction analysis of non-tagged integrin beta1. *J Biomed Biotechnol* **2010**: 927585.

Kohler, T., L.K. Curty, F. Barja, C. van Delden & J.C. Pechere, (2000) Swarming of *Pseudomonas aeruginosa* is dependent on cell-to-cell signaling and requires flagella and pili. *J Bacteriol* **182**: 5990-5996.

Kohlstedt, M., J. Becker & C. Wittmann, (2010) Metabolic fluxes and beyond-systems biology understanding and engineering of microbial metabolism. *Appl Microbiol Biotechnol* **88**: 1065-1075.

Kumar, A. & M. Snyder, (2002) Protein complexes take the bait. *Nature* **415**: 123-124.

Kuroki, M., Y. Igarashi, M. Ishii & H. Arai, (2014) Fine-tuned regulation of the dissimilatory nitrite reductase gene by oxygen and nitric oxide in *Pseudomonas aeruginosa*. *Environ Microbiol Rep* **6**: 792-801.

La Rosa, R., F. de la Pena, M.A. Prieto & F. Rojo, (2014) The Crc protein inhibits the production of polyhydroxyalkanoates in *Pseudomonas putida* under balanced carbon/nitrogen growth conditions. *Environ Microbiol* **16**: 278-290.

Lambert, J.P., G. Ivosev, A.L. Couzens, B. Larsen, M. Taipale, Z.Y. Lin, Q. Zhong, S. Lindquist, M. Vidal, R. Aebersold, T. Pawson, R. Bonner, S. Tate & A.C. Gingras, (2013) Mapping differential interactomes by affinity purification coupled with data-independent mass spectrometry acquisition. *Nat Methods* **10**: 1239-1245.

Lanciano, P., A. Vergnes, S. Grimaldi, B. Guigliarelli & A. Magalon, (2007) Biogenesis of a respiratory complex is orchestrated by a single accessory protein. *J Biol Chem* **282**: 17468-17474.

Lee, G.N. & J. Na, (2013) Future of microbial polyesters. *Microb Cell Fact* **12**: 54.
Lee, I.Y., M.K. Kim, Y.H. Park & S.Y. Lee, (1996) Regulatory effects of cellular nicotinamide nucleotides and enzyme activities on poly(3-hydroxybutyrate) synthesis in recombinant *Escherichia coli*. *Biotechnol Bioeng* **52**: 707-712.
Lee, J.W., T.Y. Kim, Y.S. Jang, S. Choi & S.Y. Lee, (2011) Systems metabolic engineering for chemicals and materials. *Trends Biotechnol* **29**: 370-378.
Lee, S.J., H. Song & S.Y. Lee, (2006) Genome-based metabolic engineering of *Mannheimia succiniciproducens* for succinic acid production. *Appl Environ Microbiol* **72**: 1939-1948.
Lewenza, S., R.K. Falsafi, G. Winsor, W.J. Gooderham, J.B. McPhee, F.S. Brinkman & R.E. Hancock, (2005) Construction of a mini-Tn5-luxCDABE mutant library in *Pseudomonas aeruginosa* PAO1: a tool for identifying differentially regulated genes. *Genome Res* **15**: 583-589.
Liang, S., Z. Xu, X. Xu, X. Zhao, C. Huang & Y. Wei, (2012) Quantitative proteomics for cancer biomarker discovery. *Comb Chem High Throughput Screen* **15**: 221-231.
Liberati, N.T., J.M. Urbach, S. Miyata, D.G. Lee, E. Drenkard, G. Wu, J. Villanueva, T. Wei & F.M. Ausubel, (2006) An ordered, nonredundant library of *Pseudomonas aeruginosa* strain PA14 transposon insertion mutants. *Proc Natl Acad Sci U S A* **103**: 2833-2838.
Lombardi, A., E. Silvestri, F. Cioffi, R. Senese, A. Lanni, F. Goglia, P. de Lange & M. Moreno, (2009) Defining the transcriptomic and proteomic profiles of rat ageing skeletal muscle by the use of a cDNA array, 2D- and Blue native-PAGE approach. *J Proteomics* **72**: 708-721.
Lunter, G. & M. Goodson, (2011) Stampy: a statistical algorithm for sensitive and fast mapping of Illumina sequence reads. *Genome Res* **21**: 936-939.
Madison, L.L. & G.W. Huisman, (1999) Metabolic engineering of poly(3-hydroxyalkanoates): from DNA to plastic. *Microbiol Mol Biol Rev* **63**: 21-53.
Magalon, A., R. Arias-Cartin & A. Walburger, (2012) Supramolecular organization in prokaryotic respiratory systems. *Adv Microb Physiol* **61**: 217-266.
Manting, E.H., A. Kaufmann, C. van der Does & A.J. Driessen, (1999) A single amino acid substitution in SecY stabilizes the interaction with SecA. *J Biol Chem* **274**: 23868-23874.
McGuirl, M.A., J.A. Bollinger, N. Cosper, R.A. Scott & D.M. Dooley, (2001) Expression, purification, and characterization of NosL, a novel Cu(I) protein of the nitrous oxide reductase (*nos*) gene cluster. *J Biol Inorg Chem* **6**: 189-195.
Mercenier, A., J.P. Simon & V. Stalon, (1980) Regulation of enzyme synthesis in the arginine deiminase pathway of *Pseudomonas aeruginosa* PAO1 [proceedings]. *Arch Int Physiol Biochim* **88**: B41-B42.
Miao, E.A., R.K. Ernst, M. Dors, D.P. Mao & A. Aderem, (2008) *Pseudomonas aeruginosa* activates caspase 1 through Ipaf. *Proc Natl Acad Sci U S A* **105**: 2562-2567.
Mulcahy, L.R., V.M. Isabella & K. Lewis, (2014) *Pseudomonas aeruginosa* biofilms in disease. *Microb Ecol* **68**: 1-12.
Muller, V.S., P.R. Jungblut, T.F. Meyer & S. Hunke, (2011) Membrane-SPINE: an improved method to identify protein-protein interaction partners of membrane proteins *in vivo*. *Proteomics* **11**: 2124-2128.
Narita, S., S. Matsuyama & H. Tokuda, (2004) Lipoprotein trafficking in *Escherichia coli*. *Arch Microbiol* **182**: 1-6.
Nelson, K.E., C. Weinel, I.T. Paulsen, R.J. Dodson, H. Hilbert, V.A. Martins dos Santos, D.E. Fouts, S.R. Gill, M. Pop, M. Holmes, L. Brinkac, M. Beanan, R.T. DeBoy, S. Daugherty, J. Kolonay, R. Madupu, W. Nelson, O. White, J. Peterson, H. Khouri, I. Hance, P. Chris Lee, E. Holtzapple, D. Scanlan, K. Tran, A. Moazzez, T. Utterback, M. Rizzo, K. Lee, D. Kosack, D. Moestl, H. Wedler, J. Lauber, D. Stjepandic, J. Hoheisel, M. Straetz, S. Heim, C. Kiewitz, J.A. Eisen, K.N. Timmis, A. Dusterhoft, B. Tummler

& C.M. Fraser, (2002) Complete genome sequence and comparative analysis of the metabolically versatile *Pseudomonas putida* KT2440. *Environ Microbiol* **4**: 799-808.

Nicke, T., T. Schnitzer, K. Munch, J. Adamczack, K. Haufschildt, S. Buchmeier, M. Kucklick, U. Felgentrager, L. Jansch, K. Riedel & G. Layer, (2013) Maturation of the cytochrome cd_1 nitrite reductase NirS from *Pseudomonas aeruginosa* requires transient interactions between the three proteins NirS, NirN and NirF. *Biosci Rep* **33**.

Noble, J.E. & M.J. Bailey, (2009) Quantitation of protein. *Methods Enzymol* **463**: 73-95.

Nurizzo, D., F. Cutruzzola, M. Arese, D. Bourgeois, M. Brunori, C. Cambillau & M. Tegoni, (1998) Conformational changes occurring upon reduction and NO binding in nitrite reductase from *Pseudomonas aeruginosa*. *Biochemistry* **37**: 13987-13996.

Nurizzo, D., M.C. Silvestrini, M. Mathieu, F. Cutruzzola, D. Bourgeois, V. Fulop, J. Hajdu, M. Brunori, M. Tegoni & C. Cambillau, (1997) N-terminal arm exchange is observed in the 2.15 A crystal structure of oxidized nitrite reductase from *Pseudomonas aeruginosa*. *Structure* **5**: 1157-1171.

O'Toole, G.A., K.A. Gibbs, P.W. Hager, P.V. Phibbs, Jr. & R. Kolter, (2000) The global carbon metabolism regulator Crc is a component of a signal transduction pathway required for biofilm development by *Pseudomonas aeruginosa*. *J Bacteriol* **182**: 425-431.

O'Toole, G.A. & R. Kolter, (1998) Flagellar and twitching motility are necessary for *Pseudomonas aeruginosa* biofilm development. *Mol Microbiol* **30**: 295-304.

Oehmen, A., F.V. Pinto, V. Silva, M.G. Albuquerque & M.A. Reis, (2014) The impact of pH control on the volumetric productivity of mixed culture PHA production from fermented molasses. *Engineering in Life Sciences* **14**: 143-152.

Ogierman, M. & V. Braun, (2003) Interactions between the outer membrane ferric citrate transporter FecA and TonB: studies of the FecA TonB box. *J Bacteriol* **185**: 1870-1885.

Oliver, S., (2000) Guilt-by-association goes global. *Nature* **403**: 601-603.

Ong, S.E. & M. Mann, (2005) Mass spectrometry-based proteomics turns quantitative. *Nat Chem Biol* **1**: 252-262.

Oren, A., (2009) Anaerobic respiration. *eLS*.

Orlando, V., (2000) Mapping chromosomal proteins *in vivo* by formaldehyde-crosslinked-chromatin immunoprecipitation. *Trends Biochem Sci* **25**: 99-104.

Orlando, V., H. Strutt & R. Paro, (1997) Analysis of chromatin structure by *in vivo* formaldehyde cross-linking. *Methods* **11**: 205-214.

Otero, J.M. & J. Nielsen, (2010) Industrial systems biology. *Biotechnol Bioeng* **105**: 439-460.

Palleroni, N.J., (1993) *Pseudomonas* classification. A new case history in the taxonomy of gram-negative bacteria. *Antonie Van Leeuwenhoek* **64**: 231-251.

Palleroni, N.J., (2003) Prokaryote taxonomy of the 20th century and the impact of studies on the genus *Pseudomonas*: a personal view. *Microbiology* **149**: 1-7.

Palleroni, N.J., R.W. Ballard, E. Ralston & M. Doudoroff, (1972) Deoxyribonucleic acid homologies among some *Pseudomonas* species. *J Bacteriol* **110**: 1-11.

Park, J.H., K.H. Lee, T.Y. Kim & S.Y. Lee, (2007) Metabolic engineering of *Escherichia coli* for the production of L-valine based on transcriptome analysis and *in silico* gene knockout simulation. *Proc Natl Acad Sci U S A* **104**: 7797-7802.

Perez-Rodriguez, R., A.C. Fisher, J.D. Perlmutter, M.G. Hicks, A. Chanal, C.L. Santini, L.F. Wu, T. Palmer & M.P. DeLisa, (2007) An essential role for the DnaK molecular chaperone in stabilizing over-expressed substrate proteins of the bacterial twin-arginine translocation pathway. *J Mol Biol* **367**: 715-730.

Poblete-Castro, I., D. Binger, A. Rodrigues, J. Becker, V.A. Martins Dos Santos & C. Wittmann, (2013) *In-silico*-driven metabolic engineering of *Pseudomonas putida* for enhanced production of poly-hydroxyalkanoates. *Metab Eng* **15**: 113-123.

Poblete-Castro, I., I.F. Escapa, C. Jager, J. Puchalka, C.M. Lam, D. Schomburg, M.A. Prieto & V.A. Martins dos Santos, (2012) The metabolic response of *P. putida* KT2442 producing high levels of polyhydroxyalkanoate under single- and multiple-nutrient-limited growth: highlights from a multi-level omics approach. *Microb Cell Fact* **11**: 34.

Poblete-Castro, I., A.L. Rodriguez, C.M. Lam & W. Kessler, (2014) Improved production of medium-chain-length polyhydroxyalkanoates in glucose-based fed-batch cultivations of metabolically engineered *Pseudomonas putida* strains. *J Microbiol Biotechnol* **24**: 59-69.

Pomowski, A., W.G. Zumft, P.M. Kroneck & O. Einsle, (2011) N_2O binding at a [4Cu:2S] copper-sulphur cluster in nitrous oxide reductase. *Nature* **477**: 234-237.

Qi, H.Y., J.B. Hyndman & H.D. Bernstein, (2002) DnaK promotes the selective export of outer membrane protein precursors in SecA-deficient *Escherichia coli*. *J Biol Chem* **277**: 51077-51083.

Rahme, L.G., E.J. Stevens, S.F. Wolfort, J. Shao, R.G. Tompkins & F.M. Ausubel, (1995) Common virulence factors for bacterial pathogenicity in plants and animals. *Science* **268**: 1899-1902.

Ranish, J.A., E.C. Yi, D.M. Leslie, S.O. Purvine, D.R. Goodlett, J. Eng & R. Aebersold, (2003) The study of macromolecular complexes by quantitative proteomics. *Nat Genet* **33**: 349-355.

Rashid, M.H. & A. Kornberg, (2000) Inorganic polyphosphate is needed for swimming, swarming, and twitching motilities of *Pseudomonas aeruginosa*. *Proc Natl Acad Sci U S A* **97**: 4885-4890.

Ren, Q., G. de Roo, K. Ruth, B. Witholt, M. Zinn & L. Thony-Meyer, (2009) Simultaneous accumulation and degradation of polyhydroxyalkanoates: futile cycle or clever regulation? *Biomacromolecules* **10**: 916-922.

Rigaut, G., A. Shevchenko, B. Rutz, M. Wilm, M. Mann & B. Seraphin, (1999) A generic protein purification method for protein complex characterization and proteome exploration. *Nat Biotechnol* **17**: 1030-1032.

Righetti, P.G., (1990) Recent developments in electrophoretic methods. *J Chromatogr* **516**: 3-22.

Rinaldo, S., G. Giardina, N. Castiglione, V. Stelitano & F. Cutruzzola, (2011) The catalytic mechanism of *Pseudomonas aeruginosa* cd_1 nitrite reductase. *Biochem Soc Trans* **39**: 195-200.

Rojo, F., (2010) Carbon catabolite repression in *Pseudomonas* : optimizing metabolic versatility and interactions with the environment. *FEMS Microbiol Rev* **34**: 658-684.

Ryan, W.J., N.D. O'Leary, M. O'Mahony & A.D. Dobson, (2013) GacS-dependent regulation of polyhydroxyalkanoate synthesis in *Pseudomonas putida* CA-3. *Appl Environ Microbiol* **79**: 1795-1802.

Sala, A., P. Bordes & P. Genevaux, (2014) Multitasking SecB chaperones in bacteria. *Front Microbiol* **5**: 666.

Sambrook, J. & D.W. Russell, (2001) *Molecular cloning: a laboratory manual (3-volume set)*. Cold spring harbor laboratory press Cold Spring Harbor, New York:.

Sanchez, A.M., G.N. Bennett & K.Y. San, (2005) Effect of different levels of NADH availability on metabolic fluxes of *Escherichia coli* chemostat cultures in defined medium. *J Biotechnol* **117**: 395-405.

Santini, S., A.R. Bizzarri, T. Yamada, C.W. Beattie & S. Cannistraro, (2014) Binding of azurin to cytochrome c_{551} as investigated by surface plasmon resonance and fluorescence. *J Mol Recognit* **27**: 124-130.

Schaefer, J.K., J. Yagi, J.R. Reinfelder, T. Cardona, K.M. Ellickson, S. Tel-Or & T. Barkay, (2004) Role of the bacterial organomercury lyase (MerB) in controlling methylmercury accumulation in mercury-contaminated natural waters. *Environ Sci Technol* **38**: 4304-4311.

Schneider, L.K., A. Wust, A. Pomowski, L. Zhang & O. Einsle, (2014) No laughing matter: the unmaking of the greenhouse gas dinitrogen monoxide by nitrous oxide reductase. *Met Ions Life Sci* **14**: 177-210.

Schobert, M. & P. Tielen, (2010) Contribution of oxygen-limiting conditions to persistent infection of *Pseudomonas aeruginosa*. *Future Microbiol* **5**: 603-621.

Schreiber, K., N. Boes, M. Eschbach, L. Jaensch, J. Wehland, T. Bjarnsholt, M. Givskov, M. Hentzer & M. Schobert, (2006) Anaerobic survival of *Pseudomonas aeruginosa* by pyruvate fermentation requires an Usp-type stress protein. *J Bacteriol* **188**: 659-668.

Schreiber, K., R. Krieger, B. Benkert, M. Eschbach, H. Arai, M. Schobert & D. Jahn, (2007) The anaerobic regulatory network required for *Pseudomonas aeruginosa* nitrate respiration. *J Bacteriol* **189**: 4310-4314.

Sharma, V., C.E. Noriega & J.J. Rowe, (2006) Involvement of NarK1 and NarK2 proteins in transport of nitrate and nitrite in the denitrifying bacterium *Pseudomonas aeruginosa* PAO1. *Appl Environ Microbiol* **72**: 695-701.

Shiro, Y., (2012) Structure and function of bacterial nitric oxide reductases: nitric oxide reductase, anaerobic enzymes. *Biochim Biophys Acta* **1817**: 1907-1913.

Silby, M.W., C. Winstanley, S.A. Godfrey, S.B. Levy & R.W. Jackson, (2011) *Pseudomonas* genomes: diverse and adaptable. *FEMS Microbiol Rev* **35**: 652-680.

Singleton, M.R. & D.B. Wigley, (2003) Multiple roles for ATP hydrolysis in nucleic acid modifying enzymes. *EMBO J* **22**: 4579-4583.

Smith, N.E., W.J. Tie, G.R. Flematti, K.A. Stubbs, B. Corry, P.V. Attwood & A. Vrielink, (2013) Mechanism of the dehydrogenase reaction of DmpFG and analysis of inter-subunit channeling efficiency and thermodynamic parameters in the overall reaction. *Int J Biochem Cell Biol* **45**: 1878-1885.

Stelzl, U. & E.E. Wanker, (2006) The value of high quality protein-protein interaction networks for systems biology. *Curr Opin Chem Biol* **10**: 551-558.

Stephanopoulos, G. & J.J. Vallino, (1991) Network rigidity and metabolic engineering in metabolite overproduction. *Science* **252**: 1675-1681.

Storbeck, S., S. Saha, J. Krausze, B.U. Klink, D.W. Heinz & G. Layer, (2011) Crystal structure of the heme d_1 biosynthesis enzyme NirE in complex with its substrate reveals new insights into the catalytic mechanism of S-adenosyl-L-methionine-dependent uroporphyrinogen III methyltransferases. *J Biol Chem* **286**: 26754-26767.

Stover, C.K., X.Q. Pham, A.L. Erwin, S.D. Mizoguchi, P. Warrener, M.J. Hickey, F.S. Brinkman, W.O. Hufnagle, D.J. Kowalik, M. Lagrou, R.L. Garber, L. Goltry, E. Tolentino, S. Westbrock-Wadman, Y. Yuan, L.L. Brody, S.N. Coulter, K.R. Folger, A. Kas, K. Larbig, R. Lim, K. Smith, D. Spencer, G.K. Wong, Z. Wu, I.T. Paulsen, J. Reizer, M.H. Saier, R.E. Hancock, S. Lory & M.V. Olson, (2000) Complete genome sequence of *Pseudomonas aeruginosa* PAO1, an opportunistic pathogen. *Nature* **406**: 959-964.

Su, S. & D.J. Hassett, (2012) Anaerobic *Pseudomonas aeruginosa* and other obligately anaerobic bacterial biofilms growing in the thick airway mucus of chronically infected cystic fibrosis patients: an emerging paradigm or "Old Hat"? *Expert Opin Ther Targets* **16**: 859-873.

Sutherland, B.W., J. Toews & J. Kast, (2008) Utility of formaldehyde cross-linking and mass spectrometry in the study of protein-protein interactions. *J Mass Spectrom* **43**: 699-715.

Tate, S., B. Larsen, R. Bonner & A.C. Gingras, (2013) Label-free quantitative proteomics trends for protein-protein interactions. *J Proteomics* **81**: 91-101.

Taubner, L.M., M.A. McGuirl, D.M. Dooley & V. Copie, (2004) 1H, 13C, 15N backbone and sidechain resonance assignments of apo-NosL, a novel copper(I) binding protein from the nitrous oxide reductase gene cluster of *Achromobacter cycloclastes*. *J Biomol NMR* **29**: 211-212.

Taubner, L.M., M.A. McGuirl, D.M. Dooley & V. Copie, (2006) Structural studies of Apo NosL, an accessory protein of the nitrous oxide reductase system: insights from structural homology with MerB, a mercury resistance protein. *Biochemistry* **45**: 12240-12252.

Timmis, K.N., (2002) *Pseudomonas putida*: a cosmopolitan opportunist par excellence. *Environ Microbiol* **4**: 779-781.

Toews, J., J.C. Rogalski, T.J. Clark & J. Kast, (2008) Mass spectrometric identification of formaldehyde-induced peptide modifications under *in vivo* protein cross-linking conditions. *Anal Chim Acta* **618**: 168-183.

Toyofuku, M., B. Roschitzki, K. Riedel & L. Eberl, (2012a) Identification of proteins associated with the *Pseudomonas aeruginosa* biofilm extracellular matrix. *J Proteome Res* **11**: 4906-4915.

Toyofuku, M., H. Uchiyama & N. Nomura, (2012b) Social Behaviours under Anaerobic Conditions in *Pseudomonas aeruginosa*. *Int J Microbiol* **2012**: 405191.

Trinkle-Mulcahy, L., (2012) Resolving protein interactions and complexes by affinity purification followed by label-based quantitative mass spectrometry. *Proteomics* **12**: 1623-1638.

Tripathi, L., L.P. Wu, M. Dechuan, J. Chen, Q. Wu & G.Q. Chen, (2013) *Pseudomonas putida* KT2442 as a platform for the biosynthesis of polyhydroxyalkanoates with adjustable monomer contents and compositions. *Bioresour Technol* **142**: 225-231.

Trunk, K., B. Benkert, N. Quack, R. Munch, M. Scheer, J. Garbe, L. Jansch, M. Trost, J. Wehland, J. Buer, M. Jahn, M. Schobert & D. Jahn, (2010) Anaerobic adaptation in *Pseudomonas aeruginosa*: definition of the Anr and Dnr regulons. *Environ Microbiol* **12**: 1719-1733.

Ugidos, A., G. Morales, E. Rial, H.D. Williams & F. Rojo, (2008) The coordinate regulation of multiple terminal oxidases by the *Pseudomonas putida* ANR global regulator. *Environ Microbiol* **10**: 1690-1702.

Unden, G. & J. Bongaerts, (1997) Alternative respiratory pathways of *Escherichia coli*: energetics and transcriptional regulation in response to electron acceptors. *Biochim Biophys Acta* **1320**: 217-234.

Van Alst, N.E., L.A. Sherrill, B.H. Iglewski & C.G. Haidaris, (2009a) Compensatory periplasmic nitrate reductase activity supports anaerobic growth of *Pseudomonas aeruginosa* PAO1 in the absence of membrane nitrate reductase. *Can J Microbiol* **55**: 1133-1144.

Van Alst, N.E., M. Wellington, V.L. Clark, C.G. Haidaris & B.H. Iglewski, (2009b) Nitrite reductase NirS is required for type III secretion system expression and virulence in the human monocyte cell line THP-1 by *Pseudomonas aeruginosa*. *Infect Immun* **77**: 4446-4454.

Vander Wauven, C., A. Pierard, M. Kley-Raymann & D. Haas, (1984) *Pseudomonas aeruginosa* mutants affected in anaerobic growth on arginine: evidence for a four-gene cluster encoding the arginine deiminase pathway. *J Bacteriol* **160**: 928-934.

Vasilescu, J., X. Guo & J. Kast, (2004) Identification of protein-protein interactions using *in vivo* cross-linking and mass spectrometry. *Proteomics* **4**: 3845-3854.

Vollack, K.U. & W.G. Zumft, (2001) Nitric oxide signaling and transcriptional control of denitrification genes in *Pseudomonas stutzeri*. *J Bacteriol* **183**: 2516-2526.

Wessel, D. & U.I. Flugge, (1984) A method for the quantitative recovery of protein in dilute solution in the presence of detergents and lipids. *Anal Biochem* **138**: 141-143.

Williams, H.D., J.E. Zlosnik & B. Ryall, (2007) Oxygen, cyanide and energy generation in the cystic fibrosis pathogen *Pseudomonas aeruginosa*. *Adv Microb Physiol* **52**: 1-71.

Withers, H., S. Swift & P. Williams, (2001) Quorum sensing as an integral component of gene regulatory networks in Gram-negative bacteria. *Curr Opin Microbiol* **4**: 186-193.

Wunsch, P., M. Herb, H. Wieland, U.M. Schiek & W.G. Zumft, (2003) Requirements for Cu(A) and Cu-S center assembly of nitrous oxide reductase deduced from complete periplasmic enzyme maturation in the nondenitrifier *Pseudomonas putida*. *J Bacteriol* **185**: 887-896.

Wunsch, P. & W.G. Zumft, (2005) Functional domains of NosR, a novel transmembrane iron-sulfur flavoprotein necessary for nitrous oxide respiration. *J Bacteriol* **187**: 1992-2001.

Wust, A., L. Schneider, A. Pomowski, W.G. Zumft, P.M. Kroneck & O. Einsle, (2012) Nature's way of handling a greenhouse gas: the copper-sulfur cluster of purple nitrous oxide reductase. *Biol Chem* **393**: 1067-1077.

Yim, H., R. Haselbeck, W. Niu, C. Pujol-Baxley, A. Burgard, J. Boldt, J. Khandurina, J.D. Trawick, R.E. Osterhout, R. Stephen, J. Estadilla, S. Teisan, H.B. Schreyer, S. Andrae, T.H. Yang, S.Y. Lee, M.J. Burk & S. Van Dien, (2011) Metabolic engineering of *Escherichia coli* for direct production of 1,4-butanediol. *Nat Chem Biol* **7**: 445-452.

Zetterquist, W., H. Marteus, P. Kalm-Stephens, E. Nas, L. Nordvall, M. Johannesson & K. Alving, (2009) Oral bacteria--the missing link to ambiguous findings of exhaled nitrogen oxides in cystic fibrosis. *Respir Med* **103**: 187-193.

Zhao, X., S.J. Norris & J. Liu, (2014) Molecular architecture of the bacterial flagellar motor in cells. *Biochemistry* **53**: 4323-4333.

Zumft, W.G., (1997) Cell biology and molecular basis of denitrification. *Microbiol Mol Biol Rev* **61**: 533-616.

7 Acknowledgements

At this point I would like to thank the people that helped me throughout my PhD time in one or another manner. First, I would like to thank Prof. Dr. Kenneth Timmis for obtaining the IPBSL funding, desposit his trust on me to conduct my work and guide me extraordinarily to succeed in my project. I would like to thank as well PD. Dr. Max Schobert for his magnificent supervision and advice throughout my work as well as the funding he provided with (DFG grant SCHO 888/4-1). Then, I feel incredibly grateful with Prof. Dr. Dieter Jahn for his scientific input, discussions and writing support in order to publish, correct my thesis and subsequently bring the work to a good end.

Furthermore, I profoundly appreciate the support given by Dr. Gabriella Molinari in order to carry out a proper PhD in terms of scientific guidance, techniques and consultation of all kind. I am deeply grateful for the supervision and scientific contribution that Dr. Sagrario Arias Rivas facilitated during the first stages of my PhD. Moreover, I highly value the outstanding assitance that Dr. Martina Jahn gave to get through the publications. I would also like to give thanks to the “mibi” for the relaxed and affable atmosphere to work.

Next, I direct my thanks to my Braunschweiger friends for rendering this time much more pleasant through conversations, hanging out, etc. Specially, Aaron, Tobito Schubeis, Rolfihno, Ignacito, Evelyn, Alexito, Sonia, Christian Lassek, Sterni, Marcia, Peppino, Marcelo Oliveira and Gehara, Christian Feiler, Carla, Sebastian, Tobi Knuuti, Christian Robledo, Jalil, Nicole and many others. They all made this period of my life something to not forget.

Very special thanks correspond to my family, for all the personal support and pacience they had all this time. They educated and raised me to become a better person in such a way only they could.

Last but not least, I would like to thank Erika, my rock, the person I leaned on when I needed to. The person who was with me all this way through and that understood me better than anyone else. Without her, I could not have succeeded in this task.

8 Appendix

P. aeruginosa protein preys found in the eluates of the baits NorB-His_{6x}, NorC-His_{6x} and NosR-His_{6x}. The fold-change enrichment of each protein is calculated by dividing its area value by the area value found in the control. Here the PA accession number and the cellular process in which the proteins are involved are shown.

Interaction partners found for NorB, NorC and NosR involved in the respiratory chains and other crucial cellular processes.

PA Nº	Interaction Partners	NorB	NorC	NosR
	1 Electron transport chain			
	1.1 NADH dehydrogenases			
PA2638	NADH dehydrogenase subunit B NuoB	3.59	29.01	11.47
PA2639	Bifunctional NADH:ubiquinone oxidoreductase subunit C/D NuoD	16.63	148.76	19.72
PA2640	NADH dehydrogenase subunit E NuoE	∞	∞	∞
PA2641	NADH dehydrogenase subunit F NuoF	∞	∞	∞
PA2642	NADH dehydrogenase subunit G NuoG	∞	∞	∞
PA2644	NADH dehydrogenase subunit I NuoI	3.40	18.98	7.62
PA2999	Na(+)-translocating NADH-quinone reductase subunit A NqrA	∞	∞	∞
PA2997	Na(+)-translocating NADH-quinone reductase subunit C NqrC	∞	ND	ND
PA2994	Na(+)-translocating NADH-quinone reductase subunit F NqrF	∞	ND	ND
PA4538	NADH dehydrogenase Ndh	∞	ND	ND
PA0023	Quinone oxidoreductase Qor	ND	∞	ND
	1.2 Other primary dehydrogenases			
PA4810	Nitrate-inducible formate dehydrogenase, gamma subunit FdnL	ND	∞	ND
PA4811	Nitrate-inducible formate dehydrogenase, beta subunit FdnH	∞	∞	∞
PA3582	Glycerol kinase GlpK	∞	∞	ND
PA1551	Ferredoxin FixG	ND	∞	ND
PA3584	Glycerol-3-phosphate dehydrogenase GlpD	∞	∞	ND
PA2951	Electron transfer flavoprotein alpha-subunit EtfA	0.70	0.97	ND
PA2952	Electron transfer flavoprotein beta-subunit EtfB	0.51	1.21	ND

PA4771	L-lactate dehydrogenase LldD	0.89	11.33	ND
PA3183	Glucose-6-phosphate 1-dehydrogenase Zwf	∞	ND	ND
PA4809	Formate dehydrogenase accessory protein FdhE	ND	∞	ND
PA2953	Electron transfer flavoprotein-ubiquinone oxidoreductase	∞	∞	∞
PA0782	Bifunctional proline dehydrogenase/pyrroline-5-carboxylate dehydrogenase PutA	0.74	17.03	4.03
PA4640	Malate:quinone oxidoreductase MqoB	1.75	6.63	ND
PA5349	Putative rubredoxin reductase RubB	∞	ND	ND
PA3452	Malate:quinone oxidoreductase MqoA	∞	∞	ND
PA2290	Glucose dehydrogenase Gcd	ND	∞	ND
PA5304	D-amino acid dehydrogenase small subunit DadA	0.33	3.09	1.12
	1.3 Succinate dehydrogenase			
PA1583	Succinate dehydrogenase flavoprotein subunit SdhA	4.01	12.38	4.08
PA1584	Succinate dehydrogenase Fe-S-subunit SdhB	7.60	17.30	6.00
PA1582	Succinate dehydrogenase D subunit SdhD	ND	5.78	3.04
	2 ATP synthase			
PA5556	F0F1 ATP synthase subunit alpha AtpA	0.87	4.43	1.92
PA5560	F0F1 ATP synthase subunit A AtpB	ND	∞	ND
PA5558	F0F1 ATP synthase subunit B AtpF	1.27	3.49	2.60
PA5553	F0F1 ATP synthase subunit epsilon AtpC	1.67	9.69	3.70
PA5554	F0F1 ATP synthase subunit beta AtpD	1.32	6.76	2.25
PA5555	F0F1 ATP synthase subunit gamma AtpG	1.13	7.52	ND
PA5557	F0F1 ATP synthase subunit delta AtpH	0.24	2.83	1.40
	3 Cytochrome oxidases			
PA1317	Cytochrome *o* ubiquinol oxidase subunit II CyoA	∞	ND	ND
PA4571	Putative cytochrome *c*	∞	ND	ND
PA1555	Cytochrome *c* CcoP2	0.26	ND	ND
PA4619	Probable *c*-type cytochrome	∞	ND	ND
PA2266	Putative cytochrome *c* precursor	∞	ND	ND
PA1552	Cytochrome *c* oxidase, cbb_3-type, CcoP subunit	0.96	1.43	ND
PA1553	Cytochrome *c* oxidase, cbb_3-type, CcoO subunit	0.88	2.46	2.02
PA4429	Putative cytochrome c_1 precursor	0.42	1.44	0.97
PA5300	Cytochrome c_5 CycB	0.45	0.69	ND
PA1556	Cytochrome *c* oxidase, cbb_3-type, CcoO subunit	0.95	5.45	5.61
PA1554	Cytochrome oxidase subunit (cbb_3-type) CcoN1	ND	6.17	ND
PA5490	Cytochrome c_4 precursor Cc4	0.52	1.17	2.24

	4 Fermentation			
PA3629	Alcohol dehydrogenase class III AdhC	∞	ND	ND
PA0835	Phosphate acetyltransferase Pta	1.43	4.22	ND
PA0836	Acetate kinase AckA	∞	∞	ND
PA5005	Putative carbamoyl transferase	2.14	6.27	2.55
PA5427	Alcohol dehydrogenase AdhA	0.42	4.94	ND
PA0888	Arginine/ornithine binding protein AotJ	0.29	0.55	ND
PA0892	Arginine/ornithine transport protein AotP	∞	∞	∞
PA2119	Alcohol dehydrogenase (Zn-dependent) Adh	∞	∞	ND
PA5171	Arginine deiminase ArcA	2.14	3.09	ND
PA5172	Ornithine carbamoyltransferase ArcB	3.80	3.69	ND
	5 Cofactor formation			
PA3813	Scaffold protein IscU	1.73	2.17	0.63
PA1481	Cytochrome C biogenesis protein CcmG	∞	ND	ND
PA1479	Cytochrome c-type biogenesis protein CcmE	2.08	4.20	2.14
PA1483	Cytochrome c-type biogenesis protein CycH	1.44	40.78	ND
PA3977	Glutamate-1-semialdehyde aminotransferase HemL	3.76	29.64	ND
PA5257	Heme biosynthesis associated protein PA5257	3.41	18.98	ND
PA4388	Potential heme catabolic process protein	∞	∞	∞
PA3914	Molybdenum cofactor biosynthetic protein A1 MoeA1	ND	ND	1.15
PA0761	L-aspartate oxidase NadB	∞	ND	ND
PA4920	NAD synthetase NadE	∞	ND	ND
PA4730	Pantoate--beta-alanine ligase PanC	∞	ND	ND
PA4919	Nicotinate phosphoribosyltransferase PncB1	∞	ND	ND
PA4376	Nicotinate phosphoribosyltransferase PncB2	∞	ND	ND
PA1796	5,10-methylene-tetrahydrofolate dehydrogenase / cyclohydrolase FolD	∞	ND	ND
PA4524	Nicotinate-nucleotide pyrophosphorylase NadC	ND	∞	ND
PA3918	Molybdenum cofactor biosynthesis protein C MoaC	∞	∞	∞
PA0024	Coproporphyrinogen III oxidase HemF	1.49	11.99	ND
PA5243	Delta-aminolevulinic acid dehydratase HemB	0.38	1.95	ND
PA2611	Siroheme synthase CysG	ND	∞	ND
PA3915	Molybdopterin biosynthetic protein B1 MoaB1	2.81	16.59	9.00
PA3029	Molybdopterin biosynthetic protein B2 MoaB2	∞	∞	ND
PA0655	Potential Ubiquinone biosynthesis protein COQ7	ND	∞	∞

PA5063	Ubiquinone/menaquinone biosynthesis methyltransferase UbiE	0.89	13.05	ND
PA5258	Potential enzyme of heme biosynthesis HemX	0.89	6.71	2.52
PA1546	Coproporphyrinogen III oxidase HemN	0.31	10.32	2.65
	6 Cell division			
PA4751	Cell division protein FtsH	30.05	76.99	19.69
PA4408	Cell division protein FtsA	1.82	4.98	ND
PA0374	Cell division ATP-binding protein FtsE	∞	∞	ND
PA0375	Cell division protein FtsX	∞	∞	ND
PA1528	Cell division protein ZipA	13.88	54.62	ND
PA5037	Potential cell division protein	5.39	27.55	9.64
PA1454	Flagellar synthesis regulator FleN	∞	ND	ND
PA3243	Septum formation inhibitor MinC	∞	ND	ND
PA4686	Chromosome segregation protein	∞	ND	ND
PA3440	Potential cell division protein	∞	∞	∞
PA4407	Cell division protein FtsZ	3.04	11.54	1.48
PA3245	Cell division topological specificity factor MinE	∞	∞	ND
PA3481	Hypothetical protein PA3481 Mrp	∞	∞	ND
PA3244	Cell division inhibitor MinD	2.55	7.07	ND
PA4480	Rod shape-determining protein MreC	∞	ND	ND
PA4481	Rod-shape-determining protein MreB	6.59	23.13	7.46
	7 TCA cycle and pyruvate knot			
PA2250	Dihydrolipoamide dehydrogenase LpdV	∞	ND	ND
PA3635	Phosphopyruvate hydratase Eno	1.28	1.96	ND
PA4329	Pyruvate kinase PykA	7.11	12.42	ND
PA5016	Dihydrolipoamide acetyltransferase AceF	9.06	18.79	ND
PA1183	C4-dicarboxylate transporter DctA	ND	∞	ND
PA0552	Phosphoglycerate kinase Pgk	ND	1.80	ND
PA5015	Pyruvate dehydrogenase subunit E1 AceE	1.55	5.19	ND
PA1770	Phosphoenolpyruvate synthase PpsA	1.09	3.04	ND
PA5192	Phosphoenolpyruvate carboxykinase PckA	1.09	2.79	ND
PA3471	Malate dehydrogenase SfcA	∞	∞	ND
PA4333	Fumarase FumA	∞	∞	ND
PA5435	Pyruvate carboxylase subunit B OadA	∞	ND	ND
PA0794	Aconitate hydratase	1.61	ND	ND
PA5046	Malic enzyme	0.44	ND	ND
PA1587	Dihydrolipoamide dehydrogenase Lpd	3.54	6.26	ND
PA0854	Fumarate hydratase FumC2	ND	∞	ND

PA1562	Aconitate hydratase AcnA	0.73	1.44	ND
PA1580	Type II citrate synthase GltA	0.71	3.45	ND
PA2623	Isocitrate dehydrogenase Icd	0.30	1.03	ND
PA2634	Isocitrate lyase AceA	2.58	ND	ND
PA0795	Methylcitrate synthase PrpC	0.64	ND	ND
PA2624	Isocitrate dehydrogenase Idh	1.27	2.96	ND
PA1585	2-oxoglutarate dehydrogenase E1 component SucA	9.14	30.46	ND
PA1586	Dihydrolipoamide succinyltransferase SucB	2.30	8.79	ND
PA1589	Succinyl-CoA synthetase subunit alpha SucD	0.72	2.50	0.54
PA1588	Succinyl-CoA synthetase subunit beta SucC	2.11	6.15	1.27
PA5006	Potential citrate synthase	∞	ND	ND
PA1787	Bifunctional aconitate hydratase 2/2-methylisocitrate dehydratase AcnB	0.55	3.61	0.72
PA2014	Methylcrotonyl-CoA carboxylase, beta-subunit LiuB	∞	∞	ND
PA2012	Methylcrotonyl-CoA carboxylase, alpha-subunit (biotin-containing)' LiuD	∞	∞	ND
PA4848	Acetyl-CoA carboxylase biotin carboxylase subunit AccC	3.93	8.47	1.72
PA3112	Acetyl-CoA carboxylase subunit beta AccD	19.11	23.44	4.64
PA3639	Acetyl-CoA carboxylase carboxyltransferase subunit alpha AccA	15.90	12.76	ND
PA3901	Fe(III) dicitrate transport protein FecA	∞	ND	ND
PA5166	Two-component response regulator DctD	∞	∞	ND
	8 Cell wall/membrane/envelope			
PA5221	2-octaprenyl-3-methyl-6-methoxy-1,4-benzoquinol hydroxylase VisC	∞	∞	ND
PA4749	Phosphoglucosamine mutase GlmM	0.90	3.62	1.90
PA5450	ABC subunit of A-band LPS efflux transporter Wzt	ND	∞	∞
PA3150	LPS biosynthesis protein WbpG	∞	∞	∞
PA5077	Gucosyltransferase MdoH	1.09	17.85	10.85
PA5278	Diaminopimelate epimerase DapF	∞	∞	ND
PA4460	Periplasmic LPS transport OstA	13.60	36.42	20.34
PA3299	Acyl-CoA synthetase FadD1	11.48	23.92	6.54
PA4067	Outer membrane protein OprG precursor	4.36	ND	ND
PA2509	Muconate cycloisomerase I CatB	∞	ND	ND

PA4406	UDP-3-O-[3-hydroxymyristoyl] N-acetylglucosamine deacetylase LpxC	1.78	ND	ND
PA2989	c-di-GMP-binding protein	∞	ND	∞
PA5164	dTDP-4-dehydrorhamnose 3,5-epimerase RmlC	∞	ND	ND
PA3337	ADP-L-glycero-D-mannoheptose 6-epimerase RfaD	∞	ND	ND
PA3300	Acyl-CoA synthetase FadD2	∞	ND	ND
PA4411	UDP-N-acetylmuramate--L-alanine ligase MurC	∞	ND	ND
PA3148	UDP-N-acetylglucosamine 2-epimerase WbpL	3.38	22.32	4.62
PA2232	Phosphomannose isomerase/GDP-mannose pyrophosphorylase	∞	ND	ND
PA4418	Penicillin-binding protein 3 FtsI	∞	ND	ND
PA4700	Penicillin-binding protein 1B MrcB	∞	ND	ND
PA3242	Lipid A biosynthesis lauroyl acyltransferase HtrB	∞	ND	ND
PA2966	Acyl carrier protein AcpP	6.57	18.88	ND
PA5546	3-demethylubiquinone-9 3-O-methyltransferase activity	∞	ND	ND
PA5011	Lipopolysaccharide heptosyltransferase I WaaC	∞	ND	ND
PA4988	3-deoxy-D-manno-octulosonic-acid transferase WaaA	∞	ND	ND
PA4693	Phosphatidylserine synthase PssA	∞	∞	ND
PA4003	Penicillin-binding protein 2 PbpA	∞	ND	ND
PA3636	2-dehydro-3-deoxyphosphooctonate aldolase KdsA	∞	ND	ND
PA0507	Putative acyl-CoA dehydrogenase	∞	∞	ND
PA5003	Protein involved in cellulose biosynthesis (CelD)	∞	ND	ND
PA5001	Glycosyltransferase	∞	ND	ND
PA4599	resistance-nodulation-cell division (RND) multidrug efflux membrane fusion protein MexC precursor MexC	∞	ND	ND
PA4206	Resistance-nodulation-cell division (RND) efflux membrane fusion protein precursor MexH	∞	ND	ND
PA0705	Alpha-1,6-rhamnosyltransferase MigA' MigA	∞	ND	ND
PA4668	Outer membrane lipoprotein LolB	∞	ND	ND
PA3552	UDP-4-amino-4-deoxy-L-arabinose--oxoglutarate aminotransferase ArnB	∞	ND	ND
PA3647	Probable outer membrane protein precursor	∞	∞	∞
PA4410	D-alanine--D-alanine ligase DdlB	∞	ND	ND

PA3644	UDP-N-acetylglucosamine acyltransferase LpxA	∞	∞	∞
PA2614	Outer-membrane lipoprotein carrier protein LolA	∞	ND	ND
PA5291	Putative choline transporter BetT2	∞	∞	ND
PA4417	UDP-N-acetylmuramoylalanyl-D-glutamate--2,6-diaminopimelate ligase MurE	∞	∞	ND
PA4412	Undecaprenyldiphospho-muramoylpentapeptide beta-N- acetylglucosaminyltransferase MurG	∞	∞	ND
PA1494	Hypothetical protein PA1494 MuiA	∞	ND	ND
PA5134	Putative carboxyl-terminal protease CtpA	4.13	5.08	0.70
PA4414	UDP-N-acetylmuramoyl-L-alanyl-D-glutamate synthetase MurD	∞	∞	ND
PA0427	Major intrinsic multiple antibiotic resistance efflux outer membrane protein OprM	ND	1.20	ND
PA4457	Arabinose-5-phosphate isomerase KdsD KpsF	∞	∞	ND
PA0973	Peptidoglycan associated lipoprotein OprL	0.20	0.39	ND
PA5045	Penicillin-binding protein 1A PonA	∞	∞	ND
PA4416	UDP-N-acetylmuramoylalanyl-D-glutamyl-2, 6-diaminopimelate--D-alanyl-D-alanyl ligase MurF	∞	∞	ND
PA4996	Bifunctional heptose 7-phosphate kinase/heptose 1-phosphate adenyltransferase RfaE	∞	∞	ND
PA4450	UDP-N-acetylglucosamine 1-carboxyvinyltransferase MurA	∞	∞	ND
PA0971	TolA protein	∞	∞	ND
PA3155	Aminotransferase WbpE	∞	∞	ND
PA2231	PslA	ND	∞	ND
PA5004	Putative glycosyl transferase	∞	∞	ND
PA0425	RND multidrug efflux membrane fusion protein MexA	2.11	2.96	1.06
PA2900	Probable outer membrane protein precursor	∞	∞	ND
PA2023	UTP-glucose-1-phosphate uridylyltransferase GalU	∞	∞	ND
PA3692	Outer membrane protein precursor LptF	2.17	7.34	ND
PA3158	Oxidoreductase WbpB	0.95	8.86	ND
PA3999	D-ala-D-ala-carboxypeptidase DacC	5.19	10.72	ND
PA1777	Major porin and structural outer membrane porin OprF precursor OprF	0.08	0.14	0.07
PA5549	Glucosamine--fructose-6-phosphate aminotransferase GlmS	∞	∞	ND

PA3141	Nucleotide sugar epimerase/dehydratase WbpM	∞	∞	ND
PA3159	UDP-glucose/GDP-mannose dehydrogenase WbpA	2.64	22.78	1.21
PA5475	Hypothetical protein PA5475	1.58	18.57	3.02
PA0070	Outer membrane lipoprotein TagQ1	0.10	1.67	0.24
PA5245	Isoprenoid biosynthesis protein with amidotransferase-like domain ElbB	∞	∞	∞
PA2000	DhcB, dehydrocarnitine CoA transferase, subunit B	∞	ND	ND
PA0958	Basic amino acid, basic peptide and imipenem outer membrane porin OprD precursor	ND	ND	0.10
PA0291	Anaerobically-induced outer membrane porin OprE precursor	ND	ND	0.12
PA1610	3-hydroxydecanoyl-(acyl carrier protein) dehydratase FabA	∞	ND	ND
PA3645	(3R)-hydroxymyristoyl-ACP dehydratase FabZ	∞	ND	ND
PA2682	Dienelactone hydrolase and related enzymes	∞	ND	ND
PA1860	O-Methyltransferase involved in polyketide biosynthesis	∞	ND	ND
PA3437	Short chain Dehydrogenase FolM	ND	∞	ND
PA2969	Putative glycerol-3-phosphate acyltransferase PlsX	∞	ND	ND
PA4454	ABC-type transport system involved in resistance to organic solvents, periplasmic component YrbD	∞	ND	ND
PA3569	3-hydroxyisobutyrate dehydrogenase MmsB	0.57	ND	ND
PA3301	2-succinyl-6-hydroxy-2,4-cyclohexadiene-1-carboxylate synthase activity	∞	ND	ND
PA2965	3-oxoacyl-(acyl carrier protein) synthase II FabF1	∞	ND	ND
PA4957	Phosphatidylserine decarboxylase Psd	∞	ND	ND
PA2553	Putative acyl-CoA thiolase	0.79	ND	ND
PA4847	Acetyl-CoA carboxylase biotin carboxyl carrier protein subunit AccB	0.67	ND	ND
PA4907	Putative short-chain dehydrogenase YdfG	1.18	1.18	ND
PA1999	DhcA, dehydrocarnitine CoA transferase, subunit A	0.81	ND	ND
PA0447	Glutaryl-CoA dehydrogenase GcdH	∞	ND	ND
PA3286	3-oxoacyl-(acyl carrier protein) synthase III	∞	ND	ND
PA5436	Acetyl-CoA carboxylase subunit A	∞	ND	ND
PA4786	3-ketoacyl-(acyl-carrier-protein) reductase	∞	ND	ND

PA2001	Acetyl-CoA acetyltransferase AtoB	0.59	ND	ND
PA0154	Protocatechuate 3,4-dioxygenase, alpha subunit PcaG	∞	ND	ND
PA3013	3-ketoacyl-CoA thiolase FoaB	∞	∞	ND
PA2009	Homogentisate 1,2-dioxygenase HmgA	∞	ND	ND
PA5092	Imidazolonepropionase HutI	∞	ND	ND
PA2513	Anthranilate dioxygenase small subunit AntB	∞	ND	ND
PA2013	Gamma-carboxygeranoyl-CoA hydratase LiuC	∞	ND	ND
PA3972	Putative acyl-CoA dehydrogenase AidB	∞	∞	ND
PA4389	Probable short-chain dehydrogenase	0.44	2.11	ND
PA3212	ABC transporter ATP-binding protein	∞	∞	ND
PA2841	Enoyl-CoA hydratase	∞	∞	ND
PA3652	Undecaprenyl pyrophosphate synthetase UppS	∞	ND	ND
PA0887	Acetyl-CoA synthetase AcsA	0.40	ND	ND
PA2537	Putative acyltransferase	0.62	3.46	ND
PA5174	Putative beta-ketoacyl synthase	∞	∞	ND
PA0745	Enoyl-CoA hydratase	5.31	5.19	1.23
PA3803	4-hydroxy-3-methylbut-2-en-1-yl diphosphate synthase GcpE	∞	∞	ND
PA4456	ABC transporter ATP-binding protein YrbF	∞	∞	∞
PA3014	Multifunctional fatty acid oxidation complex subunit alpha FaoA	1.33	4.17	ND
PA2968	Malonyl-CoA-[acyl-carrier-protein] transacylase FabD	2.36	3.27	ND
PA4661	Lipid A 3-O-deacylase PagL	∞	∞	ND
PA2815	Acyl-CoA dehydrogenase YafH	∞	∞	ND
PA2967	3-ketoacyl-(acyl-carrier-protein) reductase FabG	2.31	3.79	0.68
PA1609	3-oxoacyl-(acyl carrier protein) synthase I FabB	1.72	3.80	ND
PA2858	Hypothetical protein PA2858 YbbP	ND	∞	ND
PA3911	Hypothetical protein PA3911	ND	1.96	1.46
PA5040	Type 4 fimbrial biogenesis outer membrane protein PilQ	1.01	3.01	ND
PA3996	Lipoyl synthase Lis	ND	∞	ND
PA5223	2-octaprenyl-6-methoxyphenyl hydroxylase UbiH	∞	∞	ND
	9 Chemotaxis/motility			
PA0413	Component of chemotactic signal transduction system ChpA	11.00	58.67	8.18
PA1457	Chemotaxis protein CheZ	3.39	41.83	7.32

PA1456	Two-component response regulator CheY	∞	ND	ND
PA3349	Putative chemotaxis protein	∞	ND	ND
PA1459	Chemotaxis-specific methylesterase CheB	1.16	ND	ND
PA1458	Two-component sensor CheA	3.11	22.24	ND
PA0395	Twitching motility protein PilT	∞	ND	ND
PA4381	Putative two-component response regulator ColR	∞	ND	ND
PA2788	Putative chemotaxis transducer	1.75	19.01	4.38
PA5072	Putative chemotaxis transducer	∞	∞	∞
PA0396	Twitching motility protein PilU	∞	ND	ND
PA5199	Two-component sensor EnvZ AmgS	∞	ND	ND
PA4307	Chemotactic transducer PctC	2.07	13.99	2.83
PA4309	Chemotactic transducer PctA	∞	∞	∞
PA4310	Chemotactic transducer PctB	∞	∞	∞
PA2654	Putative chemotaxis transducer	1.92	9.42	2.65
PA0415	Putative chemotaxis protein ChpC	∞	∞	ND
PA3115	Motility protein FimV	0.59	ND	ND
PA1646	Chemotaxis transducer	∞	∞	∞
PA1092	Flagellin type B FliC	0.18	0.25	0.15
PA3103	General secretion pathway protein E XcpR	ND	∞	ND
PA1101	Flagellar MS-ring protein FliF	ND	∞	ND
PA0410	Twitching motility protein PilI	∞	∞	ND
PA4553	Type 4 fimbrial biogenesis protein PilX	∞	∞	ND
PA3919	NYN ribonuclease and ATPase of PhoH family domainsYlaK	∞	∞	ND
PA0411	Twitching motility protein PilJ	0.55	1.60	0.42
PA4525	Type 4 fimbrial precursor PilA	2.23	4.92	1.58
PA4959	FimX	∞	∞	ND
PA4856	Regulator of exopolysaccharide and type III secretion RetS	ND	∞	ND
PA4493	Putative two-component response regulator RoxR	1.94	8.38	ND
PA5044	Type 4 fimbrial biogenesis protein PilM	∞	∞	ND
PA5043	Type 4 fimbrial biogenesis protein PilN	0.87	1.87	ND
PA2960	Type 4 fimbrial biogenesis protein PilZ	ND	∞	ND
PA1094	Flagellar capping protein FliD	2.22	8.60	ND
PA5117	GTP-binding protein TypA/BipA	∞	∞	ND
PA4526	Type 4 fimbrial biogenesis protein PilB	∞	∞	ND
PA4290	Chemotaxis transducer	ND	∞	ND
PA0409	Twitching motility protein PilH	0.18	0.47	ND

PA0408	Twitching motility protein PilG	0.27	0.82	0.38
PA1636	Two-component sensor KdpD	ND	∞	ND
PA3805	Type 4 fimbrial biogenesis protein PilF	0.71	2.30	ND
PA5042	Type 4 fimbrial biogenesis protein PilO	∞	∞	ND
PA1179	Two-component response regulator PhoP	15.25	16.75	ND
PA1097	Transcriptional regulator FleQ	∞	∞	ND
PA4554	Type 4 fimbrial biogenesis protein PilY1	∞	∞	ND
PA1336	Putative two-component sensor AauS	∞	∞	ND
PA1461	Flagellar motor protein MotD	∞	∞	∞
PA0180	Putative chemotaxis transducer CttP	∞	∞	∞
PA2867	Putative chemotaxis transducer	2.74	8.19	1.29
PA2652	Putative chemotaxis transducer	1.20	7.25	1.67
PA4633	Putative chemotaxis transducer	∞	∞	∞
PA1608	Chemotaxis transducer	∞	∞	∞
	10 Protein transport			
PA4747	Preprotein translocase subunit SecG	∞	ND	ND
PA3822	Preprotein translocase subunit YajC	13.35	30.23	12.57
PA4403	Preprotein translocase subunit SecA	7.55	23.72	7.29
PA5128	Preprotein translocase subunit SecB	0.95	ND	ND
PA3821	Preprotein translocase subunit SecD	3.56	18.39	8.21
PA3820	Preprotein translocase subunit SecF	1.59	13.39	3.81
PA5568	Putative inner membrane protein translocase component YidC	0.65	2.60	2.01
PA0373	Signal recognition particle receptor FtsY	∞	∞	ND
PA3746	Signal recognition particle protein Ffh	∞	∞	∞
	11 Amino acid metabolism			
PA3397	Ferredoxin--NADP+ reductase Fpr	ND	2.12	ND
PA2827	Methionine sulfoxide reductase B YeaA	∞	ND	ND
PA4442	Bifunctional sulfate adenylyltransferase subunit 1/adenylylsulfate kinase protein CysN	∞	∞	ND
PA0389	Methionine biosynthetic process protein	∞	ND	ND
PA0432	S-adenosyl-L-homocysteine hydrolase SahH	2.85	5.61	ND
PA1681	Chorismate synthase AroC	∞	∞	∞
PA0400	Cystathionine gamma-lyase MetC	∞	∞	ND
PA3831	Leucyl aminopeptidase PepA	3.27	ND	ND
PA5066	Phosphoribosyl-AMP cyclohydrolase HisI	∞	ND	∞
PA4758	Carbamoyl phosphate synthase small subunit CarA	1.38	ND	ND
PA0390	Homoserine O-acetyltransferase MetX	∞	ND	ND

PA4722	Aspartate/tyrosine/aromatic aminotransferase	∞	ND	ND
PA0896	Arginine/ornithine succinyltransferase AI subunit AruF	∞	ND	ND
PA0302	Polyamine transport protein PotG	∞	ND	ND
PA0534	Polyamine catabolic process PauB1	1.45	ND	ND
PA5421	Glutathione-independent formaldehyde dehydrogenase FdhA	∞	ND	ND
PA2776	Glycine/D-amino acid oxidases PauB3	∞	ND	ND
PA5418	Sarcosine oxidase alpha subunit SoxA	∞	ND	ND
PA0296	Glutamine synthetase SpuI	∞	ND	ND
PA4839	Arginine decarboxylase SpeA	∞	ND	ND
PA0266	4-aminobutyrate aminotransferase GabT	0.81	ND	ND
PA4694	Ketol-acid reductoisomerase IlvC	190.75	225.30	86.39
PA1010	Dihydrodipicolinate synthase DapA	0.82	ND	ND
PA5013	Branched-chain amino acid aminotransferase IlvE	∞	ND	ND
PA4695	Acetolactate synthase 3 regulatory subunit IlvH	∞	ND	ND
PA4449	ATP phosphoribosyltransferase catalytic subunit HisG	∞	ND	ND
PA4939	ATP phosphoribosyltransferase regulatory subunit HisX	∞	ND	ND
PA3139	Aromatic amino acid aminotransferase	∞	ND	ND
PA1810	Binding protein component of ABC transporter	∞	ND	ND
PA0865	4-hydroxyphenylpyruvate dioxygenase Hpd	∞	ND	ND
PA2265	Gluconate dehydrogenase Gad	∞	ND	ND
PA2579	L-Tryptophan:oxygen 2,3-oxidoreductase (decyclizing) KynA' KynA	∞	ND	ND
PA0035	Tryptophan synthase subunit alpha TrpA	∞	ND	ND
PA5141	1-(5-phosphoribosyl)-5-[(5-phosphoribosylamino)methylideneamino] imidazole-4-carboxamide isomerase HisA	∞	ND	ND
PA3068	NAD-dependent glutamate dehydrogenase GdhB	5.29	48.85	8.04
PA5508	Putative glutamine synthetase PauA7	0.79	8.78	ND
PA1339	Amino acid ABC transporter ATP binding protein AatP	1.53	20.61	4.15
PA3525	Argininosuccinate synthase ArgG	∞	ND	ND
PA5263	Argininosuccinate lyase ArgH	1.15	ND	ND
PA5204	N-acetylglutamate synthase ArgA	ND	∞	ND

PA4402	Bifunctional ornithine acetyltransferase/N-acetylglutamate synthase protein ArgJ	∞	∞	ND
PA3814	Cysteine desulfurase IscS	1.33	2.63	ND
PA5173	Carbamate kinase ArcC	2.74	3.16	0.59
PA1750	Phospho-2-dehydro-3-deoxyheptonate aldolase	0.47	ND	ND
PA5142	imidazole glycerol phosphate synthase subunit HisH1	∞	ND	ND
PA2011	Hydroxymethylglutaryl-CoA lyase LiuE	∞	ND	ND
PA1818	Orn/Arg/Lys decarboxylase LdcC LdcA	∞	ND	ND
PA0897	Arginine/ornithine succinyltransferase AruG	∞	∞	ND
PA2709	Cysteine synthase A CysK	∞	∞	ND
PA4443	Sulfate adenylyltransferase subunit 2 CysD	∞	ND	ND
PA5119	Glutamine synthetase GlnA	9.67	9.23	2.25
PA5076	Putative binding protein component of ABC transporter	0.67	ND	ND
PA2828	Aminotransferase AlaT	∞	ND	ND
PA0870	Aromatic amino acid aminotransferase PhhC	0.54	ND	ND
PA3165	Histidinol-phosphate aminotransferase HisC2	ND	∞	ND
PA3083	Aminopeptidase N PepN	∞	∞	ND
PA5415	Serine hydroxymethyltransferase GlyA1	∞	ND	ND
PA5152	ABC transporter ATP-binding protein	∞	ND	ND
PA0904	Aspartate kinase LysC	∞	ND	ND
PA5143	Imidazoleglycerol-phosphate dehydratase HisB	∞	∞	ND
PA0899	Succinylarginine dihydrolase AruB	∞	ND	ND
PA3736	Homoserine dehydrogenase Hom	∞	∞	∞
PA5495	Homoserine kinase ThrB	ND	∞	ND
PA3862	Hypothetical protein PA3862 DauB	ND	∞	ND
PA0603	ABC transporter ATP-binding protein AgtA	∞	∞	ND
PA0300	Polyamine transport protein SpuD	0.26	0.58	ND
PA0298	Glutamine synthetase SpuB	ND	∞	ND
PA4759	Dihydrodipicolinate reductase DapB	∞	∞	ND
PA5429	Aspartate ammonia-lyase AspA	ND	0.59	ND
PA0399	Cystathionine beta-synthase	∞	∞	ND
PA4548	D-amino acid oxidase YfiT	ND	∞	ND
PA4756	Carbamoyl phosphate synthase large subunit CarB	0.79	1.48	ND
PA0430	5,10-methylenetetrahydrofolate reductase MetF	∞	∞	ND
PA2445	Glycine dehydrogenase GcvP2	ND	0.78	ND
PA0353	Dihydroxy-acid dehydratase IlvD	∞	∞	ND

PA2442	Glycine cleavage system protein T2 GcvT2	ND	1.69	ND
PA4565	Gamma-glutamyl kinase ProB	∞	∞	ND
PA3156	Acetyltransferase WbpD	ND	∞	ND
PA4506	Dipeptide transporter ATP-binding subunit DppF	0.56	2.15	ND
PA3735	Threonine synthase ThrC	1.50	6.41	2.57
PA4602	Serine hydroxymethyltransferase GlyA3	0.92	1.97	ND
PA3538	ABC transporter ATP-binding protein	∞	∞	ND
PA1342	Putative binding protein component of ABC transporter AatJ	10.91	0.59	0.17
PA3816	O-acetylserine synthase CysE	1.85	5.30	4.05
PA0895	Bifunctional succinylornithine transaminase/acetylornithine aminotransferase AruC	1.38	6.17	ND
PA3364	Aliphatic amidase expression-regulating protein AmiC	∞	∞	ND
PA3666	Tetrahydrodipicolinate succinylase DapD	∞	∞	ND
PA5125	Two-component response regulator NtrC	∞	∞	ND
	12 Iron-sulfur proteins			
PA5489	Thiol:disulfide interchange protein DsbA	∞	ND	ND
PA1008	Bacterioferritin comigratory protein Bcp	∞	ND	∞
PA4061	Probable thioredoxin YbbN	∞	ND	ND
PA0953	Thioredoxin HelX	0.57	2.29	ND
PA2616	Thioredoxin reductase 1 TrxB1	0.94	1.73	ND
PA4845	Thiol:disulfide interchange protein precursor DipZ	ND	∞	ND
PA1847	Potential iron-sulfur cluster assembly protein NfuA	2.61	5.27	ND
PA5240	Thioredoxin TrxA	2.14	3.81	ND
PA2532	Thiol peroxidase Tpx	1.26	4.70	1.00
PA3809	Ferredoxin (2Fe-2S) Fdx2	∞	ND	ND
PA0665	Iron-sulfur cluster insertion protein ErpA	∞	∞	ND
PA0962	DNA-binding stress protein Dps	0.20	ND	ND
PA4764	Ferric uptake regulation protein Fur	7.80	3.53	1.55
PA3815	Iron-sulfur cluster binding protein IscR	∞	ND	∞
PA4956	Thiosulfate:cyanide sulfurtransferase RhdA	∞	∞	ND
PA3531	Bacterioferritin BfrB	13.60	27.23	ND
PA4235	Bacterioferritin FtnA	6.07	45.75	14.20
PA1292	Putative 3-mercaptopyruvate sulfurtransferase	0.90	3.46	1.42
	13 Alginate			

PA5322	Phosphomannomutase AlgC	1.32	7.52	1.19
PA4446	AlgW protein	∞	∞	ND
PA5261	Alginate biosynthesis regulatory protein AlgR	∞	∞	ND
PA0405	Putative transcriptional regulator AlgH	∞	ND	ND
PA5483	Two-component response regulator AlgB	ND	∞	ND
	14 Proteases/chaperones			
PA4558	Peptidyl-prolyl cis-trans isomerase, FkbP-type YaaD	∞	∞	ND
PA5053	ATP-dependent protease peptidase subunit HslV	∞	ND	ND
PA1767	Membrane-bound serine protease (ClpP class)	1.63	ND	ND
PA1832	Putative periplasmic protease SohB	∞	ND	ND
PA3326	ATP-dependent Clp protease proteolytic subunit ClpP2	∞	ND	ND
PA2725	Putative chaperone	ND	∞	ND
PA1068	HSP90 family protein	ND	∞	ND
PA4542	ClpB protein	6.28	9.64	1.17
PA0277	Zn-dependent protease with chaperone function	∞	ND	ND
PA3913	Putative protease YhbU	ND	7.24	ND
PA0779	Putative ATP-dependent protease AsrA	∞	∞	ND
PA5193	Hsp33-like chaperonin YrfI	∞	∞	ND
PA4941	Protease subunit HflC	13.92	14.04	11.57
PA1805	Peptidyl-prolyl *cis-trans* isomerase D PpiD	6.29	22.33	4.38
PA4176	Peptidyl-prolyl *cis-trans* isomerase C2 PpiC2	0.10	0.31	ND
PA0580	O-sialoglycoprotein endopeptidase Gcp	∞	ND	ND
PA3365	Putative chaperone AmiB	ND	∞	ND
PA0459	Putative ClpA/B protease ATP binding subunit ClpC	3.15	8.56	1.31
PA2973	Putative peptidase	∞	∞	ND
PA5054	ATP-dependent protease ATP-binding subunit HslU	18.23	13.06	ND
PA3810	Chaperone protein HscA	∞	∞	ND
PA3811	Co-chaperone HscB	∞	∞	ND
PA4572	Peptidyl-prolyl cis-trans isomerase FklB	∞	∞	∞
PA4632	Potential Zn-dependent protease with chaperone function	1.60	1.90	0.69
PA0090	ClpV1	∞	∞	ND
PA4760	Chaperone protein DnaJ	8.84	6.06	ND
PA5440	Putative peptidase YegQ	∞	∞	∞

PA1803	Lon protease LopA	∞	∞	ND
PA1793	Peptidyl-prolyl *cis-trans* isomerase B PpiB	1.62	4.10	0.63
PA1802	ATP-dependent protease ATP-binding subunit ClpX	2.74	11.17	3.05
PA1801	ATP-dependent Clp protease proteolytic subunit ClpP	0.91	8.76	ND
PA1800	Trigger factor Tig	1.15	2.01	0.85
PA0837	Peptidyl-prolyl cis-trans isomerase SlyD	∞	∞	ND
PA4942	Protease subunit HflK	6.51	7.96	5.62
PA2620	ATP-binding protease component ClpA	∞	∞	ND
PA4386	Co-chaperonin GroES	1.89	5.33	1.15
PA4385	Chaperonin GroEL	0.95	2.27	0.71
PA0766	Serine protease MucD precursor	8.16	17.06	ND
PA3262	Putative peptidyl-prolyl cis-trans isomerase, FkbP-type	1.54	7.74	1.41
PA3785	Potential cooper(I)-binding chaperone PA3785	∞	∞	∞
PA1596	Heat shock protein 90 HtpG	3.75	5.15	1.13
PA4761	Molecular chaperone DnaK	3.12	3.09	ND
PA3257	Periplasmic tail-specific protease Prc	∞	∞	ND
PA1246	Alkaline protease secretion protein AprD	ND	∞	ND
PA3842	Chaperone SpcS	ND	∞	ND
PA0768	Signal peptidase I LepB	∞	ND	ND
PA0767	GTP-binding protein LepA	∞	ND	ND
PA4370	Metalloproteinase outer membrane protein precursor IcmP	0.98	2.44	ND
PA3841	Exoenzyme S ExoS	ND	∞	ND
	15 Stress/detoxification			
PA5373	Betaine aldehyde dehydrogenase BetB	∞	ND	ND
PA2664	Nitric oxide dioxygenase Fhp	19.04	8.22	ND
PA2813	Glutathione S-transferase YliJ	ND	∞	ND
PA2821	Glutathione S-transferase	∞	ND	ND
PA3529	Putative peroxidase TsaA	0.86	2.00	0.44
PA0838	Glutathione peroxidase BtuE	ND	∞	ND
PA0139	Alkyl hydroperoxide reductase subunit C AhpC	2.81	5.82	ND
PA5027	Hypothetical protein UspA	∞	∞	ND
PA4723	Supressor protein DksA	∞	∞	∞
PA0652	cAMP-regulatory protein Vfr	5.82	19.98	9.54
PA4236	Catalase KatA	3.19	17.03	ND

PA2582	Activator of osmoprotectant ProP	5.50	17.69	5.47
PA0456	Putative cold-shock protein	2.71	5.16	1.57
PA5372	Choline dehydrogenase BetA	∞	∞	∞
PA3309	Universal stress protein UspK	7.87	11.42	6.22
PA4352	Universal stress protein UspA	2.07	5.69	ND
PA5200	Osmolarity response regulator	∞	∞	ND
PA2622	Cold-shock protein CspD	ND	∞	ND
PA0961	Cold-shock protein	∞	ND	ND
PA3126	Heat-shock protein IbpA	∞	∞	ND
PA4762	Heat shock protein GrpE	3.17	3.19	ND
PA4366	Superoxide dismutase SodB	0.50	1.35	ND
PA1159	Cold-shock protein	0.45	2.23	ND
PA4427	ClpXP protease specificity-enhancing factor SspB (stringent starvation factor)	∞	∞	ND
PA4428	Stringent starvation protein A SspA	∞	ND	ND
PA0783	Sodium/proline symporter PutP	ND	∞	ND
PA5374	Transcriptional regulator BetL	ND	∞	ND
PA5344	Putative transcriptional regulator OxyR	∞	∞	ND
PA1207	Glutathione-regulated potassium-efflux system protein KefB	ND	∞	ND
PA0016	Potassium transporter peripheral membrane component TrkA	∞	∞	ND
PA0407	Glutathione synthetase GshB	∞	ND	ND
PA0905	Carbon storage regulator RsmA	1.43	ND	ND
PA0176	Aerotaxis transducer Aer2	∞	ND	ND
PA4777	PmrB: two-component regulator system signal sensor kinase PmrB	∞	ND	ND
PA5338	guanosine-3',5'-bis(diphosphate) 3'-pyrophosphohydrolase SpoT	∞	ND	ND
PA1561	Aerotaxis receptor Aer	2.50	16.48	3.24
PA2582	Potential activator of osmoprotectant transporter ProP	5.50	17.69	5.47
	16 DNA/RNA metabolism			
PA3686	Adenylate kinase Adk	0.30	0.45	ND
PA5426	Phosphoribosylaminoimidazole carboxylase, catalytic subunit PurE	∞	∞	ND
PA0342	Thymidylate synthase ThyA	∞	ND	ND
PA3108	Amidophosphoribosyltransferase PurF	∞	∞	ND

PA5321	Deoxyuridine 5'-triphosphate nucleotidohydrolase Dut	∞	ND	ND
PA5241	Exopolyphosphatase Ppx	∞	ND	ND
PA1013	Phosphoribosylaminoimidazole-succinocarboxamide synthase PurC	1.03	ND	ND
PA5298	Xanthine phosphoribosyltransferase Xpt	ND	∞	ND
PA3763	Phosphoribosylformylglycinamidine synthase PurL	ND	∞	ND
PA3050	Dihydroorotate dehydrogenase 2 PyrD	∞	ND	ND
PA1920	Anaerobic ribonucleoside triphosphate reductase NrdD	ND	0.79	ND
PA4854	Bifunctional phosphoribosylaminoimidazolecarboxamide formyltransferase/IMP cyclohydrolase PurH	∞	ND	ND
PA1155	Ribonucleotide-diphosphate reductase subunit beta NrdB	0.08	3.24	1.07
PA3654	Uridylate kinase PyrH	∞	ND	ND
PA3970	AMP nucleosidase Amn	∞	ND	ND
PA1156	Ribonucleotide-diphosphate reductase subunit alpha NrdA	0.65	7.27	1.37
PA5497	NrdJa	0.23	4.78	1.20
PA5496	NrdJb	0.29	5.10	1.15
PA0945	Phosphoribosylaminoimidazole synthetase PurM	1.13	2.52	ND
PA3480	Deoxycytidine triphosphate deaminase Dcd	∞	∞	ND
PA3807	Nucleoside diphosphate kinase Ndk	1.05	1.86	ND
PA0387	Putative deoxyribonucleotide triphosphate pyrophosphatase YggV	1.15	ND	ND
PA0401	Dihydroorotase	∞	∞	ND
PA0402	Aspartate carbamoyltransferase catalytic subunit PyrB	∞	∞	ND
PA3637	CTP synthetase PyrG	5.94	9.26	ND
PA3770	Inosine 5'-monophosphate dehydrogenase GuaB	4.25	5.66	ND
PA3769	GMP synthase GuaA	∞	∞	ND
PA4938	Adenylosuccinate synthetase PurA	0.94	2.51	0.67
PA3295	Putative HIT family protein	1.63	11.35	ND
PA3004	5'-methylthioadenosine phosphorylase	∞	∞	ND
PA4670	Ribose-phosphate pyrophosphokinase Prs	8.94	12.94	ND
PA4314	Formyltetrahydrofolate deformylase PurU1	∞	∞	ND

PA3168	DNA gyrase subunit A GyrA	1.87	7.54	ND
PA0004	DNA gyrase subunit B GyrB	3.05	20.06	6.46
PA0002	DNA polymerase III subunit beta DnaN	∞	∞	ND
PA5332	Catabolite repression control protein Crc	∞	ND	ND
PA0001	Chromosomal replication initiation protein DnaA	∞	ND	ND
PA5562	Chromosome partitioning protein Spo0J	2.35	10.20	ND
PA3940	Putative DNA binding protein	0.26	ND	ND
PA4964	DNA topoisomerase IV subunit A ParC	∞	∞	ND
PA3620	DNA mismatch repair protein MutS	∞	ND	ND
PA5348	Putative DNA-binding protein	0.82	ND	ND
PA2738	Integration host factor subunit alpha HimA	∞	ND	ND
PA3528	Ribonuclease T Rnt	∞	ND	ND
PA3297	ATP-dependent helicase HrpA	∞	ND	ND
PA4931	Replicative DNA helicase DnaB	ND	∞	ND
PA3640	DNA polymerase III subunit alpha DnaE	∞	ND	ND
PA4946	DNA mismatch repair protein MutL	ND	∞	ND
PA5493	DNA polymerase I PolA	∞	ND	ND
PA5443	DNA-dependent helicase II UvrD	∞	∞	ND
PA4763	DNA repair protein RecN RecN	∞	∞	ND
PA1816	DNA polymerase III subunit epsilon DnaQ	ND	∞	ND
PA2545	Exonuclease III XthA	ND	∞	ND
PA1532	DNA polymerase III subunits gamma and tau DnaX	∞	∞	∞
PA4967	DNA topoisomerase IV subunit B ParE	∞	∞	ND
PA3011	DNA topoisomerase I TopA	∞	∞	ND
PA2613	Recombination factor protein RarA	∞	∞	∞
PA4234	Excinuclease ABC subunit A UvrA	∞	∞	ND
PA3263	Recombination associated protein YaiD	∞	∞	ND
PA3617	Recombinase A RecA	2.64	8.76	3.08
PA1804	DNA-binding protein HU HupB	0.81	0.77	0.09
PA0428	Putative ATP-dependent RNA helicase RhlE	3.52	21.93	5.80
PA4232	Single-stranded DNA-binding protein Ssb	4.12	10.40	1.96
PA3466	Putative ATP-dependent RNA helicase SrmB	∞	∞	ND
PA2016	Regulator of *liu* genes LiuR	∞	ND	ND
PA2840	Putative ATP-dependent RNA helicase DeaD	∞	ND	ND
PA3225	Putative transcriptional regulator	∞	ND	ND
PA3002	Transcription-repair coupling factor Mfd	∞	∞	ND
PA1315	Putative transcriptional regulator	∞	ND	ND

PA4057	Transcriptional regulator NrdR	∞	ND	∞
PA0770	Ribonuclease III Rnc	∞	ND	ND
PA3308	ATP-dependent helicase HepA	∞	∞	ND
PA5308	Leucine-responsive regulatory protein Lrp	∞	∞	ND
PA3689	Transcriptional regulator YhdM	∞	ND	ND
PA3563	DNA-binding transcriptional regulator FruR	∞	ND	ND
PA2259	Transcriptional regulator PtxS	∞	ND	ND
PA4600	Transcriptional regulator NfxB	∞	ND	ND
PA3731	Hypothetical protein PA3731	4.40	4.01	0.56
PA4052	Transcription antitermination protein NusB	∞	ND	ND
PA3266	Cold acclimation protein B CapB	3.74	6.89	3.43
PA4937	Exoribonuclease RNase R Rnr	∞	∞	ND
PA1754	Transcriptional regulator CysB	∞	∞	ND
PA5239	Transcription termination factor Rho	4.74	10.61	2.61
PA4270	DNA-directed RNA polymerase subunit beta RpoB	2.68	12.60	2.65
PA4238	DNA-directed RNA polymerase subunit alpha RpoA	3.39	8.86	1.78
PA4269	DNA-directed RNA polymerase subunit beta' RpoC	2.97	16.96	3.18
	17 Inorganic ion transport and metabolism			
PA5500	Zinc transport protein ZnuC	ND	∞	ND
PA1429	Cation-transporting P-type ATPase	∞	∞	ND
PA1772	Ribonuclease activity regulator protein RraA	∞	ND	ND
PA4056	Riboflavin-specific deaminase/reductase RibD	∞	ND	ND
PA4044	1-deoxy-D-xylulose-5-phosphate synthase Dxs	∞	ND	ND
PA0546	S-adenosylmethionine synthetase MetK	0.94	2.74	ND
PA4569	Octaprenyl-diphosphate synthase IspB	0.58	ND	ND
PA4053	6,7-dimethyl-8-ribityllumazine synthase RibE	∞	ND	ND
PA5203	Glutamate--cysteine ligase GshA	∞	ND	ND
PA3171	3-demethylubiquinone-9 3-methyltransferase UbiG	0.48	3.87	2.05
PA0381	Thiazole synthase ThiG	∞	∞	ND
PA1766	Hypothetical protein PA1766	∞	∞	∞
PA4286	Lipoate-protein ligase A	∞	ND	ND
PA0871	Pterin-4-alpha-carbinolamine dehydratase PhhB	∞	∞	ND
PA0299	Putative aminotransferase SpuC	2.03	7.16	ND

PA5320	Bifunctional phosphopantothenoylcysteine decarboxylase/phosphopantothenate synthase CoaC	∞	∞	ND
PA4054	Bifunctional 3,4-dihydroxy-2-butanone 4-phosphate synthase/GTP cyclohydrolase II-like protein RibB	∞	∞	ND
PA1752	2-dehydropantoate 2-reductase	∞	∞	ND
PA3975	Phosphomethylpyrimidine kinase ThiD	∞	∞	ND
PA0316	D-3-phosphoglycerate dehydrogenase SerA	1.27	10.61	2.39
PA1549	Cation-transporting P-type ATPase FixI	ND	∞	ND

The proteomic data reveals the enrichment of proteins in the co-purification using NorB, NorC and NosR as bait expressed as protein abundance (area value) in comparison to the appropriate experiment control. Each number represents the average area of the protein in the bait-preys co-purifications versus the average area of the protein in the control experiment. ND = proteins not reproducibly detected as prey. ∞ = proteins detected as a prey but not found in the control. PA accession numbers are shown.